CORA Cork Open Research Archive
Cartlann Taighde Oscailte Chorcaí

Title	Competition between N and O: use of diazine N-oxides as a test case for the Marcus theory rationale for ambident reactivity
Authors	Sheehy, Kevin;Bateman, Lorraine M.;Flosbach, Niko T.;Breugst, Martin;Byrne, Peter A.
Publication date	2020-07-23
Original Citation	Sheehy, K., Bateman, L. M., Flosbach, N. T., Breugst, M. and Byrne, P. (2020) 'Competition Between N and O: Use of Diazine N-Oxides as a Test Case for the Marcus Theory Rationale for Ambident Reactivity', Chemical Science, doi: 10.1039/D0SC02834G
Type of publication	Article (peer-reviewed)
Link to publisher's version	https://pubs.rsc.org/en/Content/ArticleLanding/2020/SC/D0SC02834G - 10.1039/D0SC02834G
Rights	© The Royal Society of Chemistry 2020. Open Access. This article is licensed under a Creative Commons Attribution 3.0 Unported Licence. - https://creativecommons.org/licenses/by/3.0/
Download date	2026-11-06 16:50:28
Item downloaded from	https://hdl.handle.net/10468/10357

UCC
University College Cork, Ireland
Coláiste na hOllscoile Corcaigh

Competition Between N and O: Use of Diazine *N*-Oxides as a Test Case for the Marcus Theory Rationale for Ambident Reactivity

Received 00th January 20xx,
Accepted 00th January 20xx

DOI: 10.1039/x0xx00000x

Kevin J. Sheehy,[a] Lorraine M. Bateman,[a,b,d] Niko T. Flosbach,[c] Martin Breugst,*[c] Peter A. Byrne,*[a,d]

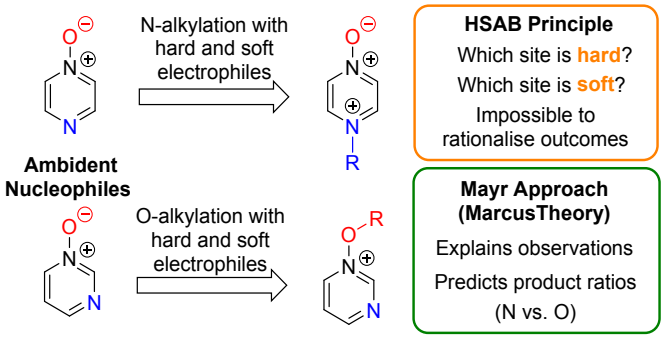
The preferred site of alkylation of diazine *N*-oxides by representative hard and soft alkylating agents was established conclusively using the ^{1}H-^{15}N HMBC NMR technique in combination with other NMR spectroscopic methods. Alkylation of pyrazine *N*-oxides (**1** and **2**) occurs preferentially on nitrogen regardless of the alkylating agent employed, while O-methylation of pyrimidine *N*-oxide (**3**) is favoured in its reaction with MeOTf. As these outcomes cannot be explained in the context of the hard/soft acid/base (HSAB) principle, we have instead turned to Marcus theory to rationalise these results. Marcus intrinsic barriers ($\Delta G_0^{\ddagger}$) and $\Delta_r G°$ values were calculated at the DLPNO-CCSD(T)/def2-TZVPPD/SMD//M06-2X-D3/6-311+G(d,p)/SMD level of theory for methylation reactions of **1** and **3** by MeI and MeOTf, and used to derive Gibbs energies of activation ($\Delta G^{\ddagger}$) for the processes of N- and O-methylation, respectively. These values, as well as those derived directly from the DFT calculations, closely reproduce the observed experimental N vs O selectivities for methylation reactions of **1** and **3**, indicating that Marcus theory can be used in a semi-quantitative manner to understand how the activation barriers for these reactions are constructed. It was found that N-alkylation of **1** is favoured due to the dominant contribution of $\Delta_r G°$ to the activation barrier in this case, while O-alkylation of **3** is favoured due to the dominant contribution of the intrinsic barrier ($\Delta G_0^{\ddagger}$) for this process. These results are of profound significance in understanding the outcomes of reactions of ambident reactants in general.

Introduction

Selectivity in Reactions of Ambident Nucleophiles

A fundamental goal in organic chemistry is to be able to understand and rationalise why chemical processes occur as they do. Naturally, therefore, an understanding of the factors that govern regioselectivity in chemical reactions is of paramount importance – i.e. if a compound contains more than one reactive site, which one is preferred, and why? Reliably accounting for the regioselectivity observed in reactions of ambident nucleophiles and electrophiles is a challenge laden with difficulties and potential pitfalls. By far the most popular rationale for this purpose[1] makes use of the principle of hard and soft acids and bases (the HSAB principle),[2] and the related concept of charge vs. orbital control.[3] The difficulty inherent in accounting for the selectivities observed in reactions of ambident nucleophiles is exemplified by the fact that the HSAB principle *predicts the incorrect product* in a very large number of cases, as has been reviewed in detail by Mayr and co-workers.[4] The data in this review call starkly into question whether the principle adequately explains the observed selectivity in reactions of ambident nucleophiles in which the expected outcome (based on HSAB theory) does match the experimental outcome.[5]

Mayr and co-workers have suggested employing Marcus theory (described below) as an alternative method of accounting qualitatively for the selectivities of reactions of ambident reactants.[4]



Scheme 1. Approaches for rationalising selectivity in reactions of diazine N-oxides as representative ambident nucleophiles.

Recently, Wang, Barnes, and co-workers conducted computational investigations to establish a theoretical basis for applying the HSAB principle in rationalising ambident reactivity, and used this, along with Marcus theory, to explain the results of their calculations on gas phase reactions of amide anions.[6] However, so far, the Marcus theory-based approach has not been adopted by the wider research community, and in fact the HSAB rationale continues to be cited in cases in which the experimental results do align, perhaps arbitrarily, with expectations based on this principle.[5] Furthermore, the elements of the intuitively alluring HSAB rationale pervade all discussions of ambident reactivity in undergraduate chemistry courses, and in the most comprehensive organic chemistry textbooks.[1] Given the clear deficiencies of the HSAB rationale in the context of ambident reactivity, it now behoves organic chemists to test Mayr's approach and other alternatives on their capacity to account for the outcomes of reactions of ambident reactants.

Herein, we focus on the notoriously difficult problem of competition between N and O nucleophilic sites (Scheme 1).[4,5c,6,7–14] We chose diazine *N*-oxides **1**, **2** and **3** (Fig. 1) as test substrates in reactions with various representative hard and soft electrophiles because, although

[a] School of Chemistry, Analytical and Biological Chemistry Research Facility, University College Cork, College Road, Cork, Ireland.
[b] School of Pharmacy, University College Cork, College Road, Ireland
[c] Department für Chemie, Universität zu Köln, Greinstraße 4, 50939 Köln, Germany.
[d] SSPC (Synthesis and Solid State Pharmaceutical Centre), Cork, Ireland.
E-mail: peter.byrne@ucc.ie, mbreugst@uni-koeln.de

Electronic Supplementary Information (ESI) available: contains experimental procedures, characterisation data for products and reaction mixtures, details of crossover experiments, copies of NMR spectra, and details on computational investigations. See DOI: 10.1039/x0xx00000x.

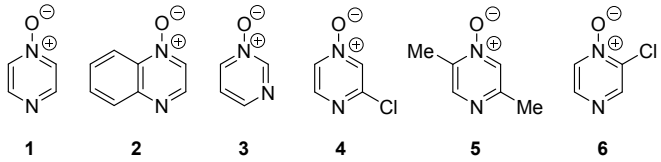


Figure 1. Representative Diazine *N*-oxides

these reactions show very high site-selectivity (i.e. for N- or O-alkylation),[7] their outcomes are intractable to rationalisation using the HSAB principle (Scheme 1), as will be discussed in the next section. An additional contributing factor that confounds any attempt to analyse the reactions of these species using the HSAB rationale is that it is not possible to unambiguously identify which nucleophilic site of a diazine *N*-oxide is the hard site, and which is the soft site (see later).[15]

In this work, we will show that the approach of Mayr and co-workers enables accurate prediction of the preferred site of alkylation of ambident nucleophiles **1–3**. Furthermore, we will also show that it is even possible to calculate the ratio of the selectivities for the different nucleophilic sites in these compounds (N vs. O) with an impressive degree of accuracy (Scheme 1).[16] Our results bolster the applicability of the Marcus theory-based approach and establish, for the first time, its capacity to semi-quantitatively account for the ratios of site-selectivities in reactions of ambident nucleophiles.

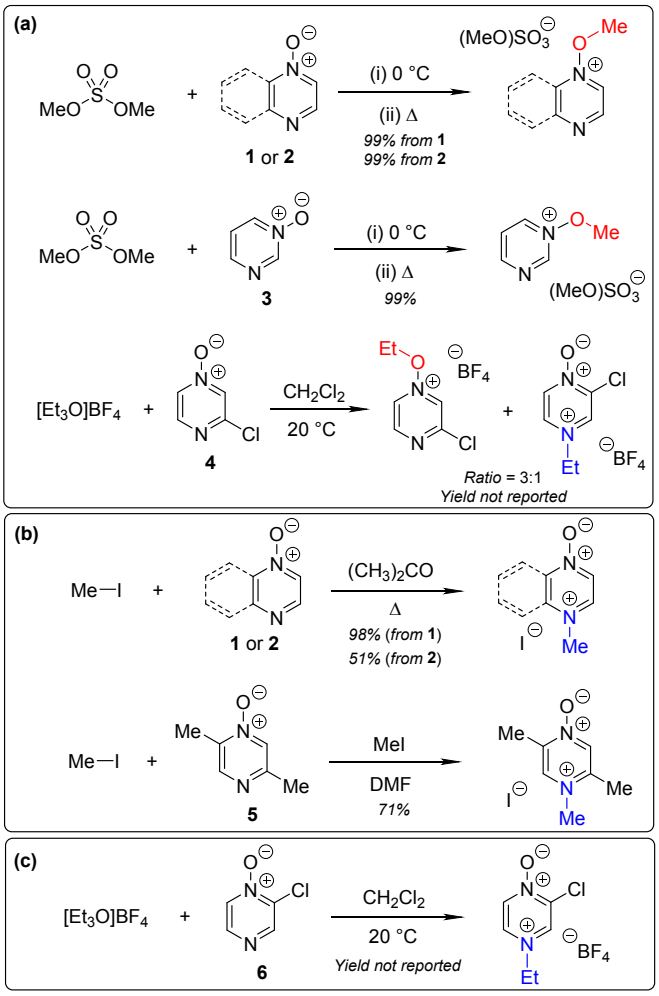
It should be noted that the limitations of the HSAB principle were highlighted by its developer (Pearson),[2d,f] and that in its original formulation,[2a,b] it was not derived with the intention of rationalising the selectivities of reactions of ambident reactants. However, thereafter, it has been[2c] and continues to be applied in this manner.[1,5] In recent years, a theoretical grounding demonstrating the applicability of the "global" HSAB principle (which does not apply to ambident reactants) has been developed.[17,18] Despite the authors' inclusion in the articles on this topic of precise statements such as "*The local HSAB principle, which makes predictions about ambident acids and bases, is on much shakier theoretical ground, so experimental evidence against it is not surprising*", [15a,17b] these papers are nonetheless cited in other articles in support of application of the HSAB principle to the analysis of reactions of ambident nucleophiles.[5c] This is illustrative of the continued application of the HSAB principle to rationalisation of ambident reactivity in the wider chemistry community despite the large body of evidence demonstrating that it does not apply in such instances.

Competition Between N and O Nucleophilic Sites

Numerous examples of reactions of ambident nucleophiles containing competing O and N nucleophilic sites exist in the literature.[6,10–14,19–32] Compounds **1–3** are particularly suitable for the present investigation for the following reasons: (i) Unlike the reactions of many other ambident nucleophiles containing N and O nucleophilic sites,[6,14,20–31] reactions of **1–3** are not influenced by the presence of a counter-cation,[33] and (ii) their alkylation products do not undergo secondary reactions (*cf.* amide alkylations).[19c,f]

There exist several literature precedents of relevance to the ambident nucleophilicity of diazine *N*-oxides. Exclusive O-alkylation has been reported to occur in reactions of pyrazine *N*-oxide (**1**), quinoxaline *N*-oxide (**2**) and pyrimidine *N*-oxide (**3**) with hard alkylating agent dimethylsulfate,[7] and predominant O-ethylation has been reported to occur in the reaction of compound **4** with hard electrophile $[Et_3O]BF_4$ (Scheme 2a).[10] Reactions of **1**, of **2** and of **5** with soft electrophile methyl iodide have been reported to yield N-alkylated adducts (Scheme 2b),[11,12] as has the reaction of **5** with benzyl chloride.[12c] In contrast, compound **6** undergoes exclusive N-ethylation on reaction with hard electrophile $[Et_3O]BF_4$ (Scheme 2c).[10] Notwithstanding the ambiguity inherent in assigning hard and soft sites in these diazine *N*-oxides, it is clear that these results cannot all simultaneously be consistent with the HSAB principle.

An additional fundamental difficulty exists in the context of reactions of diazine *N*-oxides: the act of establishing the structure of the product is itself fraught with ambiguity. The spectral features of the products of O-alkylation and N-alkylation of a particular diazine *N*-oxide are not necessarily readily distinguishable. Most instances in the literature in which product structures have been assigned have been based on the results of chemical derivatisations,[12] prior to the development of modern spectroscopic methods. In only one instance (involving two compounds) have modern two-dimensional NMR spectroscopic techniques been used to establish the precise structures of alkylation products of diazine *N*-oxides.[10,34] Hence, even



Scheme 2. Alkylation of diazine *N*-oxides **1–6** using various hard and soft electrophiles. (a) O-alkylation using hard electrophiles,[7,10] (b) N-alkylation using soft electrophiles,[11,12] (c) N-alkylation using a hard electrophile.[10]

This journal is © The Royal Society of Chemistry 20xx

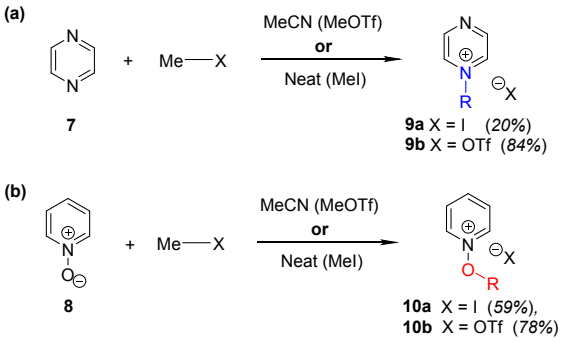
in instances in which structural assignments have been made, it is not certain that the correct product structures have been identified.

To unambiguously establish the ratios of N vs. O selectivity for the alkylation reactions of **1–3**, we took advantage of the technique of indirect detection natural abundance ^{1}H-^{15}N HMBC NMR spectroscopy.[34–38] This is an extremely useful diagnostic tool but, is very notably under-exploited – to our knowledge, there are only a handful of examples of its use to establish the site of attachment of an alkyl electrophile to an ambident reactant.[10,31,34,37] We have also conducted high level quantum chemical calculations to help us in understanding the outcomes of these experiments.

Background Data and Reference δ_N Values

In order to be able to employ ^{1}H-^{15}N HMBC NMR spectral data in a diagnostic manner to establish the site of alkylation of ambident nucleophiles **1–3**, we have made use of a set of results described in our recent publication.[39] In this preliminary study, we carried out various alkylations of representative diazines and azine *N*-oxides (see examples shown in Scheme 3, involving N-methylation of **7** and O-methylation of **8**), and monitored the change in the ^{15}N NMR chemical shifts (referred to as $\Delta(\delta_N)$ values) of each nitrogen atom in the N-alkylated product relative to its δ_N value in the starting material using ^{1}H-^{15}N HMBC NMR spectroscopy. We consistently observed that upon N-alkylation of diazines, a large upfield shift of the δ_N value of the alkylated nitrogen atom occurs (i.e. $\Delta(\delta_N) << 0$ ppm).[40] In fact, across a total of 22 examples from the chemical literature and our own work, involving N-methylation or ethylation of pyridrines, diazines, diazine *N*-oxides, quinolines, and isoquinolines, the average upfield $\Delta(\delta_N)$ value of the alkylated nitrogen atom is −115 ppm.[10,41] Similarly, the average upfield $\Delta(\delta_N)$ value associated with N-benzhydrylation was −91 ppm (3 examples). In contrast, the shift upfield in the *N*-oxide nitrogen δ_N value upon O-alkylation is significantly smaller – across 7 examples involving N-methylation or ethylation, the average upfield $\Delta(\delta_N)$ value was determined to be only −40 ppm, while for O-benzhydrylation the average $\Delta(\delta_N)$ value was −45 ppm. That the upfield signal in each case belongs to the alkylated nitrogen atom is shown by the existence of a correlation in the ^{1}H-^{15}N HMBC NMR spectrum of the product between the upfield ^{15}N signal and the proton(s) of the N- or O-alkyl group.

From the above, we can conclude that there is a characteristic $\Delta(\delta_N)$ value associated with N-alkylation of an aromatic *N*-heterocycle, distinct from (and significantly larger than) the $\Delta(\delta_N)$ value associated with O-alkylation of an aromatic *N*-oxide. Analogous observations have been made in an ^{15}N NMR spectroscopic study of protonation of pyridine and 4-methylpyridine *N*-oxide, which induces $\Delta(\delta_N)$ values of −113.3 ppm[41a] and −50.1 ppm,[41b] respectively. Furthermore, complexation of aromatic N-heterocycles to metals has been shown to result in upfield $\Delta(\delta_N)$ values of *ca.* −100 ppm).[42]



Scheme 3. Examples of use of hard and soft methylating agents to effect (a) N-methylation of **7**; (b) O-methylation of **8**. X = I or OTf throughout. Isolated yields are shown in parentheses.

Our previous investigation also allowed us to determine that in the ^{1}H-^{13}C HMBC NMR spectra of N-alkylated products, three-bond correlations exist between the N-alkyl group carbons and hydrogens and the *ortho* carbons and hydrogens of the aromatic moiety.[39] No correlations were observed in the ^{1}H-^{13}C HMBC NMR spectra of O-alkylated products between the O-alkyl group carbons and hydrogens and the *ortho* carbons and hydrogens. Furthermore, these unambiguous NMR spectroscopic correlation methods also allowed us to establish definitive diagnostic trends in the ^{13}C NMR chemical shifts of the alkyl group carbons immediately bound to aromatic nitrogen or aromatic *N*-oxide oxygen. For example, the *N*-methyl carbon of the adduct of N-methylation of an aromatic nitrogen nucleophile was shown to typically have a δ_C value in the range 36 – 53 ppm, while the O-methyl carbon of the adduct of aromatic *N*-oxide methylation typically exhibits a δ_C value in the range 62 – 75 ppm.[39] Consequently, it should be possible to employ a combination of $\Delta(\delta_N)$ values (obtained from ^{1}H-^{15}N HMBC NMR spectra) in tandem with ^{1}H-^{13}C HMBC and ^{13}C{^{1}H} NMR spectroscopic data to distinguish between N- and O-alkylated diazine *N*-oxides.

Results

Site of Alkylation of Diazine *N*-Oxides

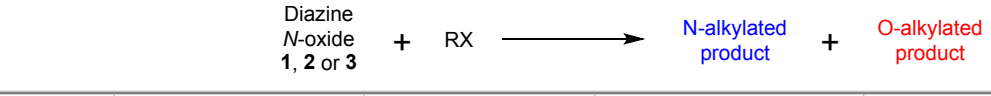
The data discussed above show that natural abundance ^{1}H-^{15}N HMBC is a highly useful diagnostic tool to determine whether or not the site of attachment of an alkyl electrophile is at a nitrogen atom. We will now describe how we have employed the ^{1}H-^{15}N HMBC NMR technique, in tandem with information from ^{13}C{^{1}H} and ^{1}H-^{13}C HSQC and HMBC NMR spectra, to establish the site of alkylation of ambident nucleophiles **1–3** in reactions with representative hard and soft alkylating agents.

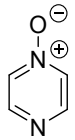
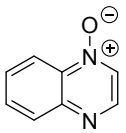
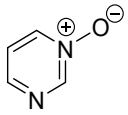
Reactions of ambident nucleophiles **1** and **2** with electrophiles MeI, MeOTf, and benzhydrylium triflates **11** and **12** were carried out using the conditions shown in Scheme 4 (pg. 5) and Table 1 (pg. 4).[44–46] The reaction of **1** with MeI in CD_3CN or CH_3CN resulted in formation of a single product, albeit with low conversion and yield – *i.e.* the process of alkylation was completely selective for one site (N or O) – see Table 1 entry (i). We did not observe any product formation in our ^{1}H NMR spectra of the reaction of **2** + MeI in CD_3CN. Product formation was only observed when the reagents were mixed together in the absence of solvent (neat); the data in Table 1 entry (v) refer to the reaction run under these conditions. As in the case of **1** + MeI, only a single product was observed by ^{1}H NMR spectroscopy. Attempted reactions of **3** with MeI in CD_3CN or MeCN did not yield any products, i.e. neither **21a** nor **23a** were observed (Scheme 4c).

The reaction of **1** with benzhydrylium triflate **11** in CH_2Cl_2 or CD_3CN also result in formation of single products (Table 1 entry (iv)).[43] The ^{1}H NMR spectrum of the reaction of **2** + **13** in CD_2Cl_2 (Scheme 4b) shows formation of two products in a 91:9 ratio (combined conversion = 93%; the remaining 7% was accounted for by hydrolysis product; see (Table 1 entry (viii)). Reaction of **3** with **11** gave ^{1}H NMR

Please do not adjust margins

Table 1. Alkylation reactions of diazine *N*-oxides **1**, **2** and **3** (as per Scheme 4) resulting in formation of O- and N-alkylated products.[a] Note that the ^{1}H NMR spectra of the reaction mixtures on their own do not show which product (O vs. N-alkylation) is favoured in each case, only the product ratio.



Diazine *N*-Oxide	#	Reaction Solvent [a]	R	X	Products		Conversion (Isolated % Yield) [b]	N/O Product Ratio [c]
					N-methyl	O-methyl		
 **1**	(i)	CD_3CN or No Solvent	Me	I	**13a**	**15a**	Reaction in CD_3CN: 24% (Solvent-free reaction 26%)	> 99:1
	(ii)	CD_3CN	Me	OTf	**13b**	**15b**	Quantitative (68% yield of **13b**) [a]	95:5
	(iii)	$(CD_3)_2SO$	Me	OTf	**13b**	**15b**	87%	> 99:1
	(iv) [a]	CD_3CN or CH_2Cl_2 [a]	CH_2Ph	OTf	**14**	**16**	Quantitative [a]	> 99:1
 **2**	(v)	No solvent	Me	I	**17a**	**19a**	(Yield = 16%) [d]	> 99:1
	(vi)	CD_3CN	Me	OTf	**17b**	**19b**	Quantitative (57% yield of **17b**) [a]	89:11
	(vii)	$(CD_3)_2SO$	Me	OTf	**17b**	**19b**	78%	> 99:1
	(viii)	CD_2Cl_2	CHPhAr [e]	OTf	**18**	**20**	93%	91:9
 **3**	(ix)	CD_3CN	Me	I	**21a**	**23a**	No products formed	-
	(x)	CD_3CN	Me	OTf	**21b**	**23b**	Quantitative [a]	7:93
	(xi)	$(CD_3)_2SO$	Me	OTf	**21b**	**23b**	76%	7:93
	(xii)	CD_2Cl_2	CHPhAr [e]	OTf	**22**	**24**	Spectra could not be interpreted	-

[a] See Supporting Information for experimental conditions employed and details of conversion calculations and yields.[44]

[b] Conversions represent the combined amount of N- and O-alkylated product formed relative to the amount added of the alkylating agent (always the limiting reagent). These were determined using integrations of appropriate signals in the ^{1}H NMR spectra. For entry (viii), the deviation from quantitative conversion was due to hydrolysis of the alkylating agent. Percentage yields (where applicable) of isolated products were determined from separate reactions run on larger scale using MeCN solvent, or with no solvent (neat reagents) for entries (i) and (v). Products **14**, **18**, **20**, **21b** and **23b** (entries (iv), (viii) and (x), respectively)) decompose upon attempted isolation, and hence no isolated yields could be obtained in these cases.

[c] The identities of the products cannot be determined directly from the ^{1}H NMR spectra. Information from other spectra is needed to establish which product is N-alkylated and which is O-alkylated, and hence to establish the N/O ratio. See main text for full details.

[d] **2** + MeI were reacted together without solvent. The product was purified prior to NMR spectral characterisation, so the conversion was not determined for this reaction. However, the low isolated yield shown above is indicative of low conversion in this reaction.

[e] Ar = *para*-tolyl.

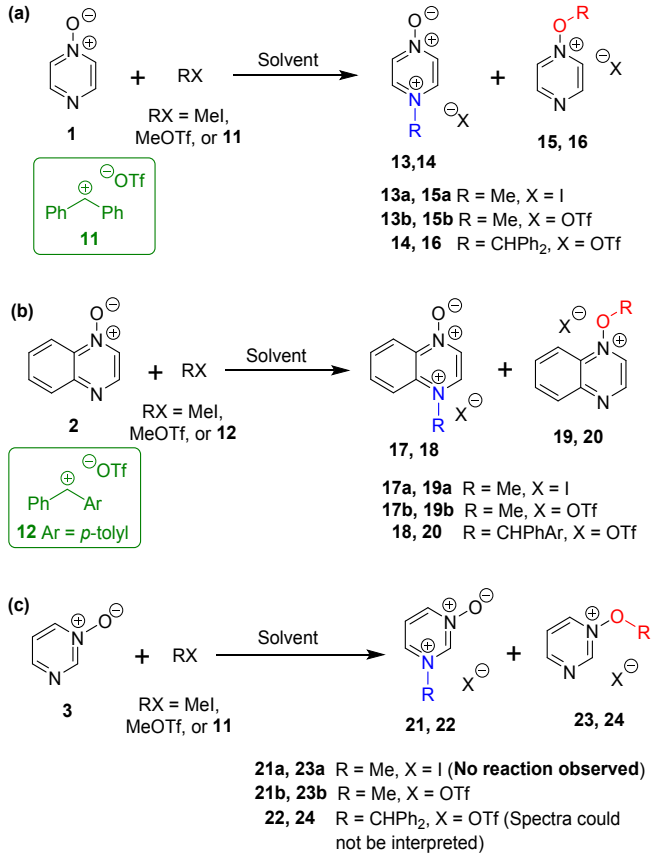
and ^{1}H-^{15}N HMBC spectra that we could not interpret,[47] containing broad and unusually-shaped signals – *i.e.* we could not detect formation of **22** or **24** (Scheme 4). We ascribe this to the very low Lewis basicity of **3**, *i.e.* the reaction of **3** + **11** is reversible, and thermodynamically disfavoured.

The reactions of **1**–**3** with MeOTf in CD_3CN yielded mixtures of O- and N-methylation products (Table 1 entries (ii), (vi), and (x)). Addition of MeOTf to $(CD_3)_2SO$ solutions of **1** and **2** resulted in formation of a single product in each case (Table 1 entries (iii) and (vii)), while the corresponding reaction of **3** gave two products (Table 1 entry (xi)).

The rates of these reactions differed greatly depending on the solvent used. Product formation was rapid for reactions in CD_3CN (i.e. complete within minutes), but was exceptionally slow in $(CD_3)_2SO$, requiring weeks for high conversions to be obtained. It is highly likely that the active methylating agent in $(CD_3)_2SO$ was the methoxysulfonium salt $[(CD_3)_2S(OMe)]OTf$,[48–50] and that this electrophile is much less reactive than MeOTf in MeCN.

Many of the initial products of the reactions of Scheme 4 and Table 1 do not survive attempts at isolation. Hence, all reactions were conducted on small scale, and the entirety of each reaction mixture

Please do not adjust margins



Scheme 4. N- and O-alkylation reactions of ambident nucleophiles **1–3**. Methylation reactions (using MeI or MeOTf) were conducted in $(CD_3)_2SO$, CD_3CN, or CH_3CN. Upon completion of reactions in CD_3CN or CH_3CN, the solvent was removed, and $(CD_3)_2SO$ was added. Benzhydrylation reactions were conducted in CD_2Cl_2.[43] See Table 1 for details of conversions and yields.

was transferred (under inert atmosphere) to a NMR tube for analysis by NMR spectroscopy. In instances in which stable, isolable products were formed, the final (stable) products were isolated from separate reactions, conducted on larger scale. The adducts of benzhydrylation of **1** and **2** are hydrolytically unstable and could not be isolated. The adduct of **2** + MeI was formed in very low conversion,[51] and the adduct of **3** + MeOTf became contaminated with multiple decomposition products;[52] hence neither adduct could be isolated in pure form. In addition, for the reactions of **1–3** with MeOTf in MeCN or CD_3CN solvent, decomposition of the minor product (detected in ^1H NMR spectra in CD_3CN) occurred upon removal of the MeCN/CD_3CN solvent under vacuum, resulting in the observation of the signals of the major product only in the ^1H NMR spectrum of the mixture upon dissolution in $(CD_3)_2SO$.[53]

In all cases shown in Table 1, it was impossible to distinguish the site of attachment of the alkyl group unambiguously using standard ^1H- or ^{13}C-based one or two-dimensional NMR techniques. That is, the identity of the product(s) in each case could not be reliably assigned as O-alkylated or N-alkylated. In the instances in which mixtures of O- and N-methylation products were obtained, product ratios could be determined using the integrations of signals in ^1H NMR spectra, but which product was favoured was not clear. The product ratios determined in this way are shown in Table 1.

In order to determine which site (N or O) of each of the ambident nucleophiles **1–3** is favoured in the alkylation reactions shown in Scheme 4 and Table 1, we made use of the indirect detection natural abundance ^1H-^{15}N HMBC NMR spectroscopic technique described above. The ^{15}N NMR chemical shifts of starting compounds **1–3** and of the observed alkylation adducts are shown in Table 2 (see pg. 6). The $\Delta(\delta_N)$ values associated with these reactions (also shown in Table 2) show the extent to which the chemical shifts of the ^{15}N nuclei of the alkylation product(s) differ from the chemical shifts of the corresponding ^{15}N nuclei in the starting materials **1–3**. As above, a negative value of $\Delta(\delta_N)$ indicates an upfield shift of the δ_N value of an ^{15}N environment upon alkylation, while a positive value indicates a downfield shift. In several instances (all described above), only one product was formed in the alkylation reactions of **1–3**, while in others, the minor product did not survive the process of removal of the MeCN or CD_3CN reaction solvent and replacement with $(CD_3)_2SO$.[53] Hence, in almost all cases, only one product could be characterized using the ^1H-^{15}N HMBC NMR technique. In the ^1H-^{15}N HMBC spectrum of the reaction of **2** + **12**, no correlations were observed to the small signals of the minor product that was shown to be present by the ^1H NMR spectrum. The only instance in which it was possible to determine the δ_N values of both the major and minor alkylation products involved methylation of **3** in $(CD_3)_2SO$ using MeOTf (Scheme 4c; through methoxysulfonium triflate).

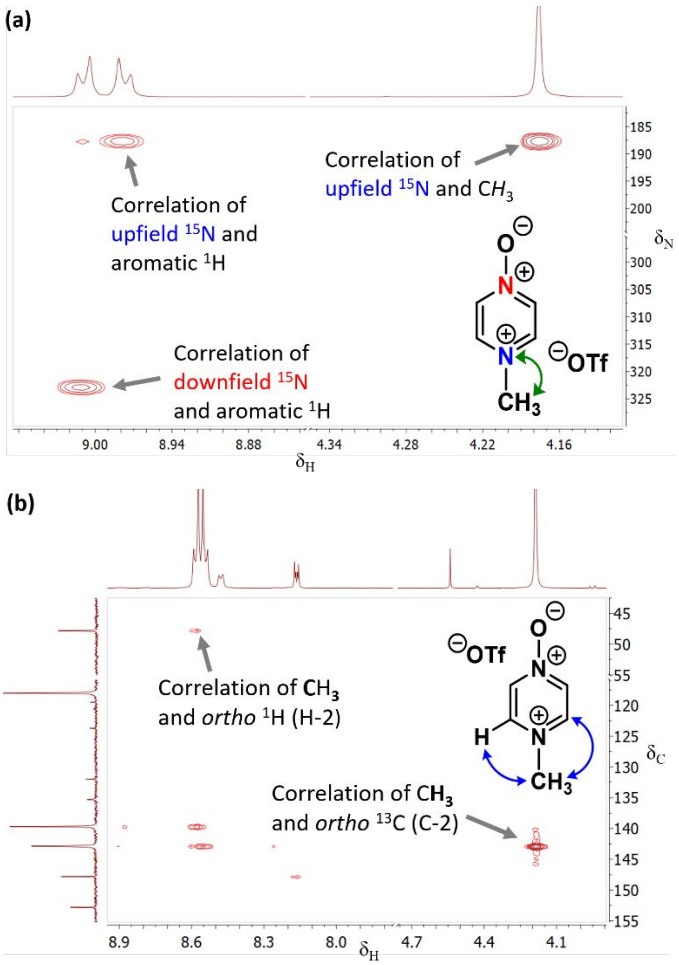
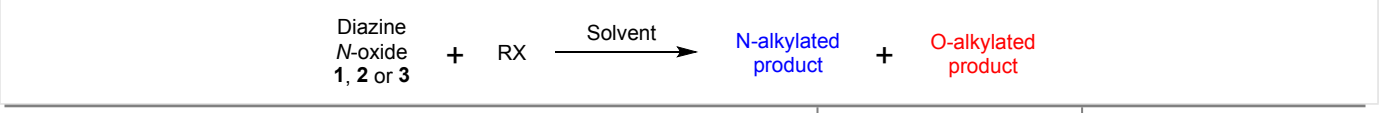
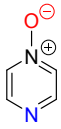
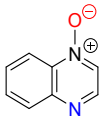
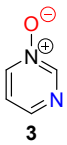


Figure 2. (a) Section of the ^1H-^{15}N HMBC NMR spectrum **of 13b** in $(CD_3)_2SO$ (from reaction of Table 2 entry (ii)) showing correlation of N-methyl ^1H signal with upfield ^{15}N signal, (b) Section of the ^1H-^{13}C HMBC NMR spectrum of **13b** in CD_3CN (from reaction of Table 2 entry (ii)) showing correlations between (i) N-methyl ^1H signal and *ortho*-^{13}C signals, and (ii) *ortho*-^1H signals and N-methyl group ^{13}C signal.

Please do not adjust margins

Table 2. δ_N and $\Delta(\delta_N)$ values associated with N- and O-alkylation reactions of diazine *N*-oxides **1**–**3** (as per Scheme 4).[a]



Diazine *N*-oxide	#	Products	R	X	Reaction solvent/ NMR Solvent [a]	δ_N of starting compound (ppm)	N-alkylation		O-alkylation	
							δ_N of product (ppm)	$\Delta(\delta_N)$ (ppm)	δ_N of product (ppm)	$\Delta(\delta_N)$ (ppm)
 **1**	(i)	**13a**, **15a**	Me	I	MeCN/ $(CD_3)_2SO$	309.3 303.9 [b]	322.3 187.1	+13.0 −116.8	Product (**15a**) not formed	
	(ii)	**13b**, **15b**	Me	OTf	MeCN/ $(CD_3)_2SO$	309.3 303.9 [b]	322.9 187.8	+13.6 −116.1	Product (**15b**) decomposed during solvent exchange	
	(iii)	**13b**, **15b**	Me	OTf	$(CD_3)_2SO$	309.3 303.9 [b]	322.9 187.7	+13.6 −116.2	Product (**15b**) not formed	
	(iv)	**14**, **16**	CH_2Ph	OTf	CD_2Cl_2	311.0 303.5	325.0 201.6	+14.0 −101.9	Product (**16**) not formed	
 **2**	(v)	**17a**, **19a**	Me	I	MeCN/ $(CD_3)_2SO$	303.2 299.3 [c,d]	314.4 178.0	+11.2 −121.3	Product (**19a**) not formed	
	(vi)	**17b**, **19b**	Me	OTf	MeCN/ $(CD_3)_2SO$	303.2 299.3 [c,d]	314.4 177.6	+11.2 −121.7	Product (**19b**) decomposed during solvent exchange	
	(vii)	**17b**, **19b**	Me	OTf	$(CD_3)_2SO$	303.2 299.3 [c,d]	314.4 177.9	+11.2 −121.4	Product (**19b**) not formed	
	(viii)	**18**, **20**	CHPhAr [e]	OTf	CD_2Cl_2	302.0 300.3	317.6 190.5	+14.4 −108.8	Signal of **20** not detected in ^1H-^{15}N HMBC	
 **3**	(ix)	**21b**, **23b**	Me	OTf	CD_3CN/ $(CD_3)_2SO$	301.3 291.7	Product (**21b**) decomposed during solvent exchange		303.4 249.4	+2.1 −42.3
	(x)	**21b**, **23b**	Me	OTf	$(CD_3)_2SO$	301.3 291.7	293.6 205.2	−7.7 −86.5	303.1 249.0	+1.8 −42.7

[a] See Supporting Information for experimental conditions employed.[45]

[b] Literature δ_N values: 309.33, 303.85 ($(CD_3)_2SO$, referenced to nitromethane at 380 ppm; equivalent to ammonia at 0 ppm).[54]

[c] These values were reported in reference 55 as δ_N −76.8 and −80.7 ppm (referenced to nitromethane at 0 ppm).

[d] The reported δ_N values for these signals was from a spectrum referenced to nitromethane at 0.0 ppm. Since our ^1H-^{15}N HMBC spectra were referenced to ammonia at 0 ppm, the literature δ_N value has been re-calculated here relative to ammonia at 0 ppm.

[e] Ar = *para*-tolyl.

The ^1H-^{15}N HMBC NMR spectra of the major or exclusive products formed in the reactions of **1** or **2** with electrophiles MeI, MeOTf, and benzhydrylium **11** and **12** (Scheme 4a and 4b) all show that the δ_N values of the upfield nitrogen nuclei are shifted upfield by over 100 ppm relative to the δ_N values of the corresponding nitrogen NMR environments in the starting materials, *i.e.* $\Delta(\delta_N) > -100$ ppm in each case (see Table 2 entries (i), (ii), (iii), (v), (vi) and (vii) for methylations and entries (iv) and (viii) for benzhydrylation reactions).[56] That the upfield signal in the ^{15}N dimension belongs the alkylated nitrogen is confirmed by the existence of a correlation in the ^1H-^{15}N HMBC NMR spectrum of this signal with the ^1H signal of the N-alkyl proton(s) (see example spectrum from the reaction of **1** + MeOTf in Fig. 2a).

In the ^1H-^{13}C HMBC NMR spectra of each of the major products of the reactions of **1** and **2**, a correlation is shown to exist between the alkyl group (aliphatic) proton(s) and the carbons *ortho* to the upfield nitrogen for all alkylation adducts (see example in Fig. 2b). A correlation between the alkyl group aliphatic carbon and the protons *ortho* to the upfield nitrogen is also evident in these spectra. The large upfield $\Delta(\delta_N)$ values and correlation data associated with the alkylation reactions of **1** and **2** are consistent with the preferential (and in some cases exclusive) occurrence of N-alkylation in these reactions.

In support of this conclusion, the $^{13}C\{^1H\}$ NMR chemical shifts of the methyl group carbon in the major products of the methylation reactions of **1** and **2** are, respectively, 44.1 and 46.6 ppm.[57] These values lie in the middle of the range of δ_C values identified in our previous work as being characteristic of N-methylation of aromatic N-heterocycles (*vide supra*).[39] The δ_C values of the minor products of these methylation reactions were, respectively, 68.9 and 70.2 ppm. These values appear in the middle of the δ_C range that is indicative of adducts of O-methylated aromatic *N*-oxides.[39,57] The δ_C values of

Please do not adjust margins

the benzhydryl group aliphatic carbons (Ar_2CH) in the products of the benzhydrylation reactions of **1** and **2** were, respectively, 77.2 and 73.2 ppm.[57] These values are characteristic of N-benzhydrylated products, based on our previous work.[39] The above data are all consistent with the conclusion that the major products formed are N-alkylation adducts **13**, **14**, **17** and **18** (Scheme 4a and 4b). These are formed in preference to O-alkylation adducts **15**, **16**, **19** and **20**.

The ^1H-^{15}N HMBC NMR spectrum of the reaction mixture produced by adding MeOTf to a $(CD_3)_2SO$ solution of **3** (Scheme 4c) showed signals for the major product at δ_N 303.1 and 249.0 ppm (Table 2, entry (x)).[58] The upfield ^{15}N NMR signal showed a correlation with the methyl group CH_3 protons, indicating that this belongs to the alkylated nitrogen. However, no correlation existed in the ^1H-^{13}C HMBC NMR spectrum for the signal of the methyl protons with the signal of the carbons *ortho* to the upfield nitrogen, nor for the signal of the methyl carbon with the signal of the protons *ortho* to upfield nitrogen. Based on the δ_N value of the upfield nitrogen signal, the δ_C value of the methyl group carbon of 70.2 ppm (characteristic of a N^+—O—CH_3 ^{13}C NMR signal of a *N*-methoxypyridinium ion),[39] and the features of the ^1H-^{13}C HMBC NMR spectrum, the spectral characteristics of the major product are very similar to those of compound **10** (the O-methylated adduct of pyridine *N*-oxide (**8**); Scheme 3b), and other aromatic *N*-oxide O-methylation adducts.[39]

We therefore conclude that the major product of this reaction is O-methylation adduct **23b** (Scheme 4c). The upfield signal (δ_N = 249.1 ppm) is assigned to the *N*—OMe nitrogen atom, and hence has a $\Delta(\delta_N)$ value of −42.7 ppm relative to the signal of the *N*-oxide nitrogen atom of **3** (at δ_N = 291.7 ppm; see Table 2 entry (x)), while the downfield signal has $\Delta(\delta_N)$ = +1.8 ppm relative to the corresponding signal of **3** (δ_N = 301.3 ppm). The upfield $\Delta(\delta_N)$ value of −42.7 ppm for this reaction is very similar to the $\Delta(\delta_N)$ values observed in formation of methoxypyridinium salts during O-methylation reactions of *N*-oxides (e.g. $\Delta(\delta_N)$ = −43.6 ppm for formation of **10** from **8** + MeOTf; Scheme 3b).[39]

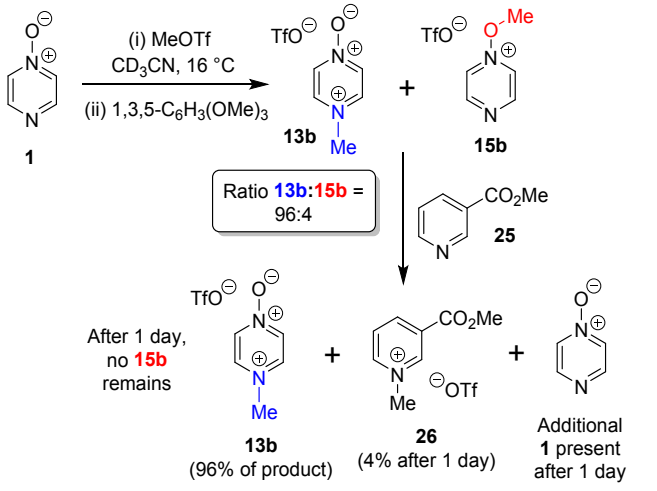
The $\Delta(\delta_N)$ value associated with formation of the minor product of the reaction of pyrimidine *N*-oxide (**3**) + $[(CD_3)_2S(OMe)]OTf$ in $(CD_3)_2SO$ is considerably larger than the $\Delta(\delta_N)$ value for O-alkylation (Table 2 entry (x); $\Delta(\delta_N)$ = −86.5 vs −42.7 ppm). In addition, the ^1H-^{13}C HMBC NMR spectrum exhibits multiple bond correlations between the N-methyl group and *ortho* aromatic ^1H and ^{13}C signals.[59] The δ_C value of the methyl group carbon of the minor product was 46.6 ppm,[57] which is characteristic of an aromatic N^+—CH_3 carbon (*vide supra*).[39] These data are consistent with the minor product being N-methylation adduct **21b** (Scheme 4c). Our spectral data on the reaction of **3** + MeOTf in CD_3CN (or MeCN) also show that **23b** is the major product formed in this solvent.[54] Although **21b** is formed in the reaction (as shown by ^1H NMR spectral analysis), it does not survive the process of solvent removal and dissolution in $(CD_3)_2SO$ (*vide supra*).

Based on the above data, we can conclude that the N- vs O-methylation ratios in the reactions of **3** with MeOTf (in CD_3CN) and $[(CD_3)_2S(OMe)]OTf$ in $(CD_3)_2SO$ are both 7:93 (in favour of O-methylation; see Table 1 entries (x) and (xi)).

Crossover Experiments

The N- vs O-alkylation ratios observed in the reactions of **1**–**3** did not change over time in the absence of perturbation. In order to establish whether or not these reactions occurred under kinetic control, we carried out several crossover experiments involving reactions of MeOTf with **1**–**3** (and of MeI with **1**) in CD_3CN followed by addition of a second nucleophile.[60] An internal standard (1,3,5-trimethoxybenzene) was added to the reaction mixture to allow the amounts of the products present to be quantified (using integrations of ^1H NMR spectral signals of the products) before and after addition of the second nucleophile, and to enable quantification of the amount of crossover product formed. Nucleophiles **7** and **25** were selected as second nucleophiles because they have been shown in separate studies to be considerably stronger Lewis bases than compounds **1**–**3**,[61] and hence are expected to out-compete **1**–**3** for any free alkylating agent present due to (i) their stronger nucleophilicity and (ii) the fact that they are present in considerable excess over **1**–**3** under the conditions of the crossover experiment.

We observed that the amount of major product formed in the methylation reactions of each of **1** and **2** remained constant with respect to the internal standard during the crossover experiments, i.e. the formation of the major product in each case is irreversible (i.e. **13a**, **13b**, and **17b** respectively). For example, the amount of **13b** formed in the reaction of **1** + MeOTf in CD_3CN at 16 °C is invariant at 96% of methylation product throughout the experiment (Scheme 5). In the reactions of **1** and **2** with MeOTf (using **25** or **7** as the second nucleophile), crossover product formed at the expense of the minor product (O-methylation adducts **15b** and **19b**) with commensurate production of starting diazine *N*-oxide (**1** or **2**). Although crossover product (**9b** or **26**) is formed from the minor products in these experiments, we conclude in each case that this is a consequence of the occurrence of an S_N2 reaction between the second nucleophile (**7** or **25**) and the minor product. If this were not the case, then repeated observations of the N/O-methylation ratios over time in alkylation reactions of **1** and **2** should show this ratio changing (to favour the major product), since formation of the major product is irreversible in each case. Consequently, we conclude that O-



Scheme 5. Crossover experiment investigating reversibility of reaction of **1** + MeOTf using 1,3,5-trimethoxybenzene as internal standard, and "crossover nucleophile" **25**. The crossover product is compound **26**.[62]

methylation of **1** and **2** are also irreversible processes in CD_3CN solvent at ambient temperatures. Thus, N-methylation of **1** and **2** are observed because they are the kinetically favoured reactions in their respective processes.

A similar crossover experiment involving the reaction of pyrimidine *N*-oxide (**3**) + MeOTf in CD_3CN (with an internal standard added) and pyrazine (**7**) as 2nd nucleophile also showed formation of crossover product **9b**. In ^{1}H NMR spectra of this reaction mixture recorded early in the reaction, the crossover product (**9b**) was observed to form primarily at the expense of N-methylation product **21b** (minor product of this reaction), but some O-methylation product (**23b**) was also consumed.[62] An amount of **3** formed that was commensurate with the amount of **9b** produced. After several days, further crossover product was observed to form at the expense of major product **23b**.[62] It is not clear from these experiments whether formation of **21b** and **23b** from **3** + MeOTf is reversible, i.e. whether **7** reacts with MeOTf formed by reversal of **21b** and/or **23b** to **3** + MeOTf, or whether crossover product **9b** is formed by direct S_N2 reactions of **7** with **21b** and/or **23b**.

Computational Investigations

Our experimental investigations indicate that ambident nucleophiles pyrazine *N*-oxide (**1**) and quinoxaline *N*-oxide (**2**) (with competing N and O nucleophilic sites) undergo preferential alkylation on nitrogen regardless of the nature of the alkylating agent used, i.e. *independent of whether the electrophile is hard or soft*. Ambident nucleophile pyrimidine *N*-oxide (**3**), by contrast, has been shown to undergo preferential O-methylation by MeOTf. In order to be able to understand and rationalise the outcomes of the reactions described above, high level quantum chemical calculations at the DLPNO-CCSD(T)/def2-TZVPPD/SMD(CH_3CN)//M06-2X-D3/6-311+G(d,p)/SMD(CH_3CN) level of theory were carried out to determine the relative Gibbs energies of the reactants, transition states and products of the reactions of each of compounds **1**, **3**, **7** (pyrazine), and **8** (pyridine *N*-oxide) (structures shown in Chart 1 and Scheme 3) with MeI and MeOTf.[63] The reactions of pyrimidine (**27**) and pyridine (**28**) with MeI and MeOTf were also investigated in the same manner. The computational results can be used to estimate the Gibbs energy of activation ($\Delta G^{\ddagger}$) and standard enthalpy and Gibbs energy of reaction ($\Delta_r H°$ and $\Delta_r G°$, respectively) for each process. The accuracy and predictive capability of this computational method have been verified by the close agreement of the $\Delta G^{\ddagger}$ values determined experimentally and computationally for the reaction of pyrazine *N*-oxide (**1**) with MeI (*vide infra*). The results of the computational investigations of the methylation reactions of **7**, **8**, **27** and **28** are presented in Table 3 (left side). Compounds **7**, **27** and **28** undergo N-methylation, and compound **8** undergoes O-methylation. These results allow us to see representative values of $\Delta G^{\ddagger}$, $\Delta_r H°$ and $\Delta_r G°$ for N- and O-methylation reactions in which there is no ambiguity over the site of methylation.

Unsurprisingly, the reactions involving MeOTf have systematically smaller calculated $\Delta G^{\ddagger}$ values and are more exergonic than the reactions involving MeI. The values of $\Delta G^{\ddagger}$ and $\Delta_r G°$ for methylation of **7** by MeI are very similar to the corresponding values for **27** (Table 3 entries (i) and (v)). The $\Delta G^{\ddagger}$ and $\Delta_r G°$ values for the reactions of **7** and **27** with MeOTf are also very similar (Table 3 entries (ii) and (vi)). This suggests that the nucleophilicities and Lewis basicities of **7** and **27** are very similar. The reactions involving pyridine (**28**; Table 3 entries (vii) and (viii)) are both more kinetically and thermodynamically favourable than the corresponding reactions of **7** and **27** with the two methylating agents.[64] The O-methylation reactions of **8** are more kinetically favourable than the corresponding reactions of **7** and **27**, despite being less thermodynamically favourable than those reactions (compare Table 3 entry (iii) with entries (i) and (v), and entry (iv) with entries (ii) and (vi)).

The reaction of pyrazine *N*-oxide (**1**) with MeOTf was found computationally to result in kinetically and thermodynamically preferred N-methylation (compare Table 3 entries (x) and (xii)). This calculation indicates that methylation of **1** by MeOTf is an irreversible process at room temperature (regardless of the site of methylation), in agreement with the results of our crossover experiments (see above). The relative magnitudes of $\Delta G^{\ddagger}$(N) and $\Delta G^{\ddagger}$(O) calculated for this reaction suggest that a small amount of O-methylated product (*ca.* 5 – 7%) should be produced, as is observed experimentally (N/O methylation ratio = 95:5 for reaction at 20 °C; see Table 2 entry (ii)).[65]

The reaction of **1** with MeI was also found to result in kinetically and thermodynamically preferred N-methylation (compare Table 3 entries (ix) and (xi)), which is consistent with the results of our crossover experiments. This reaction has been observed experimentally to be very slow. Only a small amount of conversion had occurred after several days, consistent with the high activation barrier found computationally (shown in Table 3) and determined through a kinetic investigation (described below). In contrast to the reaction of **1** with MeOTf (above), O-methylation of **1** by MeI was found computationally to be thermodynamically disfavoured and therefore reversible (Table 3 entry (xi)). No O-methyl adduct (**17a**) was observed experimentally for this reaction, which is consistent with kinetically disfavoured and reversible O-methylation.

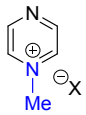
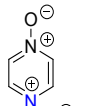
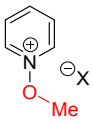
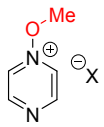
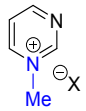
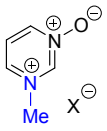
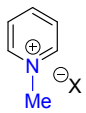
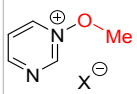
The $\Delta G^{\ddagger}$(N) and $\Delta_r G°$(N) values for N-methylation of **1** (by MeOTf or MeI) are similar to the corresponding values for diazines **7** and **27** (compare Table 3 entry (x) with entries (ii) and (vi), and entry (ix) with entries (i) and (v)). In contrast, the $\Delta G^{\ddagger}$(O) and $\Delta_r G°$(O) values for O-methylation of **1** (by MeOTf or MeI) are significantly less favourable than the corresponding reactions of *N*-oxide **8** (compare Table 3 entry (xii) with entry (iv), and entry (xi) with entry (iii)). The implication of this is that the oxygen site of **1** is deactivated relative to the oxygen site of **8**, both as a nucleophile and as a Lewis base.[66]

Our calculations on the reaction of pyrimidine *N*-oxide (**3**) with MeOTf indicate that, despite the fact that N-methylation (formation of **21b**) is thermodynamically favoured over O-methylation (formation of **23b**), the kinetically preferred process in this reaction is O-methylation (compare Table 3 entries (xiv) and (xvi)). The difference between the calculated values of $\Delta G^{\ddagger}$(N) and $\Delta G^{\ddagger}$(O) suggests that a small amount of N-methylation (*ca.* 1–3%) should occur. These results are in quite close agreement with the experimental observations – O-methylation is indeed favoured, and approximately 7% of the product formed is N-methylation adduct **21b** (in CD_3CN or $(CD_3)_2SO$; see Table 2 entries (ix) and (x))).[67] These calculations indicate that both reactions are essentially irreversible (however, see the results of our crossover experiment involving **3** + MeOTf above).[63] Our calculations on the reaction of **3** with MeI

This journal is © The Royal Society of Chemistry 20xx

Table 3. Calculated $\Delta G^{‡}$, $\Delta_r H°$ and $\Delta_r G°$ values for methylation of nucleophiles **1**, **3**, **7**, **8**, **27,** and **28** by MeI and MeOTf in CH_3CN.[a,b]



Nucleophiles with single alkylation site [c]							Ambident Nucleophiles						
#	Nu	X	Product & number	$\Delta G^{‡}$	$\Delta_r G°$	$\Delta_r H°$ [b]	#	Nu	X	Product & number	$\Delta G^{‡}$	$\Delta_r G°$	$\Delta_r H°$ [b]
(i)	**7**	I	 **9a**	+131	−21	−37	(ix)	**1**	I	 **13a**	+133	−20	−37
(ii)	**7**	OTf	**9b**	+107	−90	−90	(x)	**1**	OTf	**13b**	+108	−88	−90
(iii)	**8**	I	 **10a**	+123	−7	−24	(xi)	**1**	I	 **15a**	+140	+31	+14
(iv)	**8**	OTf	**10b**	+97	−75	−76	(xii)	**1**	OTf	**15b**	+115	−38	−38
(v)	**27**	I	 **29a**	+130	−23	−39	(xiii)	**3**	I	 **21a**	+138	+4	−13
(vi)	**27**	OTf	**29b**	+106	−91	−91	(xiv)	**3**	OTf	**21b**	+113	−64	−66
(vii)	**28**	I	 **30a**	+120	−48	−64	(xv)	**3**	I	 **23a**	+127	+38	+3
(viii)	**28**	OTf	**30b**	+96	−117	−117	(xvi)	**3**	OTf	**23b**	+103	−48	−49

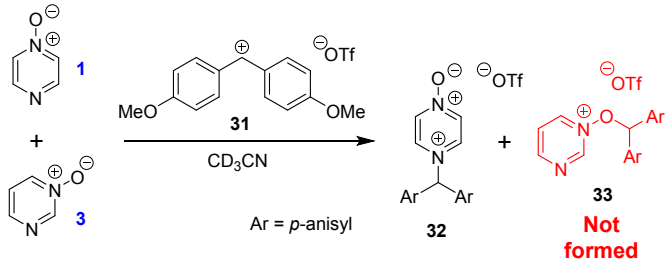
[a] Enthalpies and Gibbs energy values (in kJ mol^{-1}) were calculated at the DLPNO-CCSD(T)/def2-TZVPPD/SMD(CH3CN)//M06-2X-D3/6-311+G(d,p)/SMD(CH3CN) level of theory, with a confidence interval of ±2 kJ mol^{-1}.

[b] $\Delta_r S°$ values calculated for these reactions were similar across all reactions of MeI ($\Delta_r S°$ = −55 ± 2 J K^{-1} mol^{-1}), and across all reactions of MeOTf ($\Delta_r S°$ = −2 ± 2 J K^{-1} mol^{-1}). These data are included in Tables S1 – S3 in the Supporting Information, along with calculated $\Delta H^{‡}$ and $\Delta S^{‡}$ values for these reactions.[68]

[c] Pyrazine (**7**) and pyrimidine (**27**) clearly have two possible alkylation sites, but the sites are identical by symmetry.

indicate that both O- and N-methylation (formation of **23a** and **21a**, respectively) are reversible. O-Methylation was found to be kinetically preferred, again despite the fact that this process is less thermodynamically favourable than N-methylation (compare Table 3 entries (xiii) and (xv)). As no product formation was observed experimentally when this reaction was attempted in CD_3CN or MeCN, it is not possible to verify the applicability of these particular computational results.

The calculated Gibbs energies of activation for N- and O-methylation of pyrimidine *N*-oxide (**3**) by MeI or MeOTf, while higher than the $\Delta G^{‡}$ values for comparable reactions of similar compounds (e.g. pyrazine *N*-oxide (**1**), pyrazine (**7**), pyridine *N*-oxide (**8**) and pyridine (**27**)), are not especially different to those $\Delta G^{‡}$ values (compare Table 3 entry



Scheme 6. Competition experiment between reversible reactions of **1** and **3** with benzhydrylium ion **31**.[44]

(xiv) with entries (ii) and (vi), entry (xiii) with entries (i) and (v), entry (xvi) with entry (iv), and entry (xv) with entry (iii)). However, comparison of the $\Delta_r G°$ values for the same reactions indicates that both O- and N-methylation reactions of pyrimidine *N*-oxide (**3**) are far less thermodynamically favourable than the corresponding reactions of **1**, **7**, **8** and **27**. This computational observation has been verified experimentally through a thermodynamic competition experiment in which product **32** (derived from pyrazine *N*-oxide (**1**) in a reversible reaction) is formed to the complete exclusion of **33** (derived from pyrimidine *N*-oxide (**3**)) when **1**, **3** and benzhydrylium ion **31** are mixed in CD_3CN (Scheme 6). It seems that the O and N nucleophilic/Lewis basic sites of **3** are deactivated in a similar manner to the O site of **1**.[66]

According to our computational data, N-methylation of both **1** and **3** results in a minor shortening of the *N*-oxide N—O bond. The calculated N—O bond lengths of diazine *N*-oxides **1** and **3** and N-methyldiazinium cations **13** and **21** are, respectively, 1.27 Å, 1.29 Å, 1.25 Å and 1.27 Å.[63] O-methylation of **1** and **3** results in a lengthening of the N—O bond (to 1.36 Å for each of **15** and **23**, the O-methylated cationic derivatives of **1** and **3**).[63] O-methylation of **1** or **3** removes the favourable electrostatic interaction between N and O, and also diminishes the partial resonance of the *N*-oxide with the aromatic system, thereby removing resonance stabilisation effects that may

help to stabilise the positive charge in the product. This may contribute to making N-methylation of **1** and **3** more thermodynamically favourable than O-methylation.

Finally, for completeness, we will comment on the values of the other thermodynamic functions associated with the above reactions. Computationally determined values of $\Delta_r S°$ do not differ greatly from each other across all reactions of MeI with **1**, **3**, **7**, **8**, **27** and **28**, or across all reactions of MeOTf with the same nucleophiles, regardless of whether N- or O-methylation is occurring.[68] Across all reactions of MeI in Table 3, $\Delta_r S°$ remains constant around −55 ± 2 J $K^{-1}mol^{-1}$, while a value of −2 ± 2 J $K^{-1}mol^{-1}$ was observed across the reactions of MeOTf (using 99% confidence intervals).[68] Therefore, the computational data suggest that enthalpy changes are primarily responsible for dictating the differences between the $\Delta_r G°$ values in the various reactions in Table 3. It is not possible to unambiguously ascribe the differences in $\Delta_r H°$ to specific effects, and hence we refrain from doing so.

Activation Barrier Calculations Using Marcus Theory

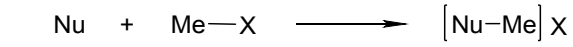
Noting the deficiencies of the HSAB principle, Mayr and co-workers have advanced Marcus theory for rationalising the outcomes of reactions of ambident nucleophiles.[4] The Marcus equation (equation 1) allows $\Delta G^{‡}$ to be separated out into its contributions from $\Delta_r G°$ (the standard Gibbs energy of reaction) and $\Delta G_0^{‡}$, the Marcus intrinsic barrier.[69–71]

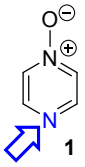
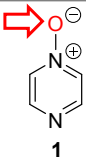
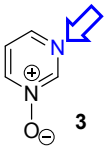
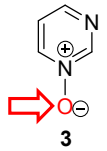
$$\Delta G^{‡} = \Delta G_0^{‡} + \frac{\Delta_r G°}{2} + \frac{(\Delta_r G°)^2}{16 \Delta G_0^{‡}} \qquad (1)$$

In reactions of ambident nucleophiles with competing sites of differing nucleophilicity, the different nucleophilic sites have different values of each of $\Delta G_0^{‡}$ and $\Delta_r G°$. Mayr and co-workers have suggested that the selectivities in such reactions can be rationalised through an appraisal of the factors that influence the values of the two parameters in the Marcus equation ($\Delta G_0^{‡}$ and $\Delta_r G°$).[4] They have employed this approach to qualitatively rationalise the outcomes of reactions of a variety of ambident nucleophiles.[4,72] In order to build up a more comprehensive understanding of the factors that influence selectivity in reactions of **1**–**3**, we have calculated values of $\Delta G_0^{‡}$ and $\Delta_r G°$ for these reactions, and used them to construct values of the activation barriers ($\Delta G^{‡}$) using the Marcus equation.

Using the procedure described in detail in the Supporting Information,[73] values of the intrinsic barrier ($\Delta G_0^{‡}$) were calculated for each of the reactions of compounds **1** and **3** with MeI and MeOTf. The $\Delta G_0^{‡}$ values for reactions of **1** and **3** are shown in Table 4.[74] It is noteworthy that, for both ambident nucleophiles **1** and **3**, the intrinsic barrier for methyl transfer to oxygen ($\Delta G_0^{‡}$(O)) is lower than that for methylation of nitrogen ($\Delta G_0^{‡}$(N)) – e.g. compare Table 4 entries (iii) and (i), and entries (vii) and (v). Hoz and co-workers previously established through computational investigations that the $\Delta G_0^{‡}$ values associated with reactions of nucleophiles centred on 2nd row elements depend on the identity of the element at the nucleophilic site, with $\Delta G_0^{‡}$ decreasing in the order C > N > O > F, i.e. from left to right across the periodic table.[75] The lower intrinsic barriers (intrinsic preference) for O-alkylation over N-alkylation we observe for **1** and **3** are in line with this general trend.

Table 4. Values of intrinsic barriers ($\Delta G_0^{‡}$) and derived values of $\Delta G^{‡}$ for methylation reactions of nucleophiles **1**, **3**, **7**, **8**, **27**, and **28** in CH_3CN, calculated using the Marcus equation (equation 1) using values of $\Delta_r G°$ from Table 3 (reproduced here).[a,b,c]



Nucleophile	#	X	$\Delta G_0^{‡}$	$\Delta_r G°$	DFT $\Delta G^{‡}$	Marcus $\Delta G^{‡}$
 **1**	(i)	OTf	+149.5	−88	+108.0	+108.7
	(ii)	I	+144.0	−20	+133.0	+134.2
 **1**	(iii)	OTf	+132.5	−38	+115.0	+114.3
	(iv)	I	+127.0	+31	+140.0	+143.0
 **3**	(v)	OTf	+145.0	−64	+113.0	+114.8
	(vi)	I	+139.5	+4	+138.0	+141.5
 **3**	(vii)	OTf	+124.0	−48	+103.0	+101.2
	(viii)	I	+118.5	+21	+127.0	+129.2

[a] The site of methylation of each nucleophile is indicated by an arrow. The Gibbs energy values have units of kJ mol^{-1} (confidence interval ±2 kJ mol^{-1}).

[b] $\Delta_r G°$ and $\Delta G^{‡}$ (DFT $\Delta G^{‡}$) values here are reproduced from Table 3.

Substitution of the calculated $\Delta G_0^{‡}$ values into equation 1 (the Marcus equation) along with the values of $\Delta_r G°$ calculated as described above (Table 3 and associated discussion; these $\Delta_r G°$ values are reproduced in Table 4 to aid the understanding of the reader) allows values of $\Delta G^{‡}$ to be calculated using the Marcus equation. Comparison of the $\Delta G^{‡}$ values obtained using the Marcus equation (shown in Marcus $\Delta G^{‡}$ column in Table 4) with the $\Delta G^{‡}$ values directly calculated as described above (values from Table 3, labelled DFT $\Delta G^{‡}$, are reproduced in Table 4) shows a close correspondence between the two methods. Importantly, the experimentally observed N vs. O selectivities for the reactions of the ambident nucleophiles **1** and **3** are reproduced quite closely by both methods of calculation.[18] Analysing how the factors that contribute to the Gibbs energy of activation for a reaction influence its magnitude (i.e. how the interplay between $\Delta G_0^{‡}$ and $\Delta_r G°$ influences $\Delta G^{‡}$) provides a very useful means of understanding the origins of the differences between the rates of different reactions. Nowhere is this more apposite than in understanding which nucleophilic site of an ambident nucleophile is kinetically preferred. A full analysis of this kind for the reactions of **1** and **3** will be described in detail below.

The applicability of Marcus theory has been challenged in recent years,[76] and alternatives have been suggested.[77,78] However, such alternatives also incorporate in some manner an intrinsic barrier or a proxy thereof. In addition to using the Marcus equation, we have

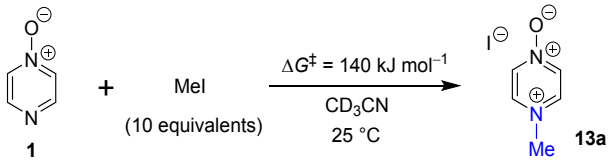
This journal is © The Royal Society of Chemistry 20xx

also used an adaptation of the Zhu equation (see the Supporting Information)[79] to calculate $\Delta G^{\ddagger}$ values for the methylation reactions of nucleophiles **1** and **3**. The $\Delta G^{\ddagger}$ values calculated using the adapted Zhu equation are very similar to the values calculated using equation 1 (see Table S5 in the Supporting Information).[73]

The experimentally observed ratio of N- to O-methylation for the reaction of **1** + MeOTf was 95:5 (Table 2). Direct calculation of the $\Delta G^{\ddagger}$ values at the DLPNO-CCSD(T)/def2-TZVPPD/SMD(CH_3CN)//M06-2X-D3/6-311+G(d,p)/SMD (CH_3CN)] level of theory indicated a N/O ratio of 94:6 for this reaction, while calculation of the N/O ratio using the Marcus equation gave a ratio of 90:10 (compare Table 4 entries (i) and (iii)). Use of the Zhu equation gave a N/O ratio of 96:4.[73] The experimentally observed ratio of N- to O-methylation for the reaction of **3** + MeOTf was 7:93. Our calculations indicated a ratio of 2:98 for this reaction, while calculation of the N/O ratio using the Marcus equation gave a ratio of 0.4 : 99.6, (compare Table 4 entries (v) and (vii)) and calculation using the Zhu equation gave a ratio of 0.5 : 99.5.[73] That the experimental selectivities (in N- vs. O-methylations of **1** and **3** by MeOTf) are reproduced quite closely using the Marcus and Zhu equations[73] and direct computation indicates that these methods are highly useful in understanding the factors that control Gibbs energies of activation in nucleophilic substitution reactions.

Experimental Verification of Accuracy of Calculated $\Delta G^{\ddagger}$

In order to verify the applicability of the computational methods discussed above to determine the magnitudes of activation barriers, we conducted a kinetic investigation on the reaction of pyrazine *N*-oxide (**1**) with MeI in CD_3CN at 25 °C using ^{1}H NMR spectroscopy to determine the concentrations of the reactants and product (**13a**). The experiment was conducted under pseudo-first order conditions, with MeI present in ten-fold excess over **1**. Using the method described in detail in the Supporting Information,[80] we determined an approximate $\Delta G^{\ddagger}$ value for this reaction of 1.4×10^2 kJ mol^{-1}. This value is within 5% of the $\Delta G^{\ddagger}$ values predicted for this reaction using the Marcus equation (134.2 kJ mol^{-1}), and using direct application of the DLPNO-CCSD(T)/def2-TZVPPD/SMD(CH_3CN)//M06-2X-D3/6-311+G(d,p)/SMD] method (133 kJ mol^{-1}). This striking agreement between computational theory and experiment demonstrates that these computational methods are capable of modelling kinetic phenomena of this type rather accurately.



Scheme 7. The reaction of **1** + MeI in CD_3CN at 25 °C under pseudo-first order conditions (excess MeI) was monitored by ^{1}H NMR spectroscopy to enable determination of an approximate $\Delta G^{\ddagger}$ value for the reaction at 25 °C.

Discussion

Rationalisation of Experimental N vs O Selectivities

The kinetic preference of compound pyrazine *N*-oxide (**1**) for N-methylation by soft electrophile MeI (forming compound **13a**) and by hard electrophile MeOTf (forming compound **13b**) has been demonstrated experimentally and computationally. The alkylation reactions of quinoxaline *N*-oxide (**2**) by MeI, MeOTf and benzhydrylium triflates (**11** or **12**) and of **1** by **11** or **12** are all also almost certainly irreversible, and all yield N-alkylated products preferentially or exclusively. The reaction of pyrimidine *N*-oxide (**3**) + MeOTf gives O-methylated product (**23b**) predominantly, and our computational investigations indicate that this is due to the kinetic favourability of formation of **23b**. Although no product formation is observed in the reaction of **3** + soft electrophile MeI (due to the formation of products **21a** and **23a** being thermodynamically disfavoured and hence reversible), our computational results indicate that O-methylation (formation of **23a**) is the kinetically favoured process in this reaction (see Table 4 entries (vi) and (viii)).

It is evident from these results that each nucleophile exhibits a preferred site of alkylation *which is independent of the nature of the electrophile used* (N for **1** and **2**, and O for **3**), *i.e.* these outcomes cannot be dictated by hard/soft acid/base interactions. A fundamentally different set of factors must dictate the observed selectivities in these reactions. We discuss an alternative rationale to account for these observations later in this article.

Although the above evidence clearly shows that the HSAB principle does not apply in this set of reactions, and thereby renders unnecessary the identification of which nucleophilic site of each of **1** – **3** is "harder" and which is "softer", it is nonetheless appropriate at this point to discuss the difficulty and ambiguity inherent in attempts at such identifications. The features that are employed to determine whether a reactant is hard or soft are charge (charge density), size, polarizability and electronegativity.[2a,b,g,18b,c] For hard bases, the donor atom is typically negatively charged and/or has a local excess of electron density, and is of small size, low polarizability and high electronegativity. For soft bases, the donor atom typically does not bear a formal negative charge and exhibits low negative charge density, and is of large size, high polarizability and low electronegativity. Derivation of functions that reliably indicate the "local hardness" and "local softness" of sites in a molecule (such as an ambident nucleophile) has proved a difficult endeavour.[15] At present, such approaches cannot be applied without ambiguity.

On the basis that oxygen is more electronegative than nitrogen, one could perhaps anticipate that the oxygen site of a diazine *N*-oxide such as **1** – **3** should be harder than the nitrogen site. However, although there is a formal negative charge on the *N*-oxide oxygen atoms in these compounds, it is not clear which nucleophilic site in each ambident nucleophile should have the highest negative charge density, thereby potentially complicating the issue. To probe this question, we calculated the charge distribution for the ambident *N*-oxides with a variety of methods (ChelpG, Merz–Singh–Kollman, natural bond order (NBO), and atoms in molecules (AIM)),[81] but found that there was no uniform agreement between methods on which site bears the highest negative charge density in compounds **1** and **3**. Full details of this are given in the Supporting Information.[81]

We now present an alternative rationale, based on Marcus theory, to explain these results (see equation 1 above). In the following discussion, the intrinsic barriers for alkylation at oxygen and nitrogen are referred to, respectively, as $\Delta G_0^{\ddagger}$(O) and $\Delta G_0^{\ddagger}$(N). The standard Gibbs energies of reaction for O- and N-alkylation are referred to, respectively, as $\Delta_r G°$(O) and $\Delta_r G°$(N).

Although O-methylation is intrinsically preferred over N-methylation (for diazine *N*-oxides, and in general; *vide supra*),[75] in reactions of **1** and **2**, the intrinsic preference for O-alkylation is modest. $\Delta G_0^{\ddagger}$(O) is calculated to be only 17 kJ mol^{-1} lower than $\Delta G_0^{\ddagger}$(N) for the reactions of **1** with MeI or MeOTf (Table 4 entry (i) vs. (iii), and entry (ii) vs. (iv)). The $\Delta_r G°$(N) values for these reactions are substantially more favourable than the corresponding $\Delta_r G°$(O) values. Consequently, the very favourable contribution of $\Delta_r G°$(N) to $\Delta G^{\ddagger}$(N) supersedes the favourable contribution of $\Delta G_0^{\ddagger}$(O) to $\Delta G^{\ddagger}$(O), such that $\Delta G^{\ddagger}$(N) is much lower than $\Delta G^{\ddagger}$(O) for alkylations of **1** and **2**. That is, the intrinsic favourability of O-alkylation is outweighed by the thermodynamic favourability of N-alkylation, so in these irreversible reactions, N-alkylation is kinetically preferred.[82]

In the reaction of pyrimidine *N*-oxide (**3**) with MeOTf, the value of $\Delta_r G°$(N) is much less favourable with respect to $\Delta_r G°$(O) than is the case for the corresponding reaction of pyrazine *N*-oxide (**1**). $\Delta G_0^{\ddagger}$(O) is calculated to be 21 kJ mol^{-1} lower than $\Delta G_0^{\ddagger}$(N) for both MeOTf and MeI (compare Table 4 entry (vii) with entry (v), and entry (viii) with entry (vi)), so O-methylation of **3** is intrinsically preferred. Since the thermodynamic favourability of N-methylation of **3** is diminished (relative to the corresponding reactions of **1**), and O-methylation is intrinsically favoured, $\Delta G^{\ddagger}$(O) is lower than $\Delta G^{\ddagger}$(N), and hence O-methylation of **3** is the kinetically dominant reaction. Instances in which N-alkylation is likely to have been "deactivated" due to steric interactions, resulting in preferential O-alkylation, have been reported previously.[4,22b,c,f,g,31] In this case, it seems likely that the free nitrogen Lewis basic site of **3** is deactivated due to an electronic effect. This Lewis basic site is connected through a network of π-bonds to an *N*-oxide group in a *meta* position relative to it, which may act as an electron withdrawing group, thereby diminishing the Lewis basicity (electron donor capacity) of the free nitrogen atom.

The reaction of **3** with MeI was calculated to be thermodynamically unfavourable ($\Delta_r G°$ > 0 for both O- and N-methylation by MeI), and therefore reversible. This is consistent with our experimental observation that no product was formed in this reaction. However, our calculations do indicate that O-methylation (formation of **23a**) is kinetically favoured over N-methylation. A similar rationale to that presented above for the reaction of **3** + MeOTf applies in this case – *i.e.* O-methylation is intrinsically preferred ($\Delta G_0^{\ddagger}$(O) < $\Delta G_0^{\ddagger}$(N)) and the thermodynamic advantage of N-methylation over O-methylation is small, and consequently O-methylation is the kinetically favoured process (see Table 4 entries (vi) and (viii)).

As discussed above, the $\Delta_r G°$ values calculated for N- and O-methylations of **3** by both MeI and MeOTf are much less favourable than the $\Delta_r G°$ values of methylation reactions of other, similar compounds (e.g. **1**, **7**, **8** and **27**; *vide supra*). In the context of our analysis based on the Marcus equation, we can make use of this information to rationalise the relatively high $\Delta G^{\ddagger}$(O) and $\Delta G^{\ddagger}$(N) values calculated for the methylation reactions of **3**. The less favourable $\Delta_r G°$ values for O- and N-methylations of **3** influence the magnitudes of the $\Delta G^{\ddagger}$ values for these reactions, causing them to be higher than the $\Delta G^{\ddagger}$ values of reactions of similar nucleophiles.

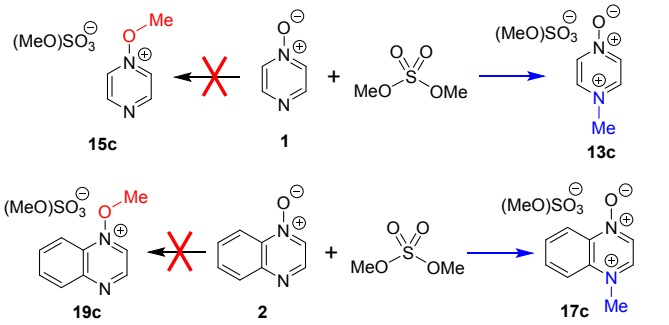
As is described in detail in the Supporting Information,[73] operationally, the value of the intrinsic barrier ($\Delta G_0^{\ddagger}$) for a reaction is accessed as the average of two identity reactions. Since there is no leaving group formed in the addition of a nucleophile to carbenium ions such as **11** and **12** (structures in Scheme 4 above), only one identity reaction of the required two can be identified to model such processes using Marcus theory. Hence, the straightforward method described in the Supporting Information[73] for accessing values of intrinsic barriers cannot be employed for reactions involving carbenium ions. Alternative methods for estimating the magnitudes of the intrinsic barriers for such reactions or analogues thereof have been reported,[83] but these do not allow quantitative determinations of the type performed above for reactions involving electrophiles from which leaving groups become cleaved. Hence only a qualitative appraisal of the outcomes of the reactions of **1** and **2** with benzhydrylium ions is possible, which we give below.

We consider that the observation of strongly preferred or exclusive N-benzhydrylation of nucleophiles pyrazine *N*-oxide (**1**) and quinoxaline *N*-oxide (**2**) in their reactions with benzhydrylium ions (**11** or **12**) arises as a consequence of the same factors that dictate the outcomes of the reactions of these nucleophiles with MeI or MeOTf. That is, in each case, O-benzhydrylation is intrinsically favoured ($\Delta G_0^{\ddagger}$(O) is smaller than $\Delta G_0^{\ddagger}$(N)) but the influence of $\Delta_r G°$(N) on $\Delta G^{\ddagger}$(N) outweighs the influence of $\Delta G_0^{\ddagger}$(O) on $\Delta G^{\ddagger}$(O), and consequently N-benzhydrylation is the kinetically preferred process. As discussed above, it was not possible to determine what occurred in the reaction of **3** + benzhydrylium ion **11**, so further comment on this is not warranted.

Literature Examples of N vs. O alkylation

We have noted in passing above that, due to the ambiguity that has up until now been inherent in determining which product is formed predominantly in reactions of ambident nucleophiles containing N and O nucleophilic sites, there exist notable cases in the literature in which the products of such reactions may have been misidentified.[8,9,84]

Comparison of the ^{1}H NMR spectrum of N-methylated product **13b** (from reactions of MeOTf with **1**; Scheme 4a) with the ^{1}H NMR spectra assigned to O-methylation adduct **15c** (Scheme 8) in reference 10 shows that the spectra are essentially identical. A similar observation can also be made on comparison of the ^{1}H NMR spectrum of N-methylated product **17b** (from **2** + MeOTf; Scheme 4b) and that assigned to O-methylated adduct **19c** in reference 7. We have identified a distinct set of signals belonging to the O-methylated adducts **15b** and **19b** that appear at different chemical shifts to the



Scheme 8. Reactions of compounds **1** and **2** with dimethylsulfate have been reported to give O-methylated products **15c** and **19c**.[7] Our data indicate that N-methylated adducts **13c** and **17c** are likely to be the major products.

This journal is © The Royal Society of Chemistry 20xx

N-methylated adducts **13b** and **17b** (*vide supra*). Furthermore, the ^{13}C NMR chemical shifts reported for the methyl group carbons (either N—CH_3 or O—CH_3) of the products are 47.2 and 44.5 ppm, respectively.[7] These δ_C values are indicative of formation of N-methylation products **13c** and **17c** (*vide supra*). Hence, our data indicate that it is highly unlikely that **1** and **2** undergo preferential O-methylation in reactions with dimethylsulfate, a close analogue of MeOTf. The methodology reported in reference 7 was predicated on the use of N-methoxypyridinium salts. That this otherwise highly successful methodology did not work for these compounds can be explained by the fact that N-methylated compounds **13c** and **17c** were almost certainly employed rather than the intended O-methylated compounds **15c** and **19c**. Problems of this type are illustrative of the need for a much more rigorous understanding of the factors that dictate the outcomes in reactions of ambident nucleophiles such as diazine *N*-oxides.

Conclusions

If one must verify on a case-by-case basis whether the predictive capabilities of a theory apply or not, then those predictive capabilities must be seriously called into question. For this reason, the continued use of the HSAB principle in rationalising the selectivities of ambident reactants in research articles and undergraduate courses and textbooks should be ceased. It appears to us that the approach of Mayr and co-workers, based around Marcus theory, is able to account for the behaviour of ambident reactants in a manner in which the HSAB principle cannot. We hope through this study to have contributed to a more general understanding of ambident reactivity, to have developed upon the approach of Mayr and co-workers to show that it can be applied to semi-quantitatively rationalise product ratios in reactions of ambident nucleophiles, and to have demonstrated the utility of ^{1}H-^{15}N HMBC NMR spectroscopy in establishing the site of attachment in reactions of nitrogen-containing compounds.

In the cases we have investigated here, calculation of $\Delta G^{‡}$ values using the equations of Marcus or Zhu yields values that reproduce closely the experimental N/O methylation ratios for reactions of ambident nucleophiles pyrazine *N*-oxide (**1**) and pyrimidine *N*-oxide (**3**). Based on this, it is reasonable to expect that calculations based on Marcus theory will allow semi-quantitative predictions of the nucleophilic site-selectivities in reactions of other ambident nucleophiles – not just those involving competition between N and O nucleophilic sites. The close agreement between the reaction selectivities determined experimentally and those calculated using the Marcus and Zhu equations (see Table 4 and associated discussion) is demonstrative of the utility of the concept of the intrinsic barrier.

The intrinsic barrier ($\Delta G_0^{‡}$) associated with an alkylation reaction of a nucleophile can be considered a property of the compounds involved in the reaction. The interplay between this quantity and the thermodynamic favourability of the reaction (quantified through $\Delta_r G°$) dictates the magnitude of the activation barrier for the reaction ($\Delta G^{‡}$). Having established herein a computational method that stands up to the stern test posed by modelling of the disparate behaviour of diazine *N*-oxides **1** and **3**, we intend in future publications to determine the magnitudes of intrinsic barriers for reactions of a wide variety of other nucleophiles, and hence establish systematic trends in intrinsic barriers (developing upon the work of Hoz).[75] This will allow the factors that control intrinsic barriers to be understood, and hence deepen our understanding of activation barriers in general.

Details on Computational Methodology

The conformational space for each structure was explored with the OPLS-2005 force field[85] and a modified Monte Carlo search algorithm implemented in Macromodel.[86] An energy cut-off of 84 kJ mol^{-1} was employed for the conformational analysis, and structures with heavy-atom root-mean-square deviations (RMSD) up to 0.5 Å after the force field optimizations where considered to be the same conformer. All remaining structures were subsequently optimized with the dispersion-corrected M06-2X functional[87] with Grimme's dispersion correction D3 (zero-damping),[88] the triple-ζ basis set 6-311+G(d,p), and SMD solvation model[89] for acetonitrile. An ultrafine grid was used throughout this study for the numerical integration of the density. Vibrational analysis verified that each structure was a minimum or a transition state and for the latter, following the intrinsic reaction coordinates (IRC) confirmed that all transition states connected the corresponding reactants and products on the potential energy surface. Thermal corrections were obtained from unscaled harmonic vibrational frequencies at the same level of theory for a standard state of 1 mol L^{-1} and 298.15 K. Entropic contributions to free energies were obtained from partition functions evaluated with Grimme's quasi-harmonic approximation.[90] This method employs the free-rotor approximation for all frequencies below 100 cm^{-1}, the rigid-rotor-harmonic-oscillator (RRHO) approximation for all frequencies above 100 cm^{-1}, and a damping function to interpolate between the two expressions. Similar results were obtained from partition functions evaluated with Cramer's and Truhlar's quasiharmonic approximation.[91] This method uses the same approximations as the usual harmonic oscillator approximation, except that all vibrational frequencies lower than 100 cm^{-1} are set equal to 100 cm^{-1}. Electronic energies were subsequently obtained from single point calculations of the M06-2X-D3 geometries employing Neese's domain-based local pair-natural orbital (DLPNO) approach to the CCSD(T) method [DLPNO-CCSD(T)] with the default normalPNO settings,[92–94] the triple-ζ def2-TZVPPD [95,96] in combination with the corresponding auxiliary basis set[97] and the SMD continuum model for acetonitrile.[89] All density functional theory calculations were performed with Gaussian 16,[98] while the DLPNO-CCSD(T) calculations were performed with ORCA 4.[99]

Acknowledgements

This work was undertaken using equipment provided by Science Foundation Ireland though a research infrastructure award for process flow spectroscopy (ProSpect) (grant: SFI 15/RI/3221) and as part of the Synthesis and Solid State Pharmaceutical Centre supported by Science Foundation Ireland (grant: SFI SSPC2 12/RC/2275). K.J.S. would like to thank the Irish Research Council for provision of a GOIPG Scholarship to fund his research (IRC

GOIPG/2018/1517). Support from the Fonds der Chemischen Industrie (Liebig scholarship to M.B.) and the University of Cologne within the excellence initiative is gratefully acknowledged. We gratefully acknowledge the Regional Computing Center of the University of Cologne for providing computing time in the DFG-funded High-Performance Computing (HPC) System CHEOPS as well as for their support, the excellent analytical services provided in the School of Chemistry and ABCRF in UCC, Prof. Justin Holmes and research group for access to an inert atmosphere glove box, Dr. Denis Lynch for assistance with NMR spectroscopy, Mick O'Shea for HRMS data, and Prof. Eoghan McGarrigle (University College Dublin) for helpful discussion.

Conflicts of interest

There are no conflicts to declare.

Notes and references

1 (a) J. Clayden, N. Greeves and S. Warren, *Organic Chemistry*, 2nd edition, Oxford University Press, New York, 2012, pp 355–357, 453–454, 506–509, 590, 658; (b) E. V. Anslyn and D. A. Dougherty, *Modern Physical Organic Chemistry,* University Science Books, Sausalito, 2006, pp 288–292, 567–568; (c) M. B. Smith, *March's Advanced Organic Chemistry,* 7th edition, Wiley, Hoboken, 2013, pp 446–450.

2 (a) R. G. Pearson, *J. Am. Chem. Soc.* 1963, **85**, 3533; (b) R. G. Pearson, *Science* 1966, **151**, 172; (c) R. G. Pearson and J. Songstad, *J. Am. Chem. Soc*. 1967, **89**, 1827; (d) R. G. Pearson, *J. Chem. Educ.* 1968, **45**, 581; (e) R. G. Pearson, *J. Chem. Educ*. 1968, **45**, 643; (f) R. G. Pearson, *Inorg. Chim. Acta* 1995, **240**, 93; (g) R. G. Parr and R. G. Pearson, *J. Am. Chem. Soc.* 1983, **105**, 7512.

3 (a) G. Klopman, *J. Am. Chem. Soc*. 1968, **90**, 223; (b) L. Salem, *J. Am. Chem. Soc*. 1968, **90**, 543; (c) T.-L. Ho, *Chem. Rev*. 1975, **75**, 1.

4 H. Mayr, M. Breugst and A. R. Ofial, *Angew. Chem. Int. Ed.* 2011, **50**, 6470.

5 For selected recent examples, see: (a) S. Maiti and P. Mal, *J. Org. Chem*. 2018, **83**, 1340; (b) S. Maiti, T. Alam and P. Mal, *Asian J. Org. Chem*. 2018, **7**, 715; (c) Y.-G. Wang and E. C. Barnes, *ACS Omega* 2018, **3**, 4557; (d) A. Burmudžija, S. Marković, J. Muškinja, A. Pejović and J. Tošović, *Reac. Kinet. Mech. Cat.* 2018, **123**, 201; (e) S. Yaragorla, A. Pareek and R. Dada, *Tetrahedron Lett.* 2017, **58**, 4642 (f) C. Slawik, C. Rickmeyer, M. Brehm, A. Böhme and G. Schürmann, *Environ. Sci. Technol*. 2017, **51**, 4018.

6 Y.-G. Wang, E. C. Barnes, S. Kaya and V. Sharma, *J. Comput. Chem.* 2019, **40**, 2761.

7 X. Ma, H. Dang, J. A. Rose, P. Rablen and S. B. Herzon, *J. Am. Chem. Soc.* 2017, **139**, 5998.

8 D. Demberelnyamba, B. K. Shin and H. Lee, *Chem. Commun.* 2002, 1538. In this paper on amide-derived ionic liquids, N-alkylation of an amide upon refluxing in acetonitrile is reported.

9 J. Yang, Q. Zhang, L. Zhu, S. Zhang, J. Li and X. Zhang, *Chem. Mater.* 2007, **19**, 2544. In this paper on amide-derived ionic liquids, N-alkylation of ε-caprolactam by alkyl tosylates and mesylates in acetonitrile at 80 °C is reported.

10 P. Cmoch, *Magn. Reson. Chem.* 2003, **41**, 693.

11 M. V. Jovanovic, *Heterocycles* 1985, **23**, 2299.

12 Assignment of N-methylated pyrazine product structures made on the basis of the results of chemical derivatisations: (a) J. K. Landquist *J. Chem. Soc.* 1953, 2816; (b) A. Ohta, M. Matsunaga, N. Iwata and T. Watanabe, *Heterocycles* 1977, **8**, 351; (c) C. F. Koelsch and W. H. Gumprecht, *J. Org. Chem.* 1958, 23, 1603.

13 R. Głaszczka, J. Jaźwiński, *J. Mol. Struct.* 2014, **1061**, 150.

14 (a) M. Breugst, T. Tokuyasu and H. Mayr, *J. Org. Chem.* 2010, **75**, 5250; (b) M. Breugst and H. Mayr, *J. Am. Chem. Soc.* 2010, **132**, 15380.

15 (a) F. H. Zadeh, P. Fuentealba, C. Cárdenas and P. W. Ayers *Phys. Chem. Chem. Phys.* 2014, **16**, 6019. See also references therein; (b) M. Torrent-Sucarrat, F. De Proft, P. Geerlings, and P.W. Ayers, *Chem. Eur. J.* 2008, **14**, 8652, and references therein.

16 J. M. Gonzales, W. D. Allen, H. F. Schaefer III, *J. Phys. Chem. A* 2005, **109**, 10613.

17 (a) P. W. Ayers, *Faraday Discuss*. 2007, **135**, 161; (b) P. W. Ayers and C. Cárdenas, *J. Chem. Phys.* 2013, **138**, 181106.

18 (a) P. W. Ayers, *J. Chem. Phys.* 2005**, 122**, 141102; (b) C. Cárdenas and P. W. Ayers, *Phys. Chem. Chem. Phys.* 2013, **15**, 13959; (c) P. W. Ayers, R. G. Parr and R. G. Pearson, *J. Chem. Phys.* 2006, **124**, 194107; (d) P. K. Chattaraj, P. W. Ayers and J. Melin *Phys. Chem. Chem. Phys.* 2007, **9**, 3853.

19 Amides: (a) Z.-J. Chen, H.-W. Xi, K. H. Lim and J.-M. Lee, *Angew. Chem. Int. Ed.* 2013, **52**, 13392; (b) T. Nanjo, E. C. de Lucca Jr. and M. C. White, *J. Am. Chem.* Soc. 2017, **139**, 14586 (c) H.-G. Cheng, M. Pu, G. Kundu and F. Schoenebeck, *Org.Lett.* 2020, **22**, 331.

20 2-Pyridone and 4-pyridone: B. Feng, Y. Li, H. Li, X. Zhang, H. Xie, H. Cao, L. Yu and Q. Xu, *J. Org. Chem.* 2018, **83**, 6769.

21 Amide anions: (a) See ref. 17a; (b) See ref. 19b.

22 Pyridone or quinolone anions: (a) See ref. 17b; (b) G. C. Hopkins, J. P. Jonak, H. J. Minnemeyer and H. Tieckelmann, *J. Org. Chem.*, 1967, **32**, 4040; (c) K. Pissinate, A. D. Villela, V. Rodrigues, B. C. Giacobbo, E. S. Grams, B. L. Abbadi, R. V. Trindade, L. R. Nery, C. D. Bonan, D. F. Back, M. M. Campos, L. A. Basso, D. S. Santos and P. Machado, *ACS Med. Chem. Lett.*, 2016, **7**, 235.

23 Imide anions: (a) L. Z. Avila, S. H. Loo and J. W. Frost, *J. Am. Chem. Soc.*, 1987, **109**, 6758; (b) A. Arévalo, S. Ovando-Segovia, M. Flores-Alamo and J. J. Garćia, *Organometallics*, 2013, **32**, 2939.

24 (a) T. H. Koch, R. J. Sluski and R. H. Moseley, *J. Am. Chem. Soc.*, 1973, **95**, 3957.; (b) D. R. Anderson, J. S. Keute, T. H. Koch and R. H. Moseley, *J. Am. Chem. Soc.*, 1977, **99**, 6332. O-alkylation is observed for silver salts of imide anions; this is ascribed to blocking of the nitrogen site due to coordination to silver in references 4 and 17a.

25 Uracil anions: (a) See ref. 9c; (b) Y.-G. Wang and E. C. Barnes, *J. Phys. Chem. A*, 2017, **121**, 8866.

26 Aryl diazoacetate anions: N. Kornblum, R. A. Smiley, R. K. Blackwood and D. C. Iffland, *J. Am. Chem. Soc.*, 1955, **77**, 6269.

27 Nitrite ion: (a) A. A. Tishkov, U. Schmidhammer, S. Roth, E. Riedle and H. Mayr, *Angew. Chem., Int. Ed.*, 2005, **44**, 4623; (b) See ref. 26.

28 Cyanate ion: See reference 4 and references therein.

29 O-alkylation of anions of 2-methylquinolin-4-ols: E. Pitta, M. K. Rogacki, O. Balabon, S. Huss, F. Cunningham, E. M. Lopez-Roman, J. Joossens, K. Augustyns, L. Ballell, R. H. Bates and P. Van der Veken, *J. Med. Chem.*, 2016, **59**, 6709.

30 Oximate anions: S. G. Smith and M. P. Hanson, *J. Org. Chem*, 1971, **36**, 1931.

31 Anions of quinolin-4-ols, quinazolin-4-ols and 1,5-naphthyrid-4-ols: E. Pitta, O. Balabon, M. K. Rogacki, J. Gómez, F. Cunningham, J. Joosens, K. Augustyns, P. van der Veken and R. Bates, *Eur. J. Med. Chem.*, 2017, **125**, 890.

32 Numerous additional literature references containing examples of competition between N- and O-alkylation of ambident nucleophiles are given in the Supporting Information, pg. S117.

This journal is © The Royal Society of Chemistry 20xx

33 The site selectivity observed in reactions of anionic ambident nucleophiles may be a consequence of one of the nucleophilic sites being blocked through coordination to a counter-cation. See references 9c, 17a, 24, 30, and also L. M. Jackman and T. S. Dunne, *J. Am. Chem. Soc.*, 1985, **107**, 2805.
34 However, see also: T. Storz, M. D. Bartberger, S. Sukits, C. Wilde and T. Soukup, *Synthesis*, 2008, **2**, 201.
35 (a) G. E. Martin and A. J. Williams, *Annu. Rev. NMR Spectro.*, 2015, **84**, 1-76; (b) R. Marek, A. Lyčka, E. Kolehmainen, E. Sievänen and J. Toušek, *Current Organic Chemistry*, 2007, **11**, 1154; (c) G. E. Martin, A. J. Williams, *Annu. Rev. NMR Spectro.* 2005, **55**, 1–119; (d) R. Marek, A. Lyčka, *Cur. Org. Chem.* 2002, **6**, 35; (e) J. Saurí, A .J. Williams, G. E. Martin in *Modern NMR Approaches to the Structure Elucidation of Natural Products*, vol. 2, ed. A.J. Williams, G.E. Martin, D. Rovnyak, RSC, Cambridge, 2016, pp. 71–116; (f) B. D. Hilton and G. E. Martin, *J. Heterocyclic Chem.*, 2012, **49**, 526; (g) S. L. Black, P. D. O'Connor, M. Boyd, A. Blaser and J. D. Kendall, *Tetrahedron*, 2018, **74**, 2797; (h) R.T. Williamson, A.V. Buevich, G.E. Martin, *Tetrahedron Lett.* 2014, **55**, 3365.
36 Applications of natural abundance ^{17}O NMR spectroscopy: (a) D. E. Frantz and D. A. Singleton, *J. Am. Chem. Soc.*, 2000, **122**, 3288; (b) M. P. Meyer, A. J. DelMonte and D. A. Singleton, *J. Am. Chem. Soc.*, 1999, **121**, 10865.
37 The natural abundance ^{1}H-^{15}N HMBC NMR experiments were obtained using an NMR spectrometer equipped with a broadband cryoprobe, which greatly enhances the capabilities of this technique. The ^{15}N resonance was acquired in little time without the need for any costly isotopic enrichment, thus overcoming the traditional barriers against direct observation ^{15}N NMR spectroscopic studies.
38 A. Salgado, C. Varela, A. M. García Collazo and P. Pevarello, *Magn. Reson. Chem.*, 2010, **48**, 614.
39 K. J. Sheehy, L. M. Bateman, N. Flosbach, M. Breugst, P. A. Byrne, *Eur. J. Org. Chem.,* 2020, DOI: 10.1002/ejoc.202000329.
40 The δ_N values of non-alkylated nitrogens of diazines undergo small downfield shifts during these reactions (i.e. $\Delta(\delta_N) \geq 0$ ppm).
41 (a) E. Lukevics, E. Leipiņš, I. Segal and M. Fleisher, *J. Organomet. Chem.*, 1991, **406**, 283; (b) Z. Dega-Szafran, M. Szafran, J. Sitkowski and L. Stefaniak, *J. Phys. Org. Chem.*, 1996, **9**, 746; (c) B. Costisella, J. Schulz, H. Teichmann, C. Donaths and M. Meisels, *Phosphorus, Sulfur, Silicon Relat. Elem.*, 1990, **53**, 367; (c) M. Szafran, Z. Dega-Szafran, A. Katrusiak, G. Buczak, T. Głowiak, J. Sitkowski and L. Stefaniak, *J. Org. Chem.*, 1998, **63**, 2898.
42 (a) L. Pazderski, *Annu. Rep. NMR Spectrosc.*, 2013, **80**, 33; (b) L. Pazderski, *Magn. Res. Chem.*, 2008, **46**, S3; (c) R. M. Shanahan, A. Hickey, L. M. Bateman, M. E. Light and G. P. McGlacken, *J. Org. Chem.*, 2020, **85**, 2585.
43 Benzhydrylium triflates were generated in the presence of nucleophiles **1**, **2** or **3** by treating the parent benzhydryl chloride with AgOTf in CD_2Cl_2. The entirety of the reaction mixture filtered into an NMR tube (to remove AgCl) under inert atmosphere. For full experimental details, see the Supporting Information.
44 Experimental data are given in section 4 of the Supporting Information, beginning on page S8.
45 A detailed description of how inert NMR spectral analysis was carried out is given on page S8 of the Supporting Information (Procedure B).
46 Note that MeCN or CD_3CN could not be used for ^{1}H-^{15}N HMBC spectroscopic characterization due to the presence of nitrogen in the solvent. Hence, for the purposes of obtaining ^{1}H-^{15}N HMBC spectra, the solvent was removed and the residue re-dissolved in $(CD_3)_2SO$. CD_2Cl_2 was not a suitable solvent for methylation reactions of diazine *N*-oxides **1**–**3** due to the negligible solubility of the adducts in this solvent.
47 The reaction of **3** with Ph_2CH^+ produced a spectrum with broad signals that could not be interpreted. See pages S36 and S37 of the Supporting Information for details.
48 Methylation of DMSO by dimethylsulfate: J. Forrester, R. V. H. Jones, P.N. Preston and E. S. C. Simpson *J. Chem. Soc., Perkin Trans. 1*, 1995, 2289.
49 Reversibility of methoxysulfonium salt formation: G. F. Koser, P. B. Kokil and M. Shah, *Tetrahedron Lett.* 1987, **28**, 5431.
50 See spectra from methylation reactions of **1**, **2** and **3** in $(CD_3)_2SO$ on pages S14–15, S24–25 and S33-35 of the Supporting Information.
51 See details on pages S18–19 of the Supporting Information.
52 Decomposition was evident in the all of the spectra obtained of this material, regardless of the method employed to synthesize it. The major product remained intact for several days if kept under inert atmosphere (invariably contaminated with decomposition products), but did not survive attempts at isolation. ^{1}H NMR spectra containing signals of the decomposition products are shown in Figures S15 and S18 of the Supporting Information (pages S29 and S33).
53 See Supporting Information pages S11–13, S21–23 and S31–33.
54 C. Sakuma, M. Maeda, K. Tabei, A. Ohta, A. Kerim and T. Kurihara, *Magn. Reson. Chem*. 1996, **34**, 567.
55 W. Städeli and W. von Philipsborn, *Helv. Chem. Acta* 1980, **63**, 504.
56 See ^{1}H-^{15}N HMBC NMR spectra in Supporting Information on pages S55, S59, S60, S62, S64, S67, S68, and S70.
57 See pages S12, S14, S16, S20, S21, S26, and S31 of the Supporting Information for details on $^{13}C\{^{1}H\}$ NMR spectra of the N- and O-alkylation products.
58 See ^{1}H-^{15}N HMBC NMR spectrum on page S71 of the SI.
59 See ^{1}H-^{13}C HMBC NMR spectrum on page S73 in the SI.
60 All crossover experiments described in this section can be found in the Supporting Information in section 5, beginning on page S38.
61 e.g. **7** is a stronger Lewis base than **2** by a factor of *ca.* 16, while **25** is a stronger Lewis base than **1** by a factor of *ca*. 20: (a) P. A. Byrne, K. J. Sheehy, S. Buckley and H. Mayr, *unpublished results*; (b) H. Mayr, J. Ammer, M. Baidya, B. Maji, T. A. Nigst, A. R. Ofial and T. Singer, *J. Am. Chem. Soc.* 2015, **137**, 2580.
62 The experimental data pertaining to this experiment can be found on pages S46–S50 in the Supporting Information.
63 Full details on our computational investigations are given in the Supporting Information, pg. S83 – S110.
64 This is consistent with a report by Mayr, Ofial and co-workers indicating greater Lewis basicity of **28** compared to **27** in reactions with reference benzhydrylium ions: See reference 61b above.
65 See page S11–12 in the Supporting Information.
66 Precedent exists for remote deactivation of a Lewis basic nitrogen site: P. A. Byrne, S. Kobayasi, M. Breugst, H. Laub and H. Mayr, *J. Phys. Org. Chem.* 2016, **29**, 759.
67 See calculation on pages S31 and S35 in the ESI.
68 As cations and anions were assumed to be solvent separated, this trend can be expected for these bimolecular reactions. See Table S1 – S3 on pages S83 – S85 of the Supporting Information.
69 For details on Marcus theory, see: (a) R. A. Marcus, *Annu. Rev. Phys. Chem.* 1964, **15**, 155; (b) R. A. Marcus, *J. Phys. Chem.* 1968, **72**, 891; (c) R. A. Marcus, *J. Am. Chem. Soc.* 1969, **91**, 7224; (d) W. J. Albery and M. M. Kreevoy, *Adv. Phys. Org. Chem.* 1978, **16**, 87; (e) W. J. Albery, *Annu. Rev. Phys. Chem.* 1980, **31**, 227; (f) R. A. Marcus, *Pure Appl. Chem.* 1997, **69**, 13; (g) R. A. Marcus, *Angew. Chem. Int. Ed.* 1993, **32**, 1111.

70 As pointed out in reference 4, the omission of the work terms from equation 1 is justified when considering intramolecular selectivity such as selectivity between nucleophilic sites of an ambident nucleophile.
71 Introductions to Marcus theory are available in chemistry textbooks: (a) E. V. Anslyn and D. A. Dougherty, *Modern Physical Organic Chemistry*, University Science Books, Sausalito, California, 2006, p. 403–406; (b) P. W. Atkins and J. De Paula, *Physical Chemistry*, Oxford University Press, Oxford, 9th edition, 2010, p. 820, 857–861; (c) M. B. Smith, *March's Advanced Organic Chemistry*, Wiley-VCH: Hoboken, New Jersey, 7th edition, 2013, p. 273–274.
72 (a) Phenoxides: R. Mayer, M. Breugst, N. Hampel, A. R. Ofial and H. Mayr, *J. Org. Chem.* 2019, **84**, 8837; (b) Carbonyl-stabilised phosphonium ylides: P. A. Byrne, K. Karaghiosoff and H. Mayr, *J. Am. Chem. Soc.* 2016, **138**, 11272; (c) Azolium enolates: B. Maji and H. Mayr, *Angew. Chem. Int. Ed.* 2013, **52**, 11163; (d) Formaldehyde *N*,*N*-dialkylhydrazones: B. Maji, K. Troshin and H. Mayr, *Angew. Chem. Int. Ed.* 2013, **52**, 11900; (e) Methylhydrazines: T. A. Nigst, J. Ammer and H. Mayr, *Angew. Chem. Int. Ed*. 2012, **51**, 1353.
73 See intrinsic barrier ($\Delta G_0^{\ddagger}$) calculations in section 9 of the Supporting Information, beginning on page S86.
74 See Table S5 on page S90 in the Supporting Information for calculated values of $\Delta G_0^{\ddagger}$ and $\Delta G^{\ddagger}$.
75 S. Hoz, H. Basch, J. L. Wolk, T. Hoz and E. Rozental, *J. Am. Chem. Soc.* 1999, **121**, 7724. Note that Similar trends were also observed across the 3rd – 5th rows of the periodic table (*p*-block elements; noble gases not included).
76 X.-Q. Zhu and J.-D. Yang, *J. Phys. Org. Chem*. 2013, **26**, 271.
77 S. S. Shaik, H. B. Schlegel and P. Wolfe, *Theoretical Aspects of Physical Organic Chemistry: The S_N2 Mechanism*; Wiley, New York, 1992.
78 (a) X.-Q. Zhu, F.-H. Deng, J.-D. Yang, X.-T. Li, Q. Chen, N.-P. Lei, F.-K. Meng, X.-P. Zhao, S.-H. Han, E.-J. Hao and Y.-Y. Mu, *Org. Biomol. Chem.* 2013, **11**, 6071; (b) Y.-H. Fu, G.-B. Shen, Y. Li, L. Yuan, J.-L. Li, L. Li, A.-K. Fu, J.-T. Chen, B.-L. Chen, L. Zhu and X.-Q. Zhu, *ChemistrySelect* 2017, **2**, 904; (c) G.-B. Shen, K. Xia, X.-T. Li, J.-L. Li, Y.-H. Fu, L. Yuan and X.-Q. Zhu, *J. Phys. Chem. A* 2016, **120**, 1779; (d) Y. Li and X.-Q. Zhu, *ACS Omega.* 2018, **3**, 872.
79 The introduction and usage of the Zhu equation is discussed in the Supporting Information, beginning on page S89.
80 See pg S111 – S116 of Supporting Information for details of the experimental determination of an approximate $\Delta G^{\ddagger}$ value for the reaction of **1** + MeI to give **13a**.
81 See Table S8 on pg S92 of the Supporting Information.
82 Numerous precedents for kinetically controlled N-alkylation of other ambident nucleophiles with competing O and N nucleophilic sites (e.g. amide anions) exist in the literature.[19b,f,j,k, 22b,c,d]
83 (a) P. A. Byrne, S. Kobayashi, E.-U. Würthwein, J. Ammer and H. Mayr, *J. Am. Chem. Soc.* 2017, **139**, 1499; (b) J. P. Richard, M. M. Toteva and J. Crugeiras, *J. Am. Chem. Soc.* 2000, **122**, 1664.
84 Amide O-alkylation appears to be kinetically favoured over N-alkylation. Although O-methylation of DMF has been shown to be reversible at temperatures > 100 °C,[19a,c,d] reports of N-alkylation of amides in refluxing acetonitrile (boiling point 82 °C at atmospheric pressure) are likely to involve misidentification of the products. Certainly, the spectral data supplied are insufficient for definitive assignment of N-alkylated products.[8,9]
85 J. L. Banks, H. S. Beard, Y. Cao, A. E. Cho, W. Damm, R. Farid, A. K. Felts, T. A. Halgren, D. T. Mainz, J. R. Maple, R. Murphy, D. M. Philipp, M. P. Repasky, L. Y. Zhang, B. J. Berne, R. A. Friesner, E. Gallicchio and R. M. Levy, *J. Comput. Chem.*, 2005, **26**, 1752–1780.
86 Schrödinger Release 2018-3; Macromodel, Schrödinger, LLC: New York, NY, 2018.
87 Y. Zhao and D. G. Truhlar, *Theor. Chem. Acc.* **2008**, *120*, 215–241.
88 S. Grimme, J. Antony, S. Ehrlich and H. Krieg,. *J. Chem. Phys.* **2010**, *132*, 154104.
89 A. V. Marenich, C. J. Cramer and D. G. Truhlar, *J. Phys. Chem. B* **2009**, *113*, 6378–6396.
90 S. Grimme, *Chem. Eur. J.* **2012**, *18*, 9955–9964.
91 R. F. Ribeiro, A. V. Marenich, C. J. Cramer and D. G. Truhlar, *J. Phys. Chem. B* **2011**, *115*, 14556–14562.
92 C. Riplinger, B. Sandhoefer, A. Hansen and F. Neese, *J. Chem. Phys.* **2013**, *139*, 134101.
93 C. Riplinger and F. Neese, *J. Chem. Phys.* **2013**, *138*, 034106.
94 D. G. Liakos and F. Neese, *J. Chem. Theory Comput.* **2015**, *11*, 4054–4063.
95 F. Weigend and R. Ahlrichs, *Phys. Chem. Chem. Phys.* **2005**, *7*, 3297–3305.
96 D. Rappopor and F. Furche, *J. Chem. Phys.* **2010,** *133*, 134105.
97 A. Hellweg, C. Hättig, S. Höfener and W. Klopper, *Theor. Chem. Acc.*, 2007, **117**, 587–597.
98 M. J. Frisch, G. W. Trucks, H. B. Schlegel, G. E. Scuseria, M. A. Robb, J. R. Cheeseman, G. Scalmani, V. Barone, G. A. Petersson, H. Nakatsuji, X. Li, M. Caricato, A. V. Marenich, J. Bloino, B. G. Janesko, R. Gomperts, B. Mennucci, H. P. Hratchian, J. V. Ortiz, A. F. Izmaylov, J. L. Sonnenberg, Williams, F. Ding, F. Lipparini, F. Egidi, J. Goings, B. Peng, A. Petrone, T. Henderson, D. Ranasinghe, V. G. Zakrzewski, J. Gao, N. Rega, G. Zheng, W. Liang, M. Hada, M. Ehara, K. Toyota, R. Fukuda, J. Hasegawa, M. Ishida, T. Nakajima, Y. Honda, O. Kitao, H. Nakai, T. Vreven, K. Throssell, J. A. Montgomery Jr., J. E. Peralta, F. Ogliaro, M. J. Bearpark, J. J. Heyd, E. N. Brothers, K. N. Kudin, V. N. Staroverov, T. A. Keith, R. Kobayashi, J. Normand, K. Raghavachari, A. P. Rendell, J. C. Burant, S. S. Iyengar, J. Tomasi, M. Cossi, J. M. Millam, M. Klene, C. Adamo, R. Cammi, J. W. Ochterski, R. L. Martin, K. Morokuma, O. Farkas, J. B. Foresman and D. J. Fox *Gaussian 16 Rev. B.01*, Wallingford, CT, 2016.
99 (a) F. Neese, *Wiley Interdiscip. Rev. Comput. Mol. Sci.*, 2012, **2**, 73–78; (b) F. Neese, *Wiley Interdiscip. Rev. Comput. Mol. Sci*., 2018, **8**, e1327.

This journal is © The Royal Society of Chemistry 20xx

Competition Between N and O: Use of Diazine *N*-Oxides as a Test Case for the Marcus Theory Rationale for Ambident Reactivity

Received 00th January 20xx,
Accepted 00th January 20xx

DOI: 10.1039/x0xx00000x

Kevin J. Sheehy,[a] Lorraine M. Bateman,[a,b,d] Niko T. Flosbach,[c] Martin Breugst,*[c] Peter A. Byrne,*[a,d]

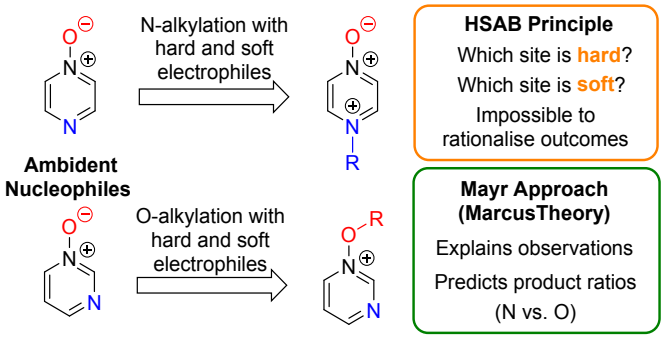
The preferred site of alkylation of diazine *N*-oxides by representative hard and soft alkylating agents was established conclusively using the ^{1}H-^{15}N HMBC NMR technique in combination with other NMR spectroscopic methods. Alkylation of pyrazine *N*-oxides (**1** and **2**) occurs preferentially on nitrogen regardless of the alkylating agent employed, while O-methylation of pyrimidine *N*-oxide (**3**) is favoured in its reaction with MeOTf. As these outcomes cannot be explained in the context of the hard/soft acid/base (HSAB) principle, we have instead turned to Marcus theory to rationalise these results. Marcus intrinsic barriers ($\Delta G_0^{\ddagger}$) and $\Delta_r G°$ values were calculated at the DLPNO-CCSD(T)/def2-TZVPPD/SMD//M06-2X-D3/6-311+G(d,p)/SMD level of theory for methylation reactions of **1** and **3** by MeI and MeOTf, and used to derive Gibbs energies of activation ($\Delta G^{\ddagger}$) for the processes of N- and O-methylation, respectively. These values, as well as those derived directly from the DFT calculations, closely reproduce the observed experimental N vs O selectivities for methylation reactions of **1** and **3**, indicating that Marcus theory can be used in a semi-quantitative manner to understand how the activation barriers for these reactions are constructed. It was found that N-alkylation of **1** is favoured due to the dominant contribution of $\Delta_r G°$ to the activation barrier in this case, while O-alkylation of **3** is favoured due to the dominant contribution of the intrinsic barrier ($\Delta G_0^{\ddagger}$) for this process. These results are of profound significance in understanding the outcomes of reactions of ambident reactants in general.

Introduction

Selectivity in Reactions of Ambident Nucleophiles

A fundamental goal in organic chemistry is to be able to understand and rationalise why chemical processes occur as they do. Naturally, therefore, an understanding of the factors that govern regioselectivity in chemical reactions is of paramount importance – i.e. if a compound contains more than one reactive site, which one is preferred, and why? Reliably accounting for the regioselectivity observed in reactions of ambident nucleophiles and electrophiles is a challenge laden with difficulties and potential pitfalls. By far the most popular rationale for this purpose[1] makes use of the principle of hard and soft acids and bases (the HSAB principle),[2] and the related concept of charge vs. orbital control.[3] The difficulty inherent in accounting for the selectivities observed in reactions of ambident nucleophiles is exemplified by the fact that the HSAB principle *predicts the incorrect product* in a very large number of cases, as has been reviewed in detail by Mayr and co-workers.[4] The data in this review call starkly into question whether the principle adequately explains the observed selectivity in reactions of ambident nucleophiles in which the expected outcome (based on HSAB theory) does match the experimental outcome.[5]

Mayr and co-workers have suggested employing Marcus theory (described below) as an alternative method of accounting qualitatively for the selectivities of reactions of ambident reactants.[4]



Scheme 1. Approaches for rationalising selectivity in reactions of diazine N-oxides as representative ambident nucleophiles.

Recently, Wang, Barnes, and co-workers conducted computational investigations to establish a theoretical basis for applying the HSAB principle in rationalising ambident reactivity, and used this, along with Marcus theory, to explain the results of their calculations on gas phase reactions of amide anions.[6] However, so far, the Marcus theory-based approach has not been adopted by the wider research community, and in fact the HSAB rationale continues to be cited in cases in which the experimental results do align, perhaps arbitrarily, with expectations based on this principle.[5] Furthermore, the elements of the intuitively alluring HSAB rationale pervade all discussions of ambident reactivity in undergraduate chemistry courses, and in the most comprehensive organic chemistry textbooks.[1] Given the clear deficiencies of the HSAB rationale in the context of ambident reactivity, it now behoves organic chemists to test Mayr's approach and other alternatives on their capacity to account for the outcomes of reactions of ambident reactants.

Herein, we focus on the notoriously difficult problem of competition between N and O nucleophilic sites (Scheme 1).[4,5c,6,7–14] We chose diazine *N*-oxides **1**, **2** and **3** (Fig. 1) as test substrates in reactions with various representative hard and soft electrophiles because, although

[a] School of Chemistry, Analytical and Biological Chemistry Research Facility, University College Cork, College Road, Cork, Ireland.
[b] School of Pharmacy, University College Cork, College Road, Ireland
[c] Department für Chemie, Universität zu Köln, Greinstraße 4, 50939 Köln, Germany.
[d] SSPC (Synthesis and Solid State Pharmaceutical Centre), Cork, Ireland.
E-mail: peter.byrne@ucc.ie, mbreugst@uni-koeln.de

Electronic Supplementary Information (ESI) available: contains experimental procedures, characterisation data for products and reaction mixtures, details of crossover experiments, copies of NMR spectra, and details on computational investigations. See DOI: 10.1039/x0xx00000x.

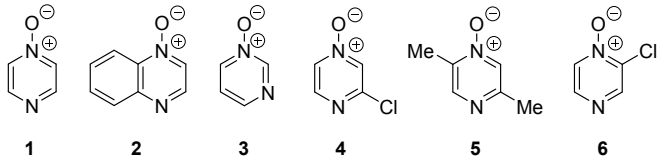


Figure 1. Representative Diazine *N*-oxides

these reactions show very high site-selectivity (i.e. for N- or O-alkylation),[7] their outcomes are intractable to rationalisation using the HSAB principle (Scheme 1), as will be discussed in the next section. An additional contributing factor that confounds any attempt to analyse the reactions of these species using the HSAB rationale is that it is not possible to unambiguously identify which nucleophilic site of a diazine *N*-oxide is the hard site, and which is the soft site (see later).[15]

In this work, we will show that the approach of Mayr and co-workers enables accurate prediction of the preferred site of alkylation of ambident nucleophiles **1–3**. Furthermore, we will also show that it is even possible to calculate the ratio of the selectivities for the different nucleophilic sites in these compounds (N vs. O) with an impressive degree of accuracy (Scheme 1).[16] Our results bolster the applicability of the Marcus theory-based approach and establish, for the first time, its capacity to semi-quantitatively account for the ratios of site-selectivities in reactions of ambident nucleophiles.

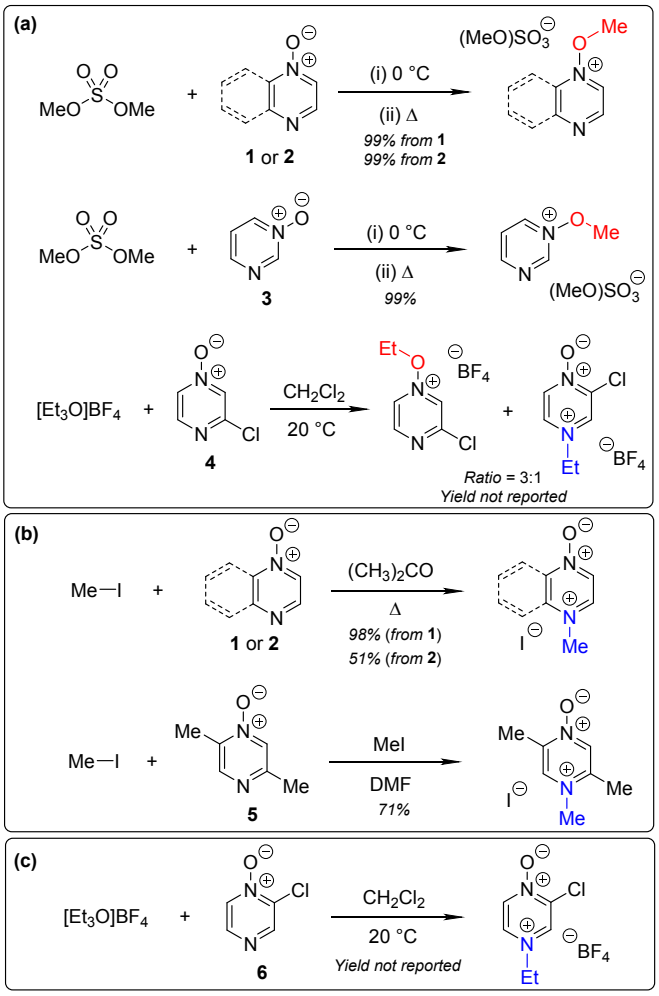
It should be noted that the limitations of the HSAB principle were highlighted by its developer (Pearson),[2d,f] and that in its original formulation,[2a,b] it was not derived with the intention of rationalising the selectivities of reactions of ambident reactants. However, thereafter, it has been[2c] and continues to be applied in this manner.[1,5] In recent years, a theoretical grounding demonstrating the applicability of the "global" HSAB principle (which does not apply to ambident reactants) has been developed.[17,18] Despite the authors' inclusion in the articles on this topic of precise statements such as "*The local HSAB principle, which makes predictions about ambident acids and bases, is on much shakier theoretical ground, so experimental evidence against it is not surprising*",[15a,17b] these papers are nonetheless cited in other articles in support of application of the HSAB principle to the analysis of reactions of ambident nucleophiles.[5c] This is illustrative of the continued application of the HSAB principle to rationalisation of ambident reactivity in the wider chemistry community despite the large body of evidence demonstrating that it does not apply in such instances.

Competition Between N and O Nucleophilic Sites

Numerous examples of reactions of ambident nucleophiles containing competing O and N nucleophilic sites exist in the literature.[6,10–14,19–32] Compounds **1–3** are particularly suitable for the present investigation for the following reasons: (i) Unlike the reactions of many other ambident nucleophiles containing N and O nucleophilic sites,[6,14,20–31] reactions of **1–3** are not influenced by the presence of a counter-cation,[33] and (ii) their alkylation products do not undergo secondary reactions (*cf.* amide alkylations).[19c,f]

There exist several literature precedents of relevance to the ambident nucleophilicity of diazine *N*-oxides. Exclusive O-alkylation has been reported to occur in reactions of pyrazine *N*-oxide (**1**), quinoxaline *N*-oxide (**2**) and pyrimidine *N*-oxide (**3**) with hard alkylating agent dimethylsulfate,[7] and predominant O-ethylation has been reported to occur in the reaction of compound **4** with hard electrophile $[Et_3O]BF_4$ (Scheme 2a).[10] Reactions of **1**, of **2** and of **5** with soft electrophile methyl iodide have been reported to yield N-alkylated adducts (Scheme 2b),[11,12] as has the reaction of **5** with benzyl chloride.[12c] In contrast, compound **6** undergoes exclusive N-ethylation on reaction with hard electrophile $[Et_3O]BF_4$ (Scheme 2c).[10] Notwithstanding the ambiguity inherent in assigning hard and soft sites in these diazine *N*-oxides, it is clear that these results cannot all simultaneously be consistent with the HSAB principle.

An additional fundamental difficulty exists in the context of reactions of diazine *N*-oxides: the act of establishing the structure of the product is itself fraught with ambiguity. The spectral features of the products of O-alkylation and N-alkylation of a particular diazine *N*-oxide are not necessarily readily distinguishable. Most instances in the literature in which product structures have been assigned have been based on the results of chemical derivatisations,[12] prior to the development of modern spectroscopic methods. In only one instance (involving two compounds) have modern two-dimensional NMR spectroscopic techniques been used to establish the precise structures of alkylation products of diazine *N*-oxides.[10,34] Hence, even



Scheme 2. Alkylation of diazine *N*-oxides **1–6** using various hard and soft electrophiles. (a) O-alkylation using hard electrophiles,[7,10] (b) N-alkylation using soft electrophiles,[11,12] (c) N-alkylation using a hard electrophile.[10]

This journal is © The Royal Society of Chemistry 20xx

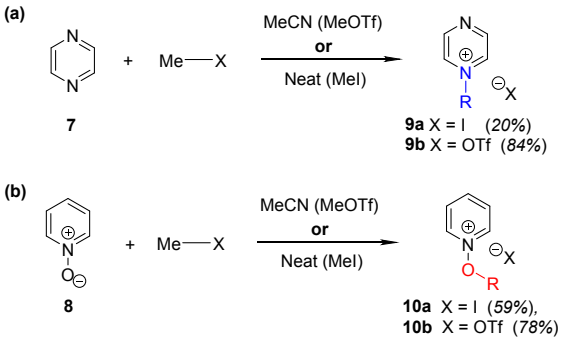
in instances in which structural assignments have been made, it is not certain that the correct product structures have been identified.

To unambiguously establish the ratios of N vs. O selectivity for the alkylation reactions of **1–3**, we took advantage of the technique of indirect detection natural abundance ^{1}H-^{15}N HMBC NMR spectroscopy.[34–38] This is an extremely useful diagnostic tool but, is very notably under-exploited – to our knowledge, there are only a handful of examples of its use to establish the site of attachment of an alkyl electrophile to an ambident reactant.[10,31,34,37] We have also conducted high level quantum chemical calculations to help us in understanding the outcomes of these experiments.

Background Data and Reference δ_N Values

In order to be able to employ ^{1}H-^{15}N HMBC NMR spectral data in a diagnostic manner to establish the site of alkylation of ambident nucleophiles **1–3**, we have made use of a set of results described in our recent publication.[39] In this preliminary study, we carried out various alkylations of representative diazines and azine *N*-oxides (see examples shown in Scheme 3, involving N-methylation of **7** and O-methylation of **8**), and monitored the change in the ^{15}N NMR chemical shifts (referred to as $\Delta(\delta_N)$ values) of each nitrogen atom in the N-alkylated product relative to its δ_N value in the starting material using ^{1}H-^{15}N HMBC NMR spectroscopy. We consistently observed that upon N-alkylation of diazines, a large upfield shift of the δ_N value of the alkylated nitrogen atom occurs (i.e. $\Delta(\delta_N) << 0$ ppm).[40] In fact, across a total of 22 examples from the chemical literature and our own work, involving N-methylation or ethylation of pyridrines, diazines, diazine *N*-oxides, quinolines, and isoquinolines, the average upfield $\Delta(\delta_N)$ value of the alkylated nitrogen atom is −115 ppm.[10,41] Similarly, the average upfield $\Delta(\delta_N)$ value associated with N-benzhydrylation was −91 ppm (3 examples). In contrast, the shift upfield in the *N*-oxide nitrogen δ_N value upon O-alkylation is significantly smaller – across 7 examples involving N-methylation or ethylation, the average upfield $\Delta(\delta_N)$ value was determined to be only −40 ppm, while for O-benzhydrylation the average $\Delta(\delta_N)$ value was −45 ppm. That the upfield signal in each case belongs to the alkylated nitrogen atom is shown by the existence of a correlation in the ^{1}H-^{15}N HMBC NMR spectrum of the product between the upfield ^{15}N signal and the proton(s) of the N- or O-alkyl group.

From the above, we can conclude that there is a characteristic $\Delta(\delta_N)$ value associated with N-alkylation of an aromatic *N*-heterocycle, distinct from (and significantly larger than) the $\Delta(\delta_N)$ value associated with O-alkylation of an aromatic *N*-oxide. Analogous observations have been made in an ^{15}N NMR spectroscopic study of protonation of pyridine and 4-methylpyridine *N*-oxide, which induces $\Delta(\delta_N)$ values of −113.3 ppm[41a] and −50.1 ppm,[41b] respectively. Furthermore, complexation of aromatic N-heterocycles to metals has been shown to result in upfield $\Delta(\delta_N)$ values of *ca.* −100 ppm).[42]



Scheme 3. Examples of use of hard and soft methylating agents to effect (a) N-methylation of **7**; (b) O-methylation of **8**. X = I or OTf throughout. Isolated yields are shown in parentheses.

Our previous investigation also allowed us to determine that in the ^{1}H-^{13}C HMBC NMR spectra of N-alkylated products, three-bond correlations exist between the N-alkyl group carbons and hydrogens and the *ortho* carbons and hydrogens of the aromatic moiety.[39] No correlations were observed in the ^{1}H-^{13}C HMBC NMR spectra of O-alkylated products between the O-alkyl group carbons and hydrogens and the *ortho* carbons and hydrogens. Furthermore, these unambiguous NMR spectroscopic correlation methods also allowed us to establish definitive diagnostic trends in the ^{13}C NMR chemical shifts of the alkyl group carbons immediately bound to aromatic nitrogen or aromatic *N*-oxide oxygen. For example, the *N*-methyl carbon of the adduct of N-methylation of an aromatic nitrogen nucleophile was shown to typically have a δ_C value in the range 36 – 53 ppm, while the O-methyl carbon of the adduct of aromatic *N*-oxide methylation typically exhibits a δ_C value in the range 62 – 75 ppm.[39] Consequently, it should be possible to employ a combination of $\Delta(\delta_N)$ values (obtained from ^{1}H-^{15}N HMBC NMR spectra) in tandem with ^{1}H-^{13}C HMBC and ^{13}C{^{1}H} NMR spectroscopic data to distinguish between N- and O-alkylated diazine *N*-oxides.

Results

Site of Alkylation of Diazine *N*-Oxides

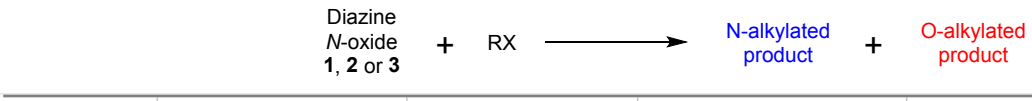
The data discussed above show that natural abundance ^{1}H-^{15}N HMBC is a highly useful diagnostic tool to determine whether or not the site of attachment of an alkyl electrophile is at a nitrogen atom. We will now describe how we have employed the ^{1}H-^{15}N HMBC NMR technique, in tandem with information from ^{13}C{^{1}H} and ^{1}H-^{13}C HSQC and HMBC NMR spectra, to establish the site of alkylation of ambident nucleophiles **1–3** in reactions with representative hard and soft alkylating agents.

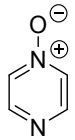
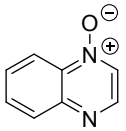
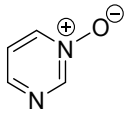
Reactions of ambident nucleophiles **1** and **2** with electrophiles MeI, MeOTf, and benzhydrylium triflates **11** and **12** were carried out using the conditions shown in Scheme 4 (pg. 5) and Table 1 (pg. 4).[44–46] The reaction of **1** with MeI in CD_3CN or CH_3CN resulted in formation of a single product, albeit with low conversion and yield – *i.e.* the process of alkylation was completely selective for one site (N or O) – see Table 1 entry (i). We did not observe any product formation in our ^{1}H NMR spectra of the reaction of **2** + MeI in CD_3CN. Product formation was only observed when the reagents were mixed together in the absence of solvent (neat); the data in Table 1 entry (v) refer to the reaction run under these conditions. As in the case of **1** + MeI, only a single product was observed by ^{1}H NMR spectroscopy. Attempted reactions of **3** with MeI in CD_3CN or MeCN did not yield any products, i.e. neither **21a** nor **23a** were observed (Scheme 4c).

The reaction of **1** with benzhydrylium triflate **11** in CH_2Cl_2 or CD_3CN also result in formation of single products (Table 1 entry (iv)).[43] The ^{1}H NMR spectrum of the reaction of **2** + **13** in CD_2Cl_2 (Scheme 4b) shows formation of two products in a 91:9 ratio (combined conversion = 93%; the remaining 7% was accounted for by hydrolysis product; see (Table 1 entry (viii)). Reaction of **3** with **11** gave ^{1}H NMR

Please do not adjust margins

Table 1. Alkylation reactions of diazine *N*-oxides **1**, **2** and **3** (as per Scheme 4) resulting in formation of O- and N-alkylated products.[a] Note that the ^{1}H NMR spectra of the reaction mixtures on their own do not show which product (O vs. N-alkylation) is favoured in each case, only the product ratio.



Diazine *N*-Oxide	#	Reaction Solvent [a]	R	X	Products		Conversion (Isolated % Yield) [b]	N/O Product Ratio [c]
					N-methyl	O-methyl		
 **1**	(i)	CD_3CN or No Solvent	Me	I	**13a**	**15a**	Reaction in CD_3CN: 24% (Solvent-free reaction 26%)	> 99:1
	(ii)	CD_3CN	Me	OTf	**13b**	**15b**	Quantitative (68% yield of **13b**) [a]	95:5
	(iii)	$(CD_3)_2SO$	Me	OTf	**13b**	**15b**	87%	> 99:1
	(iv) [a]	CD_3CN or CH_2Cl_2 [a]	CH_2Ph	OTf	**14**	**16**	Quantitative [a]	> 99:1
 **2**	(v)	No solvent	Me	I	**17a**	**19a**	(Yield = 16%) [d]	> 99:1
	(vi)	CD_3CN	Me	OTf	**17b**	**19b**	Quantitative (57% yield of **17b**) [a]	89:11
	(vii)	$(CD_3)_2SO$	Me	OTf	**17b**	**19b**	78%	> 99:1
	(viii)	CD_2Cl_2	CHPhAr [e]	OTf	**18**	**20**	93%	91:9
 **3**	(ix)	CD_3CN	Me	I	**21a**	**23a**	No products formed	-
	(x)	CD_3CN	Me	OTf	**21b**	**23b**	Quantitative [a]	7:93
	(xi)	$(CD_3)_2SO$	Me	OTf	**21b**	**23b**	76%	7:93
	(xii)	CD_2Cl_2	CHPhAr [e]	OTf	**22**	**24**	Spectra could not be interpreted	-

[a] See Supporting Information for experimental conditions employed and details of conversion calculations and yields.[44]

[b] Conversions represent the combined amount of N- and O-alkylated product formed relative to the amount added of the alkylating agent (always the limiting reagent). These were determined using integrations of appropriate signals in the ^{1}H NMR spectra. For entry (viii), the deviation from quantitative conversion was due to hydrolysis of the alkylating agent. Percentage yields (where applicable) of isolated products were determined from separate reactions run on larger scale using MeCN solvent, or with no solvent (neat reagents) for entries (i) and (v). Products **14**, **18**, **20**, **21b** and **23b** (entries (iv), (viii) and (x), respectively)) decompose upon attempted isolation, and hence no isolated yields could be obtained in these cases.

[c] The identities of the products cannot be determined directly from the ^{1}H NMR spectra. Information from other spectra is needed to establish which product is N-alkylated and which is O-alkylated, and hence to establish the N/O ratio. See main text for full details.

[d] **2** + MeI were reacted together without solvent. The product was purified prior to NMR spectral characterisation, so the conversion was not determined for this reaction. However, the low isolated yield shown above is indicative of low conversion in this reaction.

[e] Ar = *para*-tolyl.

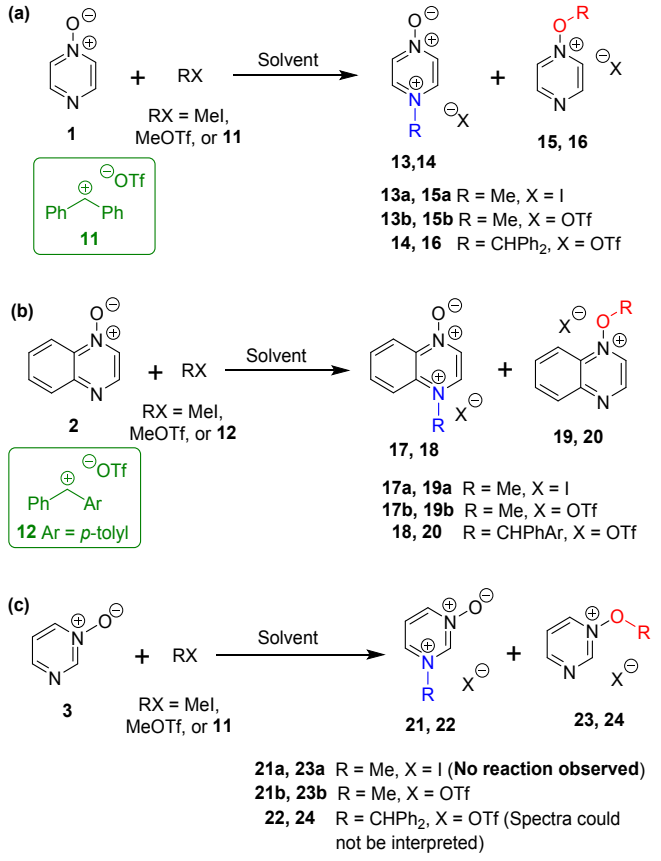
and ^{1}H-^{15}N HMBC spectra that we could not interpret,[47] containing broad and unusually-shaped signals – *i.e.* we could not detect formation of **22** or **24** (Scheme 4). We ascribe this to the very low Lewis basicity of **3**, *i.e.* the reaction of **3** + **11** is reversible, and thermodynamically disfavoured.

The reactions of **1**–**3** with MeOTf in CD_3CN yielded mixtures of O- and N-methylation products (Table 1 entries (ii), (vi), and (x)). Addition of MeOTf to $(CD_3)_2SO$ solutions of **1** and **2** resulted in formation of a single product in each case (Table 1 entries (iii) and (vii)), while the corresponding reaction of **3** gave two products (Table 1 entry (xi)).

The rates of these reactions differed greatly depending on the solvent used. Product formation was rapid for reactions in CD_3CN (i.e. complete within minutes), but was exceptionally slow in $(CD_3)_2SO$, requiring weeks for high conversions to be obtained. It is highly likely that the active methylating agent in $(CD_3)_2SO$ was the methoxysulfonium salt $[(CD_3)_2S(OMe)]OTf$,[48–50] and that this electrophile is much less reactive than MeOTf in MeCN.

Many of the initial products of the reactions of Scheme 4 and Table 1 do not survive attempts at isolation. Hence, all reactions were conducted on small scale, and the entirety of each reaction mixture

Please do not adjust margins



Scheme 4. N- and O-alkylation reactions of ambident nucleophiles **1–3**. Methylation reactions (using MeI or MeOTf) were conducted in $(CD_3)_2SO$, CD_3CN, or CH_3CN. Upon completion of reactions in CD_3CN or CH_3CN, the solvent was removed, and $(CD_3)_2SO$ was added. Benzhydrylation reactions were conducted in CD_2Cl_2.[43] See Table 1 for details of conversions and yields.

was transferred (under inert atmosphere) to a NMR tube for analysis by NMR spectroscopy. In instances in which stable, isolable products were formed, the final (stable) products were isolated from separate reactions, conducted on larger scale. The adducts of benzhydrylation of **1** and **2** are hydrolytically unstable and could not be isolated. The adduct of **2** + MeI was formed in very low conversion,[51] and the adduct of **3** + MeOTf became contaminated with multiple decomposition products;[52] hence neither adduct could be isolated in pure form. In addition, for the reactions of **1–3** with MeOTf in MeCN or CD_3CN solvent, decomposition of the minor product (detected in ^1H NMR spectra in CD_3CN) occurred upon removal of the MeCN/CD_3CN solvent under vacuum, resulting in the observation of the signals of the major product only in the ^1H NMR spectrum of the mixture upon dissolution in $(CD_3)_2SO$.[53]

In all cases shown in Table 1, it was impossible to distinguish the site of attachment of the alkyl group unambiguously using standard ^1H- or ^{13}C-based one or two-dimensional NMR techniques. That is, the identity of the product(s) in each case could not be reliably assigned as O-alkylated or N-alkylated. In the instances in which mixtures of O- and N-methylation products were obtained, product ratios could be determined using the integrations of signals in ^1H NMR spectra, but which product was favoured was not clear. The product ratios determined in this way are shown in Table 1.

In order to determine which site (N or O) of each of the ambident nucleophiles **1–3** is favoured in the alkylation reactions shown in Scheme 4 and Table 1, we made use of the indirect detection natural abundance ^1H-^{15}N HMBC NMR spectroscopic technique described above. The ^{15}N NMR chemical shifts of starting compounds **1–3** and of the observed alkylation adducts are shown in Table 2 (see pg. 6). The $\Delta(\delta_N)$ values associated with these reactions (also shown in Table 2) show the extent to which the chemical shifts of the ^{15}N nuclei of the alkylation product(s) differ from the chemical shifts of the corresponding ^{15}N nuclei in the starting materials **1–3**. As above, a negative value of $\Delta(\delta_N)$ indicates an upfield shift of the δ_N value of an ^{15}N environment upon alkylation, while a positive value indicates a downfield shift. In several instances (all described above), only one product was formed in the alkylation reactions of **1–3**, while in others, the minor product did not survive the process of removal of the MeCN or CD_3CN reaction solvent and replacement with $(CD_3)_2SO$.[53] Hence, in almost all cases, only one product could be characterized using the ^1H-^{15}N HMBC NMR technique. In the ^1H-^{15}N HMBC spectrum of the reaction of **2** + **12**, no correlations were observed to the small signals of the minor product that was shown to be present by the ^1H NMR spectrum. The only instance in which it was possible to determine the δ_N values of both the major and minor alkylation products involved methylation of **3** in $(CD_3)_2SO$ using MeOTf (Scheme 4c; through methoxysulfonium triflate).

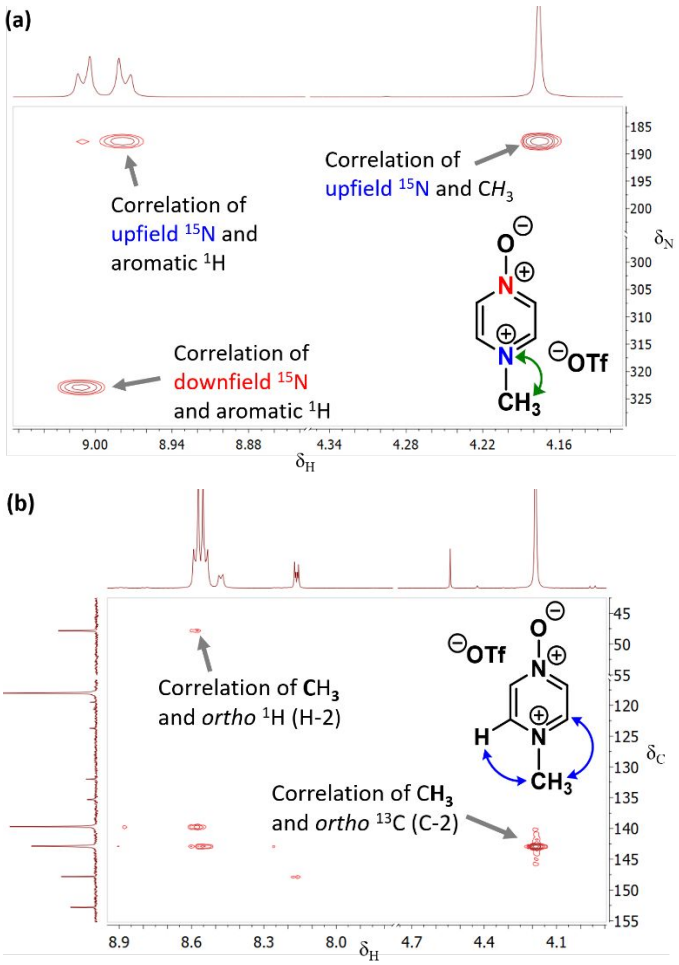
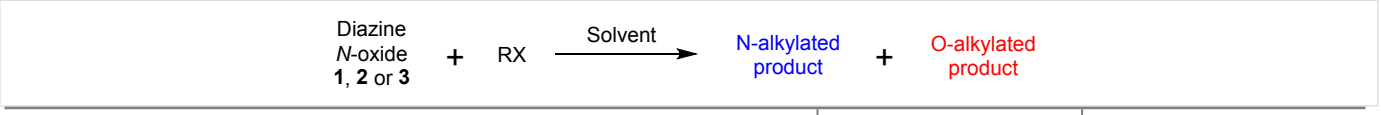
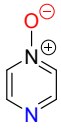
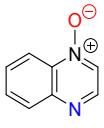
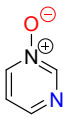


Figure 2. (a) Section of the ^1H-^{15}N HMBC NMR spectrum **of 13b** in $(CD_3)_2SO$ (from reaction of Table 2 entry (ii)) showing correlation of N-methyl ^1H signal with upfield ^{15}N signal, (b) Section of the ^1H-^{13}C HMBC NMR spectrum of **13b** in CD_3CN (from reaction of Table 2 entry (ii)) showing correlations between (i) N-methyl ^1H signal and *ortho*-^{13}C signals, and (ii) *ortho*-^1H signals and N-methyl group ^{13}C signal.

Please do not adjust margins

Table 2. δ_N and $\Delta(\delta_N)$ values associated with N- and O-alkylation reactions of diazine *N*-oxides **1**–**3** (as per Scheme 4).[a]



Diazine *N*-oxide	#	Products	R	X	Reaction solvent/ NMR Solvent [a]	δ_N of starting compound (ppm)	N-alkylation		O-alkylation	
							δ_N of product (ppm)	$\Delta(\delta_N)$ (ppm)	δ_N of product (ppm)	$\Delta(\delta_N)$ (ppm)
 **1**	(i)	**13a**, **15a**	Me	I	MeCN/ $(CD_3)_2SO$	309.3 303.9 [b]	322.3 187.1	+13.0 −116.8	Product (**15a**) not formed	
	(ii)	**13b**, **15b**	Me	OTf	MeCN/ $(CD_3)_2SO$	309.3 303.9 [b]	322.9 187.8	+13.6 −116.1	Product (**15b**) decomposed during solvent exchange	
	(iii)	**13b**, **15b**	Me	OTf	$(CD_3)_2SO$	309.3 303.9 [b]	322.9 187.7	+13.6 −116.2	Product (**15b**) not formed	
	(iv)	**14**, **16**	CH_2Ph	OTf	CD_2Cl_2	311.0 303.5	325.0 201.6	+14.0 −101.9	Product (**16**) not formed	
 **2**	(v)	**17a**, **19a**	Me	I	MeCN/ $(CD_3)_2SO$	303.2 299.3 [c,d]	314.4 178.0	+11.2 −121.3	Product (**19a**) not formed	
	(vi)	**17b**, **19b**	Me	OTf	MeCN/ $(CD_3)_2SO$	303.2 299.3 [c,d]	314.4 177.6	+11.2 −121.7	Product (**19b**) decomposed during solvent exchange	
	(vii)	**17b**, **19b**	Me	OTf	$(CD_3)_2SO$	303.2 299.3 [c,d]	314.4 177.9	+11.2 −121.4	Product (**19b**) not formed	
	(viii)	**18**, **20**	CHPhAr [e]	OTf	CD_2Cl_2	302.0 300.3	317.6 190.5	+14.4 −108.8	Signal of **20** not detected in ^1H-^{15}N HMBC	
 **3**	(ix)	**21b**, **23b**	Me	OTf	CD_3CN/ $(CD_3)_2SO$	301.3 291.7	Product (**21b**) decomposed during solvent exchange		303.4 249.4	+2.1 −42.3
	(x)	**21b**, **23b**	Me	OTf	$(CD_3)_2SO$	301.3 291.7	293.6 205.2	−7.7 −86.5	303.1 249.0	+1.8 −42.7

[a] See Supporting Information for experimental conditions employed.[45]

[b] Literature δ_N values: 309.33, 303.85 ($(CD_3)_2SO$, referenced to nitromethane at 380 ppm; equivalent to ammonia at 0 ppm).[54]

[c] These values were reported in reference 55 as δ_N −76.8 and −80.7 ppm (referenced to nitromethane at 0 ppm).

[d] The reported δ_N values for these signals was from a spectrum referenced to nitromethane at 0.0 ppm. Since our ^1H-^{15}N HMBC spectra were referenced to ammonia at 0 ppm, the literature δ_N value has been re-calculated here relative to ammonia at 0 ppm.

[e] Ar = *para*-tolyl.

The ^1H-^{15}N HMBC NMR spectra of the major or exclusive products formed in the reactions of **1** or **2** with electrophiles MeI, MeOTf, and benzhydrylium **11** and **12** (Scheme 4a and 4b) all show that the δ_N values of the upfield nitrogen nuclei are shifted upfield by over 100 ppm relative to the δ_N values of the corresponding nitrogen NMR environments in the starting materials, *i.e.* $\Delta(\delta_N) > -100$ ppm in each case (see Table 2 entries (i), (ii), (iii), (v), (vi) and (vii) for methylations and entries (iv) and (viii) for benzhydrylation reactions).[56] That the upfield signal in the ^{15}N dimension belongs the alkylated nitrogen is confirmed by the existence of a correlation in the ^1H-^{15}N HMBC NMR spectrum of this signal with the ^1H signal of the N-alkyl proton(s) (see example spectrum from the reaction of **1** + MeOTf in Fig. 2a).

In the ^1H-^{13}C HMBC NMR spectra of each of the major products of the reactions of **1** and **2**, a correlation is shown to exist between the alkyl group (aliphatic) proton(s) and the carbons *ortho* to the upfield nitrogen for all alkylation adducts (see example in Fig. 2b). A correlation between the alkyl group aliphatic carbon and the protons *ortho* to the upfield nitrogen is also evident in these spectra. The large upfield $\Delta(\delta_N)$ values and correlation data associated with the alkylation reactions of **1** and **2** are consistent with the preferential (and in some cases exclusive) occurrence of N-alkylation in these reactions.

In support of this conclusion, the $^{13}C\{^1H\}$ NMR chemical shifts of the methyl group carbon in the major products of the methylation reactions of **1** and **2** are, respectively, 44.1 and 46.6 ppm.[57] These values lie in the middle of the range of δ_C values identified in our previous work as being characteristic of N-methylation of aromatic N-heterocycles (*vide supra*).[39] The δ_C values of the minor products of these methylation reactions were, respectively, 68.9 and 70.2 ppm. These values appear in the middle of the δ_C range that is indicative of adducts of O-methylated aromatic *N*-oxides.[39,57] The δ_C values of

Please do not adjust margins

the benzhydryl group aliphatic carbons (Ar_2CH) in the products of the benzhydrylation reactions of **1** and **2** were, respectively, 77.2 and 73.2 ppm.[57] These values are characteristic of N-benzhydrylated products, based on our previous work.[39] The above data are all consistent with the conclusion that the major products formed are N-alkylation adducts **13**, **14**, **17** and **18** (Scheme 4a and 4b). These are formed in preference to O-alkylation adducts **15**, **16**, **19** and **20**.

The ^1H-^{15}N HMBC NMR spectrum of the reaction mixture produced by adding MeOTf to a $(CD_3)_2SO$ solution of **3** (Scheme 4c) showed signals for the major product at δ_N 303.1 and 249.0 ppm (Table 2, entry (x)).[58] The upfield ^{15}N NMR signal showed a correlation with the methyl group CH_3 protons, indicating that this belongs to the alkylated nitrogen. However, no correlation existed in the ^1H-^{13}C HMBC NMR spectrum for the signal of the methyl protons with the signal of the carbons *ortho* to the upfield nitrogen, nor for the signal of the methyl carbon with the signal of the protons *ortho* to upfield nitrogen. Based on the δ_N value of the upfield nitrogen signal, the δ_C value of the methyl group carbon of 70.2 ppm (characteristic of a N^+—O—CH_3 ^{13}C NMR signal of a *N*-methoxypyridinium ion),[39] and the features of the ^1H-^{13}C HMBC NMR spectrum, the spectral characteristics of the major product are very similar to those of compound **10** (the O-methylated adduct of pyridine *N*-oxide (**8**); Scheme 3b), and other aromatic *N*-oxide O-methylation adducts.[39]

We therefore conclude that the major product of this reaction is O-methylation adduct **23b** (Scheme 4c). The upfield signal (δ_N = 249.1 ppm) is assigned to the *N*—OMe nitrogen atom, and hence has a $\Delta(\delta_N)$ value of −42.7 ppm relative to the signal of the *N*-oxide nitrogen atom of **3** (at δ_N = 291.7 ppm; see Table 2 entry (x)), while the downfield signal has $\Delta(\delta_N)$ = +1.8 ppm relative to the corresponding signal of **3** (δ_N = 301.3 ppm). The upfield $\Delta(\delta_N)$ value of −42.7 ppm for this reaction is very similar to the $\Delta(\delta_N)$ values observed in formation of methoxypyridinium salts during O-methylation reactions of *N*-oxides (e.g. $\Delta(\delta_N)$ = −43.6 ppm for formation of **10** from **8** + MeOTf; Scheme 3b).[39]

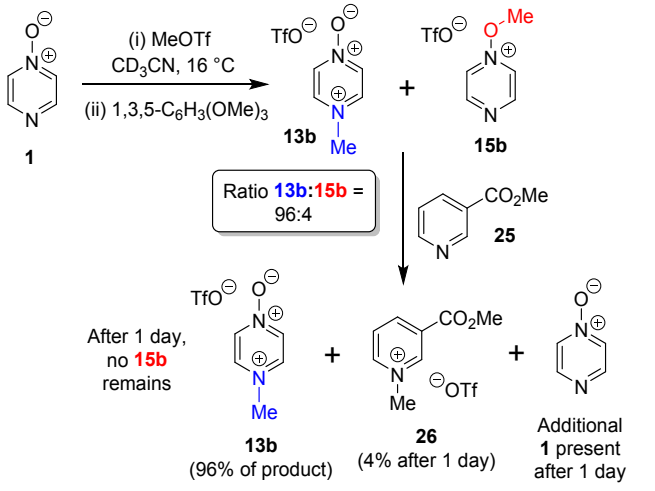
The $\Delta(\delta_N)$ value associated with formation of the minor product of the reaction of pyrimidine *N*-oxide (**3**) + $[(CD_3)_2S(OMe)]OTf$ in $(CD_3)_2SO$ is considerably larger than the $\Delta(\delta_N)$ value for O-alkylation (Table 2 entry (x); $\Delta(\delta_N)$ = −86.5 vs −42.7 ppm). In addition, the ^1H-^{13}C HMBC NMR spectrum exhibits multiple bond correlations between the N-methyl group and *ortho* aromatic ^1H and ^{13}C signals.[59] The δ_C value of the methyl group carbon of the minor product was 46.6 ppm,[57] which is characteristic of an aromatic N^+—CH_3 carbon (*vide supra*).[39] These data are consistent with the minor product being N-methylation adduct **21b** (Scheme 4c). Our spectral data on the reaction of **3** + MeOTf in CD_3CN (or MeCN) also show that **23b** is the major product formed in this solvent.[54] Although **21b** is formed in the reaction (as shown by ^1H NMR spectral analysis), it does not survive the process of solvent removal and dissolution in $(CD_3)_2SO$ (*vide supra*).

Based on the above data, we can conclude that the N- vs O-methylation ratios in the reactions of **3** with MeOTf (in CD_3CN) and $[(CD_3)_2S(OMe)]OTf$ in $(CD_3)_2SO$ are both 7:93 (in favour of O-methylation; see Table 1 entries (x) and (xi)).

Crossover Experiments

The N- vs O-alkylation ratios observed in the reactions of **1**–**3** did not change over time in the absence of perturbation. In order to establish whether or not these reactions occurred under kinetic control, we carried out several crossover experiments involving reactions of MeOTf with **1**–**3** (and of MeI with **1**) in CD_3CN followed by addition of a second nucleophile.[60] An internal standard (1,3,5-trimethoxybenzene) was added to the reaction mixture to allow the amounts of the products present to be quantified (using integrations of ^1H NMR spectral signals of the products) before and after addition of the second nucleophile, and to enable quantification of the amount of crossover product formed. Nucleophiles **7** and **25** were selected as second nucleophiles because they have been shown in separate studies to be considerably stronger Lewis bases than compounds **1**–**3**,[61] and hence are expected to out-compete **1**–**3** for any free alkylating agent present due to (i) their stronger nucleophilicity and (ii) the fact that they are present in considerable excess over **1**–**3** under the conditions of the crossover experiment.

We observed that the amount of major product formed in the methylation reactions of each of **1** and **2** remained constant with respect to the internal standard during the crossover experiments, i.e. the formation of the major product in each case is irreversible (i.e. **13a**, **13b**, and **17b** respectively). For example, the amount of **13b** formed in the reaction of **1** + MeOTf in CD_3CN at 16 °C is invariant at 96% of methylation product throughout the experiment (Scheme 5). In the reactions of **1** and **2** with MeOTf (using **25** or **7** as the second nucleophile), crossover product formed at the expense of the minor product (O-methylation adducts **15b** and **19b**) with commensurate production of starting diazine *N*-oxide (**1** or **2**). Although crossover product (**9b** or **26**) is formed from the minor products in these experiments, we conclude in each case that this is a consequence of the occurrence of an S_N2 reaction between the second nucleophile (**7** or **25**) and the minor product. If this were not the case, then repeated observations of the N/O-methylation ratios over time in alkylation reactions of **1** and **2** should show this ratio changing (to favour the major product), since formation of the major product is irreversible in each case. Consequently, we conclude that O-



Scheme 5. Crossover experiment investigating reversibility of reaction of **1** + MeOTf using 1,3,5-trimethoxybenzene as internal standard, and "crossover nucleophile" **25**. The crossover product is compound **26**.[62]

methylation of **1** and **2** are also irreversible processes in CD_3CN solvent at ambient temperatures. Thus, N-methylation of **1** and **2** are observed because they are the kinetically favoured reactions in their respective processes.

A similar crossover experiment involving the reaction of pyrimidine *N*-oxide (**3**) + MeOTf in CD_3CN (with an internal standard added) and pyrazine (**7**) as 2nd nucleophile also showed formation of crossover product **9b**. In ^1H NMR spectra of this reaction mixture recorded early in the reaction, the crossover product (**9b**) was observed to form primarily at the expense of N-methylation product **21b** (minor product of this reaction), but some O-methylation product (**23b**) was also consumed.[62] An amount of **3** formed that was commensurate with the amount of **9b** produced. After several days, further crossover product was observed to form at the expense of major product **23b**.[62] It is not clear from these experiments whether formation of **21b** and **23b** from **3** + MeOTf is reversible, i.e. whether **7** reacts with MeOTf formed by reversal of **21b** and/or **23b** to **3** + MeOTf, or whether crossover product **9b** is formed by direct S_N2 reactions of **7** with **21b** and/or **23b**.

Computational Investigations

Our experimental investigations indicate that ambident nucleophiles pyrazine *N*-oxide (**1**) and quinoxaline *N*-oxide (**2**) (with competing N and O nucleophilic sites) undergo preferential alkylation on nitrogen regardless of the nature of the alkylating agent used, i.e. *independent of whether the electrophile is hard or soft*. Ambident nucleophile pyrimidine *N*-oxide (**3**), by contrast, has been shown to undergo preferential O-methylation by MeOTf. In order to be able to understand and rationalise the outcomes of the reactions described above, high level quantum chemical calculations at the DLPNO-CCSD(T)/def2-TZVPPD/SMD(CH_3CN)//M06-2X-D3/6-311+G(d,p)/SMD(CH_3CN) level of theory were carried out to determine the relative Gibbs energies of the reactants, transition states and products of the reactions of each of compounds **1**, **3**, **7** (pyrazine), and **8** (pyridine *N*-oxide) (structures shown in Chart 1 and Scheme 3) with MeI and MeOTf.[63] The reactions of pyrimidine (**27**) and pyridine (**28**) with MeI and MeOTf were also investigated in the same manner. The computational results can be used to estimate the Gibbs energy of activation ($\Delta G^{\ddagger}$) and standard enthalpy and Gibbs energy of reaction ($\Delta_r H°$ and $\Delta_r G°$, respectively) for each process. The accuracy and predictive capability of this computational method have been verified by the close agreement of the $\Delta G^{\ddagger}$ values determined experimentally and computationally for the reaction of pyrazine *N*-oxide (**1**) with MeI (*vide infra*). The results of the computational investigations of the methylation reactions of **7**, **8**, **27** and **28** are presented in Table 3 (left side). Compounds **7**, **27** and **28** undergo N-methylation, and compound **8** undergoes O-methylation. These results allow us to see representative values of $\Delta G^{\ddagger}$, $\Delta_r H°$ and $\Delta_r G°$ for N- and O-methylation reactions in which there is no ambiguity over the site of methylation.

Unsurprisingly, the reactions involving MeOTf have systematically smaller calculated $\Delta G^{\ddagger}$ values and are more exergonic than the reactions involving MeI. The values of $\Delta G^{\ddagger}$ and $\Delta_r G°$ for methylation of **7** by MeI are very similar to the corresponding values for **27** (Table 3 entries (i) and (v)). The $\Delta G^{\ddagger}$ and $\Delta_r G°$ values for the reactions of **7** and **27** with MeOTf are also very similar (Table 3 entries (ii) and (vi)). This suggests that the nucleophilicities and Lewis basicities of **7** and **27** are very similar. The reactions involving pyridine (**28**; Table 3 entries (vii) and (viii)) are both more kinetically and thermodynamically favourable than the corresponding reactions of **7** and **27** with the two methylating agents.[64] The O-methylation reactions of **8** are more kinetically favourable than the corresponding reactions of **7** and **27**, despite being less thermodynamically favourable than those reactions (compare Table 3 entry (iii) with entries (i) and (v), and entry (iv) with entries (ii) and (vi)).

The reaction of pyrazine *N*-oxide (**1**) with MeOTf was found computationally to result in kinetically and thermodynamically preferred N-methylation (compare Table 3 entries (x) and (xii)). This calculation indicates that methylation of **1** by MeOTf is an irreversible process at room temperature (regardless of the site of methylation), in agreement with the results of our crossover experiments (see above). The relative magnitudes of $\Delta G^{\ddagger}$(N) and $\Delta G^{\ddagger}$(O) calculated for this reaction suggest that a small amount of O-methylated product (*ca.* 5 – 7%) should be produced, as is observed experimentally (N/O methylation ratio = 95:5 for reaction at 20 °C; see Table 2 entry (ii)).[65]

The reaction of **1** with MeI was also found to result in kinetically and thermodynamically preferred N-methylation (compare Table 3 entries (ix) and (xi)), which is consistent with the results of our crossover experiments. This reaction has been observed experimentally to be very slow. Only a small amount of conversion had occurred after several days, consistent with the high activation barrier found computationally (shown in Table 3) and determined through a kinetic investigation (described below). In contrast to the reaction of **1** with MeOTf (above), O-methylation of **1** by MeI was found computationally to be thermodynamically disfavoured and therefore reversible (Table 3 entry (xi)). No O-methyl adduct (**17a**) was observed experimentally for this reaction, which is consistent with kinetically disfavoured and reversible O-methylation.

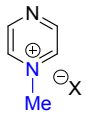
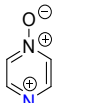
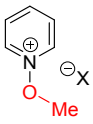
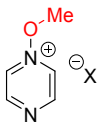
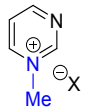
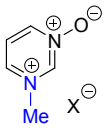
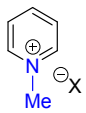
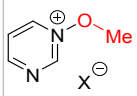
The $\Delta G^{\ddagger}$(N) and $\Delta_r G°$(N) values for N-methylation of **1** (by MeOTf or MeI) are similar to the corresponding values for diazines **7** and **27** (compare Table 3 entry (x) with entries (ii) and (vi), and entry (ix) with entries (i) and (v)). In contrast, the $\Delta G^{\ddagger}$(O) and $\Delta_r G°$(O) values for O-methylation of **1** (by MeOTf or MeI) are significantly less favourable than the corresponding reactions of *N*-oxide **8** (compare Table 3 entry (xii) with entry (iv), and entry (xi) with entry (iii)). The implication of this is that the oxygen site of **1** is deactivated relative to the oxygen site of **8**, both as a nucleophile and as a Lewis base.[66]

Our calculations on the reaction of pyrimidine *N*-oxide (**3**) with MeOTf indicate that, despite the fact that N-methylation (formation of **21b**) is thermodynamically favoured over O-methylation (formation of **23b**), the kinetically preferred process in this reaction is O-methylation (compare Table 3 entries (xiv) and (xvi)). The difference between the calculated values of $\Delta G^{\ddagger}$(N) and $\Delta G^{\ddagger}$(O) suggests that a small amount of N-methylation (*ca.* 1–3%) should occur. These results are in quite close agreement with the experimental observations – O-methylation is indeed favoured, and approximately 7% of the product formed is N-methylation adduct **21b** (in CD_3CN or $(CD_3)_2SO$; see Table 2 entries (ix) and (x))).[67] These calculations indicate that both reactions are essentially irreversible (however, see the results of our crossover experiment involving **3** + MeOTf above).[63] Our calculations on the reaction of **3** with MeI

This journal is © The Royal Society of Chemistry 20xx

Table 3. Calculated $\Delta G^{‡}$, $\Delta_r H°$ and $\Delta_r G°$ values for methylation of nucleophiles **1**, **3**, **7**, **8**, **27,** and **28** by MeI and MeOTf in CH_3CN.[a,b]



Nucleophiles with single alkylation site [c]							Ambident Nucleophiles							
#	Nu	X	Product & number	$\Delta G^{‡}$	$\Delta_r G°$	$\Delta_r H°$ [b]	#	Nu	X	Product & number	$\Delta G^{‡}$	$\Delta_r G°$	$\Delta_r H°$ [b]
(i)	**7**	I	 **9a**	+131	−21	−37	(ix)	**1**	I	 **13a**	+133	−20	−37
(ii)	**7**	OTf	**9b**	+107	−90	−90	(x)	**1**	OTf	**13b**	+108	−88	−90
(iii)	**8**	I	 **10a**	+123	−7	−24	(xi)	**1**	I	 **15a**	+140	+31	+14
(iv)	**8**	OTf	**10b**	+97	−75	−76	(xii)	**1**	OTf	**15b**	+115	−38	−38
(v)	**27**	I	 **29a**	+130	−23	−39	(xiii)	**3**	I	 **21a**	+138	+4	−13
(vi)	**27**	OTf	**29b**	+106	−91	−91	(xiv)	**3**	OTf	**21b**	+113	−64	−66
(vii)	**28**	I	 **30a**	+120	−48	−64	(xv)	**3**	I	 **23a**	+127	+38	+3
(viii)	**28**	OTf	**30b**	+96	−117	−117	(xvi)	**3**	OTf	**23b**	+103	−48	−49

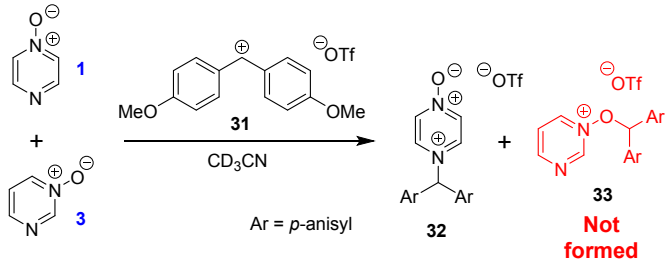
[a] Enthalpies and Gibbs energy values (in kJ mol^{-1}) were calculated at the DLPNO-CCSD(T)/def2-TZVPPD/SMD(CH3CN)//M06-2X-D3/6-311+G(d,p)/SMD(CH3CN) level of theory, with a confidence interval of ±2 kJ mol^{-1}.

[b] $\Delta_r S°$ values calculated for these reactions were similar across all reactions of MeI ($\Delta_r S°$ = −55 ± 2 J K^{-1} mol^{-1}), and across all reactions of MeOTf ($\Delta_r S°$ = −2 ± 2 J K^{-1} mol^{-1}). These data are included in Tables S1 – S3 in the Supporting Information, along with calculated $\Delta H^{‡}$ and $\Delta S^{‡}$ values for these reactions.[68]

[c] Pyrazine (**7**) and pyrimidine (**27**) clearly have two possible alkylation sites, but the sites are identical by symmetry.

indicate that both O- and N-methylation (formation of **23a** and **21a**, respectively) are reversible. O-Methylation was found to be kinetically preferred, again despite the fact that this process is less thermodynamically favourable than N-methylation (compare Table 3 entries (xiii) and (xv)). As no product formation was observed experimentally when this reaction was attempted in CD_3CN or MeCN, it is not possible to verify the applicability of these particular computational results.

The calculated Gibbs energies of activation for N- and O-methylation of pyrimidine *N*-oxide (**3**) by MeI or MeOTf, while higher than the $\Delta G^{‡}$ values for comparable reactions of similar compounds (e.g. pyrazine *N*-oxide (**1**), pyrazine (**7**), pyridine *N*-oxide (**8**) and pyridine (**27**)), are not especially different to those $\Delta G^{‡}$ values (compare Table 3 entry



Scheme 6. Competition experiment between reversible reactions of **1** and **3** with benzhydrylium ion **31**.[44]

(xiv) with entries (ii) and (vi), entry (xiii) with entries (i) and (v), entry (xvi) with entry (iv), and entry (xv) with entry (iii)). However, comparison of the $\Delta_r G°$ values for the same reactions indicates that both O- and N-methylation reactions of pyrimidine *N*-oxide (**3**) are far less thermodynamically favourable than the corresponding reactions of **1**, **7**, **8** and **27**. This computational observation has been verified experimentally through a thermodynamic competition experiment in which product **32** (derived from pyrazine *N*-oxide (**1**) in a reversible reaction) is formed to the complete exclusion of **33** (derived from pyrimidine *N*-oxide (**3**)) when **1**, **3** and benzhydrylium ion **31** are mixed in CD_3CN (Scheme 6). It seems that the O and N nucleophilic/Lewis basic sites of **3** are deactivated in a similar manner to the O site of **1**.[66]

According to our computational data, N-methylation of both **1** and **3** results in a minor shortening of the *N*-oxide N—O bond. The calculated N—O bond lengths of diazine *N*-oxides **1** and **3** and N-methyldiazinium cations **13** and **21** are, respectively, 1.27 Å, 1.29 Å, 1.25 Å and 1.27 Å.[63] O-methylation of **1** and **3** results in a lengthening of the N—O bond (to 1.36 Å for each of **15** and **23**, the O-methylated cationic derivatives of **1** and **3**).[63] O-methylation of **1** or **3** removes the favourable electrostatic interaction between N and O, and also diminishes the partial resonance of the *N*-oxide with the aromatic system, thereby removing resonance stabilisation effects that may

help to stabilise the positive charge in the product. This may contribute to making N-methylation of **1** and **3** more thermodynamically favourable than O-methylation.

Finally, for completeness, we will comment on the values of the other thermodynamic functions associated with the above reactions. Computationally determined values of $\Delta_rS°$ do not differ greatly from each other across all reactions of MeI with **1**, **3**, **7**, **8**, **27** and **28**, or across all reactions of MeOTf with the same nucleophiles, regardless of whether N- or O-methylation is occurring.[68] Across all reactions of MeI in Table 3, $\Delta_rS°$ remains constant around −55 ± 2 J K^{-1}mol^{-1}, while a value of −2 ± 2 J K^{-1}mol^{-1} was observed across the reactions of MeOTf (using 99% confidence intervals).[68] Therefore, the computational data suggest that enthalpy changes are primarily responsible for dictating the differences between the $\Delta_rG°$ values in the various reactions in Table 3. It is not possible to unambiguously ascribe the differences in $\Delta_rH°$ to specific effects, and hence we refrain from doing so.

Activation Barrier Calculations Using Marcus Theory

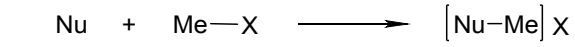
Noting the deficiencies of the HSAB principle, Mayr and co-workers have advanced Marcus theory for rationalising the outcomes of reactions of ambident nucleophiles.[4] The Marcus equation (equation 1) allows $\Delta G^{‡}$ to be separated out into its contributions from $\Delta_rG°$ (the standard Gibbs energy of reaction) and $\Delta G_0^{‡}$, the Marcus intrinsic barrier.[69–71]

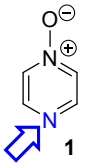
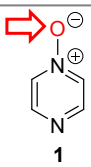
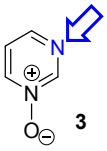
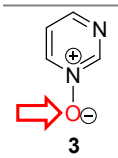
$$\Delta G^{‡} = \Delta G_0^{‡} + \frac{\Delta_r G°}{2} + \frac{(\Delta_r G°)^2}{16 \Delta G_0^{‡}} \qquad (1)$$

In reactions of ambident nucleophiles with competing sites of differing nucleophilicity, the different nucleophilic sites have different values of each of $\Delta G_0^{‡}$ and $\Delta_rG°$. Mayr and co-workers have suggested that the selectivities in such reactions can be rationalised through an appraisal of the factors that influence the values of the two parameters in the Marcus equation ($\Delta G_0^{‡}$ and $\Delta_rG°$).[4] They have employed this approach to qualitatively rationalise the outcomes of reactions of a variety of ambident nucleophiles.[4,72] In order to build up a more comprehensive understanding of the factors that influence selectivity in reactions of **1**–**3**, we have calculated values of $\Delta G_0^{‡}$ and $\Delta_rG°$ for these reactions, and used them to construct values of the activation barriers ($\Delta G^{‡}$) using the Marcus equation.

Using the procedure described in detail in the Supporting Information,[73] values of the intrinsic barrier ($\Delta G_0^{‡}$) were calculated for each of the reactions of compounds **1** and **3** with MeI and MeOTf. The $\Delta G_0^{‡}$ values for reactions of **1** and **3** are shown in Table 4.[74] It is noteworthy that, for both ambident nucleophiles **1** and **3**, the intrinsic barrier for methyl transfer to oxygen ($\Delta G_0^{‡}$(O)) is lower than that for methylation of nitrogen ($\Delta G_0^{‡}$(N)) – e.g. compare Table 4 entries (iii) and (i), and entries (vii) and (v). Hoz and co-workers previously established through computational investigations that the $\Delta G_0^{‡}$ values associated with reactions of nucleophiles centred on 2nd row elements depend on the identity of the element at the nucleophilic site, with $\Delta G_0^{‡}$ decreasing in the order C > N > O > F, i.e. from left to right across the periodic table.[75] The lower intrinsic barriers (intrinsic preference) for O-alkylation over N-alkylation we observe for **1** and **3** are in line with this general trend.

Table 4. Values of intrinsic barriers ($\Delta G_0^{‡}$) and derived values of $\Delta G^{‡}$ for methylation reactions of nucleophiles **1**, **3**, **7**, **8**, **27**, and **28** in CH_3CN, calculated using the Marcus equation (equation 1) using values of $\Delta_rG°$ from Table 3 (reproduced here).[a,b,c]



Nucleophile	#	X	$\Delta G_0^{‡}$	$\Delta_rG°$	DFT $\Delta G^{‡}$	Marcus $\Delta G^{‡}$
 **1**	(i)	OTf	+149.5	−88	+108.0	+108.7
	(ii)	I	+144.0	−20	+133.0	+134.2
 **1**	(iii)	OTf	+132.5	−38	+115.0	+114.3
	(iv)	I	+127.0	+31	+140.0	+143.0
 **3**	(v)	OTf	+145.0	−64	+113.0	+114.8
	(vi)	I	+139.5	+4	+138.0	+141.5
 **3**	(vii)	OTf	+124.0	−48	+103.0	+101.2
	(viii)	I	+118.5	+21	+127.0	+129.2

[a] The site of methylation of each nucleophile is indicated by an arrow. The Gibbs energy values have units of kJ mol^{-1} (confidence interval ±2 kJ mol^{-1}).

[b] $\Delta_rG°$ and $\Delta G^{‡}$ (DFT $\Delta G^{‡}$) values here are reproduced from Table 3.

Substitution of the calculated $\Delta G_0^{‡}$ values into equation 1 (the Marcus equation) along with the values of $\Delta_rG°$ calculated as described above (Table 3 and associated discussion; these $\Delta_rG°$ values are reproduced in Table 4 to aid the understanding of the reader) allows values of $\Delta G^{‡}$ to be calculated using the Marcus equation. Comparison of the $\Delta G^{‡}$ values obtained using the Marcus equation (shown in Marcus $\Delta G^{‡}$ column in Table 4) with the $\Delta G^{‡}$ values directly calculated as described above (values from Table 3, labelled DFT $\Delta G^{‡}$, are reproduced in Table 4) shows a close correspondence between the two methods. Importantly, the experimentally observed N vs. O selectivities for the reactions of the ambident nucleophiles **1** and **3** are reproduced quite closely by both methods of calculation.[18] Analysing how the factors that contribute to the Gibbs energy of activation for a reaction influence its magnitude (i.e. how the interplay between $\Delta G_0^{‡}$ and $\Delta_rG°$ influences $\Delta G^{‡}$) provides a very useful means of understanding the origins of the differences between the rates of different reactions. Nowhere is this more apposite than in understanding which nucleophilic site of an ambident nucleophile is kinetically preferred. A full analysis of this kind for the reactions of **1** and **3** will be described in detail below.

The applicability of Marcus theory has been challenged in recent years,[76] and alternatives have been suggested.[77,78] However, such alternatives also incorporate in some manner an intrinsic barrier or a proxy thereof. In addition to using the Marcus equation, we have

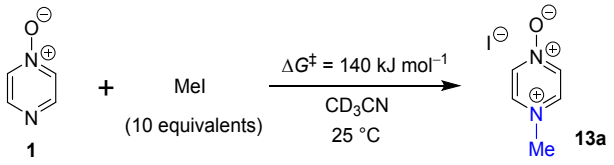
This journal is © The Royal Society of Chemistry 20xx

also used an adaptation of the Zhu equation (see the Supporting Information)[79] to calculate $\Delta G^{\ddagger}$ values for the methylation reactions of nucleophiles **1** and **3**. The $\Delta G^{\ddagger}$ values calculated using the adapted Zhu equation are very similar to the values calculated using equation 1 (see Table S5 in the Supporting Information).[73]

The experimentally observed ratio of N- to O-methylation for the reaction of **1** + MeOTf was 95:5 (Table 2). Direct calculation of the $\Delta G^{\ddagger}$ values at the DLPNO-CCSD(T)/def2-TZVPPD/SMD(CH_3CN)//M06-2X-D3/6-311+G(d,p)/SMD (CH_3CN)] level of theory indicated a N/O ratio of 94:6 for this reaction, while calculation of the N/O ratio using the Marcus equation gave a ratio of 90:10 (compare Table 4 entries (i) and (iii)). Use of the Zhu equation gave a N/O ratio of 96:4.[73] The experimentally observed ratio of N- to O-methylation for the reaction of **3** + MeOTf was 7:93. Our calculations indicated a ratio of 2:98 for this reaction, while calculation of the N/O ratio using the Marcus equation gave a ratio of 0.4 : 99.6, (compare Table 4 entries (v) and (vii)) and calculation using the Zhu equation gave a ratio of 0.5 : 99.5.[73] That the experimental selectivities (in N- vs. O-methylations of **1** and **3** by MeOTf) are reproduced quite closely using the Marcus and Zhu equations[73] and direct computation indicates that these methods are highly useful in understanding the factors that control Gibbs energies of activation in nucleophilic substitution reactions.

Experimental Verification of Accuracy of Calculated $\Delta G^{\ddagger}$

In order to verify the applicability of the computational methods discussed above to determine the magnitudes of activation barriers, we conducted a kinetic investigation on the reaction of pyrazine *N*-oxide (**1**) with MeI in CD_3CN at 25 °C using ^{1}H NMR spectroscopy to determine the concentrations of the reactants and product (**13a**). The experiment was conducted under pseudo-first order conditions, with MeI present in ten-fold excess over **1**. Using the method described in detail in the Supporting Information,[80] we determined an approximate $\Delta G^{\ddagger}$ value for this reaction of 1.4×10^2 kJ mol^{-1}. This value is within 5% of the $\Delta G^{\ddagger}$ values predicted for this reaction using the Marcus equation (134.2 kJ mol^{-1}), and using direct application of the DLPNO-CCSD(T)/def2-TZVPPD/SMD(CH_3CN)//M06-2X-D3/6-311+G(d,p)/SMD] method (133 kJ mol^{-1}). This striking agreement between computational theory and experiment demonstrates that these computational methods are capable of modelling kinetic phenomena of this type rather accurately.



1 13a

Scheme 7. The reaction of **1** + MeI in CD_3CN at 25 °C under pseudo-first order conditions (excess MeI) was monitored by ^{1}H NMR spectroscopy to enable determination of an approximate $\Delta G^{\ddagger}$ value for the reaction at 25 °C.

Discussion

Rationalisation of Experimental N vs O Selectivities

The kinetic preference of compound pyrazine *N*-oxide (**1**) for N-methylation by soft electrophile MeI (forming compound **13a**) and by hard electrophile MeOTf (forming compound **13b**) has been demonstrated experimentally and computationally. The alkylation reactions of quinoxaline *N*-oxide (**2**) by MeI, MeOTf and benzhydrylium triflates (**11** or **12**) and of **1** by **11** or **12** are all also almost certainly irreversible, and all yield N-alkylated products preferentially or exclusively. The reaction of pyrimidine *N*-oxide (**3**) + MeOTf gives O-methylated product (**23b**) predominantly, and our computational investigations indicate that this is due to the kinetic favourability of formation of **23b**. Although no product formation is observed in the reaction of **3** + soft electrophile MeI (due to the formation of products **21a** and **23a** being thermodynamically disfavoured and hence reversible), our computational results indicate that O-methylation (formation of **23a**) is the kinetically favoured process in this reaction (see Table 4 entries (vi) and (viii)).

It is evident from these results that each nucleophile exhibits a preferred site of alkylation *which is independent of the nature of the electrophile used* (N for **1** and **2**, and O for **3**), *i.e.* these outcomes cannot be dictated by hard/soft acid/base interactions. A fundamentally different set of factors must dictate the observed selectivities in these reactions. We discuss an alternative rationale to account for these observations later in this article.

Although the above evidence clearly shows that the HSAB principle does not apply in this set of reactions, and thereby renders unnecessary the identification of which nucleophilic site of each of **1** – **3** is "harder" and which is "softer", it is nonetheless appropriate at this point to discuss the difficulty and ambiguity inherent in attempts at such identifications. The features that are employed to determine whether a reactant is hard or soft are charge (charge density), size, polarizability and electronegativity.[2a,b,g,18b,c] For hard bases, the donor atom is typically negatively charged and/or has a local excess of electron density, and is of small size, low polarizability and high electronegativity. For soft bases, the donor atom typically does not bear a formal negative charge and exhibits low negative charge density, and is of large size, high polarizability and low electronegativity. Derivation of functions that reliably indicate the "local hardness" and "local softness" of sites in a molecule (such as an ambident nucleophile) has proved a difficult endeavour.[15] At present, such approaches cannot be applied without ambiguity.

On the basis that oxygen is more electronegative than nitrogen, one could perhaps anticipate that the oxygen site of a diazine *N*-oxide such as **1** – **3** should be harder than the nitrogen site. However, although there is a formal negative charge on the *N*-oxide oxygen atoms in these compounds, it is not clear which nucleophilic site in each ambident nucleophile should have the highest negative charge density, thereby potentially complicating the issue. To probe this question, we calculated the charge distribution for the ambident *N*-oxides with a variety of methods (ChelpG, Merz–Singh–Kollman, natural bond order (NBO), and atoms in molecules (AIM)),[81] but found that there was no uniform agreement between methods on which site bears the highest negative charge density in compounds **1** and **3**. Full details of this are given in the Supporting Information.[81]

We now present an alternative rationale, based on Marcus theory, to explain these results (see equation 1 above). In the following discussion, the intrinsic barriers for alkylation at oxygen and nitrogen are referred to, respectively, as $\Delta G_0^{\ddagger}$(O) and $\Delta G_0^{\ddagger}$(N). The standard Gibbs energies of reaction for O- and N-alkylation are referred to, respectively, as $\Delta_r G°$(O) and $\Delta_r G°$(N).

Although O-methylation is intrinsically preferred over N-methylation (for diazine *N*-oxides, and in general; *vide supra*),[75] in reactions of **1** and **2**, the intrinsic preference for O-alkylation is modest. $\Delta G_0^{\ddagger}$(O) is calculated to be only 17 kJ mol^{-1} lower than $\Delta G_0^{\ddagger}$(N) for the reactions of **1** with MeI or MeOTf (Table 4 entry (i) vs. (iii), and entry (ii) vs. (iv)). The $\Delta_r G°$(N) values for these reactions are substantially more favourable than the corresponding $\Delta_r G°$(O) values. Consequently, the very favourable contribution of $\Delta_r G°$(N) to $\Delta G^{\ddagger}$(N) supersedes the favourable contribution of $\Delta G_0^{\ddagger}$(O) to $\Delta G^{\ddagger}$(O), such that $\Delta G^{\ddagger}$(N) is much lower than $\Delta G^{\ddagger}$(O) for alkylations of **1** and **2**. That is, the intrinsic favourability of O-alkylation is outweighed by the thermodynamic favourability of N-alkylation, so in these irreversible reactions, N-alkylation is kinetically preferred.[82]

In the reaction of pyrimidine *N*-oxide (**3**) with MeOTf, the value of $\Delta_r G°$(N) is much less favourable with respect to $\Delta_r G°$(O) than is the case for the corresponding reaction of pyrazine *N*-oxide (**1**). $\Delta G_0^{\ddagger}$(O) is calculated to be 21 kJ mol^{-1} lower than $\Delta G_0^{\ddagger}$(N) for both MeOTf and MeI (compare Table 4 entry (vii) with entry (v), and entry (viii) with entry (vi)), so O-methylation of **3** is intrinsically preferred. Since the thermodynamic favourability of N-methylation of **3** is diminished (relative to the corresponding reactions of **1**), and O-methylation is intrinsically favoured, $\Delta G^{\ddagger}$(O) is lower than $\Delta G^{\ddagger}$(N), and hence O-methylation of **3** is the kinetically dominant reaction. Instances in which N-alkylation is likely to have been "deactivated" due to steric interactions, resulting in preferential O-alkylation, have been reported previously.[4,22b,c,f,g,31] In this case, it seems likely that the free nitrogen Lewis basic site of **3** is deactivated due to an electronic effect. This Lewis basic site is connected through a network of π-bonds to an *N*-oxide group in a *meta* position relative to it, which may act as an electron withdrawing group, thereby diminishing the Lewis basicity (electron donor capacity) of the free nitrogen atom.

The reaction of **3** with MeI was calculated to be thermodynamically unfavourable ($\Delta_r G° > 0$ for both O- and N-methylation by MeI), and therefore reversible. This is consistent with our experimental observation that no product was formed in this reaction. However, our calculations do indicate that O-methylation (formation of **23a**) is kinetically favoured over N-methylation. A similar rationale to that presented above for the reaction of **3** + MeOTf applies in this case – *i.e.* O-methylation is intrinsically preferred ($\Delta G_0^{\ddagger}$(O) < $\Delta G_0^{\ddagger}$(N)) and the thermodynamic advantage of N-methylation over O-methylation is small, and consequently O-methylation is the kinetically favoured process (see Table 4 entries (vi) and (viii)).

As discussed above, the $\Delta_r G°$ values calculated for N- and O-methylations of **3** by both MeI and MeOTf are much less favourable than the $\Delta_r G°$ values of methylation reactions of other, similar compounds (e.g. **1**, **7**, **8** and **27**; *vide supra*). In the context of our analysis based on the Marcus equation, we can make use of this information to rationalise the relatively high $\Delta G^{\ddagger}$(O) and $\Delta G^{\ddagger}$(N) values calculated for the methylation reactions of **3**. The less favourable $\Delta_r G°$ values for O- and N-methylations of **3** influence the magnitudes of the $\Delta G^{\ddagger}$ values for these reactions, causing them to be higher than the $\Delta G^{\ddagger}$ values of reactions of similar nucleophiles.

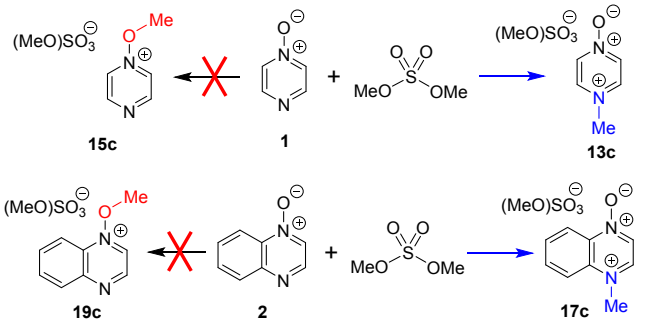
As is described in detail in the Supporting Information,[73] operationally, the value of the intrinsic barrier ($\Delta G_0^{\ddagger}$) for a reaction is accessed as the average of two identity reactions. Since there is no leaving group formed in the addition of a nucleophile to carbenium ions such as **11** and **12** (structures in Scheme 4 above), only one identity reaction of the required two can be identified to model such processes using Marcus theory. Hence, the straightforward method described in the Supporting Information[73] for accessing values of intrinsic barriers cannot be employed for reactions involving carbenium ions. Alternative methods for estimating the magnitudes of the intrinsic barriers for such reactions or analogues thereof have been reported,[83] but these do not allow quantitative determinations of the type performed above for reactions involving electrophiles from which leaving groups become cleaved. Hence only a qualitative appraisal of the outcomes of the reactions of **1** and **2** with benzhydrylium ions is possible, which we give below.

We consider that the observation of strongly preferred or exclusive N-benzhydrylation of nucleophiles pyrazine *N*-oxide (**1**) and quinoxaline *N*-oxide (**2**) in their reactions with benzhydrylium ions (**11** or **12**) arises as a consequence of the same factors that dictate the outcomes of the reactions of these nucleophiles with MeI or MeOTf. That is, in each case, O-benzhydrylation is intrinsically favoured ($\Delta G_0^{\ddagger}$(O) is smaller than $\Delta G_0^{\ddagger}$(N)) but the influence of $\Delta_r G°$(N) on $\Delta G^{\ddagger}$(N) outweighs the influence of $\Delta G_0^{\ddagger}$(O) on $\Delta G^{\ddagger}$(O), and consequently N-benzhydrylation is the kinetically preferred process. As discussed above, it was not possible to determine what occurred in the reaction of **3** + benzhydrylium ion **11**, so further comment on this is not warranted.

Literature Examples of N vs. O alkylation

We have noted in passing above that, due to the ambiguity that has up until now been inherent in determining which product is formed predominantly in reactions of ambident nucleophiles containing N and O nucleophilic sites, there exist notable cases in the literature in which the products of such reactions may have been misidentified.[8,9,84]

Comparison of the ^{1}H NMR spectrum of N-methylated product **13b** (from reactions of MeOTf with **1**; Scheme 4a) with the ^{1}H NMR spectra assigned to O-methylation adduct **15c** (Scheme 8) in reference 10 shows that the spectra are essentially identical. A similar observation can also be made on comparison of the ^{1}H NMR spectrum of N-methylated product **17b** (from **2** + MeOTf; Scheme 4b) and that assigned to O-methylated adduct **19c** in reference 7. We have identified a distinct set of signals belonging to the O-methylated adducts **15b** and **19b** that appear at different chemical shifts to the



Scheme 8. Reactions of compounds **1** and **2** with dimethylsulfate have been reported to give O-methylated products **15c** and **19c**.[7] Our data indicate that N-methylated adducts **13c** and **17c** are likely to be the major products.

This journal is © The Royal Society of Chemistry 20xx

N-methylated adducts **13b** and **17b** (*vide supra*). Furthermore, the ^{13}C NMR chemical shifts reported for the methyl group carbons (either N—CH_3 or O—CH_3) of the products are 47.2 and 44.5 ppm, respectively.[7] These δ_C values are indicative of formation of N-methylation products **13c** and **17c** (*vide supra*). Hence, our data indicate that it is highly unlikely that **1** and **2** undergo preferential O-methylation in reactions with dimethylsulfate, a close analogue of MeOTf. The methodology reported in reference 7 was predicated on the use of N-methoxypyridinium salts. That this otherwise highly successful methodology did not work for these compounds can be explained by the fact that N-methylated compounds **13c** and **17c** were almost certainly employed rather than the intended O-methylated compounds **15c** and **19c**. Problems of this type are illustrative of the need for a much more rigorous understanding of the factors that dictate the outcomes in reactions of ambident nucleophiles such as diazine *N*-oxides.

Conclusions

If one must verify on a case-by-case basis whether the predictive capabilities of a theory apply or not, then those predictive capabilities must be seriously called into question. For this reason, the continued use of the HSAB principle in rationalising the selectivities of ambident reactants in research articles and undergraduate courses and textbooks should be ceased. It appears to us that the approach of Mayr and co-workers, based around Marcus theory, is able to account for the behaviour of ambident reactants in a manner in which the HSAB principle cannot. We hope through this study to have contributed to a more general understanding of ambident reactivity, to have developed upon the approach of Mayr and co-workers to show that it can be applied to semi-quantitatively rationalise product ratios in reactions of ambident nucleophiles, and to have demonstrated the utility of ^{1}H-^{15}N HMBC NMR spectroscopy in establishing the site of attachment in reactions of nitrogen-containing compounds.

In the cases we have investigated here, calculation of $\Delta G^{‡}$ values using the equations of Marcus or Zhu yields values that reproduce closely the experimental N/O methylation ratios for reactions of ambident nucleophiles pyrazine *N*-oxide (**1**) and pyrimidine *N*-oxide (**3**). Based on this, it is reasonable to expect that calculations based on Marcus theory will allow semi-quantitative predictions of the nucleophilic site-selectivities in reactions of other ambident nucleophiles – not just those involving competition between N and O nucleophilic sites. The close agreement between the reaction selectivities determined experimentally and those calculated using the Marcus and Zhu equations (see Table 4 and associated discussion) is demonstrative of the utility of the concept of the intrinsic barrier.

The intrinsic barrier ($\Delta G_0^{‡}$) associated with an alkylation reaction of a nucleophile can be considered a property of the compounds involved in the reaction. The interplay between this quantity and the thermodynamic favourability of the reaction (quantified through $\Delta_r G°$) dictates the magnitude of the activation barrier for the reaction ($\Delta G^{‡}$). Having established herein a computational method that stands up to the stern test posed by modelling of the disparate behaviour of diazine *N*-oxides **1** and **3**, we intend in future publications to determine the magnitudes of intrinsic barriers for reactions of a wide variety of other nucleophiles, and hence establish systematic trends in intrinsic barriers (developing upon the work of Hoz).[75] This will allow the factors that control intrinsic barriers to be understood, and hence deepen our understanding of activation barriers in general.

Details on Computational Methodology

The conformational space for each structure was explored with the OPLS-2005 force field[85] and a modified Monte Carlo search algorithm implemented in Macromodel.[86] An energy cut-off of 84 kJ mol^{-1} was employed for the conformational analysis, and structures with heavy-atom root-mean-square deviations (RMSD) up to 0.5 Å after the force field optimizations where considered to be the same conformer. All remaining structures were subsequently optimized with the dispersion-corrected M06-2X functional[87] with Grimme's dispersion correction D3 (zero-damping),[88] the triple-ζ basis set 6-311+G(d,p), and SMD solvation model[89] for acetonitrile. An ultrafine grid was used throughout this study for the numerical integration of the density. Vibrational analysis verified that each structure was a minimum or a transition state and for the latter, following the intrinsic reaction coordinates (IRC) confirmed that all transition states connected the corresponding reactants and products on the potential energy surface. Thermal corrections were obtained from unscaled harmonic vibrational frequencies at the same level of theory for a standard state of 1 mol L^{-1} and 298.15 K. Entropic contributions to free energies were obtained from partition functions evaluated with Grimme's quasi-harmonic approximation.[90] This method employs the free-rotor approximation for all frequencies below 100 cm^{-1}, the rigid-rotor-harmonic-oscillator (RRHO) approximation for all frequencies above 100 cm^{-1}, and a damping function to interpolate between the two expressions. Similar results were obtained from partition functions evaluated with Cramer's and Truhlar's quasiharmonic approximation.[91] This method uses the same approximations as the usual harmonic oscillator approximation, except that all vibrational frequencies lower than 100 cm^{-1} are set equal to 100 cm^{-1}. Electronic energies were subsequently obtained from single point calculations of the M06-2X-D3 geometries employing Neese's domain-based local pair-natural orbital (DLPNO) approach to the CCSD(T) method [DLPNO-CCSD(T)] with the default normalPNO settings,[92–94] the triple-ζ def2-TZVPPD [95,96] in combination with the corresponding auxiliary basis set[97] and the SMD continuum model for acetonitrile.[89] All density functional theory calculations were performed with Gaussian 16,[98] while the DLPNO-CCSD(T) calculations were performed with ORCA 4.[99]

Acknowledgements

This work was undertaken using equipment provided by Science Foundation Ireland though a research infrastructure award for process flow spectroscopy (ProSpect) (grant: SFI 15/RI/3221) and as part of the Synthesis and Solid State Pharmaceutical Centre supported by Science Foundation Ireland (grant: SFI SSPC2 12/RC/2275). K.J.S. would like to thank the Irish Research Council for provision of a GOIPG Scholarship to fund his research (IRC

GOIPG/2018/1517). Support from the Fonds der Chemischen Industrie (Liebig scholarship to M.B.) and the University of Cologne within the excellence initiative is gratefully acknowledged. We gratefully acknowledge the Regional Computing Center of the University of Cologne for providing computing time in the DFG-funded High-Performance Computing (HPC) System CHEOPS as well as for their support, the excellent analytical services provided in the School of Chemistry and ABCRF in UCC, Prof. Justin Holmes and research group for access to an inert atmosphere glove box, Dr. Denis Lynch for assistance with NMR spectroscopy, Mick O'Shea for HRMS data, and Prof. Eoghan McGarrigle (University College Dublin) for helpful discussion.

Conflicts of interest

There are no conflicts to declare.

Notes and references

1 (a) J. Clayden, N. Greeves and S. Warren, *Organic Chemistry*, 2nd edition, Oxford University Press, New York, 2012, pp 355–357, 453–454, 506–509, 590, 658; (b) E. V. Anslyn and D. A. Dougherty, *Modern Physical Organic Chemistry,* University Science Books, Sausalito, 2006, pp 288–292, 567–568; (c) M. B. Smith, *March's Advanced Organic Chemistry,* 7th edition, Wiley, Hoboken, 2013, pp 446–450.

2 (a) R. G. Pearson, *J. Am. Chem. Soc.* 1963, **85**, 3533; (b) R. G. Pearson, *Science* 1966, **151**, 172; (c) R. G. Pearson and J. Songstad, *J. Am. Chem. Soc*. 1967, **89**, 1827; (d) R. G. Pearson, *J. Chem. Educ.* 1968, **45**, 581; (e) R. G. Pearson, *J. Chem. Educ*. 1968, **45**, 643; (f) R. G. Pearson, *Inorg. Chim. Acta* 1995, **240**, 93; (g) R. G. Parr and R. G. Pearson, *J. Am. Chem. Soc.* 1983, **105**, 7512.

3 (a) G. Klopman, *J. Am. Chem. Soc*. 1968, **90**, 223; (b) L. Salem, *J. Am. Chem. Soc*. 1968, **90**, 543; (c) T.-L. Ho, *Chem. Rev*. 1975, **75**, 1.

4 H. Mayr, M. Breugst and A. R. Ofial, *Angew. Chem. Int. Ed.* 2011, **50**, 6470.

5 For selected recent examples, see: (a) S. Maiti and P. Mal, *J. Org. Chem*. 2018, **83**, 1340; (b) S. Maiti, T. Alam and P. Mal, *Asian J. Org. Chem*. 2018, **7**, 715; (c) Y.-G. Wang and E. C. Barnes, *ACS Omega* 2018, **3**, 4557; (d) A. Burmudžija, S. Marković, J. Muškinja, A. Pejović and J. Tošović, *Reac. Kinet. Mech. Cat.* 2018, **123**, 201; (e) S. Yaragorla, A. Pareek and R. Dada, *Tetrahedron Lett.* 2017, **58**, 4642 (f) C. Slawik, C. Rickmeyer, M. Brehm, A. Böhme and G. Schürmann, *Environ. Sci. Technol*. 2017, **51**, 4018.

6 Y.-G. Wang, E. C. Barnes, S. Kaya and V. Sharma, *J. Comput. Chem.* 2019, **40**, 2761.

7 X. Ma, H. Dang, J. A. Rose, P. Rablen and S. B. Herzon, *J. Am. Chem. Soc.* 2017, **139**, 5998.

8 D. Demberelnyamba, B. K. Shin and H. Lee, *Chem. Commun.* 2002, 1538. In this paper on amide-derived ionic liquids, N-alkylation of an amide upon refluxing in acetonitrile is reported.

9 J. Yang, Q. Zhang, L. Zhu, S. Zhang, J. Li and X. Zhang, *Chem. Mater.* 2007, **19**, 2544. In this paper on amide-derived ionic liquids, N-alkylation of ε-caprolactam by alkyl tosylates and mesylates in acetonitrile at 80 °C is reported.

10 P. Cmoch, *Magn. Reson. Chem.* 2003, **41**, 693.

11 M. V. Jovanovic, *Heterocycles* 1985, **23**, 2299.

12 Assignment of N-methylated pyrazine product structures made on the basis of the results of chemical derivatisations: (a) J. K. Landquist *J. Chem. Soc.* 1953, 2816; (b) A. Ohta, M. Matsunaga, N. Iwata and T. Watanabe, *Heterocycles* 1977, **8**, 351; (c) C. F. Koelsch and W. H. Gumprecht, *J. Org. Chem.* 1958, 23, 1603.

13 R. Głaszczka, J. Jaźwiński, *J. Mol. Struct*. 2014, **1061**, 150.

14 (a) M. Breugst, T. Tokuyasu and H. Mayr, *J. Org. Chem.* 2010, **75**, 5250; (b) M. Breugst and H. Mayr, *J. Am. Chem. Soc.* 2010, **132**, 15380.

15 (a) F. H. Zadeh, P. Fuentealba, C. Cárdenas and P. W. Ayers *Phys. Chem. Chem. Phys.* 2014, **16**, 6019. See also references therein; (b) M. Torrent-Sucarrat, F. De Proft, P. Geerlings, and P.W. Ayers, *Chem. Eur. J.* 2008, **14**, 8652, and references therein.

16 J. M. Gonzales, W. D. Allen, H. F. Schaefer III, *J. Phys. Chem. A* 2005, **109**, 10613.

17 (a) P. W. Ayers, *Faraday Discuss*. 2007, **135**, 161; (b) P. W. Ayers and C. Cárdenas, *J. Chem. Phys.* 2013, **138**, 181106.

18 (a) P. W. Ayers, *J. Chem. Phys.* 2005**, 122**, 141102; (b) C. Cárdenas and P. W. Ayers, *Phys. Chem. Chem. Phys.* 2013, **15**, 13959; (c) P. W. Ayers, R. G. Parr and R. G. Pearson, *J. Chem. Phys.* 2006, **124**, 194107; (d) P. K. Chattaraj, P. W. Ayers and J. Melin *Phys. Chem. Chem. Phys.* 2007, **9**, 3853.

19 Amides: (a) Z.-J. Chen, H.-W. Xi, K. H. Lim and J.-M. Lee, *Angew. Chem. Int. Ed.* 2013, **52**, 13392; (b) T. Nanjo, E. C. de Lucca Jr. and M. C. White, *J. Am. Chem.* Soc. 2017, **139**, 14586 (c) H.-G. Cheng, M. Pu, G. Kundu and F. Schoenebeck, *Org.Lett.* 2020, **22**, 331.

20 2-Pyridone and 4-pyridone: B. Feng, Y. Li, H. Li, X. Zhang, H. Xie, H. Cao, L. Yu and Q. Xu, *J. Org. Chem.* 2018, **83**, 6769.

21 Amide anions: (a) See ref. 17a; (b) See ref. 19b.

22 Pyridone or quinolone anions: (a) See ref. 17b; (b) G. C. Hopkins, J. P. Jonak, H. J. Minnemeyer and H. Tieckelmann, *J. Org. Chem.*, 1967, **32**, 4040; (c) K. Pissinate, A. D. Villela, V. Rodrigues, B. C. Giacobbo, E. S. Grams, B. L. Abbadi, R. V. Trindade, L. R. Nery, C. D. Bonan, D. F. Back, M. M. Campos, L. A. Basso, D. S. Santos and P. Machado, *ACS Med. Chem. Lett.*, 2016, **7**, 235.

23 Imide anions: (a) L. Z. Avila, S. H. Loo and J. W. Frost, *J. Am. Chem. Soc.*, 1987, **109**, 6758; (b) A. Arévalo, S. Ovando-Segovia, M. Flores-Alamo and J. J. Garćia, *Organometallics*, 2013, **32**, 2939.

24 (a) T. H. Koch, R. J. Sluski and R. H. Moseley, *J. Am. Chem. Soc.*, 1973, **95**, 3957.; (b) D. R. Anderson, J. S. Keute, T. H. Koch and R. H. Moseley, *J. Am. Chem. Soc.*, 1977, **99**, 6332. O-alkylation is observed for silver salts of imide anions; this is ascribed to blocking of the nitrogen site due to coordination to silver in references 4 and 17a.

25 Uracil anions: (a) See ref. 9c; (b) Y.-G. Wang and E. C. Barnes, *J. Phys. Chem. A*, 2017, **121**, 8866.

26 Aryl diazoacetate anions: N. Kornblum, R. A. Smiley, R. K. Blackwood and D. C. Iffland, *J. Am. Chem. Soc.*, 1955, **77**, 6269.

27 Nitrite ion: (a) A. A. Tishkov, U. Schmidhammer, S. Roth, E. Riedle and H. Mayr, *Angew. Chem., Int. Ed.*, 2005, **44**, 4623; (b) See ref. 26.

28 Cyanate ion: See reference 4 and references therein.

29 O-alkylation of anions of 2-methylquinolin-4-ols: E. Pitta, M. K. Rogacki, O. Balabon, S. Huss, F. Cunningham, E. M. Lopez-Roman, J. Joossens, K. Augustyns, L. Ballell, R. H. Bates and P. Van der Veken, *J. Med. Chem.*, 2016, **59**, 6709.

30 Oximate anions: S. G. Smith and M. P. Hanson, *J. Org. Chem*, 1971, **36**, 1931.

31 Anions of quinolin-4-ols, quinazolin-4-ols and 1,5-naphthyrid-4-ols: E. Pitta, O. Balabon, M. K. Rogacki, J. Gómez, F. Cunningham, J. Joosens, K. Augustyns, P. van der Veken and R. Bates, *Eur. J. Med. Chem.*, 2017, **125**, 890.

32 Numerous additional literature references containing examples of competition between N- and O-alkylation of ambident nucleophiles are given in the Supporting Information, pg. S117.

This journal is © The Royal Society of Chemistry 20xx

33 The site selectivity observed in reactions of anionic ambident nucleophiles may be a consequence of one of the nucleophilic sites being blocked through coordination to a counter-cation. See references 9c, 17a, 24, 30, and also L. M. Jackman and T. S. Dunne, *J. Am. Chem. Soc.*, 1985, **107**, 2805.
34 However, see also: T. Storz, M. D. Bartberger, S. Sukits, C. Wilde and T. Soukup, *Synthesis*, 2008, **2**, 201.
35 (a) G. E. Martin and A. J. Williams, *Annu. Rev. NMR Spectro.*, 2015, **84**, 1-76; (b) R. Marek, A. Lyčka, E. Kolehmainen, E. Sievänen and J. Toušek, *Current Organic Chemistry*, 2007, **11**, 1154; (c) G. E. Martin, A. J. Williams, *Annu. Rev. NMR Spectro.* 2005, **55**, 1–119; (d) R. Marek, A. Lyčka, *Cur. Org. Chem.* 2002, **6**, 35; (e) J. Saurí, A .J. Williams, G. E. Martin in *Modern NMR Approaches to the Structure Elucidation of Natural Products*, vol. 2, ed. A.J. Williams, G.E. Martin, D. Rovnyak, RSC, Cambridge, 2016, pp. 71–116; (f) B. D. Hilton and G. E. Martin, *J. Heterocyclic Chem.*, 2012, **49**, 526; (g) S. L. Black, P. D. O'Connor, M. Boyd, A. Blaser and J. D. Kendall, *Tetrahedron*, 2018, **74**, 2797; (h) R.T. Williamson, A.V. Buevich, G.E. Martin, *Tetrahedron Lett.* 2014, **55**, 3365.
36 Applications of natural abundance ^{17}O NMR spectroscopy: (a) D. E. Frantz and D. A. Singleton, *J. Am. Chem. Soc.*, 2000, **122**, 3288; (b) M. P. Meyer, A. J. DelMonte and D. A. Singleton, *J. Am. Chem. Soc.*, 1999, **121**, 10865.
37 The natural abundance ^{1}H-^{15}N HMBC NMR experiments were obtained using an NMR spectrometer equipped with a broadband cryoprobe, which greatly enhances the capabilities of this technique. The ^{15}N resonance was acquired in little time without the need for any costly isotopic enrichment, thus overcoming the traditional barriers against direct observation ^{15}N NMR spectroscopic studies.
38 A. Salgado, C. Varela, A. M. García Collazo and P. Pevarello, *Magn. Reson. Chem.*, 2010, **48**, 614.
39 K. J. Sheehy, L. M. Bateman, N. Flosbach, M. Breugst, P. A. Byrne, *Eur. J. Org. Chem.,* 2020, DOI: 10.1002/ejoc.202000329.
40 The δ_N values of non-alkylated nitrogens of diazines undergo small downfield shifts during these reactions (i.e. $\Delta(\delta_N) \geq 0$ ppm).
41 (a) E. Lukevics, E. Leipiņš, I. Segal and M. Fleisher, *J. Organomet. Chem.*, 1991, **406**, 283; (b) Z. Dega-Szafran, M. Szafran, J. Sitkowski and L. Stefaniak, *J. Phys. Org. Chem.*, 1996, **9**, 746; (c) B. Costisella, J. Schulz, H. Teichmann, C. Donaths and M. Meisels, *Phosphorus, Sulfur, Silicon Relat. Elem.*, 1990, **53**, 367; (c) M. Szafran, Z. Dega-Szafran, A. Katrusiak, G. Buczak, T. Głowiak, J. Sitkowski and L. Stefaniak, *J. Org. Chem.*, 1998, **63**, 2898.
42 (a) L. Pazderski, *Annu. Rep. NMR Spectrosc.*, 2013, **80**, 33; (b) L. Pazderski, *Magn. Res. Chem.*, 2008, **46**, S3; (c) R. M. Shanahan, A. Hickey, L. M. Bateman, M. E. Light and G. P. McGlacken, *J. Org. Chem.*, 2020, **85**, 2585.
43 Benzhydrylium triflates were generated in the presence of nucleophiles **1**, **2** or **3** by treating the parent benzhydryl chloride with AgOTf in CD_2Cl_2. The entirety of the reaction mixture filtered into an NMR tube (to remove AgCl) under inert atmosphere. For full experimental details, see the Supporting Information.
44 Experimental data are given in section 4 of the Supporting Information, beginning on page S8.
45 A detailed description of how inert NMR spectral analysis was carried out is given on page S8 of the Supporting Information (Procedure B).
46 Note that MeCN or CD_3CN could not be used for ^{1}H-^{15}N HMBC spectroscopic characterization due to the presence of nitrogen in the solvent. Hence, for the purposes of obtaining ^{1}H-^{15}N HMBC spectra, the solvent was removed and the residue re-dissolved in $(CD_3)_2SO$. CD_2Cl_2 was not a suitable solvent for methylation reactions of diazine *N*-oxides **1**–**3** due to the negligible solubility of the adducts in this solvent.
47 The reaction of **3** with Ph_2CH^+ produced a spectrum with broad signals that could not be interpreted. See pages S36 and S37 of the Supporting Information for details.
48 Methylation of DMSO by dimethylsulfate: J. Forrester, R. V. H. Jones, P.N. Preston and E. S. C. Simpson *J. Chem. Soc., Perkin Trans. 1*, 1995, 2289.
49 Reversibility of methoxysulfonium salt formation: G. F. Koser, P. B. Kokil and M. Shah, *Tetrahedron Lett.* 1987, **28**, 5431.
50 See spectra from methylation reactions of **1**, **2** and **3** in $(CD_3)_2SO$ on pages S14–15, S24–25 and S33-35 of the Supporting Information.
51 See details on pages S18–19 of the Supporting Information.
52 Decomposition was evident in the all of the spectra obtained of this material, regardless of the method employed to synthesize it. The major product remained intact for several days if kept under inert atmosphere (invariably contaminated with decomposition products), but did not survive attempts at isolation. ^{1}H NMR spectra containing signals of the decomposition products are shown in Figures S15 and S18 of the Supporting Information (pages S29 and S33).
53 See Supporting Information pages S11–13, S21–23 and S31–33.
54 C. Sakuma, M. Maeda, K. Tabei, A. Ohta, A. Kerim and T. Kurihara, *Magn. Reson. Chem*. 1996, **34**, 567.
55 W. Städeli and W. von Philipsborn, *Helv. Chem. Acta* 1980, **63**, 504.
56 See ^{1}H-^{15}N HMBC NMR spectra in Supporting Information on pages S55, S59, S60, S62, S64, S67, S68, and S70.
57 See pages S12, S14, S16, S20, S21, S26, and S31 of the Supporting Information for details on ^{13}C{^{1}H} NMR spectra of the N- and O-alkylation products.
58 See ^{1}H-^{15}N HMBC NMR spectrum on page S71 of the SI.
59 See ^{1}H-^{13}C HMBC NMR spectrum on page S73 in the SI.
60 All crossover experiments described in this section can be found in the Supporting Information in section 5, beginning on page S38.
61 e.g. **7** is a stronger Lewis base than **2** by a factor of *ca.* 16, while **25** is a stronger Lewis base than **1** by a factor of *ca*. 20: (a) P. A. Byrne, K. J. Sheehy, S. Buckley and H. Mayr, *unpublished results*; (b) H. Mayr, J. Ammer, M. Baidya, B. Maji, T. A. Nigst, A. R. Ofial and T. Singer, *J. Am. Chem. Soc.* 2015, **137**, 2580.
62 The experimental data pertaining to this experiment can be found on pages S46–S50 in the Supporting Information.
63 Full details on our computational investigations are given in the Supporting Information, pg. S83 – S110.
64 This is consistent with a report by Mayr, Ofial and co-workers indicating greater Lewis basicity of **28** compared to **27** in reactions with reference benzhydrylium ions: See reference 61b above.
65 See page S11–12 in the Supporting Information.
66 Precedent exists for remote deactivation of a Lewis basic nitrogen site: P. A. Byrne, S. Kobayasi, M. Breugst, H. Laub and H. Mayr, *J. Phys. Org. Chem.* 2016, **29**, 759.
67 See calculation on pages S31 and S35 in the ESI.
68 As cations and anions were assumed to be solvent separated, this trend can be expected for these bimolecular reactions. See Table S1 – S3 on pages S83 – S85 of the Supporting Information.
69 For details on Marcus theory, see: (a) R. A. Marcus, *Annu. Rev. Phys. Chem.* 1964, **15**, 155; (b) R. A. Marcus, *J. Phys. Chem.* 1968, **72**, 891; (c) R. A. Marcus, *J. Am. Chem. Soc.* 1969, **91**, 7224; (d) W. J. Albery and M. M. Kreevoy, *Adv. Phys. Org. Chem.* 1978, **16**, 87; (e) W. J. Albery, *Annu. Rev. Phys. Chem.* 1980, **31**, 227; (f) R. A. Marcus, *Pure Appl. Chem.* 1997, **69**, 13; (g) R. A. Marcus, *Angew. Chem. Int. Ed.* 1993, **32**, 1111.

70 As pointed out in reference 4, the omission of the work terms from equation 1 is justified when considering intramolecular selectivity such as selectivity between nucleophilic sites of an ambident nucleophile.
71 Introductions to Marcus theory are available in chemistry textbooks: (a) E. V. Anslyn and D. A. Dougherty, *Modern Physical Organic Chemistry*, University Science Books, Sausalito, California, 2006, p. 403–406; (b) P. W. Atkins and J. De Paula, *Physical Chemistry*, Oxford University Press, Oxford, 9th edition, 2010, p. 820, 857–861; (c) M. B. Smith, *March's Advanced Organic Chemistry*, Wiley-VCH: Hoboken, New Jersey, 7th edition, 2013, p. 273–274.
72 (a) Phenoxides: R. Mayer, M. Breugst, N. Hampel, A. R. Ofial and H. Mayr, *J. Org. Chem.* 2019, **84**, 8837; (b) Carbonyl-stabilised phosphonium ylides: P. A. Byrne, K. Karaghiosoff and H. Mayr, *J. Am. Chem. Soc.* 2016, **138**, 11272; (c) Azolium enolates: B. Maji and H. Mayr, *Angew. Chem. Int. Ed.* 2013, **52**, 11163; (d) Formaldehyde *N*,*N*-dialkylhydrazones: B. Maji, K. Troshin and H. Mayr, *Angew. Chem. Int. Ed.* 2013, **52**, 11900; (e) Methylhydrazines: T. A. Nigst, J. Ammer and H. Mayr, *Angew. Chem. Int. Ed*. 2012, **51**, 1353.
73 See intrinsic barrier ($\Delta G_0^{\ddagger}$) calculations in section 9 of the Supporting Information, beginning on page S86.
74 See Table S5 on page S90 in the Supporting Information for calculated values of $\Delta G_0^{\ddagger}$ and $\Delta G^{\ddagger}$.
75 S. Hoz, H. Basch, J. L. Wolk, T. Hoz and E. Rozental, *J. Am. Chem. Soc.* 1999, **121**, 7724. Note that Similar trends were also observed across the 3rd – 5th rows of the periodic table (*p*-block elements; noble gases not included).
76 X.-Q. Zhu and J.-D. Yang, *J. Phys. Org. Chem*. 2013, **26**, 271.
77 S. S. Shaik, H. B. Schlegel and P. Wolfe, *Theoretical Aspects of Physical Organic Chemistry: The S_N2 Mechanism*; Wiley, New York, 1992.
78 (a) X.-Q. Zhu, F.-H. Deng, J.-D. Yang, X.-T. Li, Q. Chen, N.-P. Lei, F.-K. Meng, X.-P. Zhao, S.-H. Han, E.-J. Hao and Y.-Y. Mu, *Org. Biomol. Chem.* 2013, **11**, 6071; (b) Y.-H. Fu, G.-B. Shen, Y. Li, L. Yuan, J.-L. Li, L. Li, A.-K. Fu, J.-T. Chen, B.-L. Chen, L. Zhu and X.-Q. Zhu, *ChemistrySelect* 2017, **2**, 904; (c) G.-B. Shen, K. Xia, X.-T. Li, J.-L. Li, Y.-H. Fu, L. Yuan and X.-Q. Zhu, *J. Phys. Chem. A* 2016, **120**, 1779; (d) Y. Li and X.-Q. Zhu, *ACS Omega.* 2018, **3**, 872.
79 The introduction and usage of the Zhu equation is discussed in the Supporting Information, beginning on page S89.
80 See pg S111 – S116 of Supporting Information for details of the experimental determination of an approximate $\Delta G^{\ddagger}$ value for the reaction of **1** + MeI to give **13a**.
81 See Table S8 on pg S92 of the Supporting Information.
82 Numerous precedents for kinetically controlled N-alkylation of other ambident nucleophiles with competing O and N nucleophilic sites (e.g. amide anions) exist in the literature.[19b,f,j,k, 22b,c,d]
83 (a) P. A. Byrne, S. Kobayashi, E.-U. Würthwein, J. Ammer and H. Mayr, *J. Am. Chem. Soc.* 2017, **139**, 1499; (b) J. P. Richard, M. M. Toteva and J. Crugeiras, *J. Am. Chem. Soc.* 2000, **122**, 1664.
84 Amide O-alkylation appears to be kinetically favoured over N-alkylation. Although O-methylation of DMF has been shown to be reversible at temperatures > 100 °C,[19a,c,d] reports of N-alkylation of amides in refluxing acetonitrile (boiling point 82 °C at atmospheric pressure) are likely to involve misidentification of the products. Certainly, the spectral data supplied are insufficient for definitive assignment of N-alkylated products.[8,9]
85 J. L. Banks, H. S. Beard, Y. Cao, A. E. Cho, W. Damm, R. Farid, A. K. Felts, T. A. Halgren, D. T. Mainz, J. R. Maple, R. Murphy, D. M. Philipp, M. P. Repasky, L. Y. Zhang, B. J. Berne, R. A. Friesner, E. Gallicchio and R. M. Levy, *J. Comput. Chem.*, 2005, **26**, 1752–1780.
86 Schrödinger Release 2018-3; Macromodel, Schrödinger, LLC: New York, NY, 2018.
87 Y. Zhao and D. G. Truhlar, *Theor. Chem. Acc.* **2008**, *120*, 215–241.
88 S. Grimme, J. Antony, S. Ehrlich and H. Krieg,. *J. Chem. Phys.* **2010**, *132*, 154104.
89 A. V. Marenich, C. J. Cramer and D. G. Truhlar, *J. Phys. Chem. B* **2009**, *113*, 6378–6396.
90 S. Grimme, *Chem. Eur. J.* **2012**, *18*, 9955–9964.
91 R. F. Ribeiro, A. V. Marenich, C. J. Cramer and D. G. Truhlar, *J. Phys. Chem. B* **2011**, *115*, 14556–14562.
92 C. Riplinger, B. Sandhoefer, A. Hansen and F. Neese, *J. Chem. Phys.* **2013**, *139*, 134101.
93 C. Riplinger and F. Neese, *J. Chem. Phys.* **2013**, *138*, 034106.
94 D. G. Liakos and F. Neese, *J. Chem. Theory Comput.* **2015**, *11*, 4054–4063.
95 F. Weigend and R. Ahlrichs, *Phys. Chem. Chem. Phys.* **2005**, *7*, 3297–3305.
96 D. Rappopor and F. Furche, *J. Chem. Phys.* **2010,** *133*, 134105.
97 A. Hellweg, C. Hättig, S. Höfener and W. Klopper, *Theor. Chem. Acc.*, 2007, **117**, 587–597.
98 M. J. Frisch, G. W. Trucks, H. B. Schlegel, G. E. Scuseria, M. A. Robb, J. R. Cheeseman, G. Scalmani, V. Barone, G. A. Petersson, H. Nakatsuji, X. Li, M. Caricato, A. V. Marenich, J. Bloino, B. G. Janesko, R. Gomperts, B. Mennucci, H. P. Hratchian, J. V. Ortiz, A. F. Izmaylov, J. L. Sonnenberg, Williams, F. Ding, F. Lipparini, F. Egidi, J. Goings, B. Peng, A. Petrone, T. Henderson, D. Ranasinghe, V. G. Zakrzewski, J. Gao, N. Rega, G. Zheng, W. Liang, M. Hada, M. Ehara, K. Toyota, R. Fukuda, J. Hasegawa, M. Ishida, T. Nakajima, Y. Honda, O. Kitao, H. Nakai, T. Vreven, K. Throssell, J. A. Montgomery Jr., J. E. Peralta, F. Ogliaro, M. J. Bearpark, J. J. Heyd, E. N. Brothers, K. N. Kudin, V. N. Staroverov, T. A. Keith, R. Kobayashi, J. Normand, K. Raghavachari, A. P. Rendell, J. C. Burant, S. S. Iyengar, J. Tomasi, M. Cossi, J. M. Millam, M. Klene, C. Adamo, R. Cammi, J. W. Ochterski, R. L. Martin, K. Morokuma, O. Farkas, J. B. Foresman and D. J. Fox *Gaussian 16 Rev. B.01*, Wallingford, CT, 2016.
99 (a) F. Neese, *Wiley Interdiscip. Rev. Comput. Mol. Sci.*, 2012, **2**, 73–78; (b) F. Neese, *Wiley Interdiscip. Rev. Comput. Mol. Sci*., 2018, **8**, e1327.

This journal is © The Royal Society of Chemistry 20xx

Competition Between N and O: Use of Diazine *N*-Oxides as a Test Case for the Marcus Theory Rationale for Ambident Reactivity

Kevin J. Sheehy,[a] Lorraine M. Bateman,[a,b,d] Niko T. Flosbach,[c] Martin Breugst,*[c] Peter A. Byrne,*[a,d]

[a] School of Chemistry, Analytical and Biological Chemistry Research Facility, University College Cork, College Road, Cork, Ireland.

[b] School of Pharmacy, University College Cork, College Road, Ireland

[c] Department für Chemie, Universität zu Köln, Greinstraße 4, 50939 Köln, Germany.

[d] SSPC (Synthesis and Solid State Pharmaceutical Centre), Cork, Ireland.

E-mail: peter.byrne@ucc.ie

mbreugst@uni-koeln.de

Contents

1. General Experimental …….…….. S3 – S4

2. Preparation and ^{1}H-^{15}N HMBC NMR spectra of diazine *N*-oxides **1**–**3**…… S4 – S6

3. Synthesis of 4-methylbenzhydryl chloride……..……...……... S7

4. Reactions of Diazines and *N*-oxides with MeI, MeOTf and benzhydrylium ions..... S8 – S38

   4.1 General Procedures ……... S8
   4.2 Reactions of Pyrazine *N*-Oxide (**1**)……...…… S9 – S17
   4.3 Reactions of Quinoxaline *N*-Oxide (**2**)……...…….....…… S18 – S27
   4.4 Reactions of Pyrimidine *N*-Oxide (**3**)……...……..... S28 – S37

5. Crossover experiments of **1**, **2**, **3** and **25** with a competing nucleophile……..... S38 – S52

   5.1 Crossover experiment of pyrazine *N*-oxide (**1**) with MeOTf and methyl nicotinate (**25**) …….. S38 – S41
   5.2 Crossover experiment of quinoxaline *N*-oxide (**2**) with MeOTf and pyrazine (**7**) S42 – S45
   5.3 Crossover experiment of pyrimidine *N*-oxide (**3**) with MeOTf and pyrazine (**7**)… S46 – S50
   5.4 Crossover experiment of 4-Methylpyrazinium-*N*-oxide iodide (**13a**) with MeOTf and methyl nicotinate (**25**) ……..... S50 – S52

6. Competition experiment: Pyrazine *N*-oxide (**1**) vs Pyrimidine *N*-oxide (**3**)……. S53 – S54

7. Full Spectra for compounds produced in Sections 4 – 6 ……..…… S55 – S82

8. Calculations of Thermodynamic and Activation Parameter Values ……...…… S83 – S85

9. Calculation of Marcus Intrinsic Barriers …...……..……...…….. S86 – S91

10. Charge Density Calculations ……..…….. S92

11. Calculation of Activation Barriers for Methyl Transfer Identity Reactions……....…. S93 – S99

12. Calculations on Reactions with Methyl Iodide and Methyl Triflate ……..…….. S100 – S110

13. Determination of 2nd Order Rate Constant…….…..……..……...….. S111 – S116

14. Additional Literature References from Main Article…….……...….. S117

15. Supporting Information References……..... S118

1. General Experimental

Commercial diazines and alkylating agents were obtained from Fluorochem, Sigma-Aldrich and Alfa Aesar.

CH_2Cl_2, CH_3CN, CD_3CN, $(CD_3)_2SO$ and $(CH_3)_2SO$ were dried over activated 3 Å molecular sieves and stored under an atmosphere of nitrogen in flasks with grease-free J. Young's valves (this is a modification of the method of Williams and Lawton).[1] Molecular sieves (10 weight percent per unit volume of compound to be dried) were activated by flame drying in the storage flask(s) for 5 – 10 minutes (depending on quantity of sieves to be dried). After flame-drying, the storage flask was immediately connected to a Schlenk line, subjected to vacuum (between 2 and 5×10^{-3} mbar), and allowed to stand until the sieves had cooled. The flask was then subjected to several vacuum/refill cycles to establish a nitrogen atmosphere inside, and the solvent/compound to be dried was then added against a flow of nitrogen.

Solvents that were used in relative bulk (CH_3CN, CH_2Cl_2) were stored in a specialised flask with two J. Young's valves, one of which was modified to facilitate easy access of a needle to the body of the flask through the side-arm of the valve. When accessing the dry solvent, the angled side-arm was sealed with a rubber septum, and the small volume contained between the septum and the sealed tap of the J. Young's valve was flushed with a stream of nitrogen gas for a minimum of five minutes prior to opening the valve. The solvent required several days after commencing drying to reach maximal dryness (according to analysis by Karl Fischer titration), but was dry enough for most purposes after one day. CH_3CN and THF stored in this manner was found to retain water contents of less than 10 ppm for more than one year.

For all reactions conducted using Schlenk glassware, the Schlenk flask was dried in an oven, then attached to vacuum via Schlenk manifold and placed under vacuum ($\leq 5 \times 10^{-3}$ mbar). The flask was then filled with nitrogen gas by the pump and fill technique (three repeats of the following cycle: evacuation to $\leq 5 \times 10^{-3}$ mbar, re-fill with nitrogen gas).[2] Solids and reagents were then introduced to the flasks under fast nitrogen flow.

NMR spectra were recorded on Bruker Avance III 600, Bruker Avance III 500, Bruker Avance I 400 and Bruker Avance III 300 NMR spectrometers. ^1H and ^{13}C NMR chemical shifts were referenced to tetramethylsilane (TMS). ^1H NMR spectra (proton coupled mode, 600 MHz, 400 MHz and 300 MHz respectively) $^{13}C\{^1H\}$ NMR spectra (proton decoupled mode; 150 MHz,100 MHz and 75 MHz, respectively), HSQC NMR spectra, HMBC NMR spectra and COSY NMR spectra were acquired at 300 K on the 300 and 600 MHz instruments and 293 K on the 400 MHz instrument. ^1H NMR spectra on the 500 MHz instrument (equipped with a 5 mm QNP probe) were recorded at 298 K. ^1H NMR spectra were acquired using a 30° pulse (Bruker zg pulse programme), an acquisition time of 2.65 seconds, and a time domain data size of 32768 or 65536 points. A relaxation delay of 5 seconds was used in most instances; exceptions to this are noted where applicable below. Signal assignments in the ^1H and ^{13}C NMR spectra were made with reference to information contained in the two-dimensional NMR spectra. ^1H-^{15}N HMBC spectra were recorded at 300 K on a Bruker Avance III 600 NMR spectrometer [600 MHz (^1H), 60.8 MHz (^{15}N)], equipped with Bruker BBFO cryoprobe (coil temperature 16 K) and referenced externally to ammonia, the value of which was uncorrected. ^1H-^{15}N HMBC spectra were acquired using the Bruker

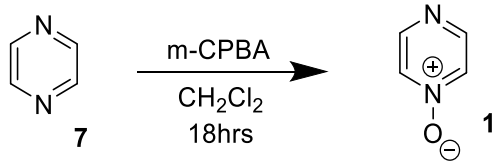
hmbcqpndqf pulse program (2D H-1/X correlation via heteronuclear zero and double quantum coherence optimised on long range couplings), with 4 scans and spectral width of 600–650 ppm. All ^{1}H-^{15}N HMBC NMR spectra shown below were processed (post-acquisition) by application of t1 noise reduction. All spectra were run at University College Cork. Spectra recorded in non-deuterated solvents were acquired using the Bruker NOESY presat (noesygppr) solvent suppression pulse sequence, using presaturation during the mixing time and relaxation delay. Chemical shifts (δ) are expressed as parts per million (ppm), positive shift being downfield from TMS; coupling constants (*J*) are expressed in Hertz (Hz). Splitting patterns in ^{1}H-NMR spectra are designated as: s (singlet), bs (broad singlet), d (doublet), dd (doublet of doublets), ddd (doublet of doublets of doublets), t (triplet), td (triplet of doublets), q (quartet), quin (quintet) and m (multiplet). Infrared spectra were measured using a FTIR UATR2 spectrometer as thin films in acetonitrile. Data are represented as follows: frequency of absorption (cm^{-1}), intensity of absorption (s = strong, m = medium, w = weak, br = broad). High resolution (precise) mass spectra (HRMS) were recorded on a Waters LCT Premier TOF LC–MS instrument using electrospray ionization in positive ionization mode (ESI+) using 50 % acetonitrile/water containing 0.1 % formic acid as eluent. Samples were made up at a concentration of approximately 1 mg ml^{-1}.

2. Preparation and ^{1}H-^{15}N HMBC NMR spectra of diazine *N*-oxides 1 – 3

Preparations of diazine *N*-oxides were achieved with modifications of established literature procedures.[3,4]

We recommend the use of a slight excess of diazine (relative to the amount of 3-chloroperbenzoic acid) in order to remove the need to use quenching agents (e.g. Ph_3P, Na_2SO_3) in these reactions.

(i) Pyrazine *N*-oxide (1) [4]



Pyrazine (**7**) (1.12 g, 14.0 mmol) was dissolved in CH_2Cl_2 (70 ml). 3-Chloroperbenzoic acid (3.08 g, 13.8 mmol) was added in one portion, and the solution was stirred for 18 hrs, turning a cloudy white colour (due to precipitated 3-chlorobenzoic acid). The reaction mixture was washed twice with saturated sodium sulfite solution (*ca.* 40 ml each) and once with a solution of brine (*ca.* 40 ml). The recovered organic phase was dried over Na_2SO_4, and the drying agent was removed by filtration. The solvent was then removed under reduced pressure. The residue was purified by column chromatography using 100% EtOAc, yielding a colourless, needle-like solid. (0.56 g, 5.8 mmol, 42%). This material was immediately transferred to a glove box upon isolation.

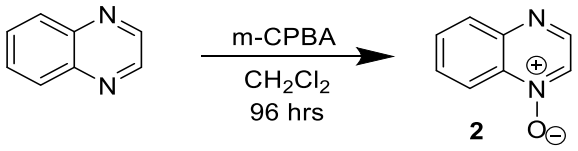
^{1}H NMR (300 MHz, $CDCl_3$) δ 8.52 – 8.44 (m, 2H), 8.15 – 8.08 (m, 2H). [5]

A further sample of **1** (0.080 g) was dissolved in CH_2Cl_2 (0.65 ml) and placed in an NMR tube by syringe under nitrogen, which was then sealed by a rubber septum cap and wrapped with PTFE tape. ^{1}H NMR and ^{1}H-^{15}N HMBC NMR spectra were recorded on this sample. The ^{15}N NMR chemical shift values reported below were attained from the ^{1}H-^{15}N HMBC NMR experiment. See the General Experimental for details on the solvent suppression protocol used during acquisition.

^{1}H NMR (600 MHz, CH_2Cl_2) δ 8.40 (app d, app *J* = 4.3 Hz, 2H), 8.08 – 8.03 (m, 2H).

^{15}N NMR (60.8 MHz, CH_2Cl_2): δ 311, 303.5

(ii) Quinoxaline *N*-oxide (2)



Quinoxaline (1.70 g, 13.1 mmol) was dissolved in 100 ml CH_2Cl_2. 3-Chloroperbenzoic acid (2.39 g, 13.8 mmol) was added in one portion, and the solution was stirred for 4 days. Precipitated 3-chlorobenzoic acid appeared in the reaction mixture after a few hours. The reaction mixture was washed twice with saturated sodium sulfite solution (*ca.* 40 ml each) and once with a solution of brine (*ca.* 40 ml). The recovered organic phase was dried over Na_2SO_4, and the drying agent was removed by filtration. The solvent was then removed under reduced pressure. The residue was purified by column chromatography in silica using 70:30 ethyl acetate/cyclohexane, yielding light tan-coloured solid (**2**). (1.27 g, 8.68 mmol, 66% yield). This material was immediately transferred to a glove box upon isolation.

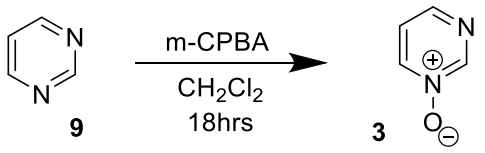
^{1}H NMR (300 MHz, $CDCl_3$) δ 8.68 (d, *J* = 3.6 Hz, 1H), 8.59 (dd, *J* = 8.6, 1.4 Hz, 1H), 8.35 (d, *J* = 3.6 Hz, 1H), 8.19 – 8.11 (m, 1H), 7.88 – 7.72 (m, 2H). [6]

A sample of the product (0.055 g) was dissolved in CH_2Cl_2 (0.65 ml) and placed in an NMR tube by syringe under nitrogen, which was then sealed by a rubber septum cap and wrapped with PTFE tape. ^{1}H NMR and ^{1}H-^{15}N HMBC NMR spectra were recorded on this sample. The ^{15}N NMR chemical shift values reported below were attained from the ^{1}H-^{15}N HMBC NMR experiment. See the General Experimental for details on the solvent suppression protocol used during acquisition.

^{1}H NMR (600 MHz, CH_2Cl_2) δ 8.62 (d, *J* = 3.5 Hz, 1H), 8.50 (app d, app *J* = 8.6 Hz, 1H), 8.31 (d, *J* = 3.5 Hz, 1H), 8.09 (app d, app *J* = 8.4 Hz, 1H), 7.82 – 7.77 (m, 1H), 7.74 – 7.69 (m, 1H).

^{15}N NMR (60.8 MHz, CH_2Cl_2): δ 302, 300.3.

(iii) Preparation of Pyrimidine *N*-oxide



Pyrimidine (**9**) (1.74 g, 21.7 mmol) was dissolved in CH_2Cl_2 (110 ml). 3-Chloroperbenzoic acid (5.62 g, 32.6 mmol) was added in one portion, and the solution was stirred for 48 hrs, turning a cloudy white colour (due to precipitated 3-chlorobenzoic acid). PPh_3 (3.90 g, 14.9 mmol) was added, and the solution was stirred for 3 hours. The solvent was removed under reduced pressure. The residue was purified by column chromatography using 90 : 10 EtOAc/Cyclohexane, yielding a white crystalline solid (**3**). (0.993 g, 10.3 mmol, 48 %). The product is very hygroscopic and hence was transferred to a glove box immediately after isolation.

^{1}H NMR (300 MHz, $CDCl_3$) δ 9.01 (m (fine splitting not resolved), 1H), 8.42 – 8.35 (m, 1H), 8.25 (dd, *J* = 4.7, 1.4 Hz, 1H), 7.35 – 7.28 (m, 1H). [7]

Authors' Note: We recommend that PPh_3 should NOT be used for quenching purposes, as it was difficult to find chromatographic conditions allowing the product to be separated from triphenylphosphine oxide, and significant loss of product occurred due to co-elution with Ph_3PO.

A sample of the product (0.047 g) was dissolved in DMSO (0.65 ml) and placed in an NMR tube by syringe under nitrogen, which was then sealed by a rubber septum cap and wrapped with PTFE tape. ^{1}H NMR and ^{1}H-^{15}N HMBC NMR spectra were recorded on this sample. The ^{15}N NMR chemical shift values reported below were attained from the ^{1}H-^{15}N HMBC NMR experiment. See the General Experimental for details on the solvent suppression protocol used during acquisition.

^{1}H NMR (600 MHz, DMSO) δ 9.04 (s, 1H), 8.58–8.52 (m, 1H), 8.25 (dd, J = 4.7, 1.0 Hz, 1H), 7.55 – 7.49 (m, 1H).

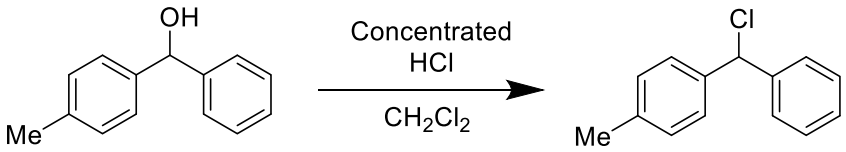
^{15}N NMR (60.8 MHz, DMSO): δ 301.3, 291.7.

A further sample of **3** (0.047 g) was dissolved in CH_2Cl_2 (0.65 ml) and placed in an NMR tube by syringe under nitrogen, which was then sealed by a rubber septum cap and wrapped with PTFE tape. The product was analysed by ^{1}H-^{15}N HMBC NMR. See the General Experimental for details on the solvent suppression protocol used during acquisition.

^{1}H NMR (600 MHz, CH_2Cl_2) δ 8.90 (s, 1H), 8.32 (app d, app *J* = 6.6 Hz, 1H), 8.16 (app d, app *J* = 4.6 Hz, 1H), 7.30 – 7.24 (m, 1H).

^{15}N NMR (60.8 MHz, CH_2Cl_2): δ 299.6, 291.4.

3. Synthesis of 4-methylbenzhydryl chloride



4-methylbenzhydrol (1.00 g, 5.04 mmol) was dissolved in dichloromethane (16 ml), and the resulting solution was cooled in an ice bath for 10 minutes. Over approximately 20 minutes, concentrated aqueous HCl (37%; 5 ml) was added dropwise from a Pasteur pipette into the solution of 4-methylbenzhydrol at 0 °C. The reaction was stirred at 0 °C for 1.5 hours, and then placed in a refrigerator overnight. The reaction was then transferred into a pre-chilled separating funnel (cooled in freezer in advance), and the dichloromethane phase was separated from the aqueous phase. The aqueous phase was extracted twice with cold dichloromethane (pre-chilled in an ice bath; *ca.* 5 ml per extraction), and the dichloromethane phases were combined and then dried over anhydrous $CaCl_2$. The $CaCl_2$ was removed by filtration. The dichloromethane phases were kept cold at all points by immersing the vessel(s) containing them in an ice bath.

Next, the solvent was removed from the filtrate under vacuum, giving a colourless oil (1.05 g, 4.85 mmol, 96%). The flask containing the product was maintained at room temperature during solvent removal, and a relatively high vacuum was used to remove the solvent as quickly as possible. A sample was removed and dissolved in $CDCl_3$, and a ^{1}H NMR spectrum was obtained.

^{1}H NMR (300 MHz, $CDCl_3$) δ 7.46 – 7.26 (m, overlaps with C*H*Cl_3 signal, contains 7H of tolyl and phenyl groups), 7.15 (app d, app *J* = 7.9 Hz, 2H), 6.11 (s, 1H, Ar_2CH), 2.34 (s, 3H, CH_3). [8]

An attempt was made to crystallise the product by triturating with *n*-pentane, and hence small signals of this solvent are present in the ^{1}H NMR spectrum recorded of the product.

The product was stored in a freezer, and remains stable at −18 °C for at least one year.

4. Reactions of Diazine *N*-oxides with MeI, MeOTf and benzhydrylium ions

4.1 General Procedures

General Procedure A: Removal of solvent without compromising inert atmosphere

The following procedure was used to remove the solvent (MeCN, CD_3CN or Et_2O) and volatile reagents (MeI or MeOTf) from a Schlenk flask containing a completed reaction mixture without exposing the product(s) to the ambient atmosphere, allowing the inert atmosphere in a reaction flask to be re-established after completion of removal of volatile materials. A second vacuum trap was attached to the Schlenk manifold on one arm and to the sealed reaction flask by the other. An inert atmosphere was established in the second trap and connective tubing by three pump and re-fill cycles.[2] The trap was then again placed under vacuum ($\leq 5 \times 10^{-3}$ mbar) and then immersed in liquid N_2 in a Dewar flask. At this point, the tap on the Schlenk flask is carefully opened and volatile reagents are removed and collected in the second trap. After approximately 30 minutes, the entirety of the trap and the Schlenk flask are re-filled with nitrogen gas through the Schlenk manifold, and the tap of the Schlenk flask is closed. The trap is removed and the Schlenk flask is re-attached directly to the Schlenk manifold.

General Procedure B: Preparation of NMR samples under inert atmosphere

The following procedure was used to place the products of the alkylation reactions (dissolved in an appropriate solvent) into NMR tubes while maintaining an inert atmosphere. The products were formed in an N_2-filled Schlenk flask using inert atmosphere techniques. The appropriate solvent was introduced to the Schlenk flask by syringe and *ca.* 10 mg of the product was dissolved. An empty NMR tube was placed in a long, tube shaped Schlenk flask, which was evacuated and re-filled with nitrogen ≥ 3 times by the pump and refill technique,[2] creating an inert atmosphere inside the flask. The solution to be examined (in DMSO or CH_2Cl_2) was added to the NMR tube by syringe under nitrogen. The NMR tube was then sealed by a rubber septum cap. The seal made by the rubber septum on the outside of the NMR tube was secured by wrapping it with PTFE tape and then a layer of Parafilm. The sealed NMR tube was then transferred to the appropriate spectrometer for analysis.

General Procedure C: Preparation of benzhydryl adducts of heterocycles and *N*-oxides

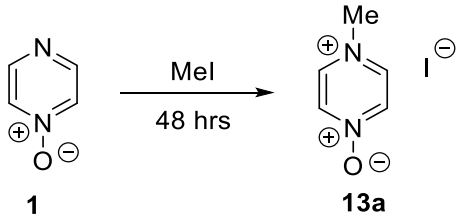
The appropriate benzhydryl chloride (1 equivalent) was weighed into a reaction vessel and transferred into a glove box containing a nitrogen atmosphere. Dry CD_2Cl_2,CH_2Cl_2 or CD_3CN (usually 0.85 ml) was added, followed by the heterocycle or *N*-oxide (1 equivalent). AgOTf (1.1 – 1.2 equivalents) was then added, causing the immediate precipitation of AgCl. The reaction vessel was sealed, and agitated (15 minutes for 4-methylbenzhydryl chloride, 60 minutes for benzhydryl chloride), and then filtered (removing AgCl) through a syringe filter into an NMR tube. The NMR tube was sealed using a rubber septum. The seal was then wrapped with PTFE tape and Parafilm. Finally, the NMR tube was placed in a long Schlenk flask and removed from the glove box and brought to the NMR spectrometer. All products underwent relatively rapid decomposition (hydrolysis) on exposure to moisture, and hence were only characterized by inert atmosphere NMR spectroscopy.

4.2 Reactions of Pyrazine *N*-Oxide (1)

Preparation of *N*-methylpyrazinium *N'*-oxide iodide (13a)

(a) Experiment Showing Isolated Yield of 13a (Solvent-Free Reaction) – Contains ^{15}N NMR data

Pyrazine *N*-oxide (**1**) (0.041 g, 0.43 mmol) was placed in a N_2-filled Schlenk flask. Methyl iodide (0.53 ml, 1.2 g, 8.5 mmol) was added by syringe to the flask. The flask was wrapped in foil and left in the dark for 48 hours, after which time the methyl iodide was removed under vacuum using General Procedure A. The resulting yellow solid (**13a**) was washed by addition of dry Et_2O, which was removed by cannula filtration (under inert atmosphere). Three aliquots of dry Et_2O (0.5 ml each) were used in this manner to wash the product, (yield = 0.026 g, 0.11 mmol, 26%) A sample of **13a** in dry $(CD_3)_2SO$ was then prepared for ^{1}H and ^{1}H-^{15}N HMBC NMR spectroscopic characterization by Procedure B



^{1}H NMR (600 MHz, $(CD_3)_2SO$) δ 9.05 – 9.01 (m, 2H), 9.00 – 8.97 (m, 2H), 4.18 (s, 3H, C*H*$_3$). [9]

^{15}N NMR (60.8 MHz, $(CD_3)_2SO$): δ 322.3 (*N*—O), 187.1 (*N*$^+$—Me).

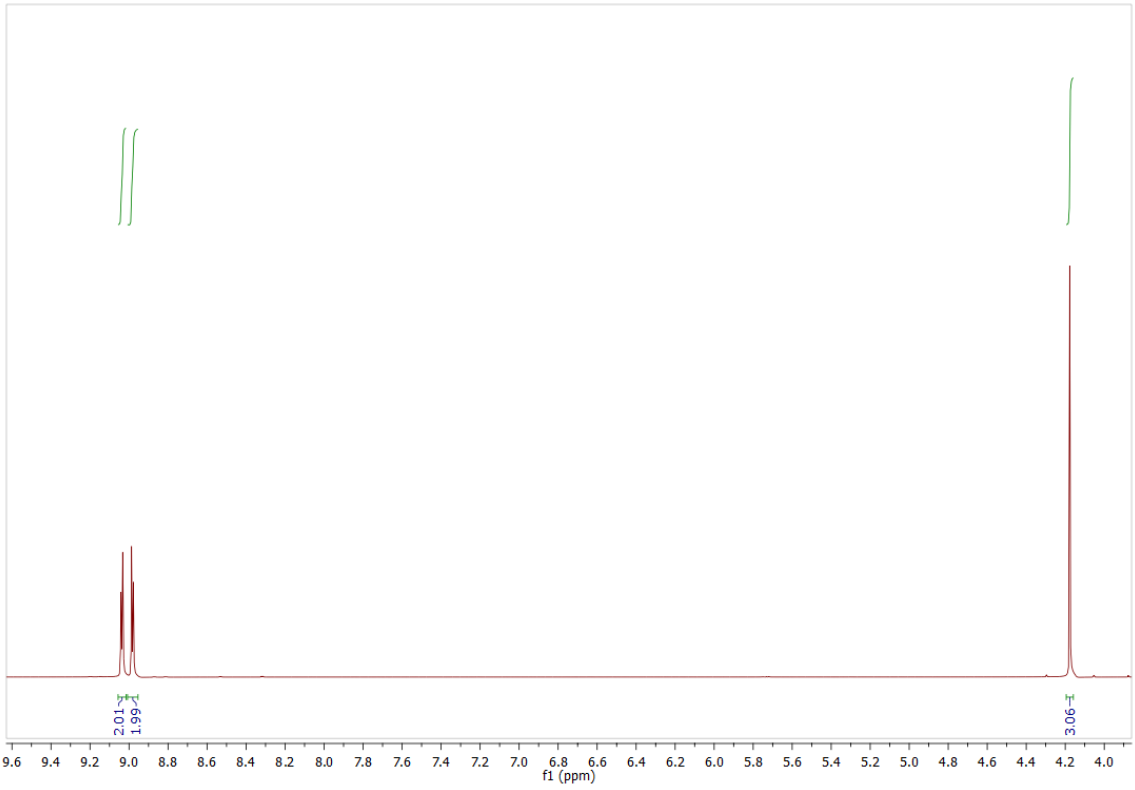
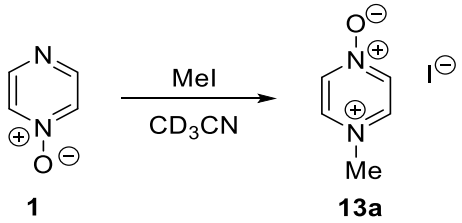


Figure S1: ^{1}H NMR spectrum in $(CD_3)_2SO$ of **13a**, showing no **15a**. The full spectrum is shown in Section 7.

(b) Experiment in CD_3CN Showing Low Conversion to 13a

In a glove box, pyrazine *N*-oxide (**1**) (0.019 g, 0.20 mmol) was dissolved in CD_3CN (0.65 ml). Methyl iodide (0.033 g, 0.23 mmol) was added dropwise by syringe to the solution of **1**. The reaction vessel was agitated throughout addition of MeI. After completion of addition of MeI, the entire reaction mixture was transferred to an NMR tube. The NMR tube was sealed with a rubber septum, and the seal was secured by wrapping with PTFE tape and then Parafilm. The NMR tube was take to the NMR spectrometer. A ^{1}H NMR spectrum recorded approximately 20 minutes after mixing of the reactants showed no conversion to **13a** (i.e. only signals of **1** and MeI were observed). After four days, a second ^{1}H NMR spectrum was obtained. This showed low conversion to **13a**. No signals of **15a** were observed.



^{1}H NMR (300 MHz, CD_3CN)

Assigned to **13a**: δ 8.74 – 8.66 (m, 2H), 8.61 – 8.51 (m, 2H), 4.20 (s, 3H, NCH_3). [9]

Assigned to **1**: δ 8.46 – 8.38 (m, 2H), 8.13 – 8.06 (m, 2H).

Relative to 1H of **13a**, 1H of **1** integrates for 3.1H. Therefore, the conversion to **13a** was 24%. A signal of H_2O is present in the second spectrum since due to ingress of into the NMR tube.

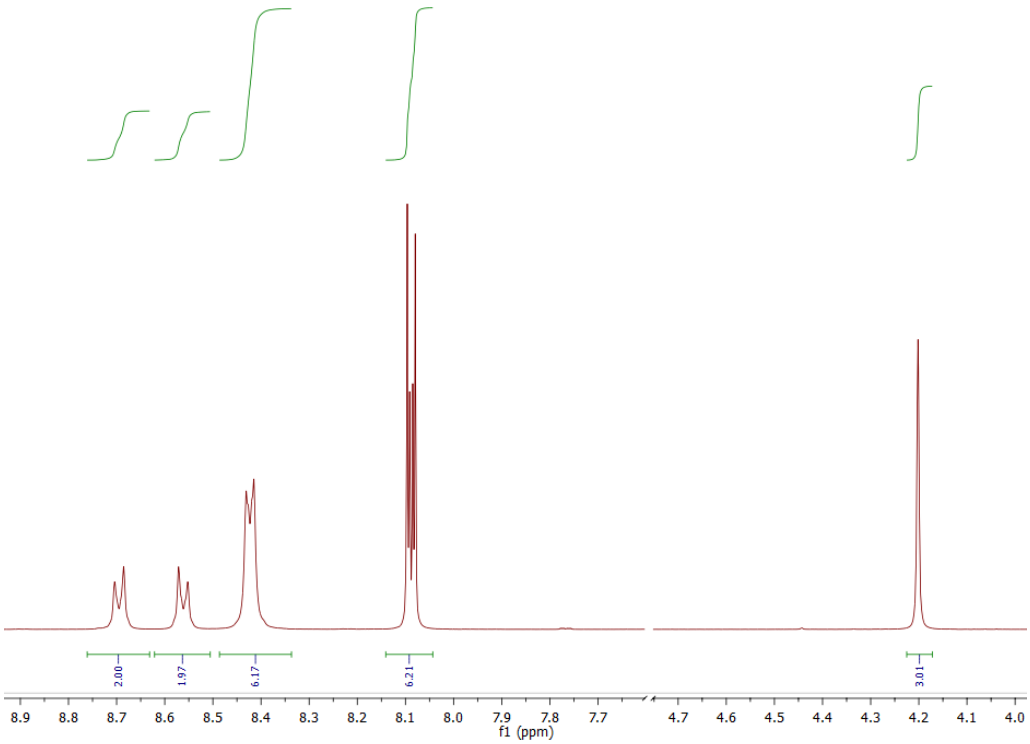
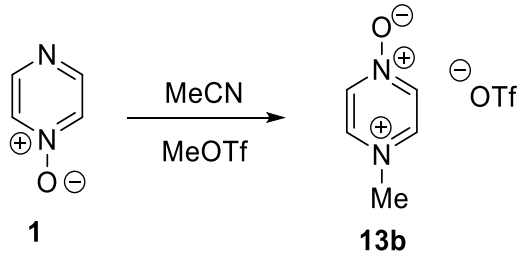


Figure S2: ^{1}H NMR spectrum of reaction of **1** + MeI in CD_3CN, forming **13a** in low conversion after 4 days, and showing that no **15a** is formed. The full spectrum is shown in Section 7.

Preparations of 13b and 15b

(a) Experiment Showing Isolated Yield of 13b

Pyrazine *N*-oxide (**1**) (0.166 g, 1.73 mmol) was dissolved in CH_3CN (5.0 ml) in a N_2-filled Schlenk flask. Methyl triflate (0.318 g, 1.94 mmol) was then added dropwise. After 96 hours, the CH_3CN was removed under vacuum using General Procedure A. The solid product (**13b**) was washed by addition of dry Et_2O, which was removed by cannula filtration (under inert atmosphere). Three aliquots of dry Et_2O (3 ml each) were used in this manner to wash the product (yield = 0.305 g, 1.17 mmol, 68%) A sample of **13b** in dry $(CD_3)_2SO$ was prepared using General Procedure B for ^1H NMR spectroscopic characterization.



^{1}H NMR (300 MHz, $(CD_3)_2SO$) δ 9.03 – 8.96 (m, 4H), 4.16 (s, 3H, C*H*$_3$). [9]

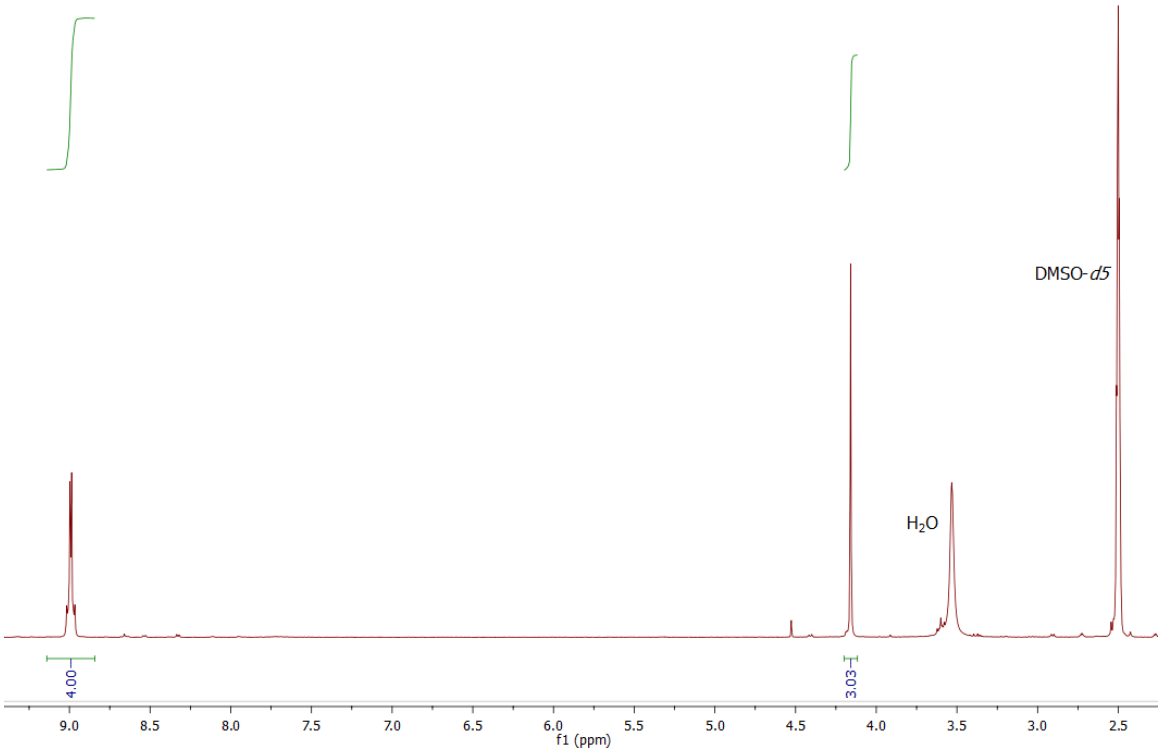
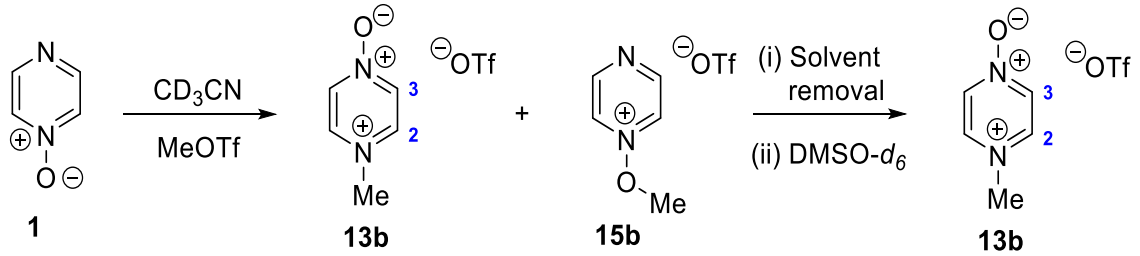


Figure S3: ^1H NMR spectrum of **13b** in $(CD_3)_2SO$. The full spectrum is shown in Section 7.

(b) Experiment Showing N- vs O-Alkylation Product Ratio (13b vs 15b) – Contains ^{15}N NMR Data

Pyrazine *N*-oxide (**1**) (0.031 g, 0.32 mmol) was dissolved in CD_3CN (0.65 ml) in a N_2-filled Schlenk flask. Methyl triflate (0.050 g, 0.030 mmol) was subsequently added dropwise. The reaction mixture was transferred to an NMR tube and analyzed by NMR spectroscopy using General Procedure B.

Note: Insufficient concentrations of **1** and **15b** in the spectra below meant that unambiguous assignments of ^{1}H and ^{13}C NMR signals to specific sites in the structures of these compounds was not possible.



^{1}H NMR (300 MHz, CD_3CN)

Signals assigned to **13b**: δ 8.64 – 8.50 (m, 4H, H-2 and H-3), 4.19 (s, 3H, NC*H*$_3$).

Signals assigned to **15b**: δ 9.48 (dd, *J* = 3.3, 1.6 Hz, 2H), 9.13 (dd, *J* = 3.3, 1.6 Hz, 2H), 4.54 (s, 3H, OC*H*$_3$). Relative to 1H of **13b**, 1H of **15b** integrates for 0.05H.

Signals assigned to the starting material **1**: δ 8.48 (d, *J* = 4.8 Hz, 1H), 8.16 (dd, *J* = 3.6, 1.5 Hz, 1H). Relative to 1H of **13b**, 1H of **1** integrates for *ca.* 0.15H.

The signal at δ 8.64 – 8.50 ppm contains 4H of **13b** and 2H of the starting material **1**. The integration of this signal is slightly low with respect to the other signals of **1** and **13b**; this is likely to be due to a slow relaxation rate of one of the contributing protons.

^{13}C{^{1}H} NMR (75 MHz, CD_3CN)

Assigned to **13b**: δ 143.1 (C-2), 139.9 (C-3), 48.1 (N*C*H$_3$)

Assigned to **15b**: δ 153.1, 132.2, 69.1 (O*C*H$_3$)

Assigned to **1**: δ 148.1, 135.6.

Quantitative product formation can be concluded in this experiment on the basis of complete consumption of MeOTf (no signal of MeOTf present in the ^{1}H NMR spectrum). Ratio of N-alkylation and O-alkylation Products (from ^{1}H NMR spectrum):

4H of Compound **13b** = 4.00 – Therefore 1H = 1.00

2H of compound **15b** = 0.10 – Therefore 1H = 0.05

$$\text{Ratio} = \frac{1.00}{1.00 + 0.05} \times 100 = 95\%\ \text{N alkylation}$$

The CD_3CN was removed using General Procedure A and the product mixture was re-dissolved in $(CD_3)_2SO$ to record a ^{1}H-^{15}N HMBC NMR spectrum. Product **15b** did not survive the solvent removal process.

^{1}H NMR (600 MHz, $(CD_3)_2SO$)

Signals assigned to **13b**: δ 9.02 – 8.99 (m, 2H), 8.99 – 8.96 (m, 2H), 4.17 (s, 3H, C*H*$_3$).

Signals assigned to **1**: δ 8.55 – 8.53 (m, 2H), 8.33 – 8.31 (m, 2H). Relative to 1H of **13b**, 1H of **1** integrates for 0.15H.

^{15}N NMR of **13b** (60.8 MHz, $(CD_3)_2SO$): δ 322.9 (*N*—O), 187.8 (*N*$^{+}$—Me).

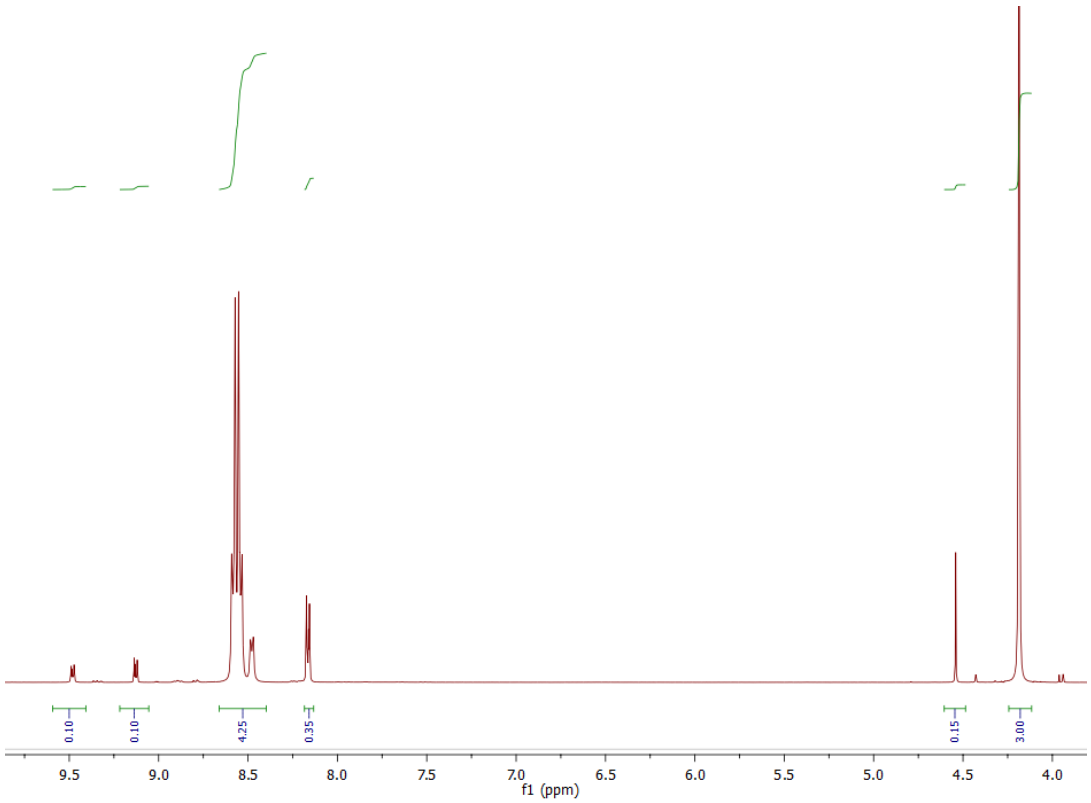


Figure S4: ^{1}H NMR spectrum of reaction mixture in CD_3CN, showing signals of **13b** (major product), some **15b** and starting material. The full spectrum is shown in Section 7.

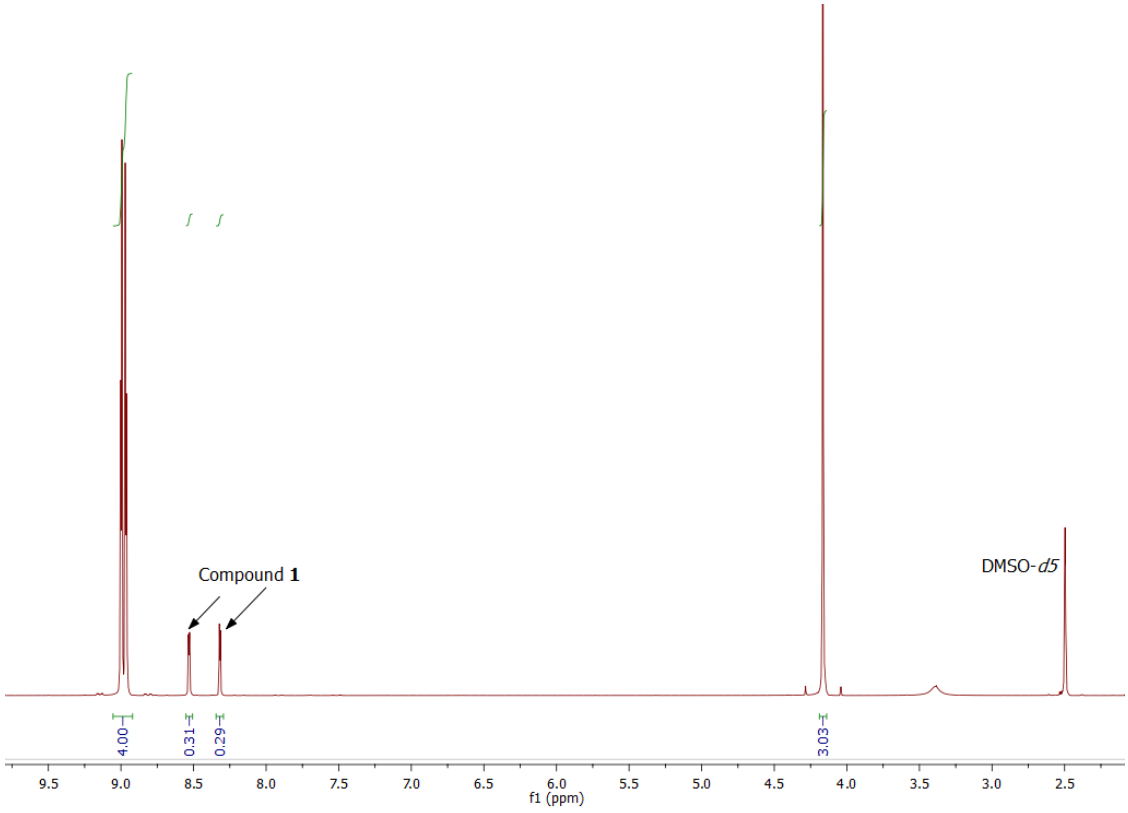
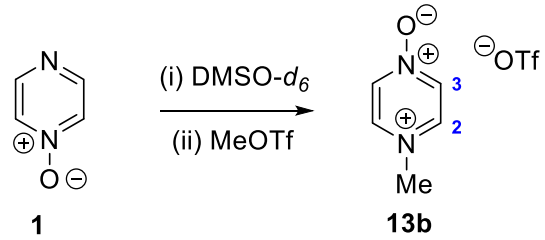


Figure S5: ^{1}H NMR spectrum of reaction mixture after removal of CD_3CN and addition of $(CD_3)_2SO$, showing signals of **13b** (major product) and starting material, but no **15b**. The full spectrum is shown in Section 7.

(c) Experiment Showing Exclusive Formation of 13b in $(CD_3)_2SO$ – Contains ^{15}N and ^{13}C NMR Data

Pyrazine *N*-oxide (**1**) (0.050 g, 0.52 mmol) was dissolved in $(CD_3)_2SO$ (0.65 ml) in a vial inside an inert atmosphere glove box. Methyl triflate (0.084 g, 0.51 mmol) was subsequently added dropwise. The reaction mixture was transferred to a NMR tube by syringe. The NMR tube was then sealed by a rubber septum cap and wrapped with PTFE tape. The septum was then covered with Parafilm and the tube transferred outside the glove box. The methoxydimethylsulfonium salt derived from $(CD_3)_2SO$ is likely to be the primary methylating agent in the reaction of **1** + MeOTf in $(CD_3)_2SO$.[10] As a consequence, the methylation of **1** is relatively slow. After 4 weeks the reaction mixture was subjected to ^1H and ^1H-^{15}N HMBC NMR spectroscopic characterization.



1 **13b**

^1H NMR (600 MHz, $(CD_3)_2SO$)

Signals assigned to **13b**: δ 9.02 – 8.98 (m, 2H), 8.98 – 8.93 (m, 2H), 4.17 (s, 3H, C*H*$_3$).

Signals assigned to **1**: δ 8.55 – 8.51 (m, 2H), 8.34 – 8.30 (m, 2H). Relative to 1H of **13b**, 1H of **1** integrates for 0.23H.

A signal assigned to the methoxydimethylsulfonium salt of $(CD_3)_2SO$ is present at 3.98 ppm. Relative to 1H of **13b**, 1H of the salt integrates for 0.15H.

$^{13}C\{^1H\}$ NMR (150 MHz, $(CD_3)_2SO$)

Signals assigned to **13b**: 142.7 (C-2) , 138.7 (C-3), 120.7 (q, *J* = 322 Hz, triflate *C*F$_3$), 46.8.

Signals assigned to **1**: δ 148.2, 134.2.

Signals assigned to methoxydimethylsulfonium salt of $(CD_3)_2SO$: 62.2.

^{15}N NMR of **13b** (60.8 MHz, $(CD_3)_2SO$)

Signals assigned to **13b**: δ 322.9 (*N*—O), 187.7 (N^+—Me).

Signals assigned to **1**: δ 310.8, 303.7.

Conversion Calculation (based on consumption of the methoxydimethylsulfonium salt as the limiting reagent):

4H of Compound **13b** corresponds to 4.00, therefore 1H = 1.00

For the methoxydimethylsulfonium salt at 3.98 ppm, 3H = 0.46, therefore 1H = 0.15.

$$\text{Conversion} = \frac{1.00}{1.00 + 0.15} \times 100 = 87\%$$

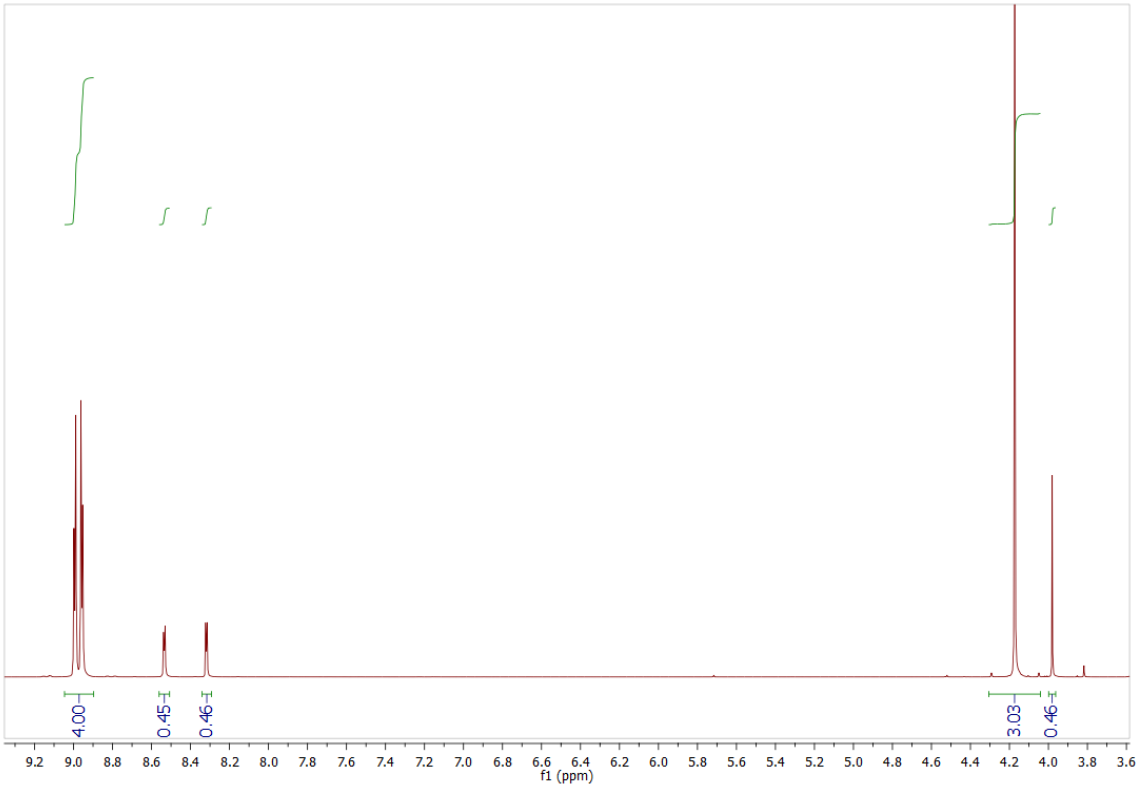


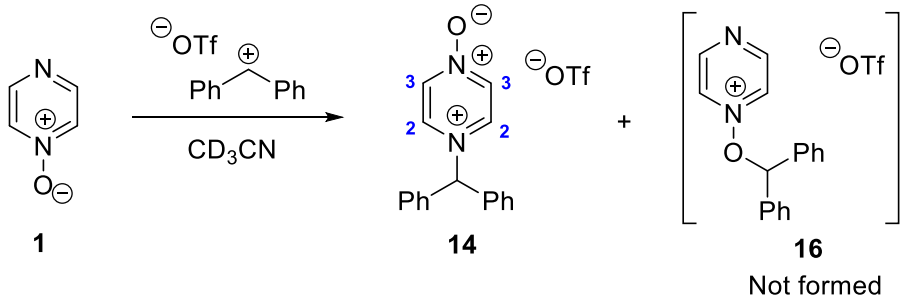
Figure S6: ^{1}H NMR spectrum showing product **13b** and **1** in $(CD_3)_2SO$. The full spectrum is shown in Section 7.

Preparation of 14

(a) Experiment in CD_3CN – Quantitative Conversion to 14 – Contains ^{13}C NMR data

The products of this reaction decompose upon exposure to moisture, and could not be isolated. The products were characterized by recording NMR spectra of the reaction mixture under inert atmosphere.

Pyrazine *N*-oxide (**1**) (0.016 g, 0.17 mmol), benzhydryl chloride (0.035 g, 0.17 mmol) and silver triflate (0.054 g, 0.21 mmol) were combined by the process described in General Procedure C to produce **14** in CD_3CN. NMR spectroscopic characterization of the product in CD_3CN was carried out. Quantitative conversion to **14** (based on consumption of the benzhydrylium ion) was observed.



^{1}H NMR (600 MHz, CD_3CN) δ 8.50 (app s,* 4H, H-2, H-3), 7.54 – 7.49 (m, 6H, Phenyl H-3, H-4 & H-5), 7.36 – 7.31 (m, 4H, Phenyl H-2 & H-6), 7.24 (s, 1H, C*H*Ph_2). Apparent singlet (app s) in ^{1}H NMR spectrum was appeared as two barely separated multiplets in other spectra of this compound.

$^{13}C\{^1H\}$ NMR (150 MHz, CD_3CN) δ 141.31 (C-3), 140.77 (C-2), 135.30 (Phenyl C-1), 131.05 (Phenyl C-4), 130.54 (Phenyl C-3 & C-5), 129.94 (Phenyl C-2 & C-6), 77.21 (*C*HPh_2).

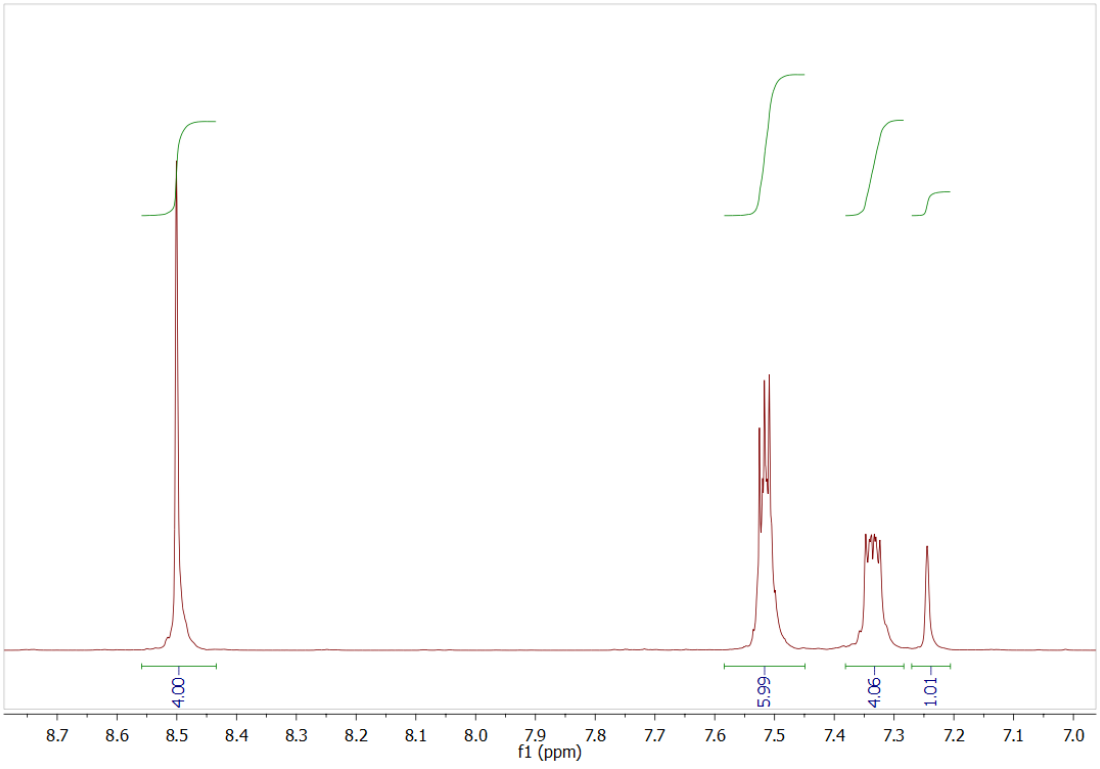
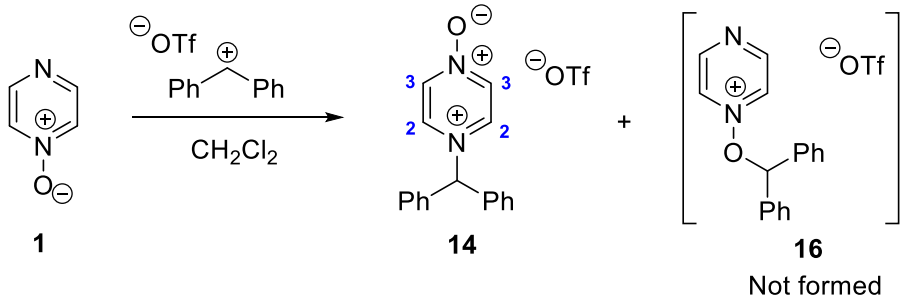


Figure S7: ^{1}H NMR spectrum in CD_2Cl_2 of **14**. The full spectrum is shown in Section 7.

(b) Experiment Showing Exclusive Formation of 14 in CH_2Cl_2 – Contains ^{15}N NMR Data

The products of this reaction decompose upon exposure to moisture, and could not be isolated. The products were characterized by recording NMR spectra of the reaction mixture under inert atmosphere.

Pyrazine *N*-oxide (**1**) (0.037 g, 0.39 mmol), benzhydryl chloride (0.077 g, 0.38 mmol) and silver triflate (0.113 g, 0.440 mmol) were combined by the process described in General Procedure C to produce **14** in CH_2Cl_2. The reaction mixture in CH_2Cl_2 was subjected to ^1H and ^1H-^{15}N HMBC NMR spectroscopic characterization using the solvent suppression protocol referred to in the General Experimental. No hydrolysis product can be definitively identified from the ^1H NMR spectrum, although a small amount of material not attributable to **14** is present. Conversion to **14** is estimated to be a minimum of 94% (based on integration of excess **1** relative to **14**).



1 **14** **16** Not formed

^{1}H NMR (600 MHz, CH_2Cl_2)

Assigned to **14**: δ 8.56 – 8.49 (m, 4H, H-2, H-3), 7.52 – 7.48 (m, 6H), 7.35 – 7.31 (m, 4H), 7.29 (s, 1H, Ph_2CH).

Assigned to **1**: δ 8.68 (app d, app *J* = 5.4 Hz, 2H), 8.48 (app d, app *J* = 5.5 Hz, 2H). Integration relative to 1H of **14** is 0.13H.

^{15}N NMR (60.8 MHz, CH_2Cl_2): δ 325.0 (*N*—O of **14**), 201.6 (N^+—Me of **14**).

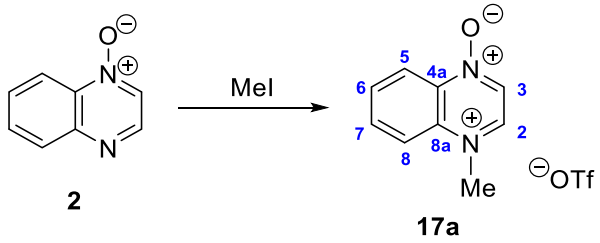
The ^1H and ^1H-^{15}N HMBC NMR spectra are shown in Section 7.

4.3 Reactions of Quinoxaline *N*-Oxide (2)

Preparations of *N*-Methylquinoxalinium *N'*-oxide iodide (17a)

(a) Experiment Showing Formation of 17a in Low Yield

Quinoxaline *N*-oxide (**2**) (0.023 g, 0.16 mmol) was placed in a N_2-filled Schlenk flask. Methyl iodide (0.684 g, 4.82 mmol) was subsequently added dropwise *via* syringe. The flask was wrapped in foil and left in the dark for 48 hours, before the methyl iodide was removed under vacuum using General Procedure A. The flask was then opened and the red solid product (**17a**) was washed by addition of Et_2O, which was removed by cannula filtration. Three aliquots of dry Et_2O (3 ml each) were used in this manner to wash the product in very low yield (2 mg, 0.007 mmol, 4% yield). The recovered product (**17a**) was dissolved in $(CD_3)_2SO$ for ^1H NMR spectroscopic characterization. Some signals from residual Et_2O are present in the ^1H NMR spectrum.



^{1}H NMR (600 MHz, $(CD_3)_2SO$) δ 9.46 (d, *J* = 5.2 Hz, 1H, H-2), 9.28 (d, *J* = 5.2 Hz, 1H, H-3), 8.61 (dd, *J* = 8.7, 1.2 Hz, 1H, H-8), 8.55 – 8.51 (m (app dd, signal resolution renders *J* values ambiguous), 1H, H-5), 8.34 (m, 1H, H-6), 8.21 – 8.15 (m, 1H, H-7), 4.49 (s, 3H, NC*H*$_3$).

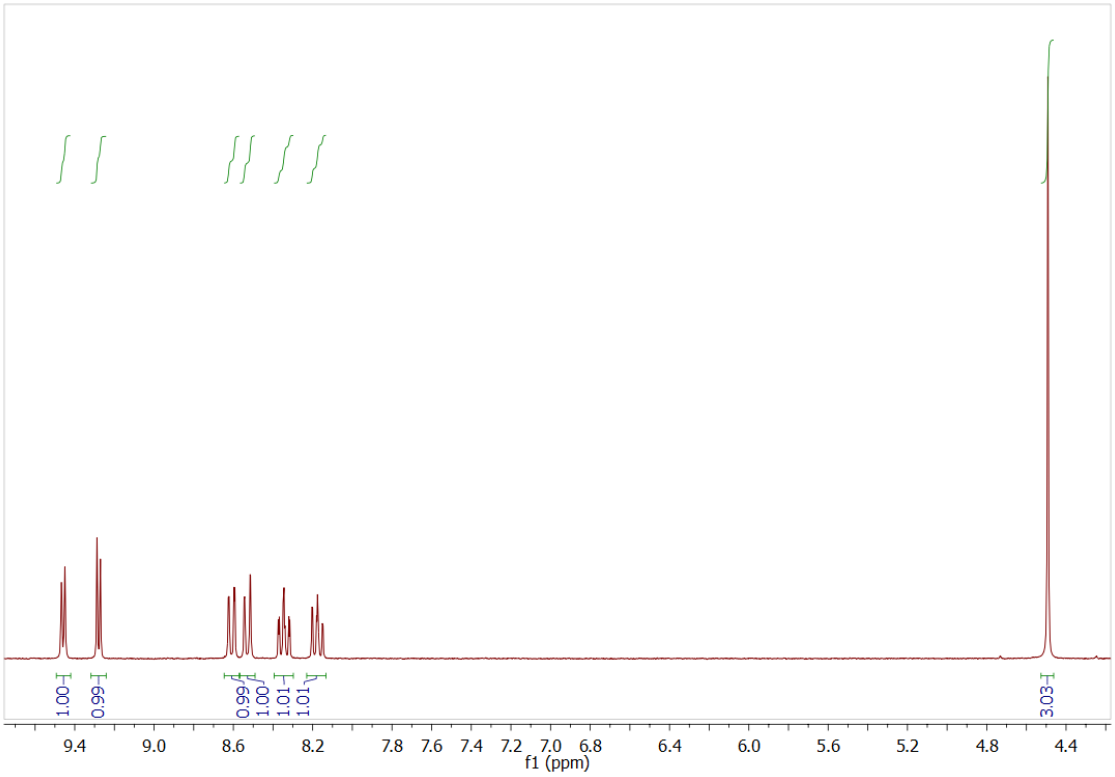
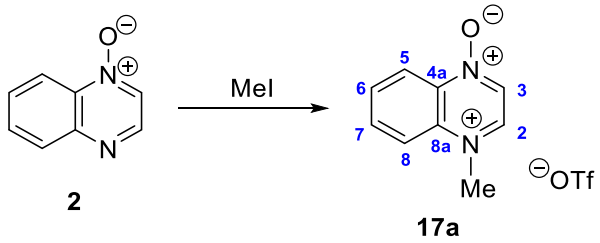


Figure S8: ^1H NMR spectrum of **17a** in $(CD_3)_2SO$. The full spectrum is shown in Section 7.

(b) Experiment Showing Formation of 17a in Low Yield – Contains ^{15}N NMR data

Quinoxaline *N*-oxide (**2**) (0.044 g, 0.30 mmol) was placed in a N_2-filled Schlenk flask. Methyl iodide (0.129 g, 0.91 mmol) was subsequently added dropwise *via* syringe. The MeI was removed under vacuum using General Procedure A after 18 hours and the solid product (**17a**) was washed by addition of dry Et_2O, which was removed by cannula filtration (under inert atmosphere). Three aliquots of dry Et_2O (0.4 ml each) were used in this manner to wash the product (yield = 0.014 g, 0.049 mmol, 16%). A sample of **17a** in dry $(CH_3)_2SO$ was then prepared for ^{1}H and ^{1}H-^{15}N HMBC NMR spectroscopic characterization using General Procedure B. Note: An initial attempt to dissolve the product in CH_2Cl_2 was unsuccessful, and a residual amount of this solvent can be seen in the spectrum.



^{1}H NMR (600 MHz, $(CH_3)_2SO$) δ 9.42 (d, *J* = 5.2 Hz, 1H, H-2), 9.25 (d, *J* = 5.2 Hz, 1H, H-3), 8.59 – 8.56 (m (app dd, *J* values ambiguous), 1H, H-8), 8.51 – 8.48 (m (app dd, *J* values ambiguous), 1H, H-5), 8.34 – 8.29 (m, 1H, H-6), 8.16 – 8.12 (m, 1H, H-7), 4.46 (s, 3H, NC*H*$_3$).

^{15}N NMR (60.8 MHz, $(CH_3)_2SO$): δ 314.7 (*N*—O), 178.3 (N^+—Me).

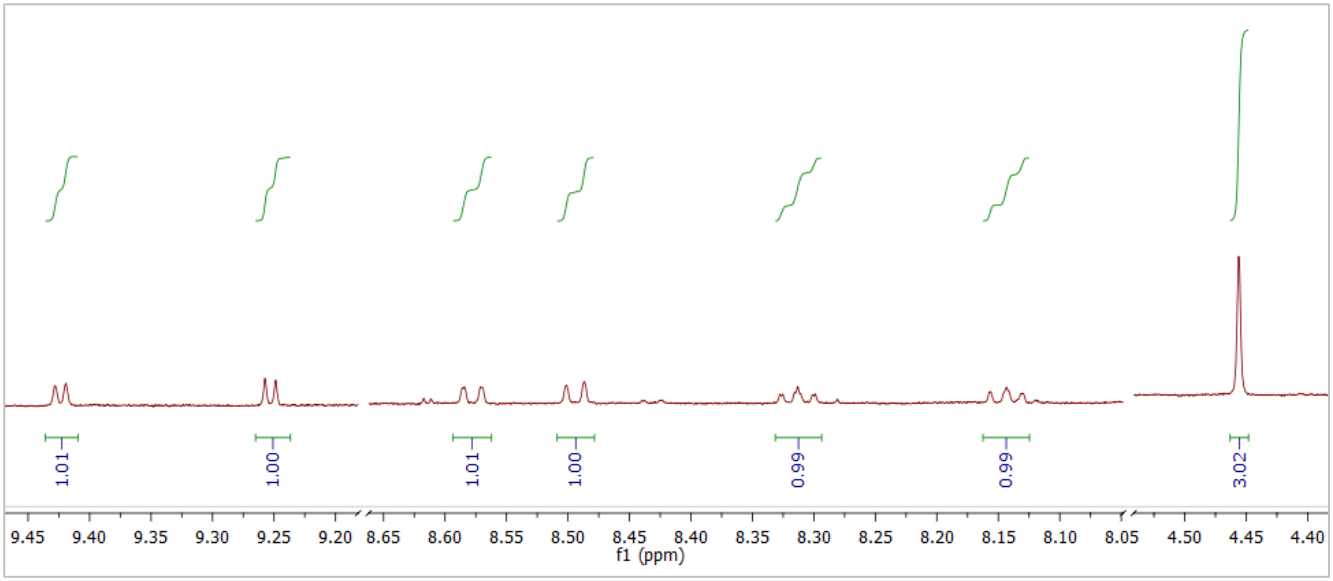


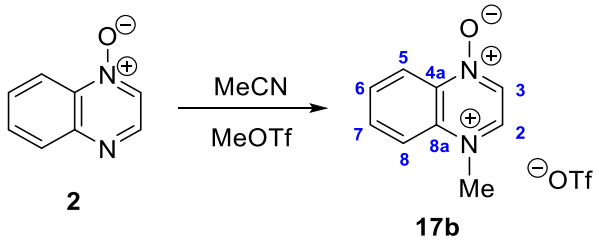
Figure S9: ^{1}H NMR spectrum of **17a** in $(CH_3)_2SO$. The full spectrum is shown in Section 7.

Note: This spectrum was recorded in non-deuterated solvent (using the solvent suppression protocol specified in the General Experimental above). Due to a combination of this and the low conversion to product that occurred in this reaction, the product signals are very small. However, the spectral details match well to the ^{1}H NMR spectrum obtained from another repetition of the same experiment, described in part (a), immediately above.

Preparations of 17b and 19b

(a) Experiment Showing Isolated Yield of 17b

Quinoxaline *N*-oxide (**2**) (0.323 g, 2.21 mmol) was dissolved in CH_3CN (10 ml) in a N_2-filled Schlenk flask. Methyl triflate (0.399 g, 2.43 mmol) was subsequently added dropwise. After 5 hours, the CH_3CN was removed under vacuum using General Procedure A, giving black crystals. The solid product (**17b**) was washed by addition of dry Et_2O, which was removed by cannula filtration (under inert atmosphere). Three aliquots of dry Et_2O (3 ml each) were used in this manner to wash the product (yield = 0.389 g, 1.25 mmol, 57%). A sample of **17b** in dry $(CD_3)_2SO$ was then prepared for ^1H and ^1H-^{13}C HMBC NMR spectroscopic characterization using General Procedure B.



2 **17b**

^{1}H NMR (300 MHz, $(CD_3)_2SO$) δ 9.45 (d, *J* = 5.2 Hz, 1H, H-2), 9.27 (d, *J* = 5.2 Hz, 1H, H-3), 8.61 (dd, *J* = 8.7, 1.2 Hz, 1H, H-8), 8.55 – 8.49 (m (app dd, signal resolution renders *J* values ambiguous), 1H, H-5), 8.39 – 8.30 (m, 1H, H-6), 8.17 (m, 1H, H-7), 4.49 (s, 3H, C*H*$_3$).

^{13}C{^{1}H} NMR (75 MHz, $(CD_3)_2SO$) δ 144.5 (C-2), 140.0 (C-4a), 136.5 (C-6), 135.9 (C-8a), 133.2 (C-7), 133.0 (C-3), 121.1 (C-5), 120.0 (C-8), 44.2 (*C*H$_3$)

IR (ATR-FTIR), cm^{-1}: 3115 (w), 3092 (w), 1629 (m), 1536 (m), 1408 (m), 1256 (s), 1029 (s), 638 (m).

HRMS-ESI+ (*m/z*): calculated for $[M]^+ = C_9H_9N_2O$ 161.0709; found 161.07069.

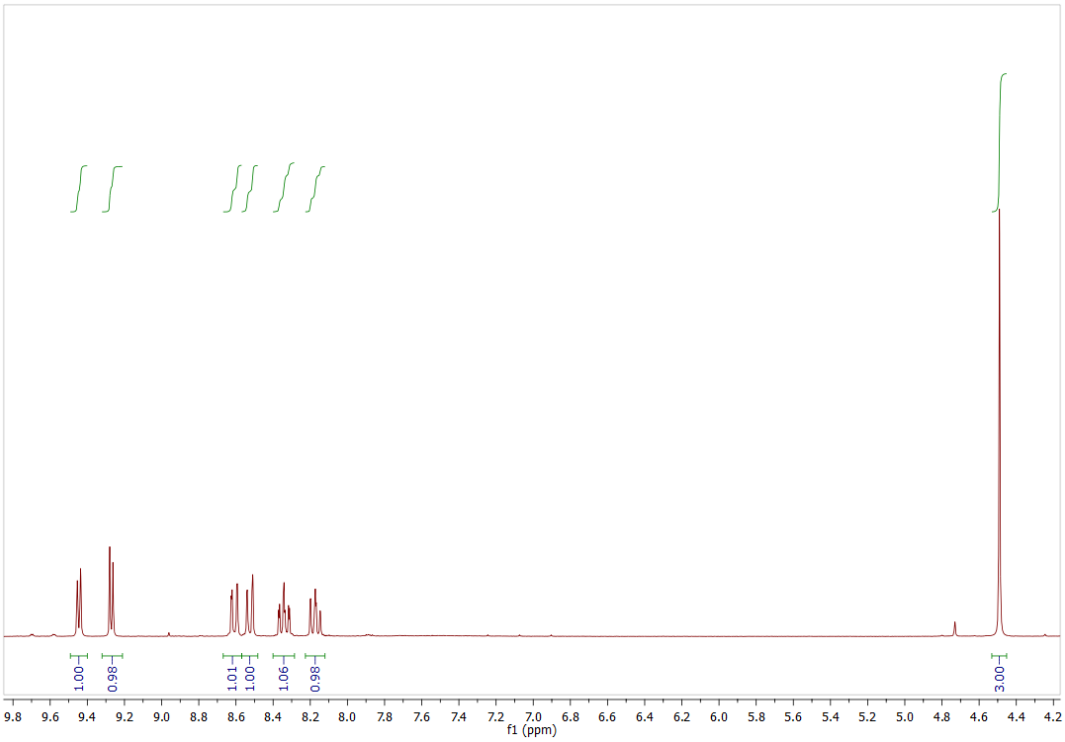
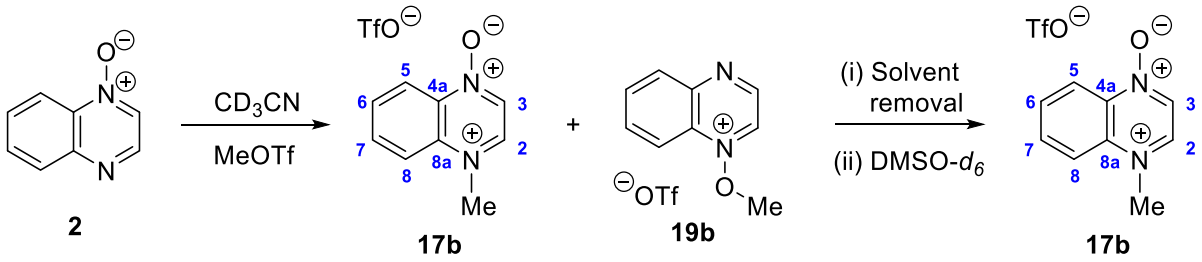


Figure S10: ^{1}H NMR spectrum in $(CD_3)_2SO$ of **17b**. The full spectrum is shown in Section 7.

(b) Experiment Showing N- vs O-Alkylation Product Ratio (17b vs 19b) – Contains ^{13}C & ^{15}N NMR Data

Quinoxaline *N*-oxide (**2**) (0.047 g, 0.32 mmol) was dissolved in CD_3CN (0.65 ml) in a N_2-filled Schlenk flask. Methyl triflate (0.045 g, 0.27 mmol) was subsequently added dropwise. The reaction mixture was transferred to an NMR tube and analyzed by NMR spectroscopy using General Procedure B.

Note: Insufficient concentrations of **2** and minor product **19b** in the following spectra meant that unambiguous assignment of hydrogen and carbon NMR signals to specific sites in the structures of these compounds was not possible.



2 **17b** **19b** **17b**

^{1}H NMR (400 MHz, CD_3CN)

Assigned to **17b**: δ 8.98 (d, *J* = 5.1 Hz, 1H, H-2), 8.79 (d, *J* = 5.2 Hz, 1H, H-3), 8.62 – 8.55 (m, 1H, H-5), 8.48 – 8.23 (m, 2H, H-5 and H-7), 8.16 – 8.06 (m, 1H, H-8), 4.47 (s, 3H, NC*H*$_3$).

Assigned to **19b**: δ 9.63 (d, *J* = 3.4 Hz, 1H), 9.56 (d, *J* = 3.2 Hz, 1H), 8.62 – 8.55 (m, 1H), 8.48 – 8.23 (m, 2H), 8.16 – 8.06 (m, 1H), 4.69 (s, 3H, OC*H*$_3$). Relative to 1H of **17b**, 1H of **19b** integrates for 0.12H.

Assigned to **2**: δ 8.69 (d, *J* = 3.6 Hz, 1H), 8.48 – 8.23 (m, 2H), 8.16 – 8.06 (m, 1H), 7.94 – 7.87 (m, 1H), 7.84 – 7.78 (m, 1H). Relative to 1H of **17b**, 1H of **2** integrates for approximately 0.33H.

The signal between 8.62 and 8.55 ppm contains a 1H signal from **17b** and a 1H signal from **19b**.

The signal between 8.48 and 8.23 ppm contains a 2H signal from **17b**, a 2H signal from **19b** and a 2H signal from **2**.

The signal between 8.16 and 8.06 ppm contains a 1H signal from **17b**, a 1H signal from **19b** and a 1H signal from **2**.

$^{13}C\{^1H\}$ NMR (100 MHz, CD_3CN)

Assigned to **17b**: δ 143.2 (C-2), 140.2 (C-4a), 136.3 (C-6), 135.5 (C-8a), 132.9 (C-7), 132.1 (C-3), 120.1 (C-5), 119.7 (C-8), 44.1 (*C*H$_3$)

Assigned to **19b**: δ 147.2, 144.7, 140.2, 136.8, 134.7, 131.7, 129.4, 119.1, 116.3, 68.9.

Ratio of N-alkylation and O-alkylation Products (from integrations in ^{1}H NMR spectrum):

3H of Compound **17b** = 3.00 – Therefore 1H = 1.00

3H of compound **19b** = 0.36 – Therefore 1H = 0.12

$$\text{Ratio} = \frac{1.00}{1.00 + 0.12} \times 100 = 89\%\ \text{N alkylation}$$

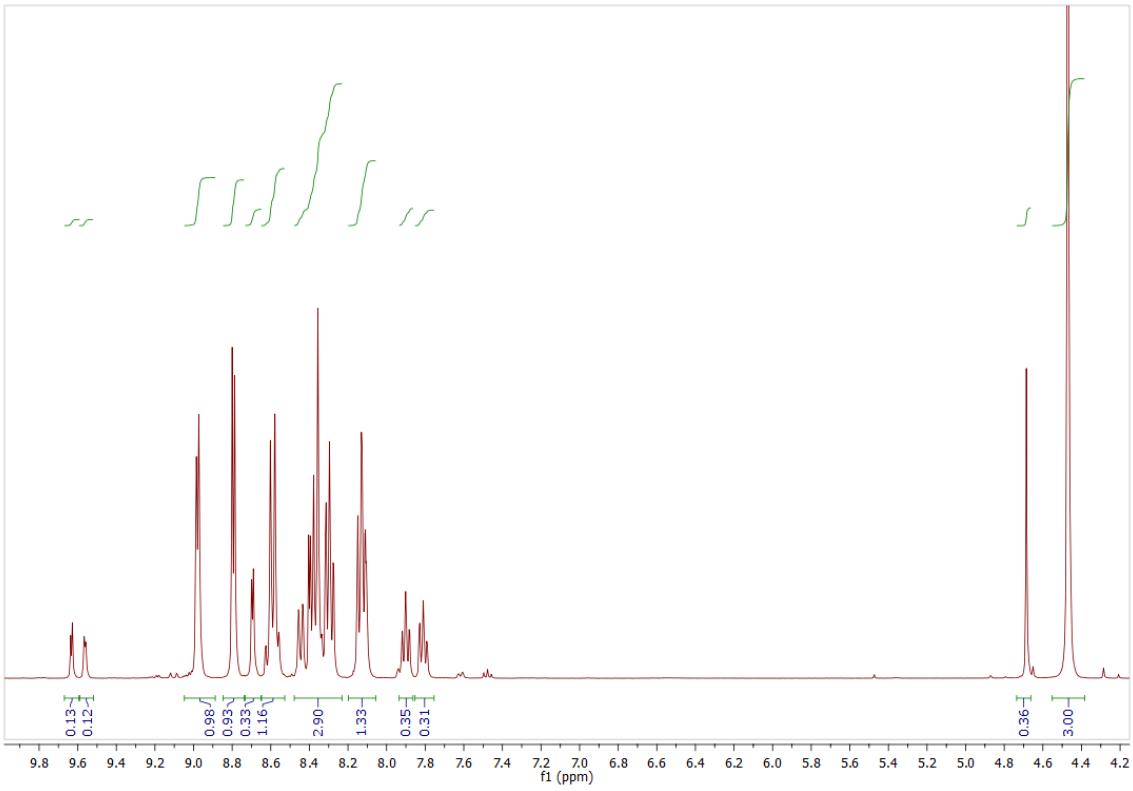


Figure S11: ^{1}H NMR Spectrum of **17b**, **19b** and **2** in CD_3CN. The full spectrum is shown in Section 7.

The CD_3CN was removed using General Procedure A and the product mixture was re-dissolved in $(CD_3)_2SO$ to allow a ^{1}H-^{15}N HMBC NMR spectrum to be recorded. Product **19b** did not survive the solvent removal process.

^{1}H NMR (600 MHz, $(CD_3)_2SO$)

Assigned to **17b**: δ 9.46 (d, *J* = 5.1 Hz, 1H, H-2), 9.29 (d, *J* = 5.1 Hz, 1H, H-3), 8.60 (app d,* app *J* = 8.6 Hz, 1H, overlaps partially with signal of **2**, H-8), 8.53 (app d,* app *J* = 8.8 Hz, 1H, H-5), 8.37 – 8.32 (m, 1H, H-6), 8.20–8.16 (m, overlaps with signal of **2**, 1H, H-7), 4.50 (s, 3H, NCH_3). See NMR spectra in experiments described above – these signals are not doublets; signal resolution in this particular spectrum is too low to observe the fine structure of these signals.

Assigned to **2**: δ 8.78 (d, *J* = 3.5 Hz, 1H), 8.63 (d, *J* = 3.5 Hz, 1H, overlaps partially with signal of **17b**), 8.46 – 8.42 (m (app d, app *J* = 8.5 Hz), 1H), 8.16 – 8.11 (m, overlaps with signal of **17b**, 1H), 7.96 – 7.92 (m, 1H), 7.88 – 7.84 (m, 1H). Relative to 1H of **17b**, 1H of **2** integrates for 0.26H.

The region between 8.64 and 8.45 ppm contains two 1H signals from **17b** and a 1H signal from **2**.

The region between 8.20 and 8.11 ppm contains a 1H signal from **17b** and a 1H signal from **2**.

^{15}N NMR (60.8 MHz, $(CD_3)_2SO$): δ 314.4 (*N*—O), 178.0 (N^+—Me).

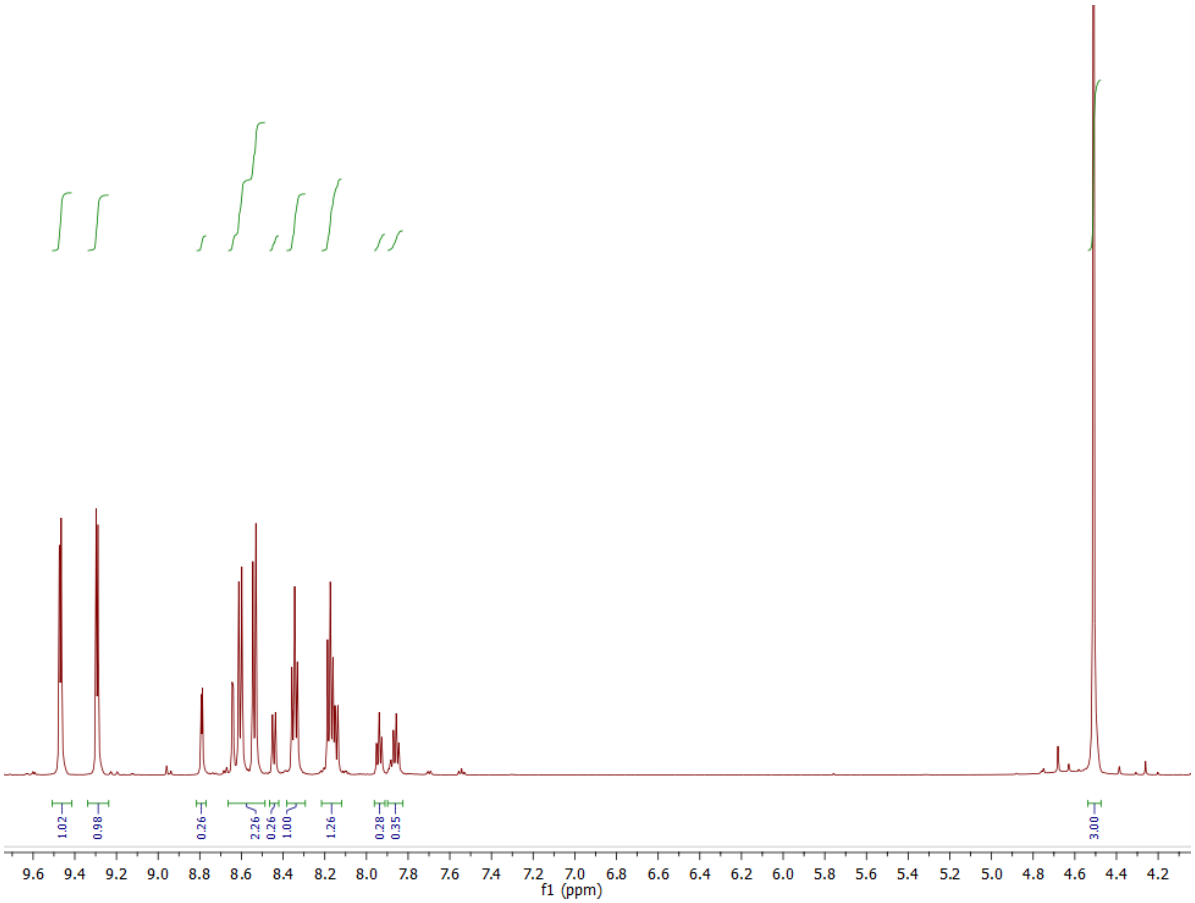
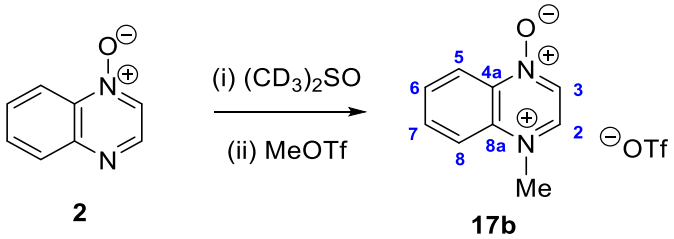


Figure S12: ^{1}H NMR Spectrum of **17b** and **2** in $(CD_3)_2SO$. Note the absence of signals assigned to **19b**. The full spectrum is shown in Section 7.

(c) Experiment Showing Exclusive Formation of 17b in $(CD_3)_2SO$ – Contains ^{15}N NMR Data

Quinoxaline *N*-oxide (**2**) (0.057 g, 0.39 mmol) was dissolved in $(CD_3)_2SO$ (0.8 ml) in a vial inside an inert atmosphere glove box. Methyl triflate (0.050 g, 0.31 mmol) was subsequently added dropwise. The reaction mixture was transferred to a NMR tube by syringe. The NMR tube was then sealed by a rubber septum cap and wrapped with PTFE tape. The septum was then covered with Parafilm and the tube transferred outside the glove box. $(CH_3)_2SO$ is known to react with methylating agents (e.g. dimethyl sulfate) to give methoxydimethylsulfonium salt.[10] The resulting methoxysulfonium salt acts as the primary methylating agent in the reaction of **2** + MeOTf in $(CD_3)_2SO$. As a consequence, the methylation of **2** is relatively slow. After 4 weeks the reaction mixture was subjected to ^1H and ^1H-^{15}N HMBC NMR spectroscopic characterization.



2 **17b**

^1H NMR (600 MHz, $(CD_3)_2SO$)

Assigned to **17b**: δ 9.46 (d, *J* = 5.1 Hz, 1H, H-2), 9.27 (d, *J* = 5.1 Hz, 1H, H-3), 8.58 (dd, *J* = 8.7, 1.1 Hz, 1H, H-8), 8.54 – 8.50 (m (app dd, signal resolution renders *J* values ambiguous), 1H, H-5), 8.34 – 8.30 (m, 1H, H-6), 8.18 – 8.14 (m, 1H, overlaps partially with signal of **2**, H-7), 4.51 (s, 3H, C*H*$_3$).

Assigned to **2**: δ 8.78 (d, *J* = 3.6 Hz, 1H), 8.62 (d, *J* = 3.6 Hz, 1H), 8.42 (dd, *J* = 8.6, 1.2 Hz, 1H), 8.14 – 8.10 (1H, overlaps partially with signal of **17b**), 7.95 – 7.89 (m, 1H), 7.87 – 7.81 (m, 1H). Relative to 1H of **17b**, 1H of **2** integrates for approximately 0.78H.

The region between 8.17 and 8.10 ppm contains a 1H signal from **17b** and a 1H signal from **2**.

A signal assigned to the methoxydimethylsulfonium salt of $(CD_3)_2SO$ is present at 3.99 ppm. Relative to 1H of **17b**, 1H of the salt integrates for 0.28H.

^{15}N NMR (60.8 MHz, $(CD_3)_2SO$)

Assigned to **17b**: δ 314.4 (*N*—O), 177.9 (N^+—Me).

Assigned to **2**: δ 302.3, 299.7.

Conversion Calculation (based on consumption of the methoxydimethylsulfonium salt as the limiting reagent):

For the methoxydimethylsulfonium salt at 3.99 ppm, 3H = 0.84 relative to 1H of **17b**, therefore 1H = 0.28.

$$\text{Conversion} = \frac{1.00}{1.00 + 0.28} \times 100 = 78\%$$

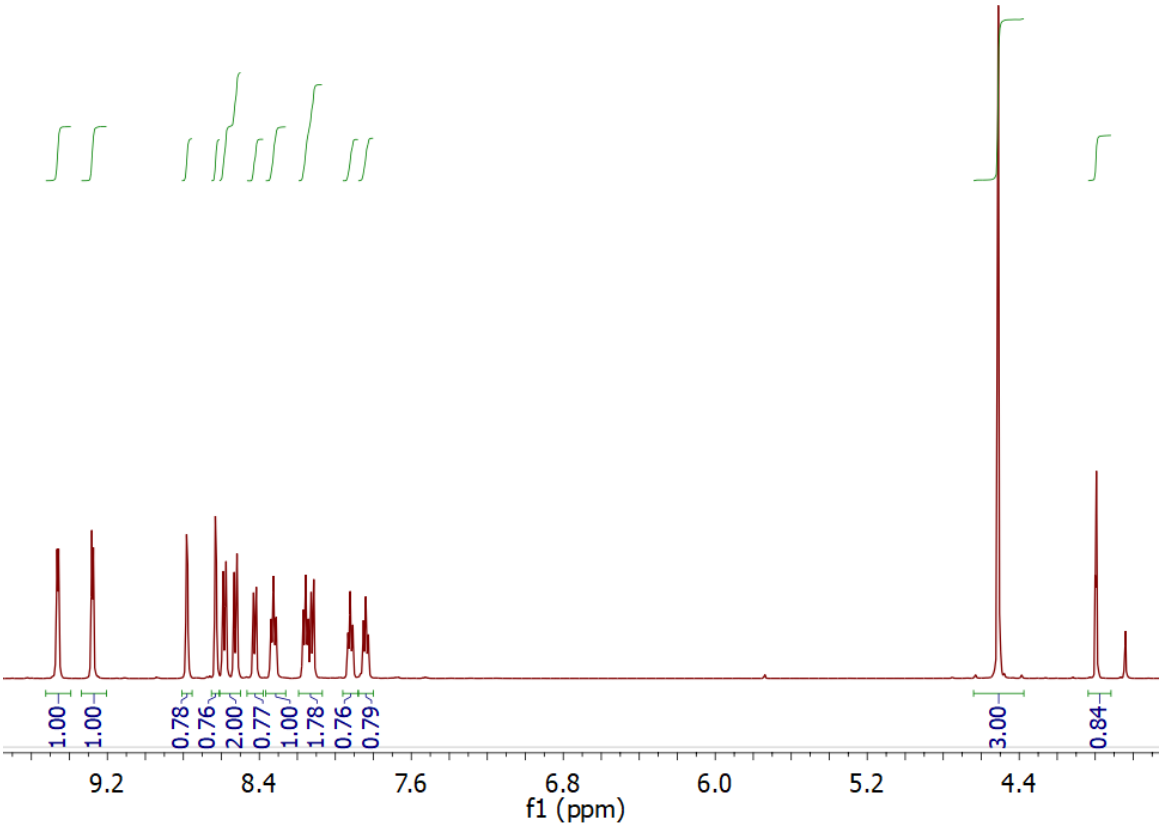
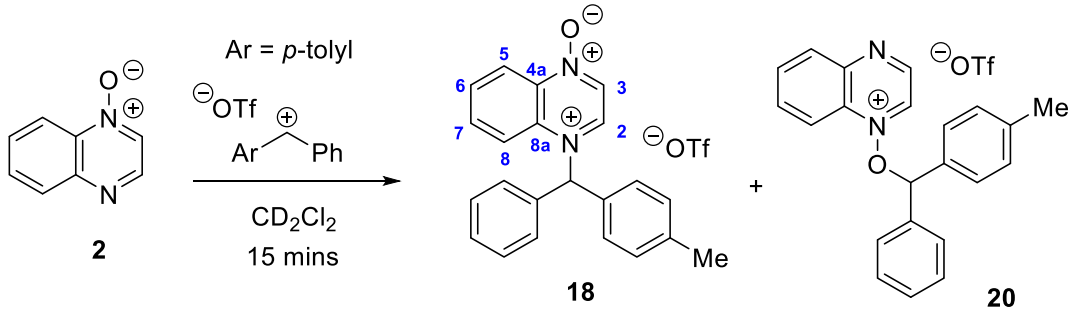


Figure S13: ^{1}H NMR Spectrum in $(CD_3)_2SO$ of **17b** and **2** in $(CD_3)_2SO$. The full spectrum is shown in Section 7.

Preparation of 18

The products of this reaction decompose upon exposure to moisture, and could not be isolated. Consequently, the products were characterized by recording NMR spectra of the reaction mixture under inert atmosphere.

Quinoxaline *N*-oxide (**2**) (0.026 g, 0.18 mmol), 4-methylbenzhydryl chloride (0.038 g, 0.18 mmol) and silver triflate (0.044 g, 0.17 mmol) were combined by the process described in Procedure C to produce **18** (major product) + **20** (minor product) in CD_2Cl_2. The reaction mixture in CD_2Cl_2 was then prepared for ^1H and ^1H-^{15}N HMBC NMR spectroscopic characterization using General Procedure B.



^{1}H NMR (600 MHz, CD_2Cl_2)

Signals assigned to **18**: δ 8.75 (d, *J* = 5.5 Hz, 1H, H-3), 8.60 (dd, *J* = 8.7, 1.1 Hz, 1H, H-8), 8.53 (d, *J* = 5.5 Hz, 1H, H-2), 8.42 (app d, app *J* = 8.9 Hz, 1H, H-5), 8.10 (m, 1H, H-7), 8.02 – 7.97 (m, 1H, H-6), 7.81 (s, 1H, C*H*PhTol), 7.51 – 7.46 (m, 3H, Phenyl H-3, H-4 & H-5), 7.39 – 7.22 (m, 6H, Phenyl H-2 & H-6, Tolyl H-2, H-3, H-5 & H-6), 2.37 (s, 3H, CH_3).

Signals assigned to **20**: δ 8.83 (d, *J* = 3.6 Hz, 1H), 8.28 (d, *J* = 8.4 Hz, 1H) and 7.87 (m, 1H). Relative to 1H of **18**, 1H of **20** integrates for 0.10H.

A peak assigned to a hydrolysis product is present at 5.38 ppm. The signals of the aromatic protons of this product also contribute to the integration of the multiplet at 7.39 – 7.22 ppm. Relative to 1H of **18**, 2H of the hydrolysis product integrates for 0.08H.

^{13}C{^{1}H} NMR (150 MHz, CD_2Cl_2)

Signals assigned to **18**: δ 141.4 (Tolyl C-4), 141.2 (C-4a), 140.7 (C-2), 137.5 (C-7), 135.6 (C-8a), 134.8 (Phenyl C-1), 133.5 (C-6), 133.1 (C-3), 130.8 (Tolyl C-3 & C-5), 130.2 (Phenyl C-4), 130.1 (Phenyl C-3 & C-5), 129.5 (Tolyl C-2 & C-6), 129.2 (Phenyl C-2 & C-6), 121.4 (C-5), 121.1 (C-8), 73.2 (*C*HPhTol), 21.3 (*C*H_3).

A ^{13}C NMR signal assigned to the *C*$F_3SO_3^-$ ion is present at δ 120.72 (q, *J* = 320 Hz).

Note: Low concentration of minor product **20** in the ^{13}C{^{1}H} NMR spectrum meant that assignment of the very small signals present in the spectrum to this compound could not be done unambiguously.

^{15}N NMR (60.8 MHz, CD_2Cl_2)

Signals assigned to **18**: δ 317.6 (*N*—O), 190.5 (*N*$^+$—Me).

No correlations were observed to the ^{1}H NMR signals of the minor product, **20**.

Ratio of N-alkylation and O-alkylation Products:

1H of compound **18** = 1.00

1H of compound **20** = 0.10

$$\text{Ratio} = \frac{1.00}{1.00 + 0.10} \times 100 = 91\%\ \text{N alkylation}$$

<u>Conversion Calculation</u> (based on consumption of the benzhydrylium ion as the limiting reagent):

1H of Compound **18** corresponds to 1.00.

For the hydrolysis product at 5.38ppm, 2H = 0.08. Therefore, since two equivalents of benzhydrylium ion are consumed in hydrolysis (formation of bis(benzhydryl) ether), the conversion was:

$$\text{Conversion} = \frac{1.00}{1.00 + 0.08} \times 100 = 93\%$$

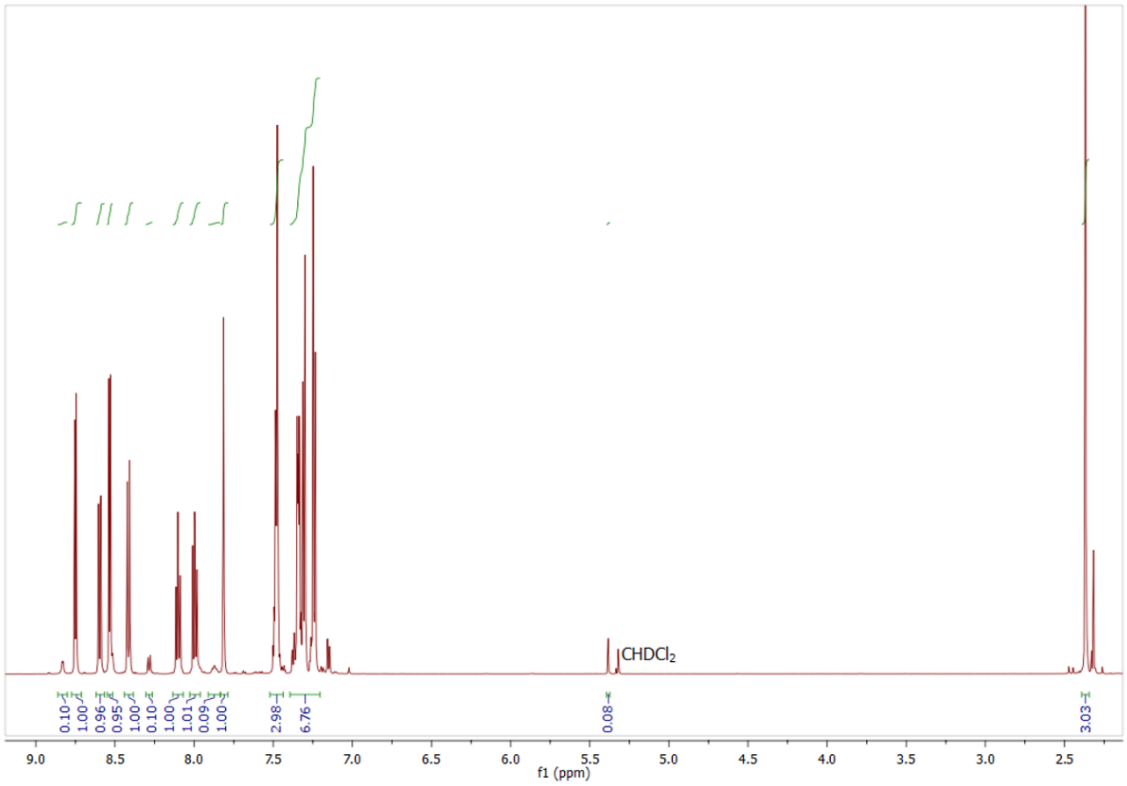


Figure S14: ^{1}H NMR spectrum in CD_2Cl_2 of **18**. The full spectrum is shown in Section 7.

4.4 Reactions of Pyrimidine *N*-Oxide (3)

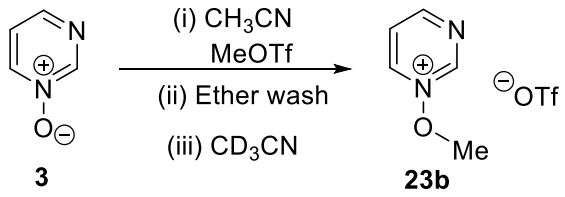
Preparations of 21b and 23b

Removing the solvent from reaction mixtures containing **21b** and/or **23b** causes decomposition of **21b**. Formation of some quantity of degradation products was observed in all instances of reactions of **3** with MeOTf (see below), regardless of whether CD_3CN, MeCN or $(CD_3)_2SO$ were used as solvent *even if the solvent was not removed*. Taking steps to protect the reaction mixture from light also did not prevent the formation of these degradation products. It is not clear whether the degradation products observed directly in reaction mixtures by ^1H NMR spectroscopy (reactions in CD_3CN or $(CD_3)_2SO$ – see below) are derived from decomposition of **21b** or **23b** or both, or if some separate process leads to the formation of the decomposition products observed in the reaction mixtures. Although **23b** survives solvent removal, attempts to isolate it from the decomposition products through crystallization under inert atmosphere (in a Schlenk flask) were unsuccessful, resulting only in formation of further decomposition product(s). Since neither **21b** nor **23b** could be isolated, it was necessary to characterize these products in the reaction mixtures in which they formed by NMR spectroscopy under inert atmosphere. A high resolution mass spectrum of **23b** (sample maintained under inert atmosphere) was also obtained by subjecting a reaction mixture known (from NMR spectroscopic analysis) to contain only a small amount of decomposition product to electrosptray ionization mass spectrometric analysis (see below). This compound (with dimethylsulfate counter-ion rather than triflate) has been characterized previously.[11]

(a) Experiment Showing Approximate Isolated Yield of 23b

Pure samples of compounds **23b** and/or **21b** could not be obtained from this reaction for the reasons given at the start of section 4.4 (just above).

Pyrimidine *N*-oxide (**3**) (0.195 g, 2.03 mmol) was dispensed into a Schenk flask and sealed in a glove box. The flask was removed from the glove box and attached to a Schlenk line, and the solid was then dissolved in dry CH_3CN (3 ml). Methyl triflate (0.342 g, 2.08 mmol) was subsequently added dropwise. The flask was wrapped with aluminium foil and the reaction mixture was stirred for 24 hours.



3 **23b**

All operations and manipulations of the product were carried out under inert atmosphere – *i.e.* the product was kept in a Schlenk flask under an atmosphere of N_2 throughout. Dry Et_2O (3 ml) was then added to the reaction mixture, which caused the separation of a yellow oil from the reaction mixture. The supernatant (CH_3CN/Et_2O) was carefully removed by cannula. Two further aliquots of dry Et_2O (3 ml each) were then used to wash the yellow oil. In each case, the Et_2O supernatant was removed by cannula, as above. The product was dried by passing a stream of N_2 gas over the oil to avoid exposing the product to vacuum (for the reasons given at the beginning of section 4.4). The oil obtained contained small amounts of decomposition products seen in all experiments involving reaction of **3** with MeOTf (see

below). The amount of decomposition product present (based on ^{1}H NMR spectroscopic analysis of theis material) is sufficiently small to quote an approximate isolated yield for **23b** of 404 mg (1.55 mmol, 77% yield) from this experiment. All attempts to purify this material further (to obtain completely pure **23b**) resulted in decomposition of the product. A small sample of the product was dissolved in dry CD_3CN and analyzed by NMR spectroscopy using General Procedure B. A separate sample of **23b** was prepared in dry MeCN (approximately 1 mg ml^{-1}) and transferred to a mass spectrometry vial contained in a Schlenk flask under an atmosphere of nitrogen. The sample was maintained under inert atmosphere until directly prior to recording the mass spectrum.

^{1}H NMR (300 MHz, CD_3CN) Signals assigned to **23b**: δ 9.77 (dd, *J* = 2.3, 0.8 Hz, 1H), 9.43 – 9.34 (m, 2H), 8.23 (ddd, *J* = 6.8, 4.9, 0.9 Hz, 1H), 4.47 (s, 3H).

HRMS-ESI+ (*m/z*): Calculated for $[M]^+ = C_5H_7N_2O$ 111.0553; found 111.0550 (44%). Calculated for $[M + H + OTf]^+ = C_6H_8N_2O_4SF_3$ 261.0157; found 261.0150 (100%). We assign the second peak to the dicationic N-protonated adduct of **23b** associated with triflate to give an entity with a single net positive charge.

Note: The ^{1}H signal at δ 9.77 in compound **23b** has an extremely long relaxation time. A 30° pulse and a relaxation delay of 60 seconds were used during acquisition of the spectrum shown in Fig. S14, leading to a set of internally consistent integrations for the ^{1}H NMR signals of **23b**.

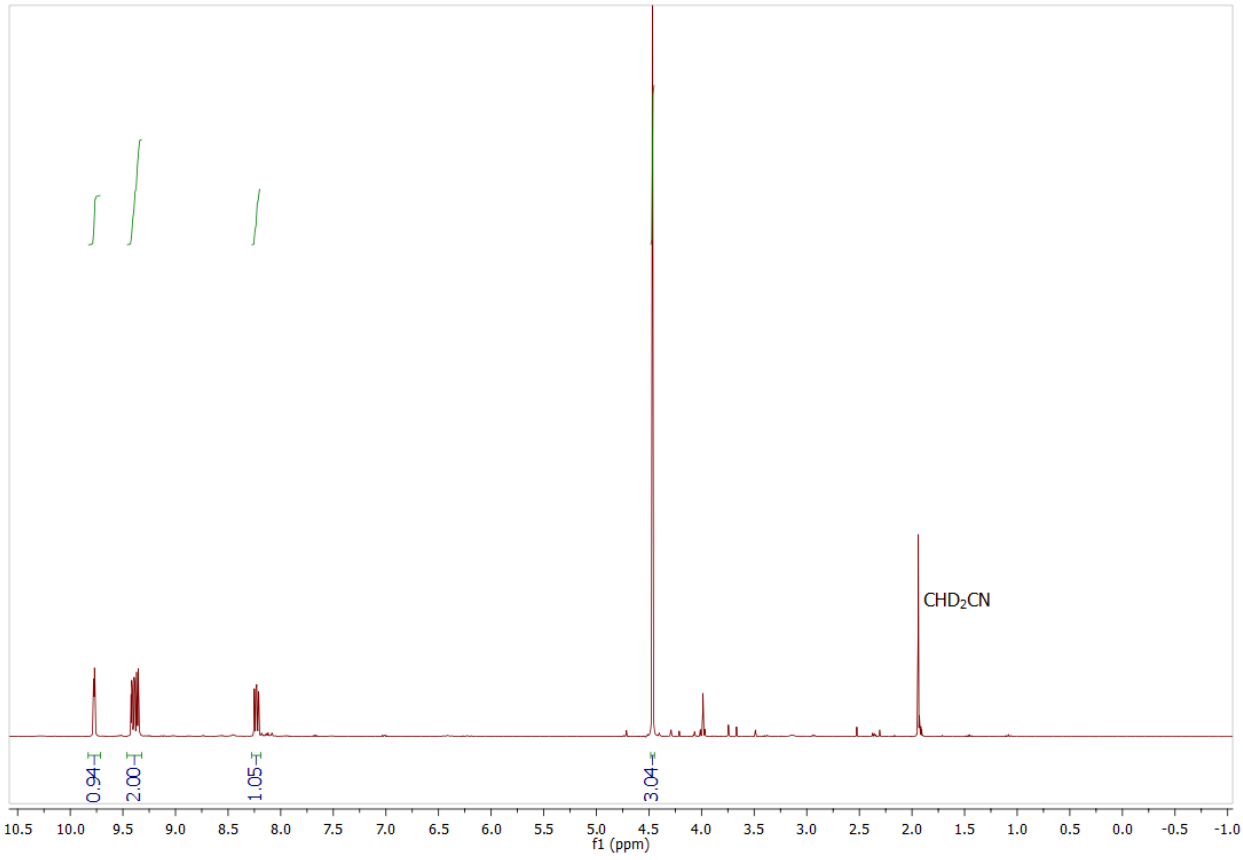
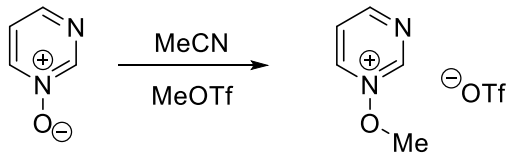


Figure S15: ^{1}H NMR spectrum in CD_3CN of **23b**. Small signals of decomposition products are present between 4.5 and 2.0 ppm.

(b) <u>Reaction in MeCN – after solvent removal only 23b is observed – Contains ^{15}N NMR Data</u>

Pure samples of compounds **23b** and/or **21b** could not be obtained from this reaction for the reasons given at the start of section 4.4.

Pyrimidine *N*-oxide (**3**) (0.046 g, 0.48 mmol) was dissolved in CH_3CN (5 ml) in a N_2-filled Schlenk flask. Methyl triflate (0.057 g, 0.35 mmol) was subsequently added dropwise. After *ca.* 20 minutes, the CH_3CN was removed under vacuum using General Procedure A and the solid product (**23b**) was washed by addition of dry Et_2O, which was removed by cannula filtration (under inert atmosphere). Three aliquots of dry Et_2O (2 ml each) were used in this manner to wash the product. A sample of **23b** in dry $(CH_3)_2SO$ was then prepared for ^{1}H and ^{1}H-^{15}N HMBC NMR spectroscopic characterization using General Procedure B.



3 **23b**

^{1}H NMR (600 MHz, $(CH_3)_2SO$)

Signals assigned to **23b**: δ 10.21 (app d, app *J* = 1.8 Hz, 1H), 9.90 – 9.83 (m, 1H), 9.44 (dd, *J* = 4.8, 1.5 Hz, 1H), 8.40 – 8.36 (m, 1H), 4.45 (s, 3H).[11]

Signals assigned to **3**: δ 9.07 (s, 1H, H-2), 8.61 – 8.56 (m, 1H, H-6), 8.33 – 8.29 (m, 1H, H-4), 7.58 – 7.52 (m, 1H, H-5).[11] Relative to 1H of **23b**, 1H of **3** integrates for approximately 0.71H.

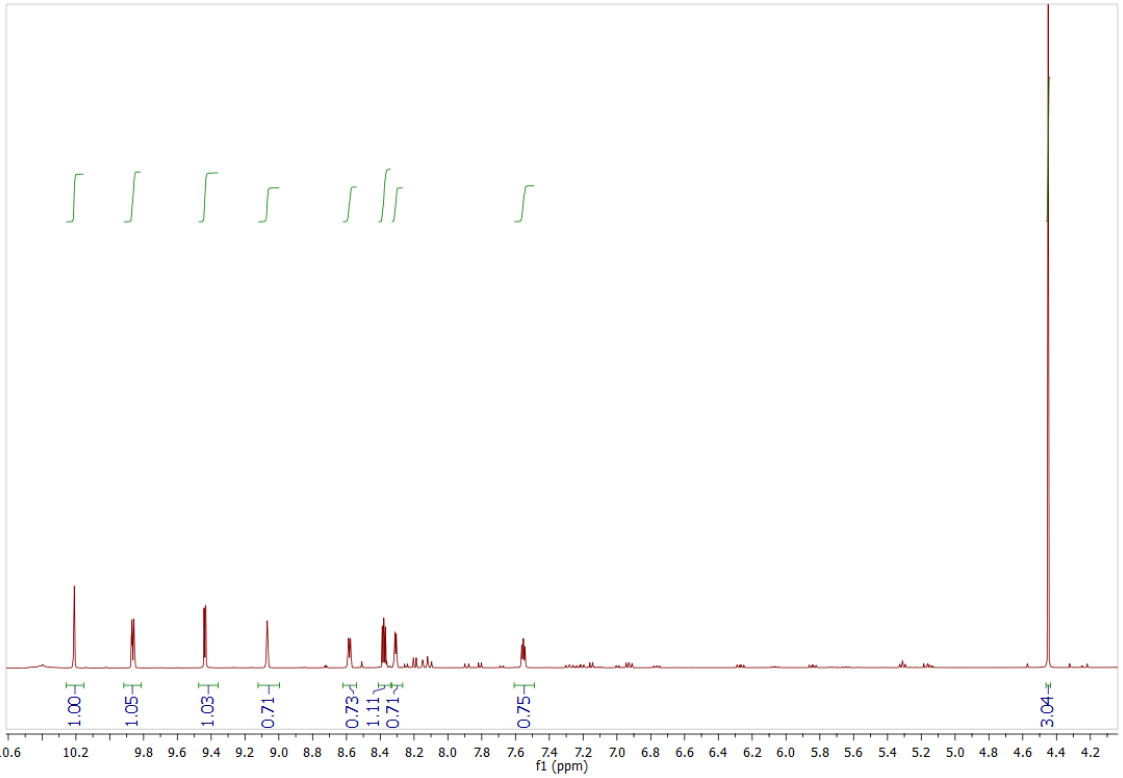
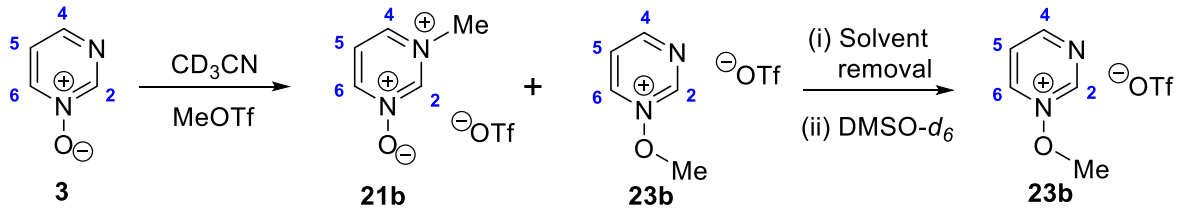


Figure S16: ^{1}H NMR spectrum in $(CH_3)_2SO$ of **23b**, containing signals assigned to **3**. The full spectrum is shown in Section 7

(c) Experiment Showing N- vs O-Alkylation Product Ratio (21b vs 23b) in CD_3CN – Contains ^{15}N and ^{13}C NMR Data

Pure samples of compounds **23b** and/or **21b** could not be obtained from this reaction for the reasons given at the start of section 4.4.

Pyrimidine *N*-oxide (**3**) (0.045 g, 0.47 mmol) was dissolved in CD_3CN (0.65 ml) in a N_2-filled Schlenk flask. Methyl triflate (0.067 g, 0.41 mmol) was then added dropwise. The reaction mixture was transferred to an NMR tube and analyzed by NMR spectroscopy using General Procedure B.



3 21b 23b 23b

^{1}H NMR (400 MHz, CD_3CN)

Signals assigned to **23b**: δ 9.81 (app d, app *J* = 1.5 Hz, 1H, H-2), 9.47 – 9.37 (m, 2H, H-4 and H-6), 8.31 – 8.24 (m, 1H, H-5), 4.51 (s, 3H, O*CH*$_3$).

Signals assigned to **21b**: δ 9.56 (s, 1H, H-2), 8.90 (app d, app *J* = 6.8 Hz, 1H), 8.58 (app d, app *J* = 6.0 Hz, 1H), 8.01 (app t, app *J* = 6.0 Hz, 1H), 4.32 (s, 3H, N*CH*$_3$). Relative to 1H of **23b**, 1H of **21b** integrates for 0.08H.

Signals assigned to starting material **3**: δ 8.98 (s, 1H, H-2), 8.50 – 8.42 (m, 1H, H-6), 8.39 – 8.33 (m, 1H, H-4), 7.55 – 7.46 (m, 1H, H-5).[11] Relative to 1H of **23b**, 1H of **3** integrates for 0.30H.

^{13}C{^{1}H} NMR (100 MHz, CD_3CN)

Signals assigned to **23b**: δ 163.6 (C-6), 150.0 (C-2), 148.1 (C-4), 125.0 (C-5), 70.2 (O*C*H$_3$).

Signals assigned to **21b**: δ 151.8, 149.1, 140.2, 124.0, 46.6 (N*C*H$_3$).

Signals assigned to starting material **3**: δ 149.1 (C-2), 145.8 (C-4), 144.5 (C-6), 121.9 (C-5).

A quartet from *C*F$_3$SO$_3^-$ is present at δ 120.6 (partially overlaps with other signals; *J* = *ca.* 320 Hz).

Ratio of N-alkylation and O-alkylation Products (from integrations in ^{1}H NMR spectrum):

2H of Compound **23b** = 2.00 – Therefore 1H = 1.00

1H of Compound **21b** = 0.08 – Therefore 1H = 0.08

$$\text{Ratio} = \frac{1.00}{1.00 + 0.08} \times 100 = 93\%\ \text{O alkylation}$$

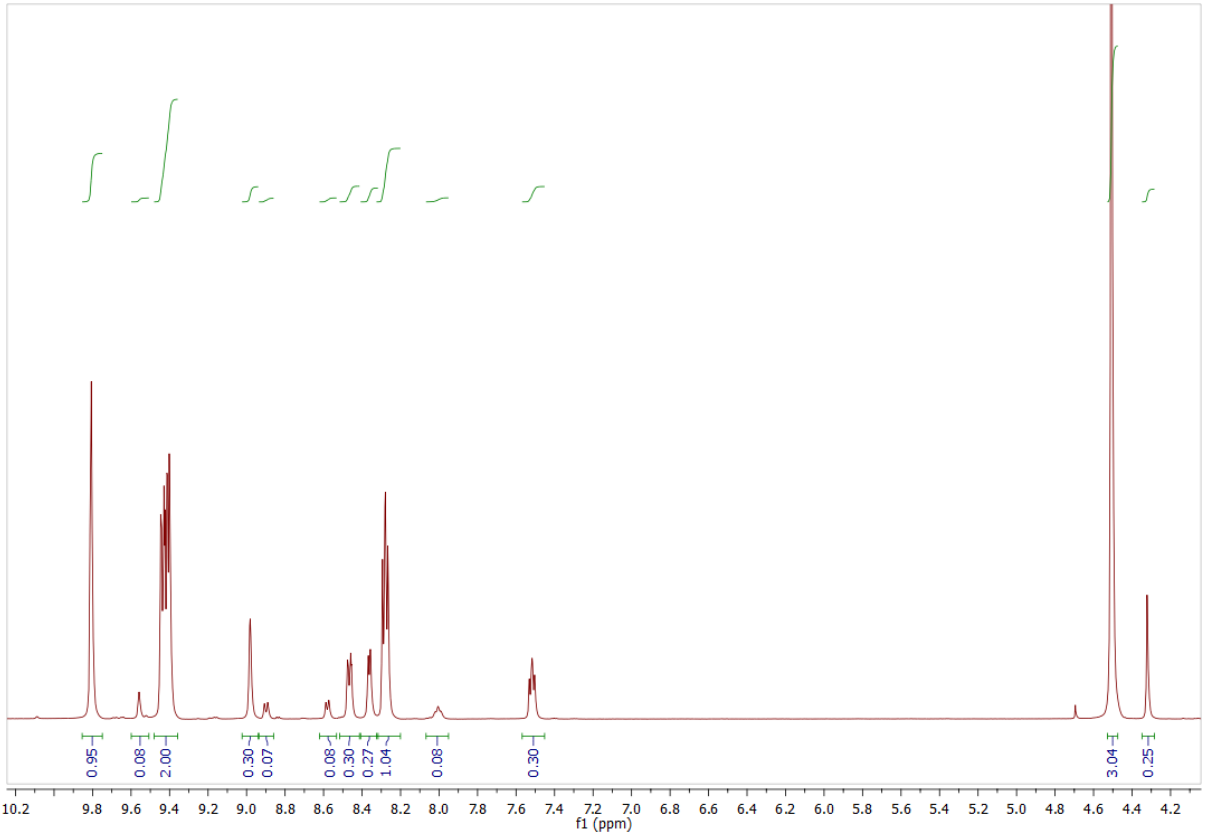


Figure S17: ^{1}H NMR spectrum in CD_3CN, containing signals assigned to **23b**, **21b** and **3**. The full spectrum is shown in Section 7.

The CD_3CN was removed and the product mixture was re-dissolved in $(CD_3)_2SO$ to allow a ^{1}H-^{15}N HMBC NMR spectrum to be measured. Product **21b** did not survive the solvent removal process.

^{1}H NMR (600 MHz, $(CD_3)_2SO$)

Signals assigned to **23b** δ 10.24 (dd, *J* = 2.2, 0.8 Hz, 1H, H-2), 9.89 (ddd, *J* = 6.8, 2.2, 1.6 Hz, 1H, H-6), 9.46 (dd, *J* = 4.8, 1.6 Hz, 1H, H-4), 8.40 (app. ddd, *J* = 6.8, 4.8, 0.8 Hz, 1H, H-5), 4.48 (s, 3H).

Signals assigned to starting material **3** δ 9.15 – 9.11 (m, 1H, H-2), 8.64 (ddd, *J* = 6.6, 2.0, 1.5 Hz, 1H, H-6), 8.38 (dd, *J* = 4.8, 1.5 Hz, 1H, H-4), 7.61 (ddd, *J* = 6.6, 4.8, 0.9 Hz, 1H, H-5).[11] Relative to 1H of **23b**, 1H of **3** integrates for approximately 1.80H.

^{15}N NMR (60.8 MHz, $(CD_3)_2SO$)

Signals assigned to **23b** δ 303.4 (free *N*), 249.4 (N^{+}—OMe)

Signals assigned to **3**: δ 300.9, 285.8.

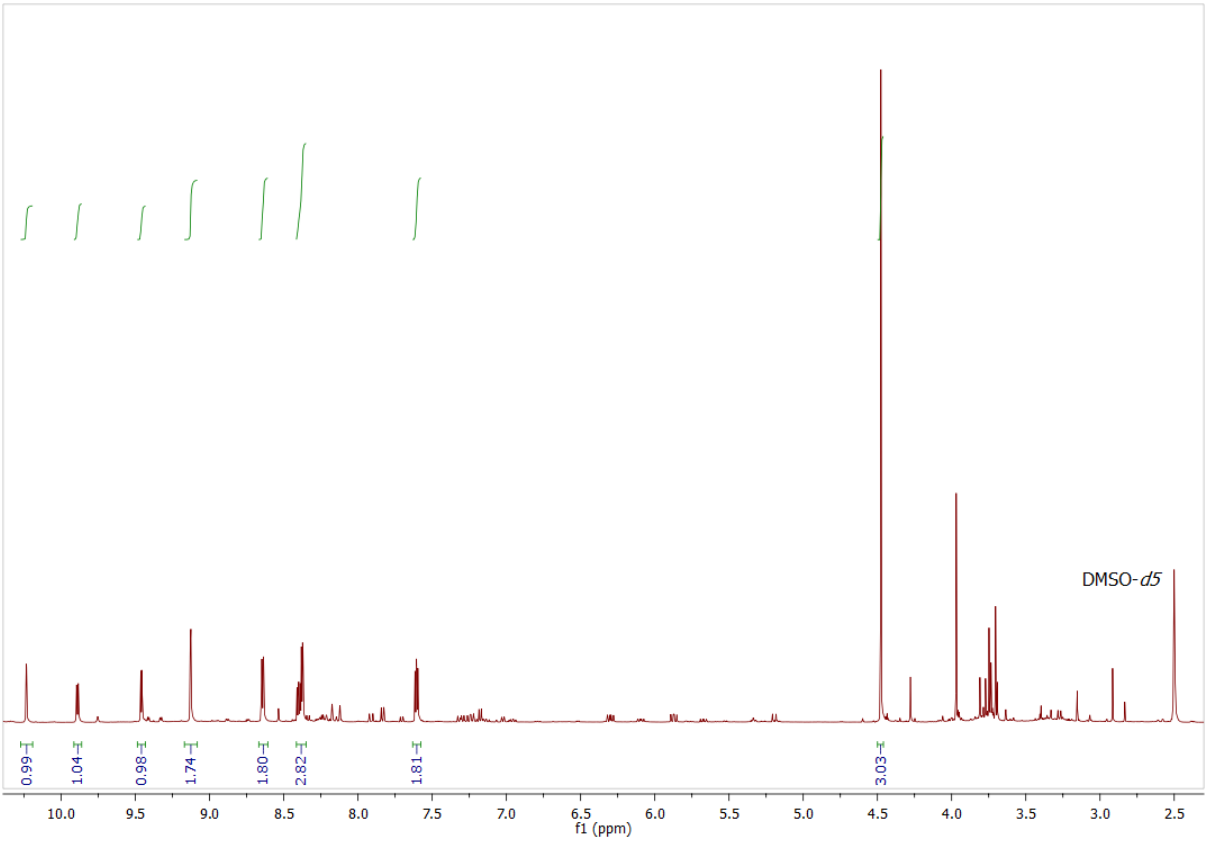
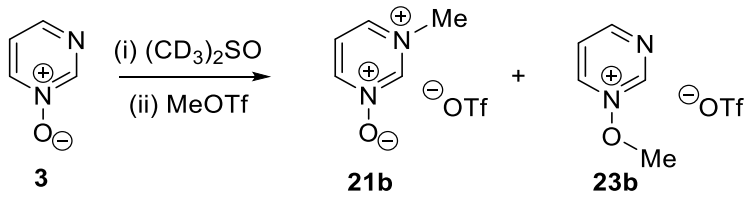


Figure S18: ^{1}H NMR spectrum in $(CD_3)_2SO$, containing signals assigned to **23b** and **3**. Signals assigned to **21b** are no longer present after solvent removal. Signals of a large amount of decomposition products are also present. The full spectrum is shown in Section 7.

(d) Experiment Showing N- vs O-Alkylation Product Ratio (21b vs 23b) in $(CD_3)_2SO$ – Contains ^{15}N and ^{13}C NMR Data

Pyrimidine *N*-oxide (**3**) (0.050 g, 0.52 mmol) was dissolved in $(CD_3)_2SO$ (0.8 ml) in a vial inside an inert atmosphere glove box. Methyl triflate (0.087 g, 0.53 mmol) was subsequently added dropwise. The reaction mixture was transferred to a NMR tube by syringe. The NMR tube was then sealed by a rubber septum cap and wrapped with PTFE tape. The septum was then covered with Parafilm and the tube transferred outside the glove box. ^{1}H NMR spectra were run periodically over the course of four weeks. Very slow consumption of **3** and growth of **21b** and **23b** was observed from these spectra. The integration of the ^{1}H NMR signal of the methylating agent (likely to be (methoxy)sulfonium triflate)[10] at δ 3.98 ppm also diminished during this time. After four weeks, ^{1}H, ^{13}C{^{1}H}, COSY, ^{1}H-^{13}C HSQC, ^{1}H-^{13}C HMBC and ^{1}H-^{15}N HMBC NMR spectra of the reaction mixture were recorded.



^{1}H NMR (600 MHz, $(CD_3)_2SO$)

Signals assigned to **23b**: δ 10.24 (dd, *J* = 2.2, 0.8 Hz, 1H, H-2, overlaps with signal of **21b**), 9.90 (ddd, *J* = 6.8, 2.2, 1.6 Hz, 1H, H-6), 9.47 (dd, *J* = 4.9, 1.6 Hz, 1H, H-4), 8.41 (ddd, *J* = 6.8, 4.9, 0.8 Hz, 1H, H-5, partially overlaps with signal of **3**), 4.48 (s, 3H, OC*H*$_3$).

Signals assigned to **21b**: δ 10.18 (s, 1H, overlaps with signal of **23b**), 9.21 – 9.17 (m, 1H), 8.89 (app d, app *J* = 6.1 Hz, 1H), 8.17 (app t, app *J* = 6.5 Hz, 1H), 4.26 (s, 3H, NC*H*$_3$). Relative to 1H of **23b**, 1H of **21b** integrates for 0.07H.

Signals assigned to **3**: δ 9.09 (m, 1H, H-2), 8.60 (ddd, *J* = 6.6, 2.0, 1.5 Hz, 1H, H-6), 8.33 (dd, *J* = 4.8, 1.5 Hz, 1H, H-4, partially overlaps with signal of **23b**), 7.58 (ddd, *J* = 6.6, 4.8, 1.0 Hz, 1H, H-5).[11] Relative to 1H of **23b**, 1H of **3** integrates for 0.61H.

A signal assigned to the methoxydimethylsulfonium salt of $(CD_3)_2SO$ is present at 3.98 ppm. Relative to 1H of **23b**, 1H of the salt integrates for approximately 0.33H.

Note: The singlet at δ 10.24 ppm has an extremely slow relaxation rate. A 30° pulse and a relaxation delay of 60 seconds were used during acquisition of the spectra above, leading to a set of internally consistent integrations for the ^{1}H NMR signals of **23b**. Use of a 90° pulse and a 60 second relaxation delay gave an integration of the signal at 10.24 ppm of 84% relative to the other 1H signals of **23b**.

^{13}C{^{1}H} NMR (151 MHz, $(CD_3)_2SO$)

Signals assigned to **23b**: δ 163.7 (C-6), 151.2 (C-2), 149.0 (C-4), 125.1 (C-5), 70.4 (O*C*H$_3$).

No signals in this ^{13}C NMR spectrum could be assigned to the small amount of **21b** present.

Signals assigned to **3**: δ 149.8 (C-2), 145.3 (C-4 or C-6), 145.2 (C-4 or C-6), 122.6 (C-5).

A signal at δ 121.1 (q, *J* = 322 Hz) is assigned to triflate ion ($^{-}$OSO$_2$*C*F$_3$). Small signal derived from decomposition products are also present (see spectra in section 7 and comment at start of section 4.4).

^{15}N NMR (60.8 MHz, $(CD_3)_2SO$)

Signals assigned to **23b**: δ 303.1 (free *N*), 249.0 (*N*$^{+}$—OMe)

Signals assigned to **21b**: δ 293.6 (*N*—O), 205.2 (*N*$^{+}$—Me)

Signals assigned to **3**: 300.7, 288.4.

Conversion Calculation (based on consumption of the methoxydimethylsulfonium salt as the limiting reagent):

3H of Compound **23b** corresponds to 3.00, therefore 1H = 1.00. 3H of compound **21b** corresponds to 0.21, therefore 1H = 0.07.

For the methoxydimethylsulfonium salt at 3.98 ppm, 3H = 1.00, therefore 1H = 0.33.

$$\text{Conversion} = \frac{1.00 + 0.07}{1.00 + 0.07 + 0.33} \times 100 = 76\%$$

Ratio of N-alkylation and O-alkylation Products (using integrations from ^{1}H NMR spectrum):

1H of Compound **23b** = 1.00

1H of Compound **21b** = 0.07

$$\text{Ratio} = \frac{1.00}{1.00 + 0.07} \times 100 = 93\%\ \text{O alkylation}$$

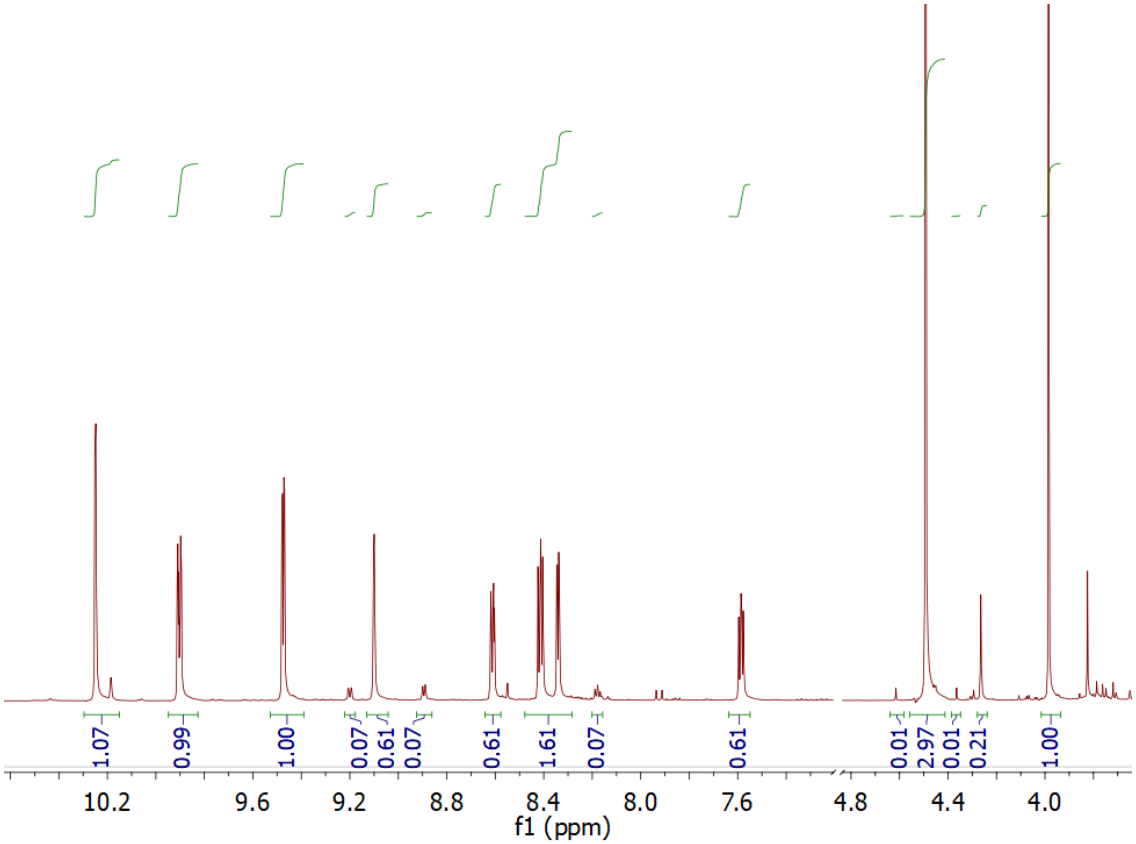
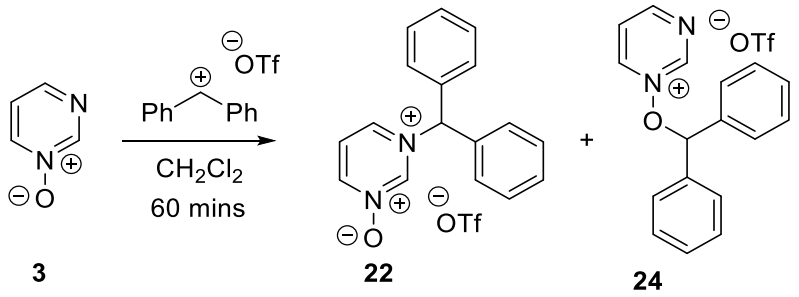


Figure S19: ^{1}H NMR spectrum in $(CD_3)_2SO$ of **23b**, containing signals assigned to **21b** and **3**. The full spectrum is shown in Section 7.

Attempted Preparation of 22 and 24

Pyrimidine *N*-oxide (**3**) (0.044 g, 0.46 mmol), benzhydryl chloride (0.093 g, 0.46 mmol) and silver triflate (0.132 g, 0.514 mmol) were combined by the process described in Procedure C in an attempt to produce **22** or **24** in CH_2Cl_2. The reaction mixture was analyzed by NMR spectroscopy using General Procedure B. As can be seen in the spectra shown below, the appearances of the signals are highly unusual, and none of these signals could be definitively assigned to any particular species. The identities of the entities formed in this process are not clear.



No evidence for product formation

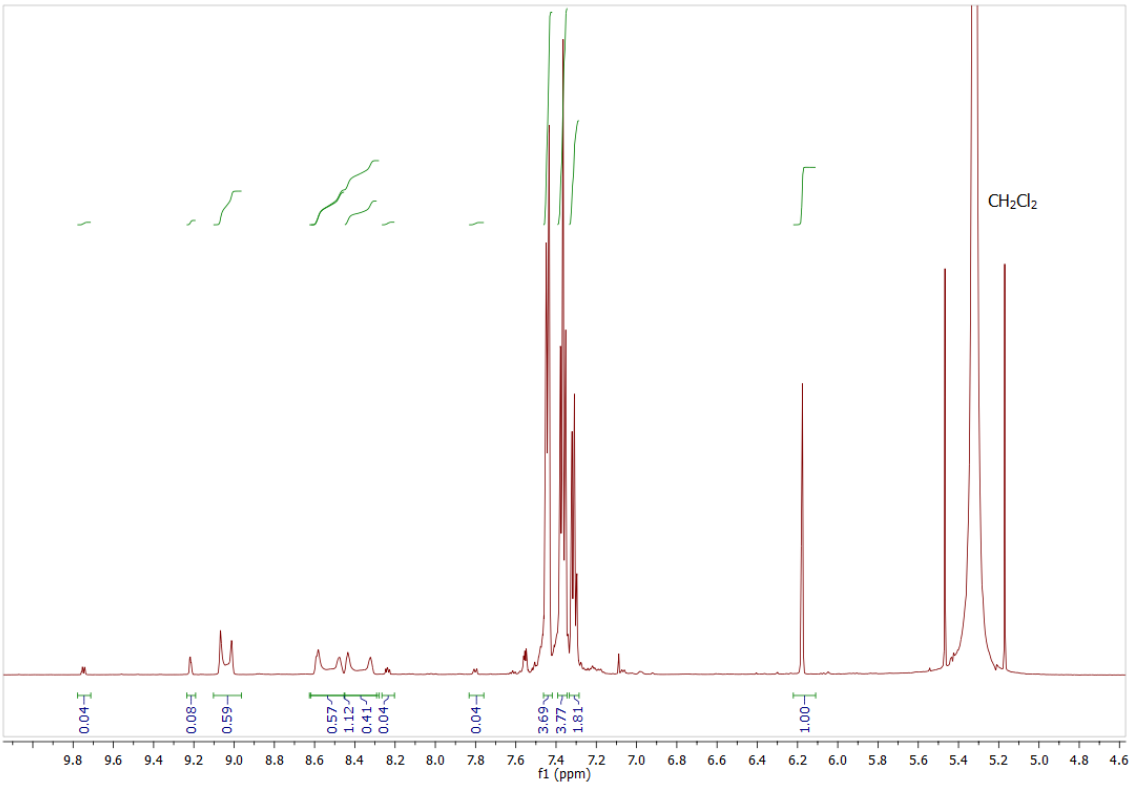


Figure S20: ^{1}H NMR spectrum in CH_2Cl_2 of the crude reaction mixture from the reaction above. Signals could not be definitively assigned to product **22** or **24**. The full spectrum is shown in Section 7.

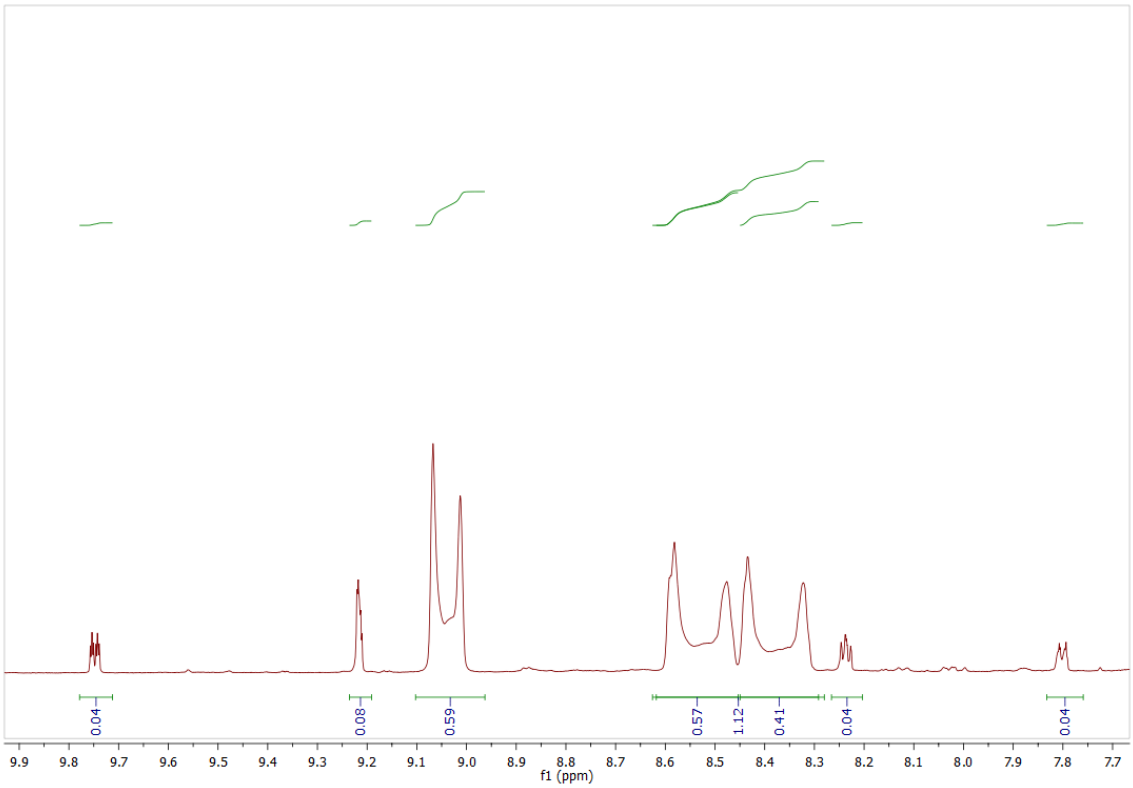


Figure S21: Expansion of the ^{1}H NMR spectrum of the crude reaction mixture from the reaction above in CH_2Cl_2, showing the broadness of the observed signals. Signals could not be definitively assigned to product **22** or **24**

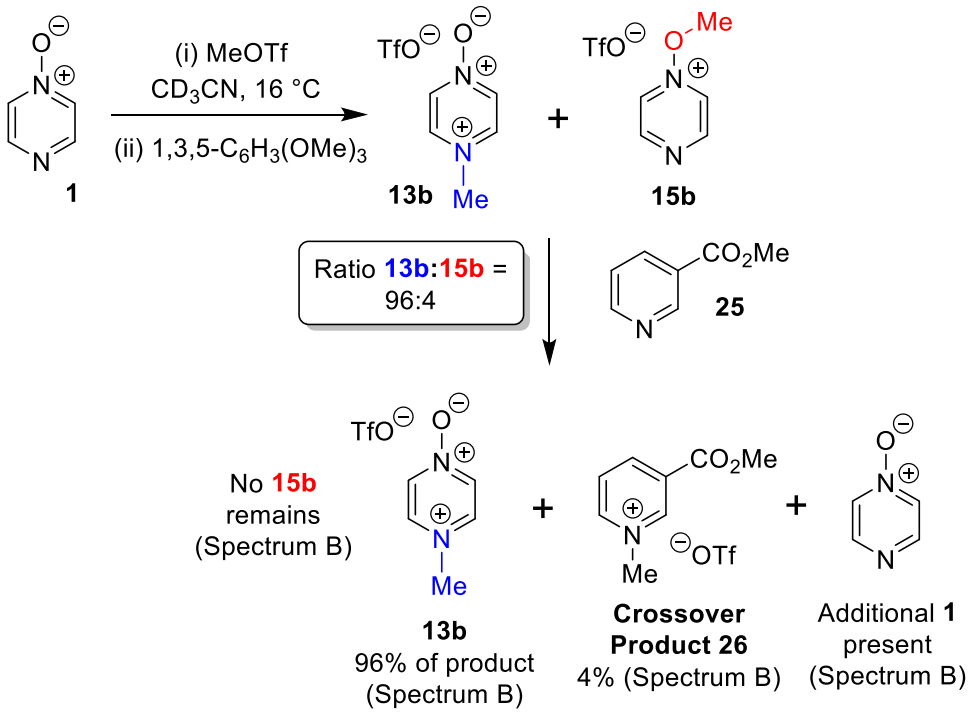
5. Crossover Experiments

General Procedure D: Crossover experiments

The following procedure was used to establish whether reactions of diazine *N*-oxides occurred under kinetic control. In a glove box containing a nitrogen atmosphere, the appropriate diazine *N*-oxide (1 equivalent) was weighed into a vial. Dry CD_3CN (usually 0.65 ml) was added. An internal standard, 1,3,5-trimethoxybenzene was subsequently added (approx. 15 mol%). The mixture was then transferred into an NMR tube, which was sealed with a rubber septum. The seal was then wrapped with PTFE tape and Parafilm. Finally, the NMR tube was placed in a long Schlenk flask and removed from the glove box and brought to the NMR spectrometer. A ^{1}H NMR spectrum was measured and the tube was removed from the spectrometer. A solution of the crossover nucleophile in CD_3CN (amounts specified below) was then injected through the septum cap. A second ^{1}H NMR spectrum was recorded immediately, and an additional spectrum was obtained after allowing the reaction mixture to stand (in the NMR tube) for two days or more.

5.1 Crossover experiment – pyrazine *N*-oxide (1) with MeOTf and methyl nicotinate (25)

The following reagents were combined in the process described in General Procedure D. Pyrazine *N*-oxide (**1**) (0.018 g, 0.19 mmol) was dissolved in CD_3CN (0.65 ml) in a vial in a glove box. Methyl triflate (0.024 g, 0.15 mmol) was subsequently added dropwise. To this mixture was added 1,3,5-trimethoxybenzene (0.003 g, 0.02 mmol). The reaction mixture was transferred to an NMR tube and analyzed by NMR spectroscopy in CD_3CN (Spectrum A). The tube was removed from the spectrometer and methyl nicotinate (**25**) (0.032 g, 0.23 mmol) in CD_3CN (0.15 ml) was injected into the tube through the septum by syringe. The mixture was agitated and a second ^{1}H NMR spectrum was recorded. No change was observed in the ratio of **13b** and **15b** in this spectrum. An additional ^{1}H NMR spectrum was recorded after 1 day (Spectrum B).



^{1}H NMR (300 MHz, CD_3CN, 15 second relaxation delay) Spectrum A:

Signals assigned to **13b**: δ 8.55 – 8.49 (m, 4H), 4.15 (s, 3H).

Signals assigned to **15b**: δ 9.45 (dd, *J* = 3.3, 1.6 Hz, 2H), 9.08 (dd, *J* = 3.3, 1.6 Hz, 2H), 4.51 (s, 3H). Relative to 1H of **13b**, 1H of **15b** integrates for 0.04H.

Signals assigned to starting material **1**: δ 8.47 – 8.40 (m, 2H), 8.13 (app dd, app *J* = 3.6, 1.5 Hz, 2H). Relative to 1H of **13b**, 1H of **1** integrates for approximately 0.28H.

Signals assigned to internal standard **trimethoxybenzene**: δ 6.09 (s, 3H), 3.74 (s, 9H). Relative to 1H of **23b**, 1H of **trimethoxybenzene** integrates for 0.14H.

Ratio of N-alkylation and O-alkylation Products:

3H of Compound **13b** = 3.00 – Therefore 1H = 1.00

2H of Compound **15b** = 0.08 – Therefore 1H = 0.04

$$\text{Ratio} = \frac{1.00}{1.00 + 0.04} \times 100 = 96\%\ \text{N alkylation}$$

Ratio of major product to internal standard:

3H of Compound **13b** = 3.00 – Therefore 1H = 1.00

3H of internal standard = 0.43 – Therefore 1H = 0.143

$$\text{Ratio} = \frac{1.00}{1.00 + 0.143} \times 100 = 87 : 13$$

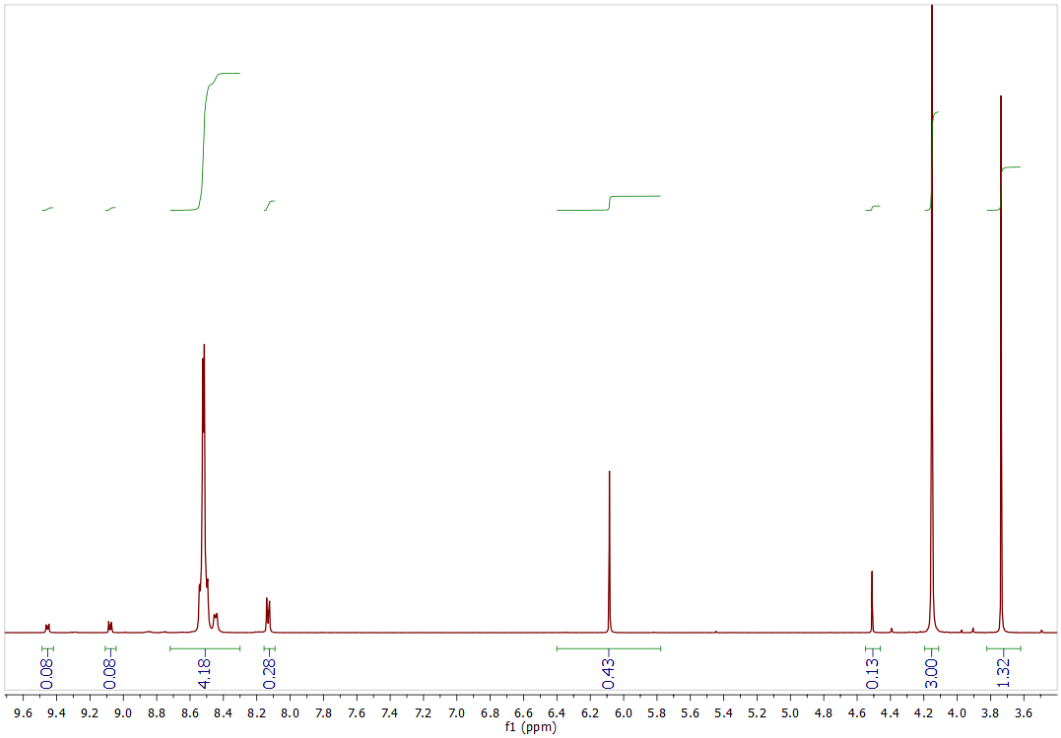


Figure S22: Spectrum A: ^{1}H NMR spectrum in CD_3CN containing signals assigned to **13b**, **15b** and **1**. Signals of the internal standard 1,3,5-trimethoxybenzene are also present. The full spectrum is shown in Section 7.

^{1}H NMR (300 MHz, CD_3CN, 15 second relaxation delay) Spectrum B:

Signals assigned to **13b**: δ 8.57 – 8.49 (m, 4H), 4.16 (s, 3H).

No signals assigned to **15b**

Signals assigned to starting material **1**: δ 8.46 – 8.38 (m, 2H), 8.08 (app dd, app *J* = 3.5, 1.5 Hz, 2H). Relative to 1H of **13b**, 1H of **1** integrates for approximately 0.39H.

Signals assigned to internal standard **trimethoxybenzene**: δ 6.08 (s, 1H), 3.73 (s, 1H). Relative to 1H of **13b**, 1H of **trimethoxybenzene** integrates for approximately 0.15H.

Signals assigned to **25**: δ 9.14 – 9.10 (m, 1H), 8.76 (dd, *J* = 4.9, 1.7 Hz, 1H), 8.30 – 8.25 (m, 1H), 7.47 (ddd, *J* = 8.0, 4.9, 0.9 Hz, 1H), 3.90 (s, 3H). Relative to 1H of **13b**, 1H of **3** integrates for 1.57H.

Signals assigned to **crossover product 26**: δ 9.22 (s, 1H), 8.92 (d, *J* = 8.1 Hz, 1H), 4.39 (s, 3H), 4.00 (s, 3H). Relative to 1H of **13b**, 1H of **26** integrates for 0.04H. [12]

Note: The singlets at 4.39 ppm and 4.16 ppm are overlapping with a minor side product, altering their integration values.

Ratio of **13b** to **crossover product 26**:
4H of Compound **13b** = 4.00 – Therefore 1H = 1.00

1H of **26** = 0.04 – Therefore 1H = 0.04

$$\text{Ratio} = \frac{1.00}{1.00 + 0.04} \times 100 = 96 : 4$$

Ratio of major product to internal standard:

4H of Compound **13b** = 4.00 – Therefore 1H = 1.00

3H of internal standard = 0.45 – Therefore 1H = 0.15

$$\text{Ratio} = \frac{1.00}{1.00 + 0.15} \times 100 = 87 : 13$$

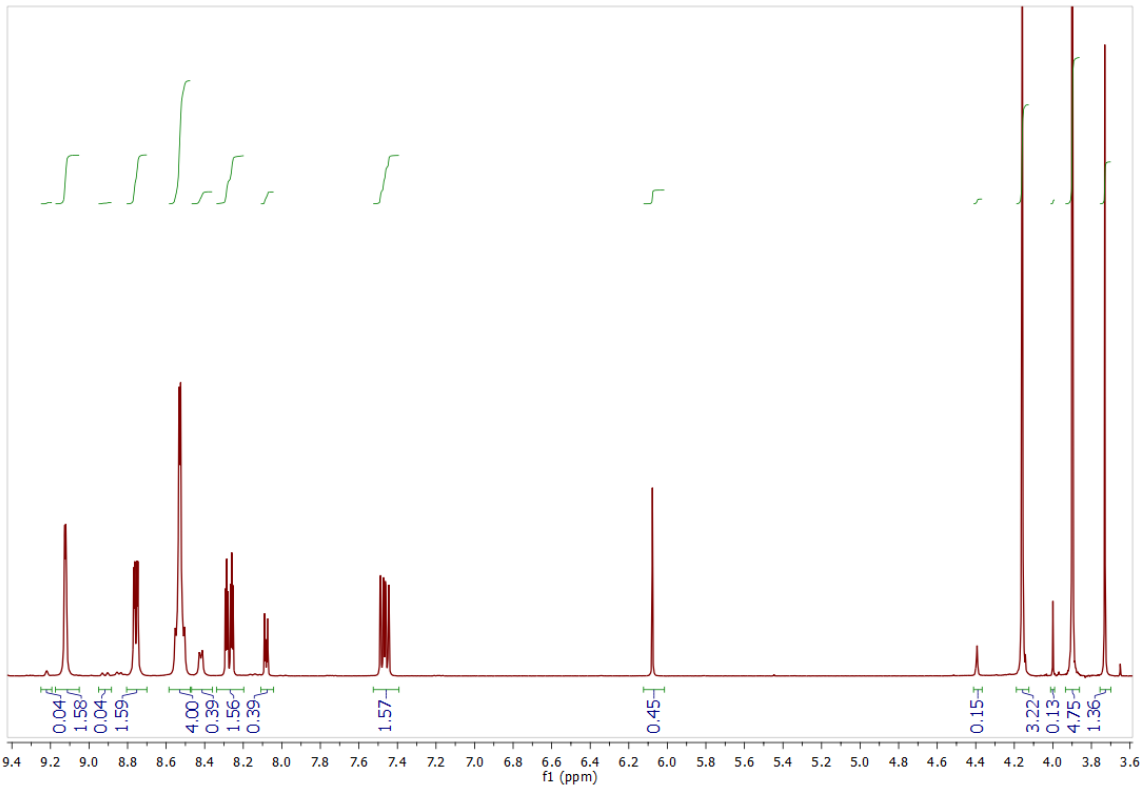


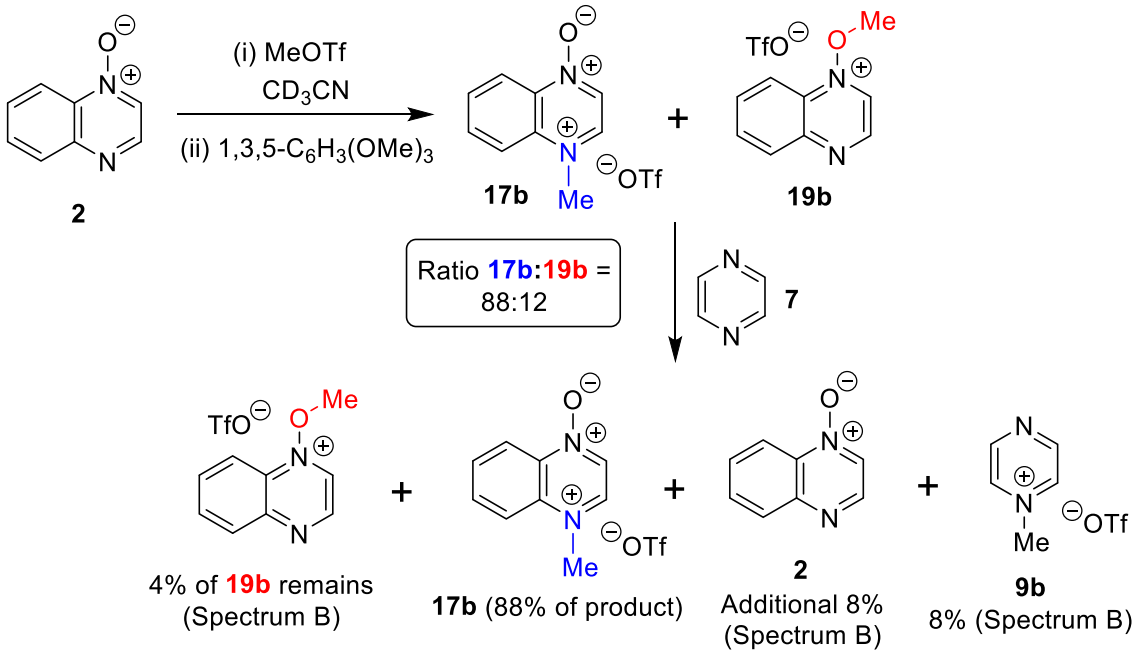
Figure S23: Spectrum B: ^{1}H NMR spectrum in CD_3CN containing signals assigned to **13b**, **25**, crossover product **26** and **1**. Signals of the internal standard 1,3,5-trimethoxybenzene are also present. No signals assigned to **15b** are observed. The full spectrum is shown in Section 7.

That the relative ratio of N-methylation product (**13b**) and the internal standard (1,3,5-trimethoxybenzene) remains constant after addition of 2nd nucleophile (**25**) demonstrates that the formation of **13b** from **1** + MeOTf is irreversible under the reaction conditions employed.

We conclude that formation of crossover product (**26**) derived from O-methylation product **15b** occurs by S_N2 reaction of **15b** + 2nd nucleophile **25**, and that **15b** does not undergo reversal to **1** + MeOTf in CD_3CN at *ca.* 20 °C (i.e. **15b** is formed irreversibly). If this were not the case, then a mixture of **13b** + **15b** should eventually convert entirely to **13b**, since **13b** is formed irreversibly. The ratio of **13b** to **15b** remains invariant with time unless a second nucleophile is added to the reaction mixture.

5.2 Crossover experiment – quinoxaline *N*-oxide (2) with MeOTf and pyrazine (7)

The following reagents were combined in the process described in General Procedure D. Quinoxaline *N*-oxide (**2**) (0.018 g, 0.12 mmol) was dissolved in CD_3CN (0.65 ml) in a vial in a glove box. Methyl triflate (0.019 g, 0.12 mmol) was subsequently added dropwise. To this mixture was added 1,3,5-trimethoxybenzene (5 mg, 0.03 mmol). The reaction mixture was transferred to an NMR tube and analyzed by NMR spectroscopy in CD_3CN (Spectrum A). The tube was removed from the spectrometer and a solution of **7** (8 mg, 0.010 mmol) in CD_3CN (0.20 ml) was injected into the tube through the rubber septum by syringe. The mixture was agitated and a second ^{1}H NMR spectrum was recorded. No change was observed in the ratio of **17b** and **19b** in this spectrum. After 1 day, and additional ^{1}H NMR spectrum was recorded (Spectrum B).



^{1}H NMR (300 MHz, CD_3CN, 15 second relaxation delay) Spectrum A:

Signals assigned to **17b**: δ 8.92 (d, *J* = 5.3 Hz, 1H), 8.75 (d, *J* = 5.3 Hz, 1H), 8.62 – 8.55 (m, overlaps with 1H of **19b**, contains 1H of **17b**), 4.43 (s, 3H).

Signals assigned to **19b**: δ 9.60 (d, *J* = 3.4 Hz, 1H), 9.49 (d, *J* = 3.4 Hz, 1H), 8.56 – 8.52 (overlaps with 1H of **17b**, contains 1H of **19b**), 4.65 (s, 3H). Relative to 1H of **17b**, 1H of **19b** integrates for 0.13H.

Signals assigned to starting material **2**: δ 8.67 (d, *J* = 3.6 Hz, 1H), 8.46 (dd, *J* = 8.6, 1.4 Hz, 1H), 8.38 – 8.23 (m, 1H), 7.92–7.84 (m, 1H), 7.83 – 7.75 (m, 1H). Relative to 1H of **17b**, 1H of **2** integrates for approximately 0.38H.

Signals assigned to internal standard **trimethoxybenzene**: δ 6.06 (s, 3H), 3.73 (s, 9H). Relative to 1H of **23b**, 1H of **trimethoxybenzene** integrates for 0.33H.

The section of the spectrum at 8.62 – 8.53 ppm contains 1H each of **17b** and **19b**. The section at 8.38 – 8.23 ppm contains a 2H signal from **17b**, a 2H signal from **19b** and a 1H signal from **2**. The section at 8.15 – 8.07 ppm contains a 1H signal from **17b,** a 1H signal from **19b** and a 1H signal from **2**.

Ratio of N-alkylation and O-alkylation Products:

1H of Compound **17b** = 1.00

1H of Compound **19b** = 0.13

$$\text{Ratio} = \frac{1.00}{1.00 + 0.13} \times 100 = 88\%\ \text{N alkylation}$$

Ratio of major product to internal standard:

1H of Compound **17b** = 1.00

3H of internal standard = 1.00 – Therefore 1H = 0.33

$$\text{Ratio} = \frac{1.00}{1.00 + 0.33} \times 100 = 75 : 25$$

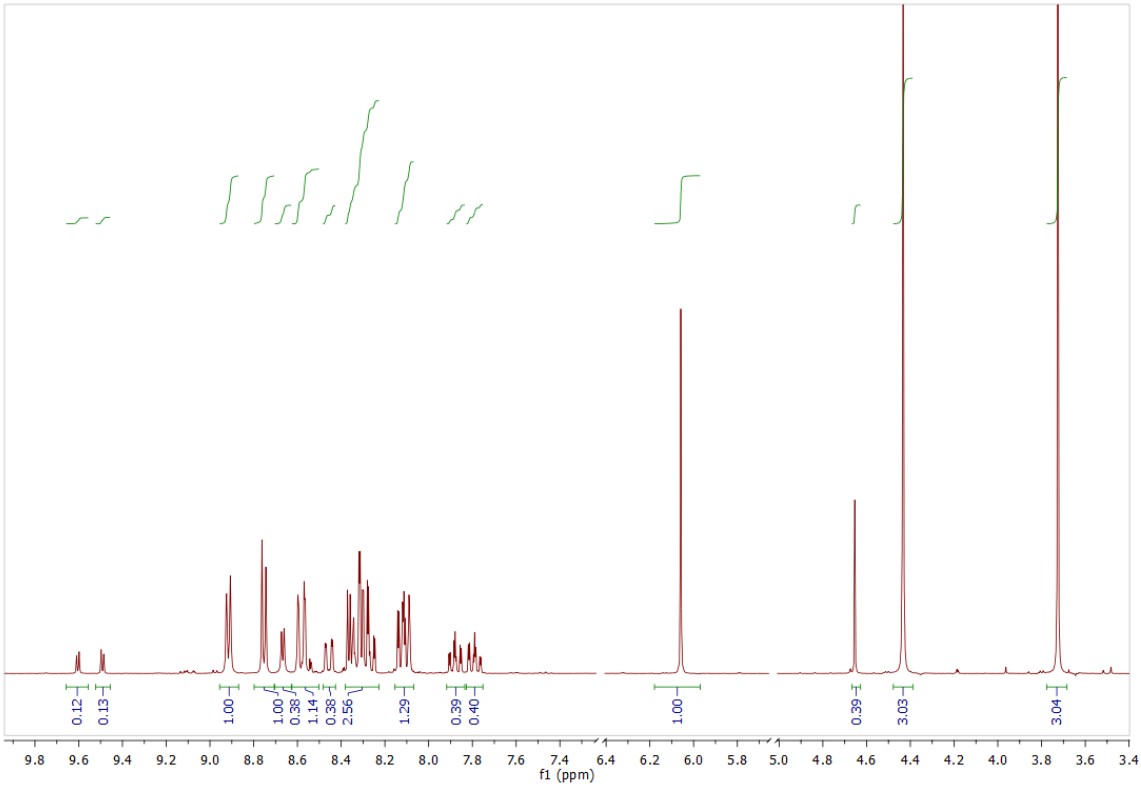


Figure S24: Spectrum A: ^{1}H NMR spectrum in CD_3CN containing signals assigned to **17b**, **19b** and **2**. Signals of the internal standard 1,3,5-trimethoxybenzene are also present. The full spectrum is shown in Section 7.

^{1}H NMR (300 MHz, CD_3CN, 15 second relaxation delay) Spectrum B:

Signals assigned to **17b**: δ 8.91 (d, *J* = 5.3 Hz, 1H), 8.76 (d, *J* = 5.3 Hz, overlaps with signal of **9b**, contains 1H of **17b**), 4.43 (s, 3H).

Signals assigned to **19b**: δ 9.61 (d, *J* = 3.4 Hz, 1H), 9.49 (d, *J* = 3.4 Hz, 1H), 8.58 (app d, app *J* = 7.3 Hz, 1H), 4.65 (s, 3H). Relative to 1H of **17b**, 1H of **19b** integrates for 0.05H.

Signals assigned to starting material **2**: δ 8.66 (d, *J* = 3.6 Hz, 1H), 8.46 (dd, *J* = 8.6, 1.4 Hz, 1H), 7.91–7.83 (m, 1H), 7.82 – 7.74 (m, 1H). Relative to 1H of **17b**, 1H of **2** integrates for approximately 0.55H.

Signals assigned to internal standard **trimethoxybenzene**: δ 6.06 (s, 3H), 3.73 (s, 9H). Relative to 1H of **17b**, 1H of **trimethoxybenzene** integrates for approximately 0.33H.

Signals assigned to **7**: δ 8.57 (s, overlaps with 1H signal of **17b**, contains 4H of **7** (relative integration = 4.05 – 1.00 = 3.05)). Relative to 1H of **17b**, 1H of **7** integrates for (3.05/4) = 0.76H.

Signals assigned to **crossover product 9b**: δ 9.41 – 9.35 (m, 2H), 8.77 – 8.73 (m, 2H, overlaps with signal of **17b**), 4.39 (s, 3H). Relative to 1H of **17b**, 1H of **9b** integrates for approximately 0.07H.

The section of the spectrum between 8.38 and 8.23 ppm contains a 2H signal from **17b**, a 2H signal from **19b** and a 1H signal from **2**. The section at 8.15 – 8.07 ppm contains a 1H signal from **17b,** a 1H signal from **19b** and a 1H signal from **2**. The signal between 8.77 and 8.71 ppm contains a 1H signal from **17b** and a 1H signal from **19b**.

Ratio of **17b** to **crossover product 9b**:

1H of Compound **17b** = 1.00

2H of crossover product = 0.14 – Therefore 1H = 0.07

$$\text{Ratio} = \frac{1.00}{1.00 + 0.07} \times 100 = 93 : 7$$

Ratio of major product to internal standard:

1H of Compound **17b** = 1.02

3H of internal standard = 1.00 – Therefore 1H = 0.33

$$\text{Ratio} = \frac{1.02}{1.02 + 0.33} \times 100 = 76 : 24$$

That the relative ratio of N-methylation product (**17b**) and the internal standard (1,3,5-trimethoxybenzene) remains constant after addition of 2nd nucleophile (**7**) demonstrates that the formation of **17b** from **2** + MeOTf is irreversible under the reaction conditions employed.

We conclude that formation of crossover product (**9b**) derived from O-methylation product **19b** occurs by S_N2 reaction of **19b** + 2nd nucleophile **7**, and that **19b** does not undergo reversal to **2** + MeOTf in CD_3CN at *ca.* 20 °C (i.e. **19b** is formed irreversibly). If this were not the case, then a mixture of **17b** + **19b** should eventually convert entirely to **17b**, since **17b** is formed irreversibly. The ratio of **17b** to **19b** remains invariant with time unless a second nucleophile is added to the reaction mixture.

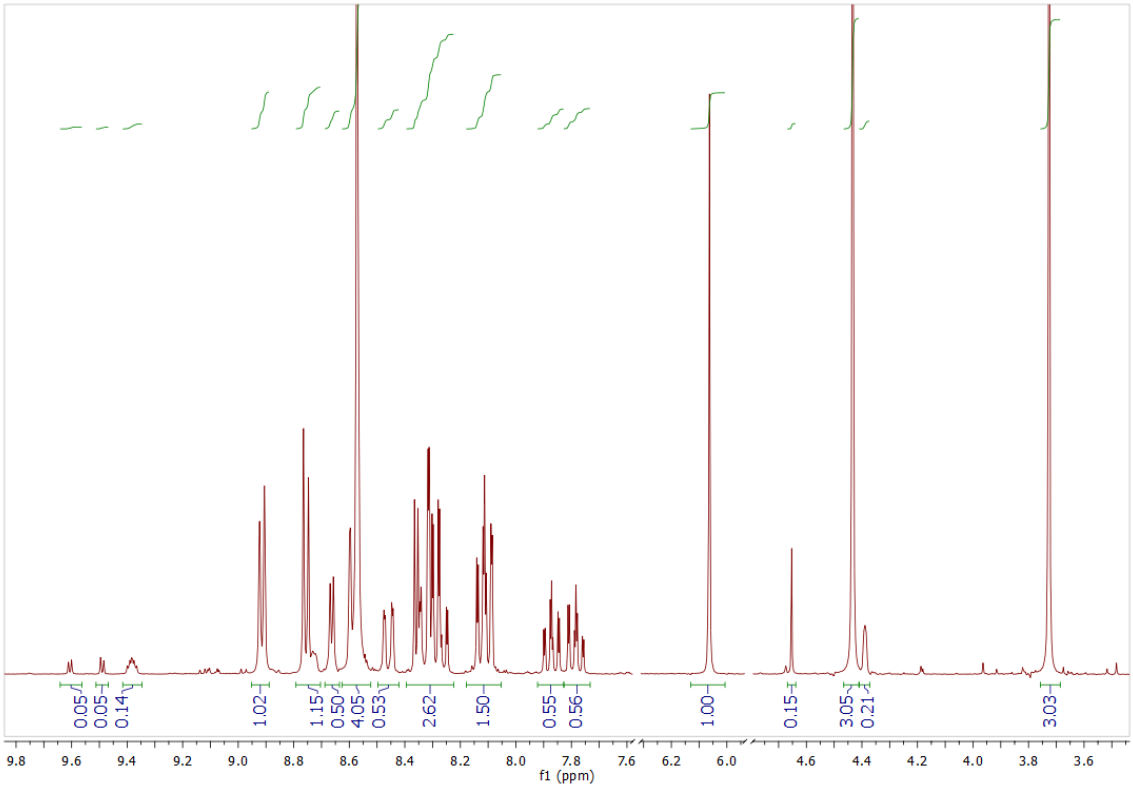
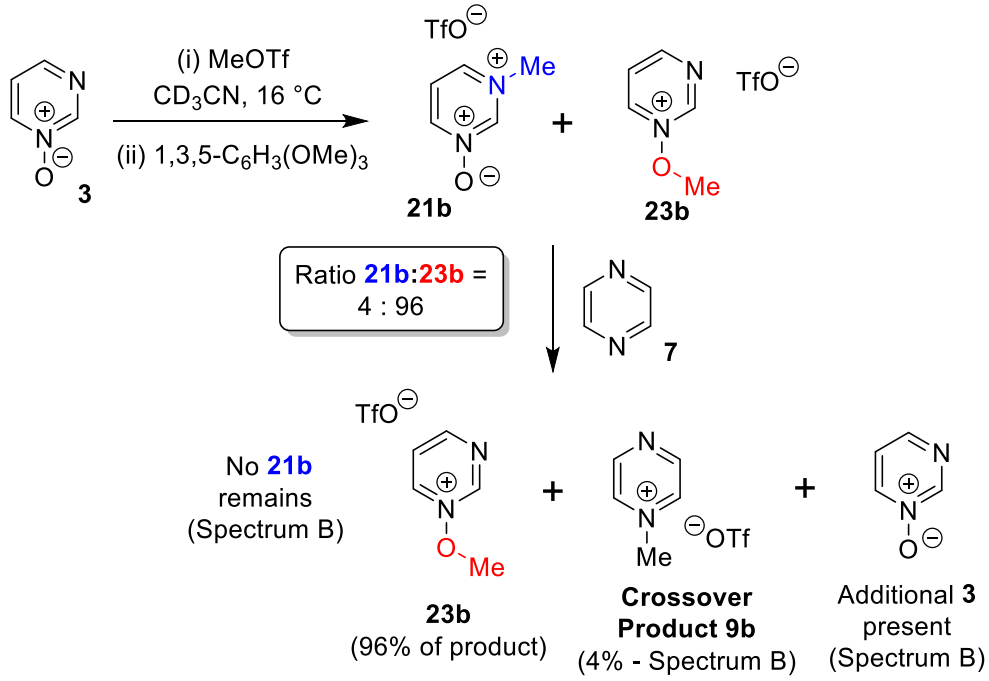


Figure S25: Spectrum B: ^{1}H NMR spectrum in CD_3CN containing signals assigned to **17b**, **7**, crossover product **9b** and **2**. Signals of the internal standard 1,3,5-trimethoxybenzene are also present. A lower proportion of signals assigned to **19b** are observed. The full spectrum is shown in Section 7.

5.3 Crossover experiment – pyrimidine *N*-oxide (3) with MeOTf and pyrazine (7)

The following reagents were combined in the process described in General Procedure D. Pyrimidine *N*-oxide (**3**) (0.014 g, 0.15 mmol) was dissolved in CD_3CN (0.65 ml) in a vial in a glove box. Methyl triflate (0.021 g, 0.13 mmol) was subsequently added dropwise. To this mixture was added 1,3,5-trimethoxybenzene (4 mg, 0.02 mmol). The reaction mixture was transferred to an NMR tube and analyzed by NMR spectroscopy in CD_3CN (Spectrum A). The tube was removed from the spectrometer and a 1.33 mol L^{-1} solution of **7** in CD_3CN (0.25 ml, 0.33 mmol) was injected into the tube through the rubber septum by syringe. The mixture was agitated and a second ^1H NMR spectrum was recorded – no change was observed in the ratio of **21b** and **23b** in this spectrum. After 1 day, the mixture was re-analyzed by ^1H NMR spectroscopy (Spectrum B). In spectrum B, only signals of starting material **3**, crossover product **9b**, **7** and **trimethoxybenzene** were observed. After two weeks, the mixture was analyzed again by ^1H NMR spectroscopy (Spectrum C). This showed that no **21b** or **23b** remained, and substantial formation of crossover product **9b** along with starting material **3** and a variety of decomposition products (the latter of which have been observed in all other experiments involving formation of **21b** and **23b** – see above).



^1H NMR (300 MHz, CD_3CN, 20 second relaxation delay) Spectrum A:

Signals assigned to **21b**: δ 9.50 – 9.36 (m, 1H), 8.98 – 8.85 (m, 1H), 8.53 (d, *J* = 6.0 Hz, 1H), 8.13 (s, 1H), 4.30 (s, 3H).

Signals assigned to **23b**: δ 9.78 – 9.77 (m, 1H), 9.43 – 9.36 (m, 2H), 8.33 – 8.17 (m, 1H), 4.51 (s, 3H). Relative to 1H of **23b**, 1H of **21b** integrates for 0.03H.

Signals assigned to starting material **3**: δ 8.95 (s, 1H), 8.41 (m, 1H), 8.34 – 8.23 (m, 1H), 7.51 – 7.43 (m, 1H). Relative to 1H of **23b**, 1H of **3** integrates for 0.31H.

Signals assigned to internal standard **trimethoxybenzene**: δ 6.11 (s, 3H), 3.76 (s, 9H). Relative to 1H of **23b**, 1H of **trimethoxybenzene** integrates for 0.18H.

The section of the spectrum between 9.50 and 9.36 ppm contains a 1H signal from **23b** and a 2H signal from **21b**. The section between 8.98 and 8.85 ppm contains a 1H signal from **21b** and a 1H signal from **3**. The section between 8.41 and 8.23 ppm contains a 1H signal from **23b** and two 1H signals from **3**.

Ratio of N-alkylation and O-alkylation Products:

3H of Compound **23b** = 3.00 – Therefore 1H = 1.00

1H of Compound **21b** = 0.03

$$\text{Ratio} = \frac{1.00}{1.00 + 0.03} \times 100 = 97\%\ \text{O alkylation}$$

Ratio of major product to internal standard:

3H of Compound **23b** = 3.00 – Therefore 1H = 1.00

3H of internal standard = 0.54 – Therefore 1H = 0.18

$$\text{Ratio} = \frac{1.00}{1.00 + 0.18} \times 100 = 85 : 15$$

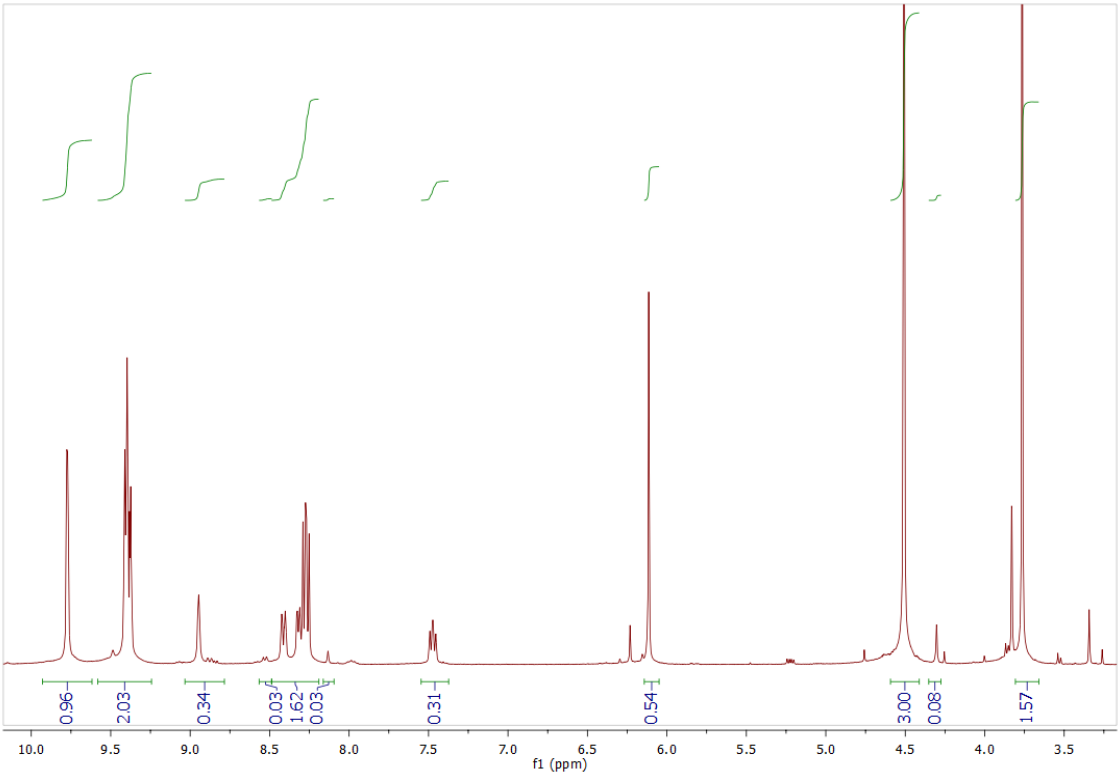


Figure S26: Spectrum A: ^{1}H NMR spectrum in CD_3CN containing signals assigned to **21b**, **23b** and **3**. Signals of the internal standard 1,3,5-trimethoxybenzene are also present. The full spectrum is shown in Section 7.

^{1}H NMR (300 MHz, CD_3CN, 20 second relaxation delay) Spectrum B:

No signals assigned to **21b**.

Signals assigned to **23b**: δ 9.78 (app dd, app *J* = 2.2, 0.7 Hz, 1H), 9.43 – 9.37 (m, 2H), 8.31 – 8.25 (m, 1H), 4.51 (s, 3H).

Signals assigned to starting material **3**: δ 8.93 (s, 1H), 8.42 – 8.36 (m, 1H), 8.31 – 8.25 (m, 1H), 7.48 – 7.40 (m, 1H). Relative to 1H of **23b**, 1H of **3** integrates for 0.43H.

Signals assigned to internal standard **trimethoxybenzene**: δ 6.11 (s, 3H), 3.76 (s, 9H). Relative to 1H of **23b**, 1H of **trimethoxybenzene** integrates for 0.18H.

Signals assigned to **7**: δ 8.60 (s, 4H). Relative to 1H of **23b**, 1H of **7** integrates for (11.32/4) = 2.83H.

Signals assigned to **crossover product 9b**: δ 9.43 – 9.37 (m, 2H), 8.76 (d, *J* = 3.1 Hz, 2H), 4.42 (s, 3H). Relative to 1H of **23b**, 1H of **9b** integrates for 0.10H.

The signal between 9.50 and 9.36 ppm contains a 1H signal from **21b** and a 2H signal from **23b**. The signal between 8.98 and 8.85 ppm contains a 1H signal from **21b** and a 1H signal from **3**. The signal between 8.31 and 8.25 ppm contains a 1H signal from **23b** and a 1H signals from **3**.

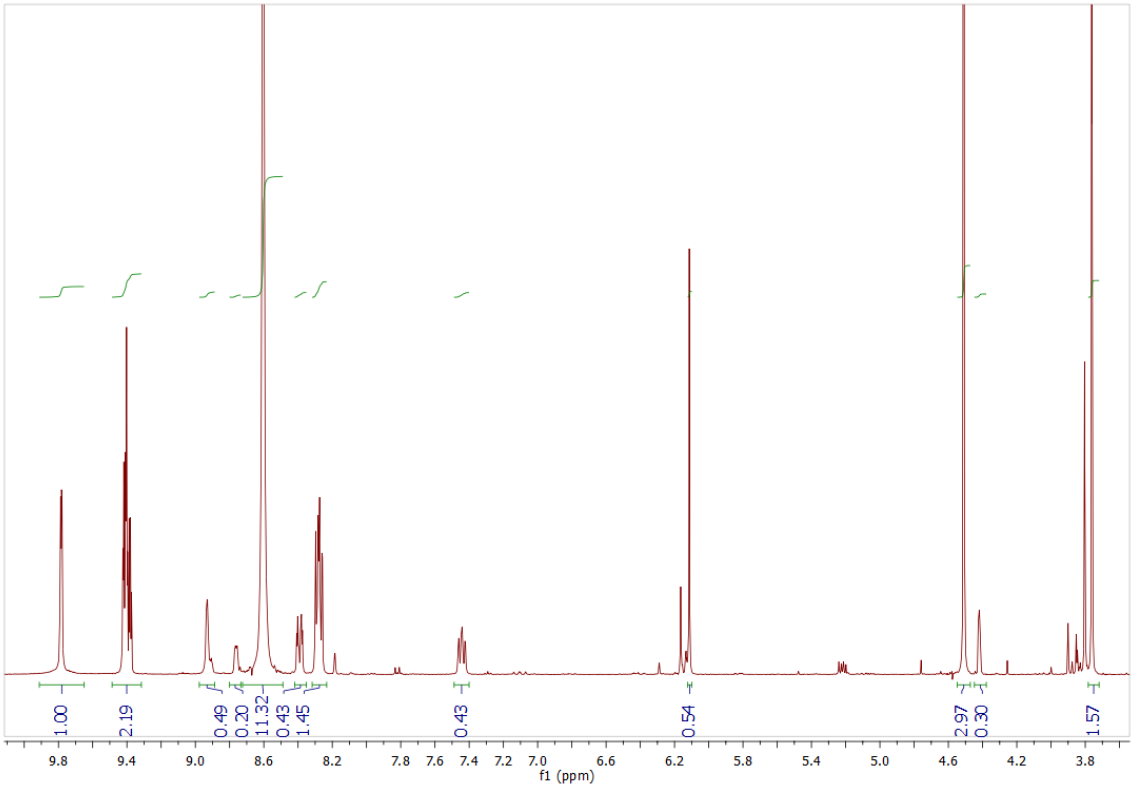


Figure S27: Spectrum B: ^{1}H NMR spectrum in CD_3CN containing signals assigned to **23b**, **7**, crossover product **9b** and **3**. Signals of the internal standard 1,3,5-trimethoxybenzene are also present. No signals of **21b** can be observed. The full spectrum is shown in Section 7.

Ratio of **23b** to **crossover product 9b**:

1H of Compound **23b** = 1.00

2H of crossover product = 0.20 – Therefore 1H = 0.10

$$\text{Ratio} = \frac{1.00}{1.00 + 0.10} \times 100 = 91 : 9$$

Ratio of major product to internal standard:

1H of Compound **23b** = 1.00

3H of internal standard = 0.54 – Therefore 1H = 0.18

$$\text{Ratio} = \frac{1.00}{1.00 + 0.18} \times 100 = 85 : 15$$

^{1}H NMR (400 MHz, CD_3CN, 20 second relaxation delay) Spectrum C: Relative integrations are given relative to 1H of crossover product **9b** since no baseline-separated signals of the internal standard are available.

No signals characteristic of **23b** are present.

Signals assigned to starting material **3**: δ 9.02 (s, 1H), 8.52 – 8.46 (m, 1H), 8.44 – 8.36 (m, 1H), 7.57 – 7.49 (m, 1H). Relative to 1H of **9b**, 1H of **3** integrates for 1.45H.

Signals assigned to **7**: δ 8.61 (s, 4H). Relative to 1H of **9b**, 1H of **7** integrates for 3.02H.

Signals assigned to **crossover product 9b**: δ 9.43 – 9.35 (m, 2H), 8.75 – 8.70 (m, 2H), 4.38 (s, 3H).

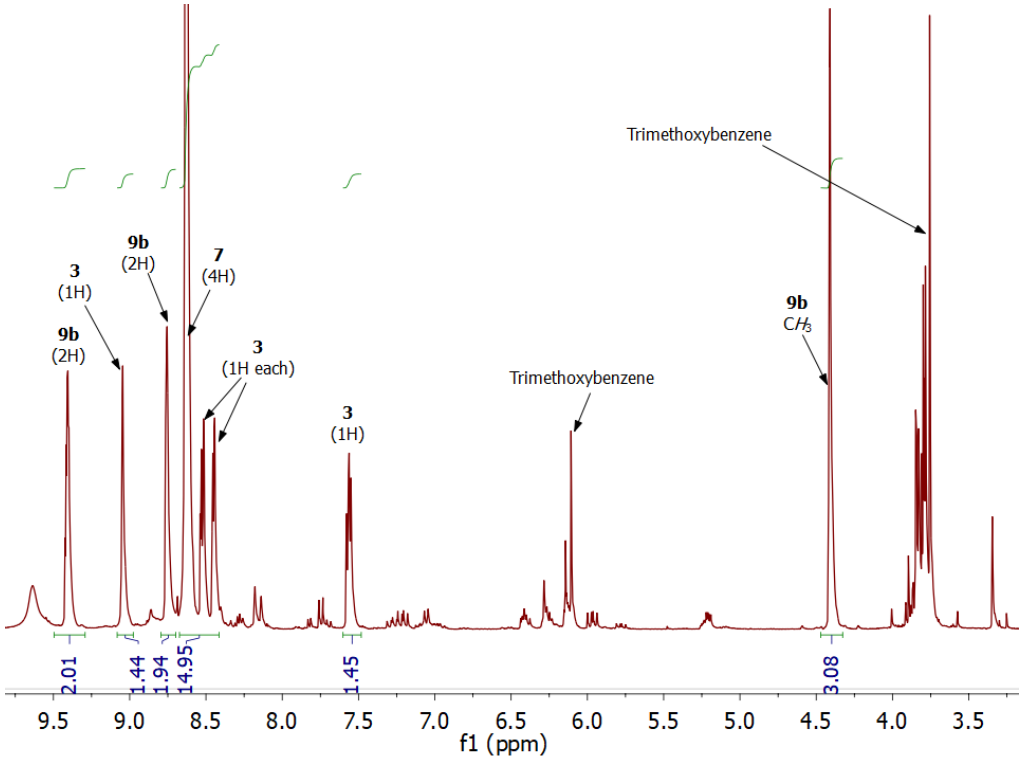


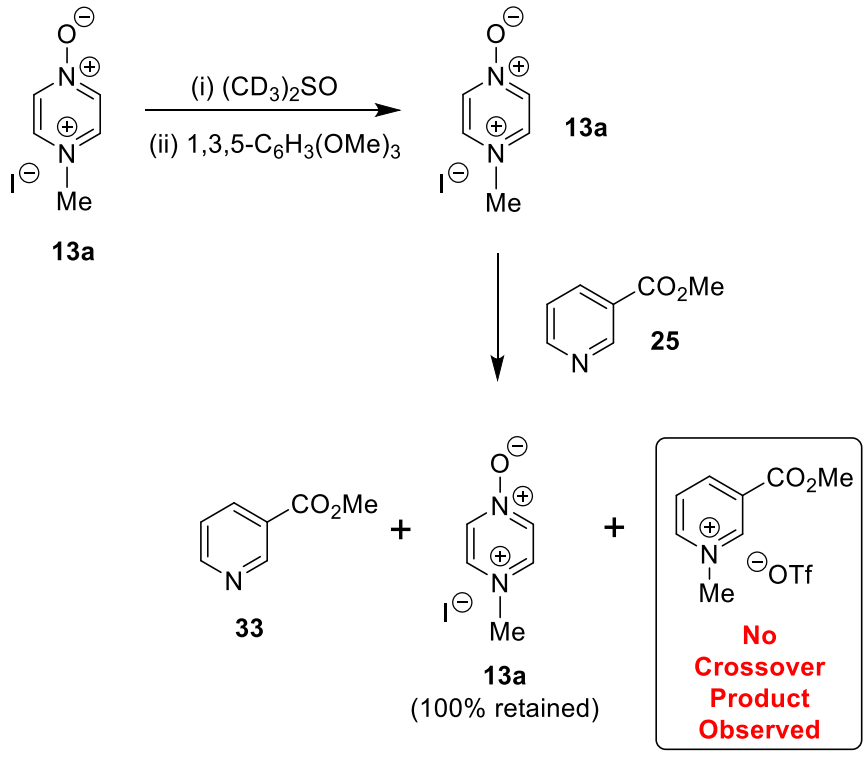
Figure S28: Spectrum C: ^{1}H NMR spectrum in CD_3CN containing signals assigned to **7**, crossover product **9b** and starting material **3**. Signals of the internal standard, 1,3,5-trimethoxybenzene, are also present, but are obscured by signals of decomposition products. No signals assigned to **23b** are observed. The full spectrum is shown in Section 7.

The signals of the internal standard (1,3,5-trimethoxybenzene) are obscured by signals of decomposition products (see ^{1}H NMR spectrum below). The relative proportion of (**7** + **9b**) to **3** is similar to the relative proportion of (**7** + **9b**) to (**3** + **23b**) in spectrum B (above), but reflects the occurrence of some decomposition of **23b** that was independent of the process of formation of crossover product **9b** by methylation of **7**.

Formation of crossover product (**9b**) derived from both N-methylation and O-methylation products (**21b** and **23b**) may indicate that **21b** and **23b** form reversibly from **3** + MeOTf, or instead that **21b** and **23b** each undergo S_N2 reactions with 2nd nucleophile **7**.

5.4 Crossover experiment – 4-methylpyrazinium-*N*-oxide iodide (13a) with MeOTf and methyl nicotinate (25)

The following reagents were combined in the process described in General Procedure D. **13a** (0.031 g, 0.13 mmol) was dissolved in $(CD_3)_2SO$ (0.7 ml) in a vial. To this solution was added 1,3,5-trimethoxybenzene (3 mg, 0.02 mmol). The mixture was transferred to an NMR tube and analyzed by NMR spectroscopy in $(CD_3)_2SO$ (Spectrum A). The tube was removed from the spectrometer and a solution of methyl nicotinate (**25**) (0.026 g, 0.19 mmol) in $(CD_3)_2SO$ (0.15 ml) was injected into the tube through the septum by syringe. The mixture was agitated and re-analyzed by NMR spectroscopy immediately, and again after one day (Spectrum B).



^{1}H NMR (300 MHz, $(CD_3)_2SO$, 10 second relaxation delay) Spectrum A:

Signals assigned to **13a**: δ 8.92 (dd, *J* = 13.3, 5.7 Hz, 4H), 4.16 (s, 3H).

Signals assigned to internal standard **trimethoxybenzene**: δ 6.06 (s, 3H), 3.68 (s, 9H). Relative to 1H of **13a**, 1H of **trimethoxybenzene** integrates for 0.18H.

Note: A singlet belonging to a small amount of an unknown contaminant is present at 8.22 ppm.

The singlet at 3.68 ppm could not be accurately integrated due to its proximity to the H_2O signal.

Ratio of major product to internal standard:

4H of Compound **13a** = 4.00 – Therefore 1H = 1.00

3H of internal standard = 0.55 – Therefore 1H = 0.18

$$\text{Ratio} = \frac{1.00}{1.00 + 0.18} \times 100 = 85 : 15$$

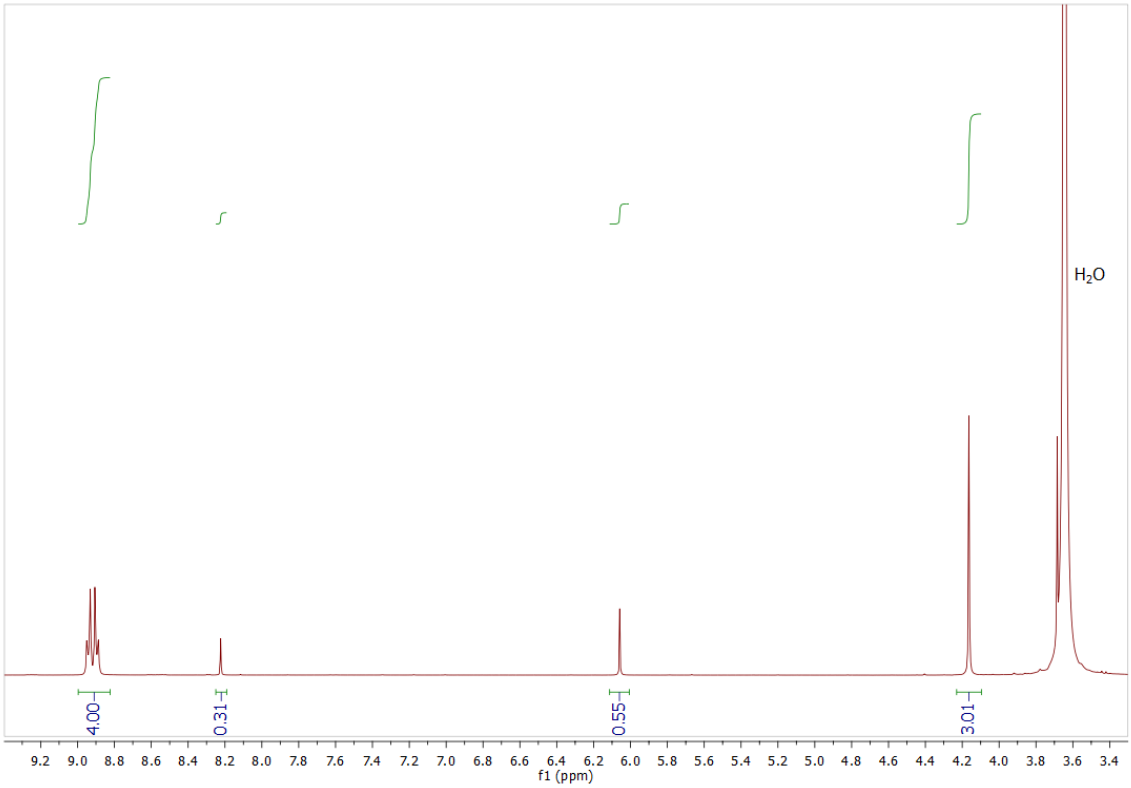


Figure S29: Spectrum A: ^{1}H NMR spectrum in $(CD_3)_2SO$ containing signals assigned to **13a**. Signals of the internal standard 1,3,5-trimethoxybenzene are also present. The full spectrum is shown in Section 7.

^{1}H NMR (300 MHz, $(CD_3)_2SO$, 10 second relaxation delay) Spectrum B:

Signals assigned to **13a**: δ 8.98 – 8.90 (m, 4H), 4.17 (s, 3H).

Signals assigned to internal standard **trimethoxybenzene**: δ 6.04 (s, 3H). Relative to 1H of **13a**, 1H of **trimethoxybenzene** integrates for 0.18H.

Signals assigned to **25**: δ 9.04 (d, *J* = 1.7 Hz, 1H), 8.78 (dd, *J* = 4.8, 1.6 Hz, 1H), 8.27 (app dt, app *J* = 8.0, 1.9 Hz, 1H), 7.56 (ddd, *J* = 8.0, 4.9 Hz (signal resolution not sufficient to determine smallest *J* value – it is of the order of < 1 Hz), 1H), 3.86 (s, 3H). Relative to 1H of **23b**, 1H of **25** integrates for 1.59H.

Note: The 9H singlet of 1,3,5-trimethoxybenzene is obscured by the signal of residual H_2O.

Ratio of major product to internal standard:

4H of Compound **13a** = 4.00 – Therefore 1H = 1.00

3H of internal standard = 0.54 – Therefore 1H = 0.18

$$\text{Ratio} = \frac{1.00}{1.00 + 0.18} \times 100 = 85 : 15$$

This experiment shows that **13a** is formed irreversibly from **1** + MeI.

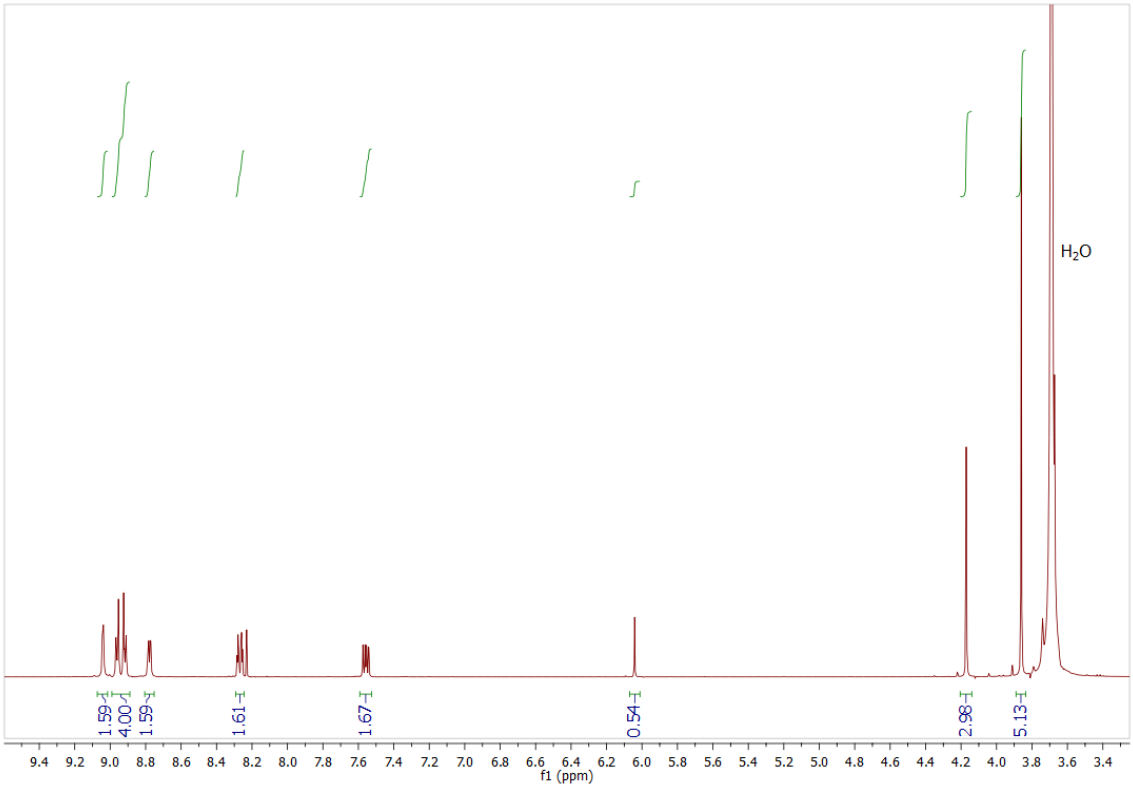
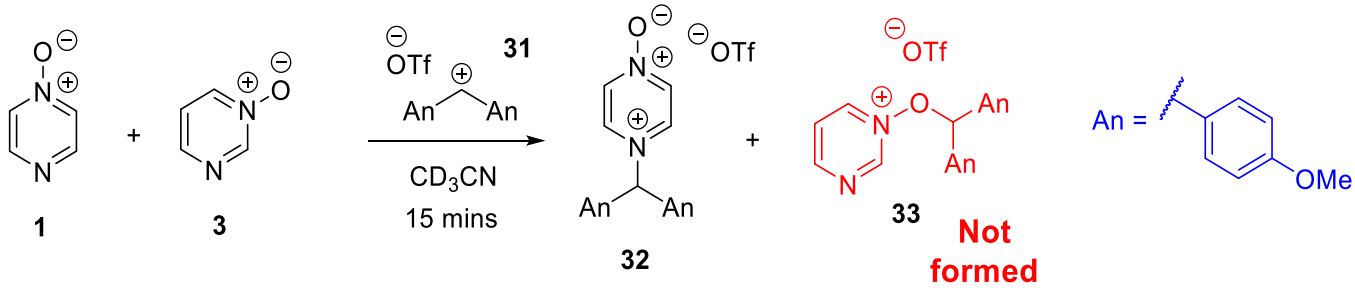


Figure S30: Spectrum B: ^{1}H NMR spectrum in $(CD_3)_2SO$ containing signals assigned to **13a** and **25**. The internal standard 1,3,5-trimethoxybenzene is also present. No signals of crossover product **26** are observed. The full spectrum is shown in Section 7.

As no change in the amount of **13a** present was observed, and no crossover product was formed, we conclude that **13a** is formed irreversibly.

6. Competition experiment: Pyrazine *N*-oxide (1) vs Pyrimidine *N*-oxide (3)

Under an atmosphere of nitrogen in a glove box, bis(methoxy)benzhydryl chloride (0.009 g, 0.03 mmol) was dissolved in dry CD_3CN (0.85 ml). Pyrazine *N*-oxide **1** (6 mg, 0.06 mmol) was then added, followed by pyrimidine *N*-oxide **3** (0.005 g, 0.05 mmol), and then AgOTf (0.013 g, 0.05 mmol), causing the immediate precipitation of AgCl. The reaction vessel was sealed, agitated for 1 – 2 minutes, and filtered (removing AgCl) through a syringe filter into an NMR tube. The NMR tube was then sealed using a rubber septum. The seal was then wrapped with PTFE tape and Parafilm. Finally, the NMR tube was placed in a long Schlenk flask, which was sealed and then removed from the glove box. The sample was brought to the NMR spectrometer inside the long NMR Schlenk flask to protect it from potential ingress of moisture. The sample was removed from this Schlenk flask directly before loading it into the NMR spectrometer.



^{1}H NMR (400 MHz, CD_3CN) – Integrations are given relative to 1H of **32**.

Signals assigned to **32**: δ 8.52–8.46 (m, overlaps with signal of **1** at δ 8.46–8.41, contains 4H of **32** (4 × pyrazinium H)), 7.30–7.20 (m, contains 4H of **32** (anisyl protons), overlaps with signal of hydrolysis product), 7.11 – 7.00 (m, 5H, contains Ar_2CH and anisyl protons), 3.84(s, 6H, OCH_3).

Signals assigned to **1**: δ 8.46–8.41 (m, 2H), 8.15–8.08 (m, 2H). 1H of **1** integrates for 0.70 relative to 1H of **32**.

Signals assigned to **3**: δ 8.92 (s, 1H), 8.41–8.32 (app d, app *J* = 6.3 Hz, 1H), 8.29 – 8.21 (m, 1H), 7.46 – 7.39 (m, 1H). 1H of **3** integrates for 1.58 relative to 1H of **32**.

Small signals arising from the presence of hydrolysis product (bis(4-methoxy)benzhydryl ether) are also present in the ^{1}H NMR spectrum (see Fig. S30 below).

No signals attributable to compound **33** are present, i.e. **32** is the only product formed.

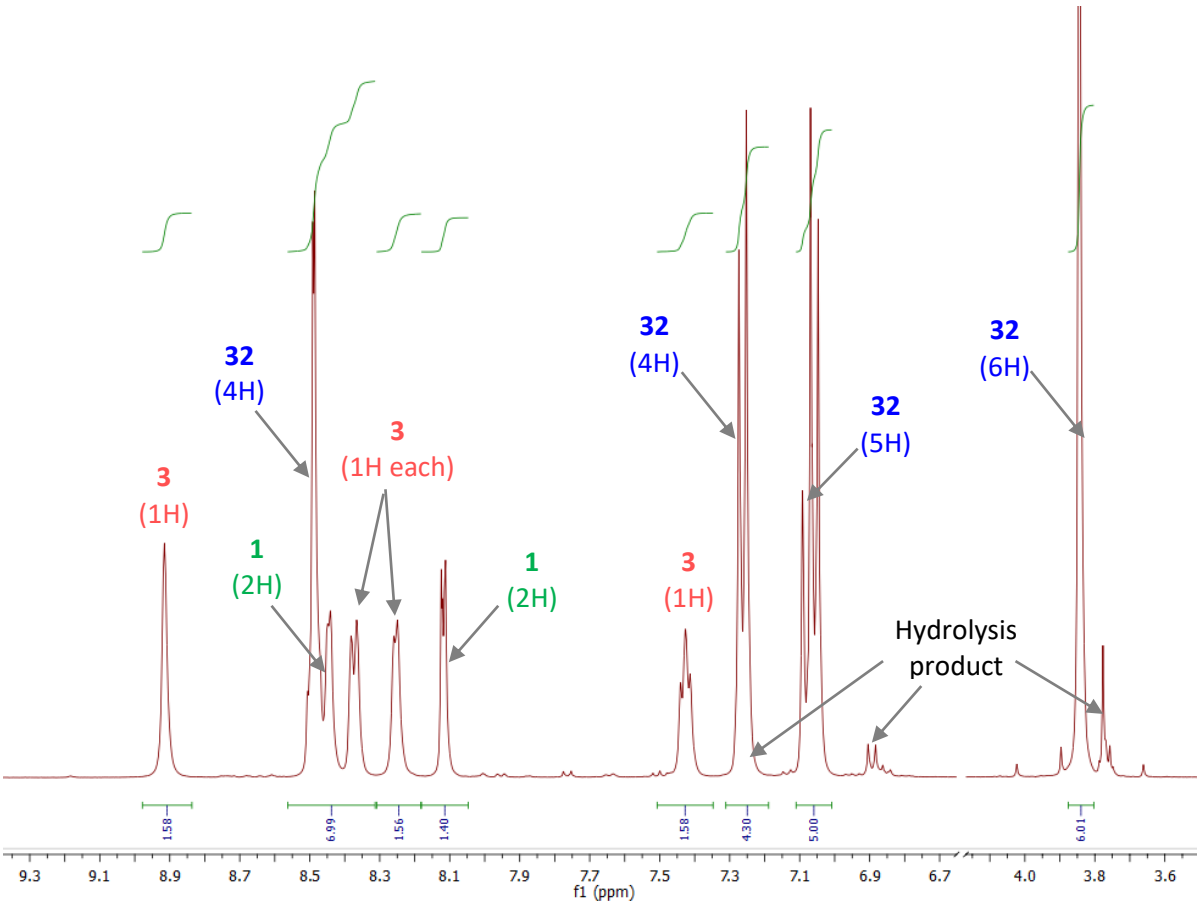


Figure S31: ^{1}H NMR spectrum in CD_3CN containing signals assigned to **1**, **3**, and **32**. No signals assigned to **33** were observed.

7. Full Spectra for compounds produced in Sections 4 – 6

13a in $(CD_3)_2SO$ (From Pyrazine *N*-oxide (1) + MeI)

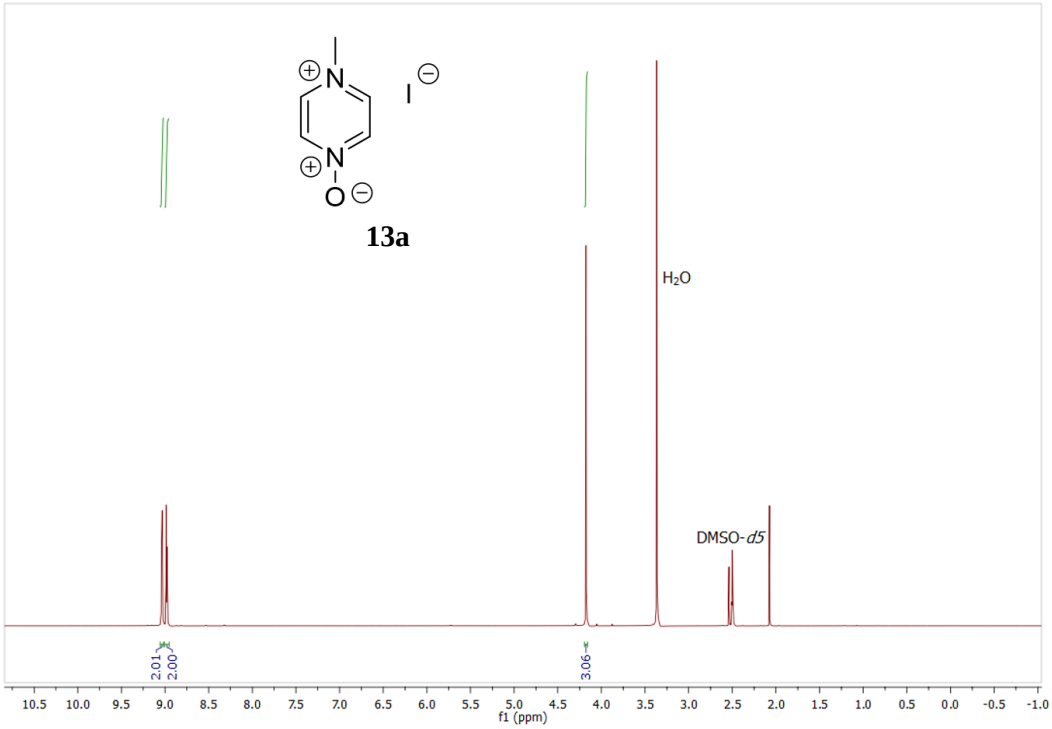


Figure S32 Full ^{1}H NMR spectrum of **13a** in $(CD_3)_2SO$ (600 MHz).

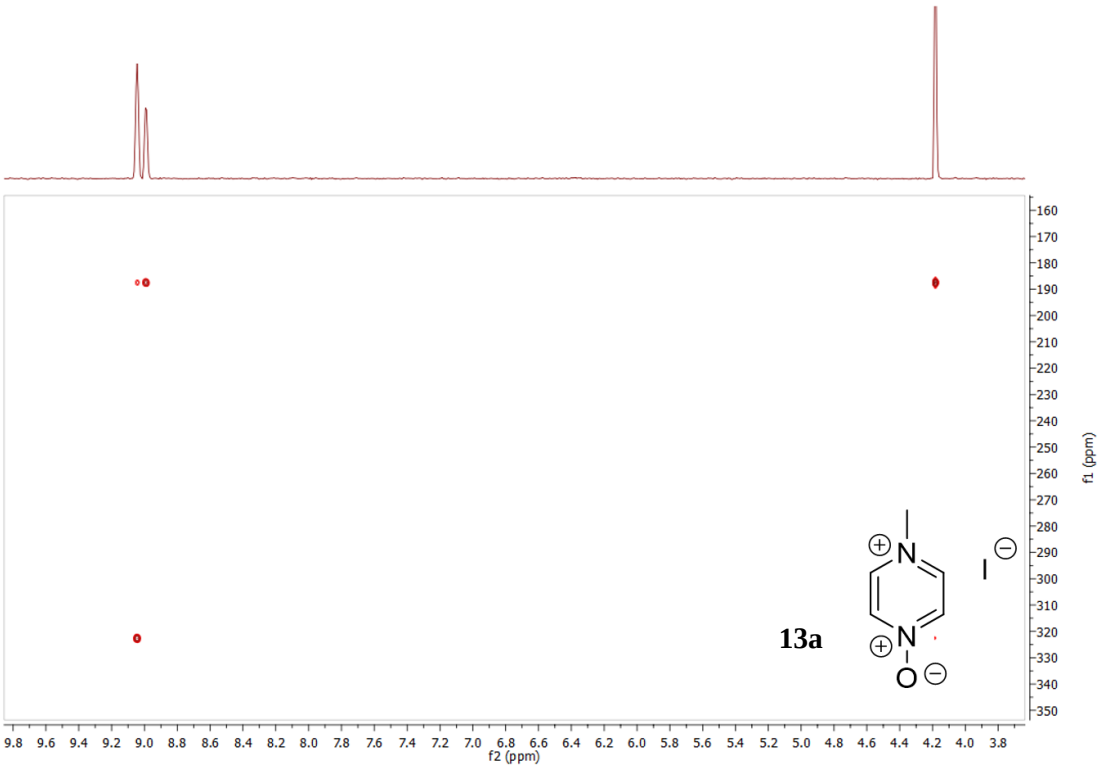


Figure S33: ^{1}H-^{15}N HMBC NMR spectrum of **27a** in $(CD_3)_2SO$.

13a in CD_3CN (From Pyrazine *N*-oxide (1) + MeI)

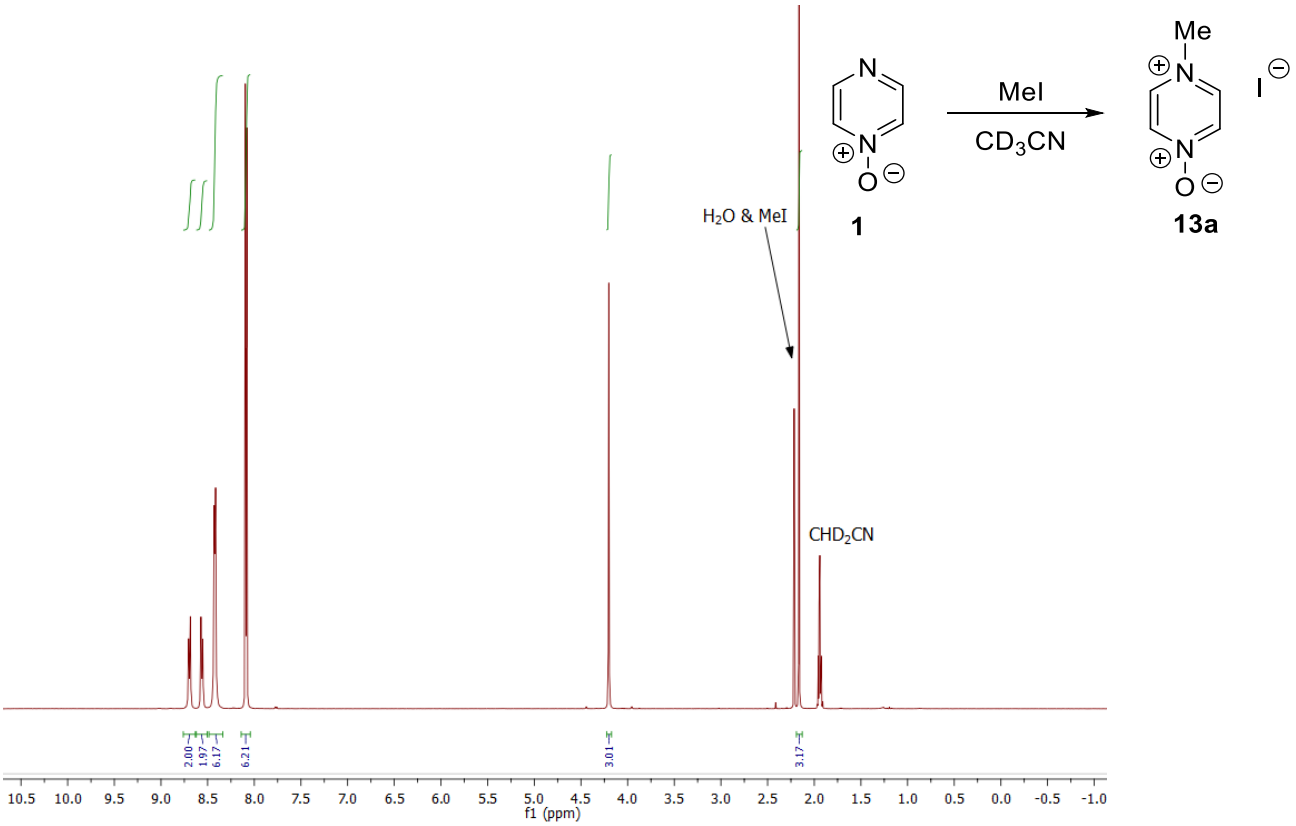


Figure S34 Full ^{1}H NMR spectrum of the reaction of **1** + MeI to give low conversion to **13a** in CD_3CN

13b in $(CD_3)_2SO$ (From Pyrazine *N*-oxide (1) + MeOTf in CH_3CN)

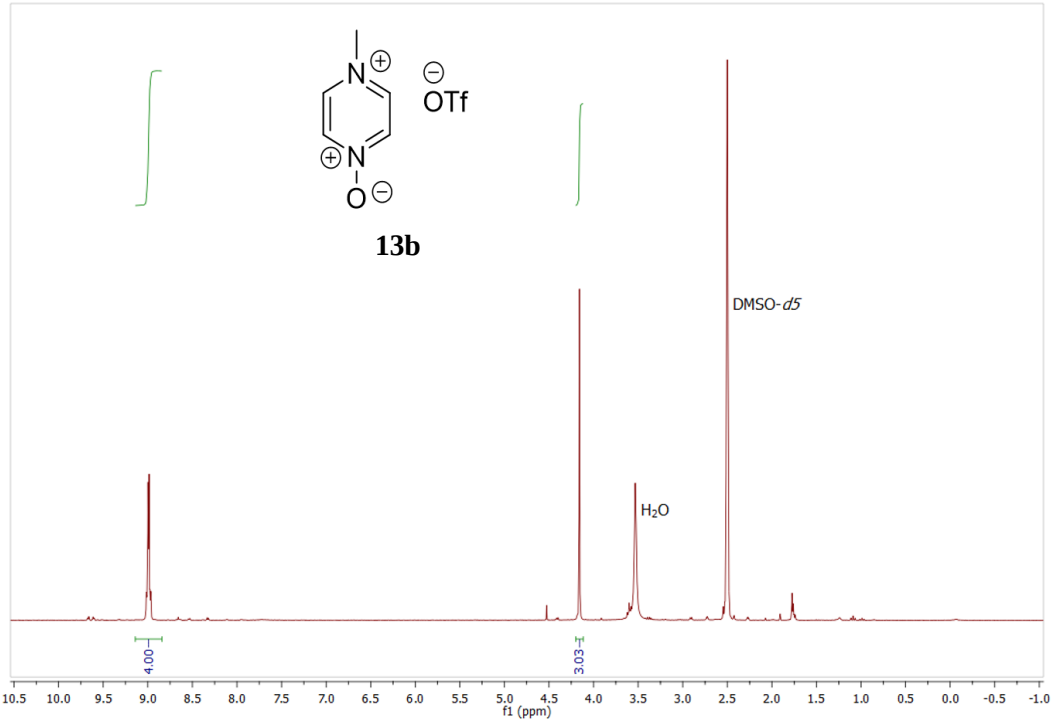


Figure S35: Full ^{1}H spectrum of **13b** in $(CD_3)_2SO$ (300 MHz).

13b and 15b in CD_3CN (From Pyrazine *N*-oxide (1) + MeOTf in CD_3CN)

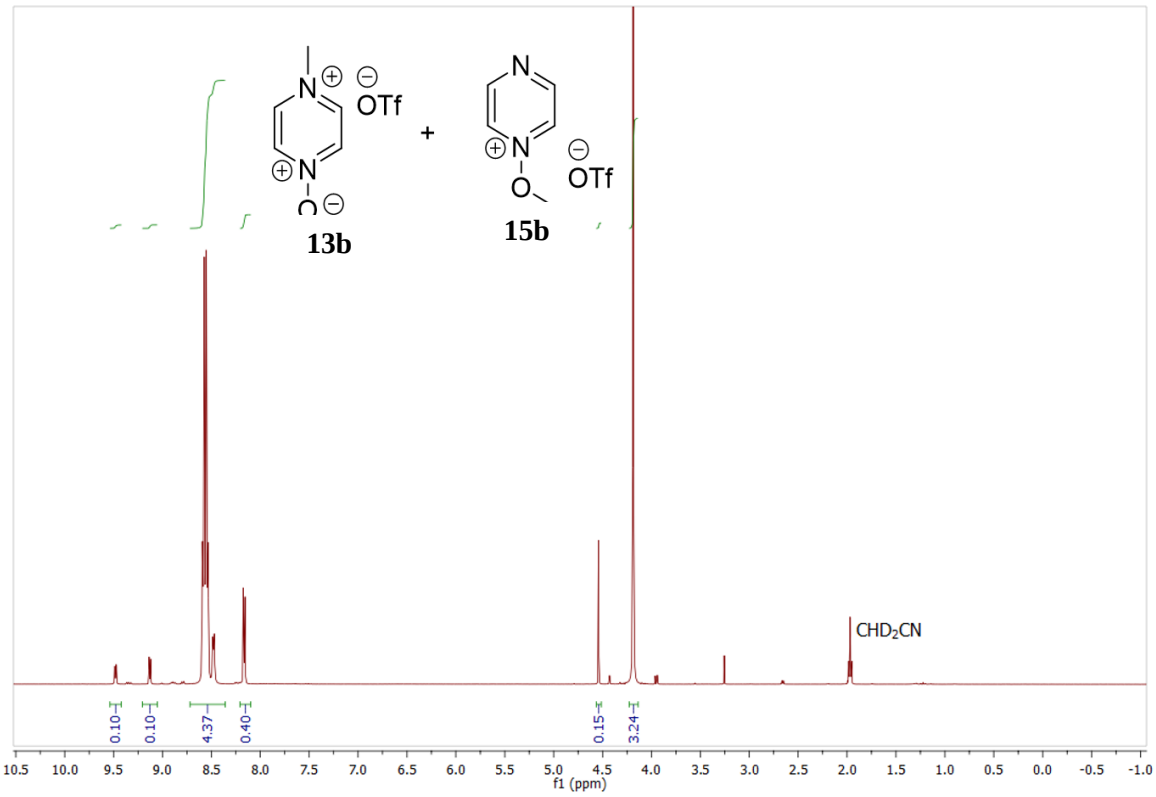


Figure S36: Full ^1H NMR spectrum of **13b**, showing some **15b** and starting material (**1**) in CD_3CN (600 MHz).

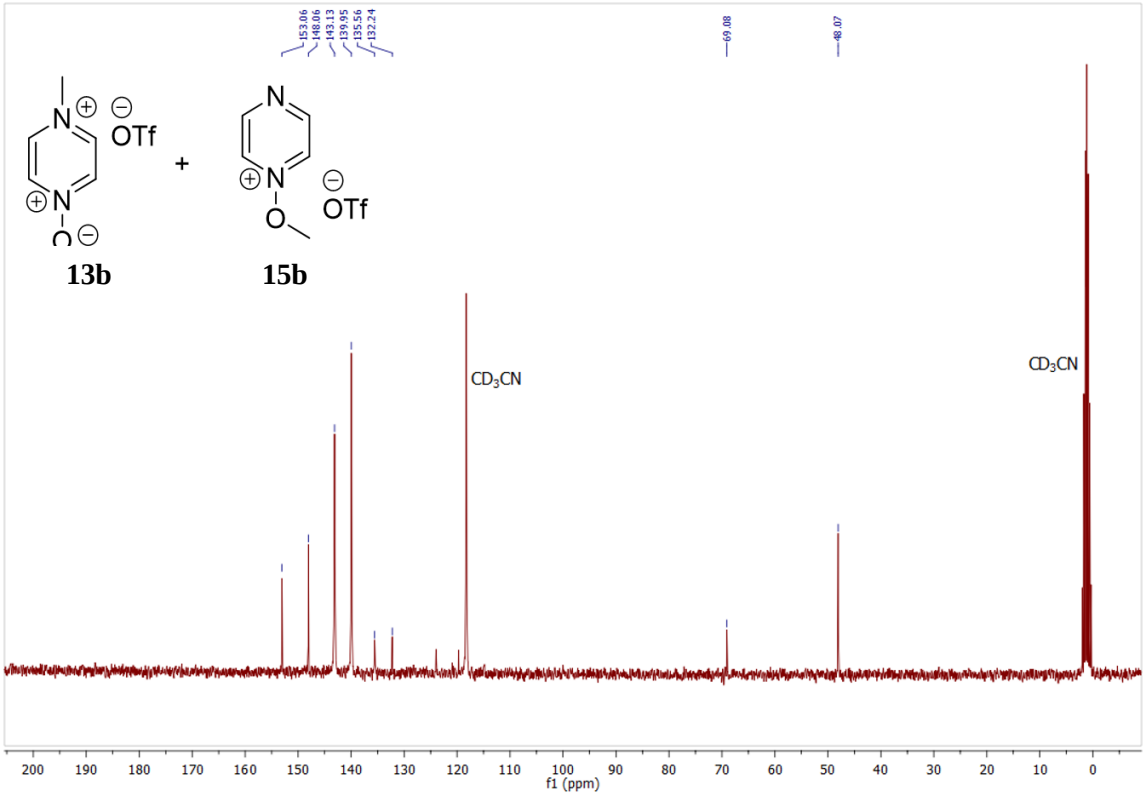


Figure S37: $^{13}C\{^1H\}$ NMR spectrum of **13b**, showing some **15b** and starting material (**1**) in CD_3CN (150 MHz).

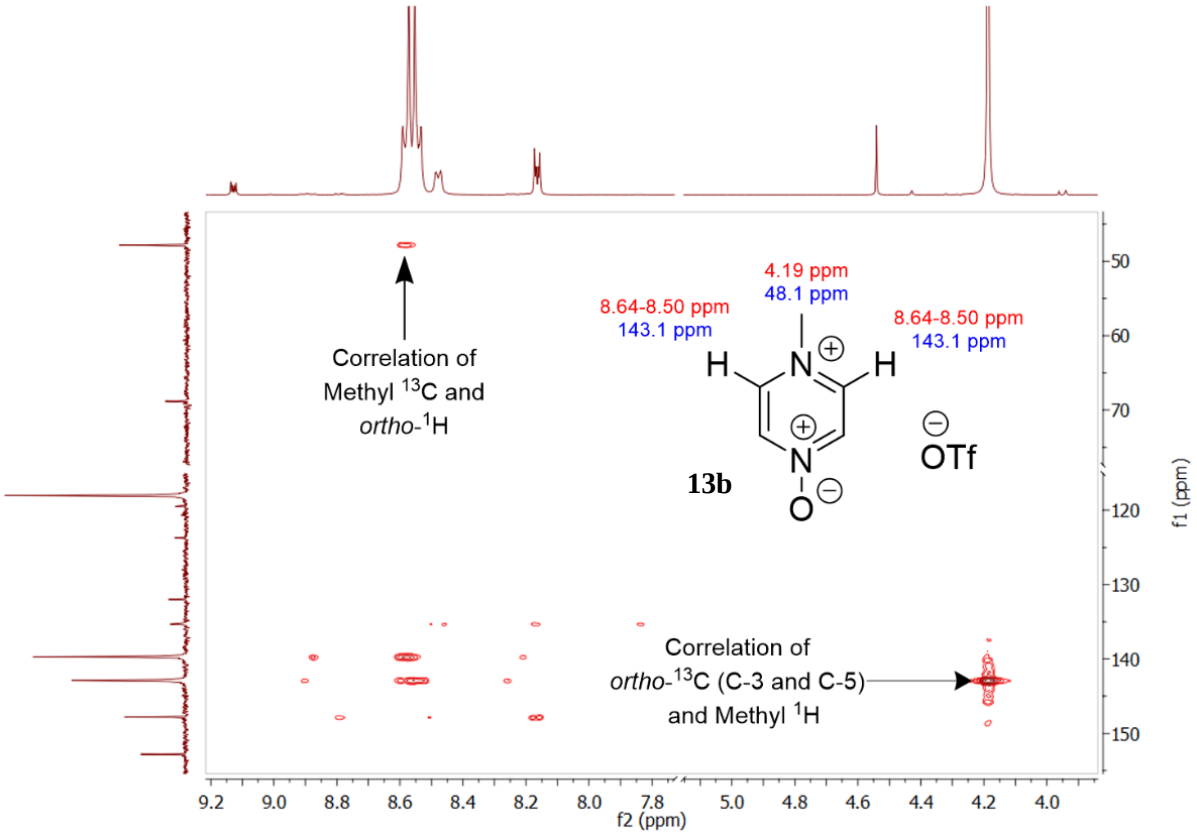


Figure S38: Section of ^{1}H-^{13}C HMBC NMR spectrum of **13b** in CD_3CN.

13b in $(CD_3)_2SO$ (From 1 + MeOTf in CD_3CN, after solvent removal)

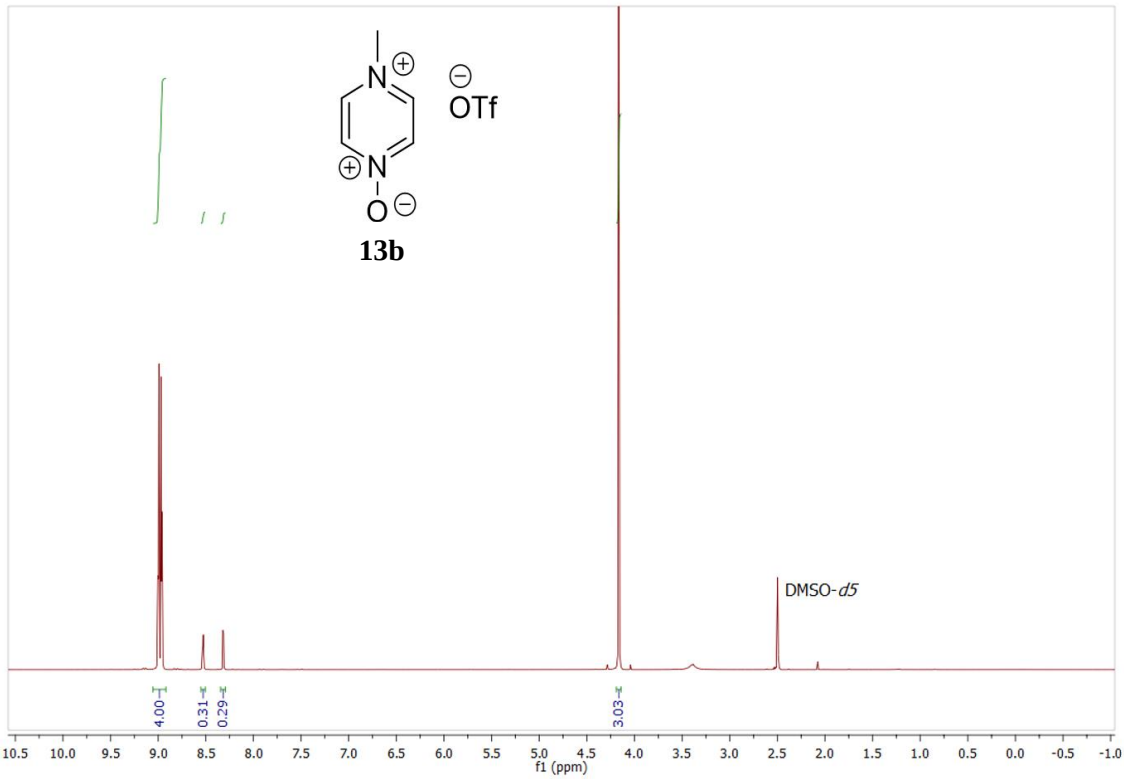


Figure S39: Full ^{1}H NMR spectrum of **13b** and **1** in $(CD_3)_2SO$ after removal of the CD_3CN reaction solvent (600 MHz).

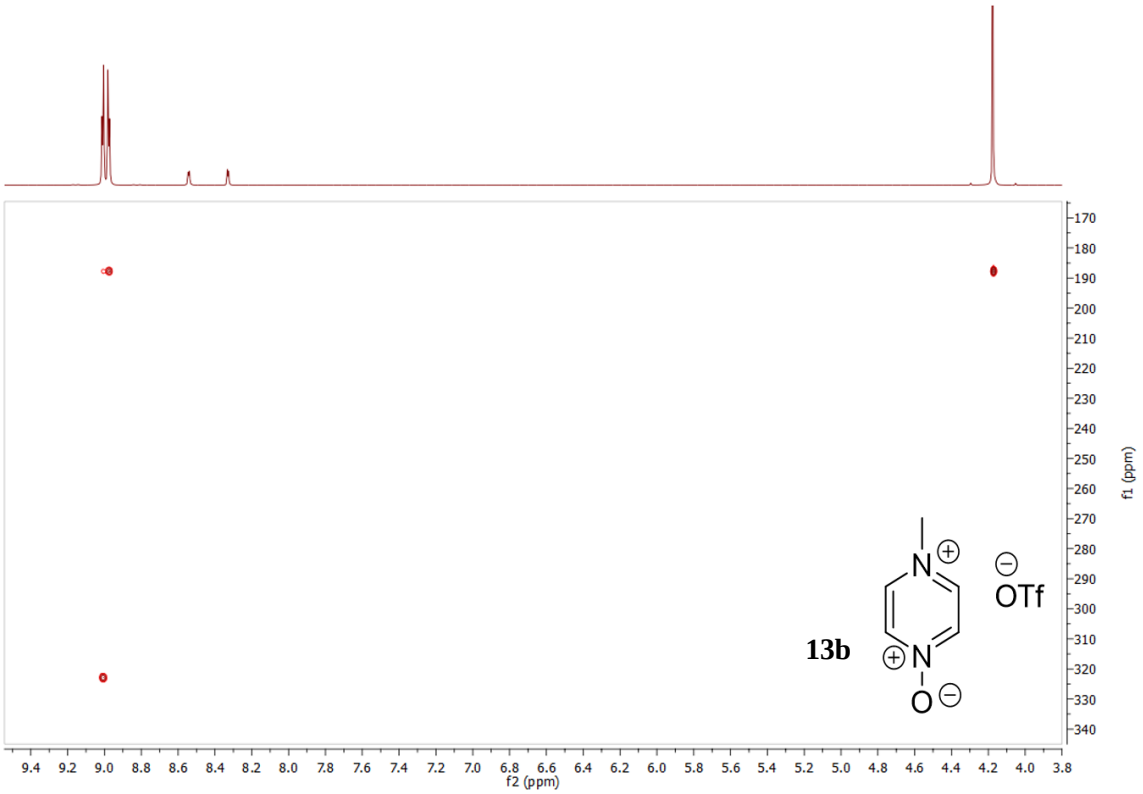


Figure S40: ^{1}H-^{15}N HMBC NMR spectrum of **13b** and **1** in $(CD_3)_2SO$. Removal of the CD_3CN caused the decomposition of **15b**.

13b in $(CD_3)_2SO$ (From Pyrazine *N*-oxide (1) + MeOTf in $(CD_3)_2SO$)

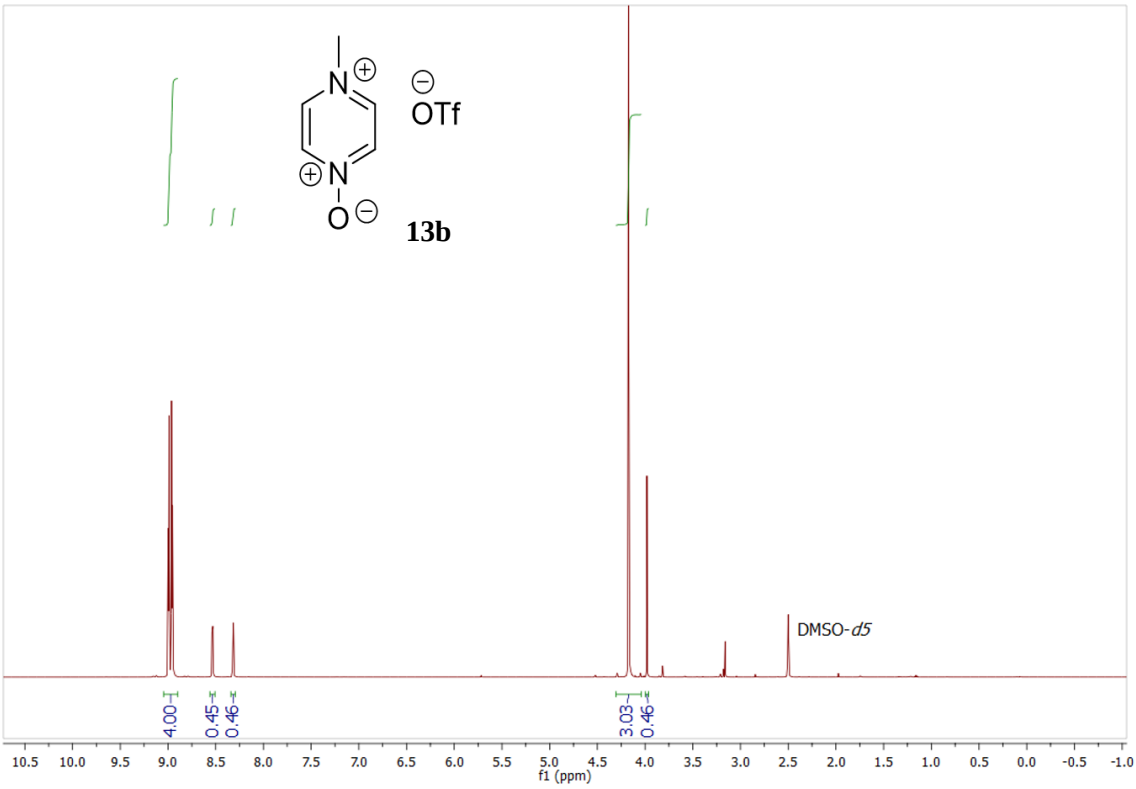


Figure S41: Full ^{1}H NMR spectrum of **13b**, showing some **1** in $(CD_3)_2SO$ (600 MHz). A signal assigned to the methoxydimethylsulfonium salt of $(CD_3)_2SO$ is present at 3.98 ppm.

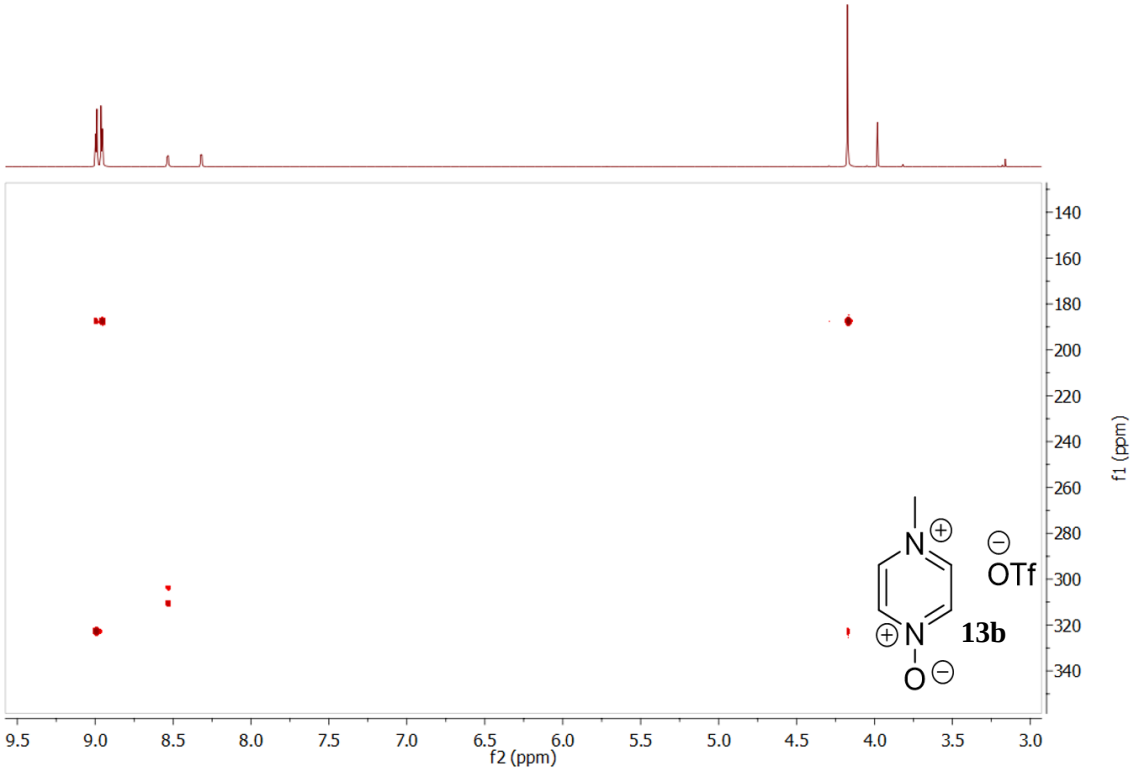


Figure S42: ^{1}H-^{15}N HMBC NMR spectrum of **13b** and **1** in $(CD_3)_2SO$.

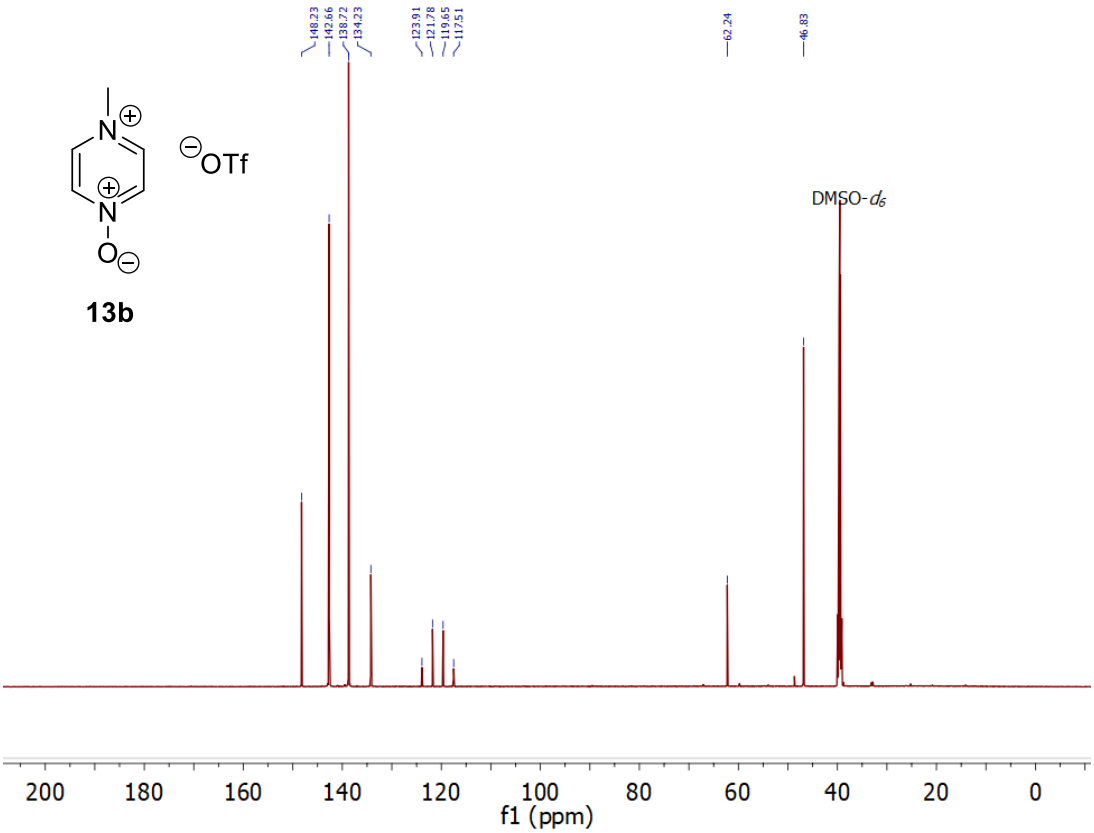


Figure S43: $^{13}C\{^{1}H\}$ NMR spectrum of **13b**, showing some **1** in $(CD_3)_2SO$ (600 MHz). A signal assigned to the methoxydimethylsulfonium salt of $(CD_3)_2SO$ is present at 62.2 ppm.

14 in CD_3CN (From Pyrazine *N*-oxide (1) + benzhydrylium ion 11 in CD_3CN)

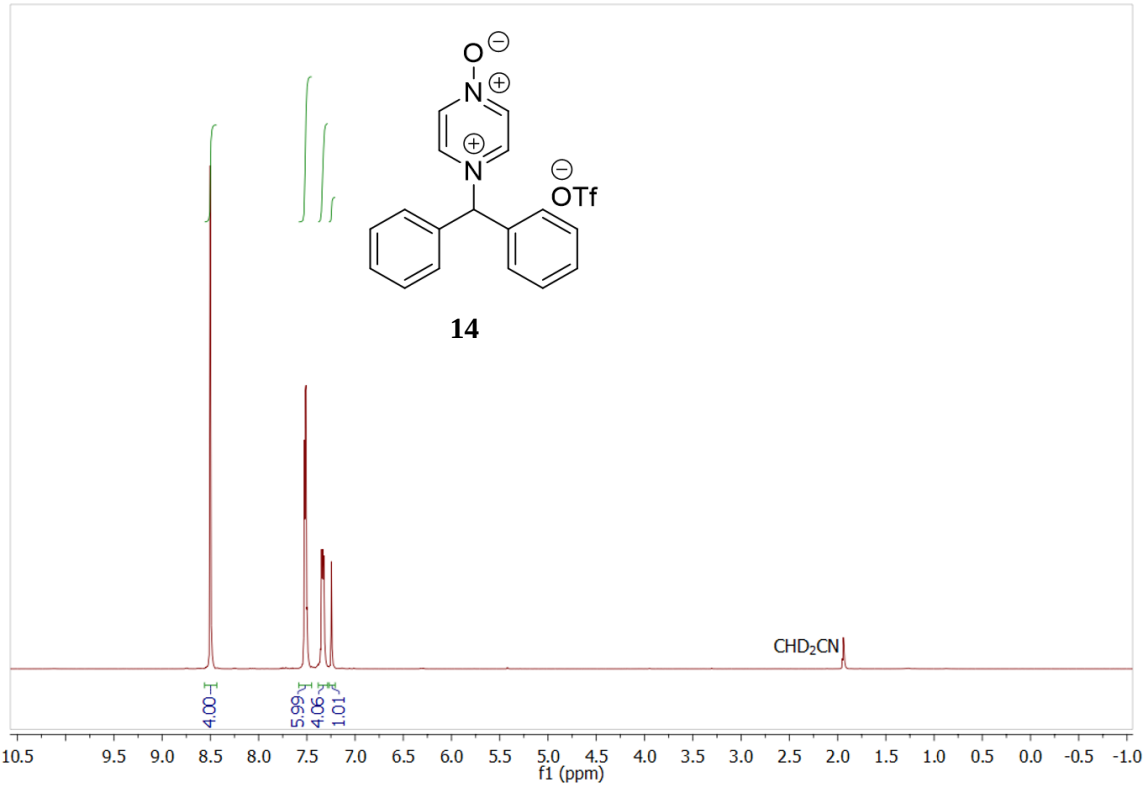


Figure S44: Full ^1H NMR spectrum of **14** in CD_3CN (400 MHz)

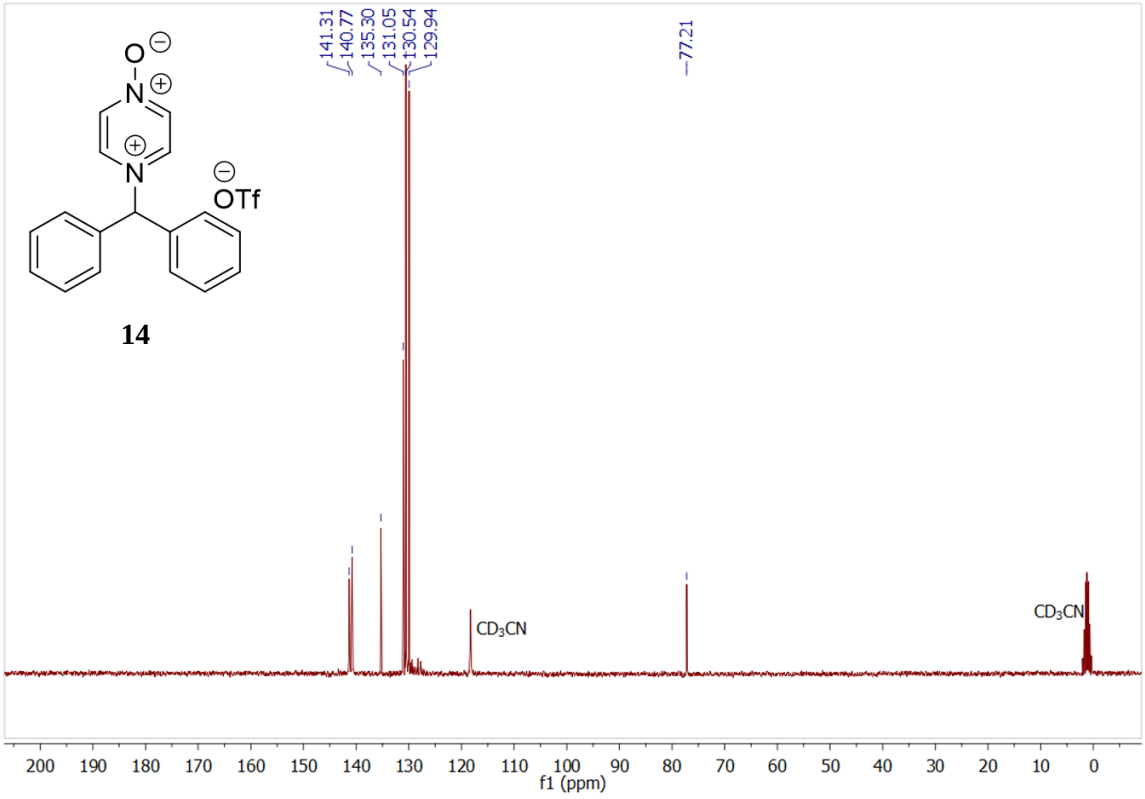


Figure S45: $^{13}C\{^1H\}$ NMR spectrum of **14** in CD_3CN (75 MHz)

14 in CH_2Cl_2 (From Pyrazine *N*-oxide (1) + benzhydrylium ion 11 in CH_2Cl_2)

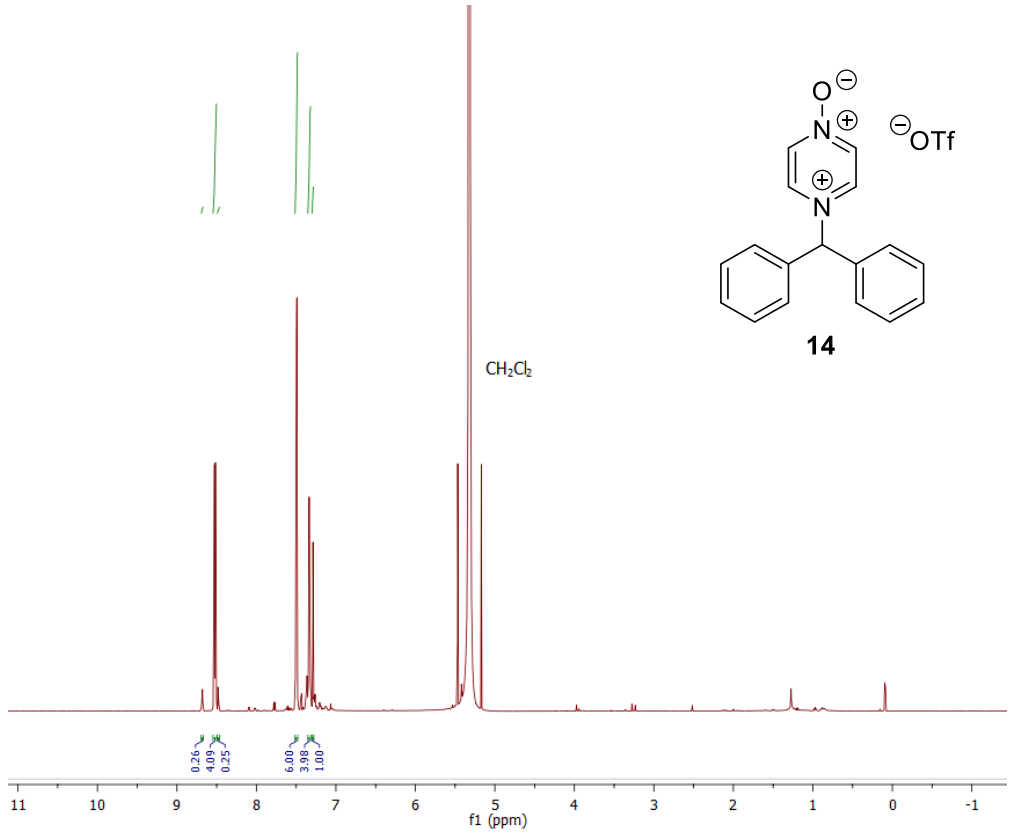


Figure S46: Full ^1H NMR spectrum of **14** in CH_2Cl_2 (600 MHz) **acquired with solvent signal suppression**.

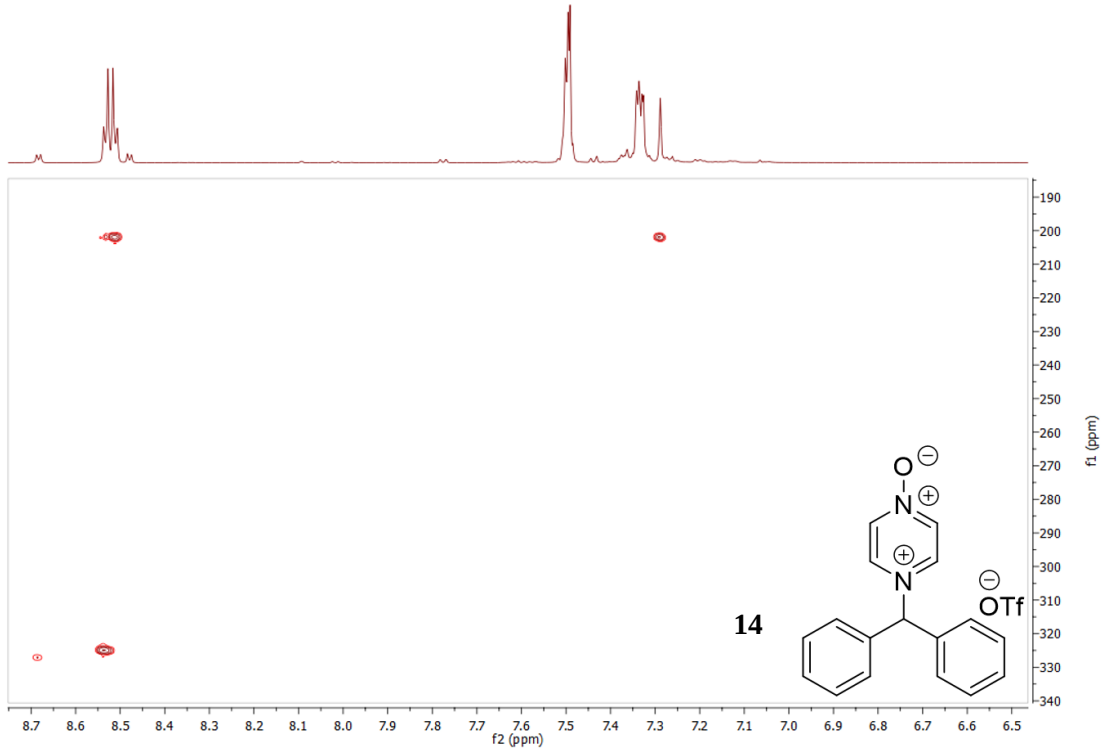


Figure S47: ^1H-^{15}N HMBC NMR spectrum of **14** in CH_2Cl_2 acquired with solvent signal suppression.

17a in $(CD_3)_2SO$ (From Quinoxaline *N*-oxide (2) + MeI)

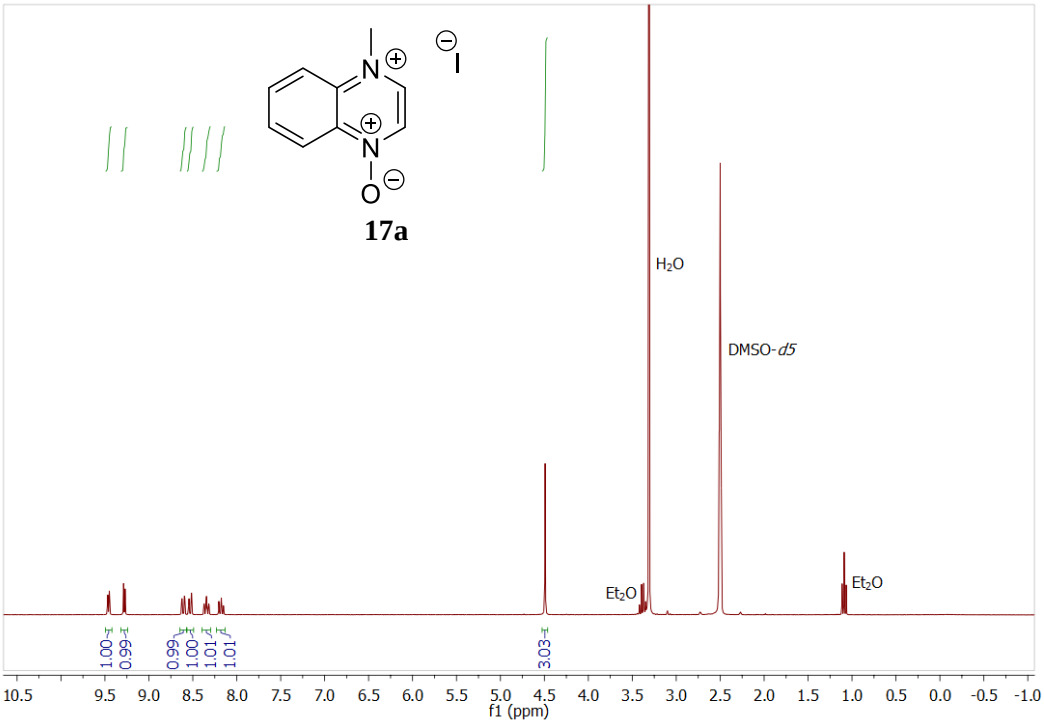


Figure S48: Full ^{1}H NMR spectrum of **17a** in $(CD_3)_2SO$ (600 MHz).

17a in $(CH_3)_2SO$ (From Quinoxaline *N*-oxide (2) + MeI)

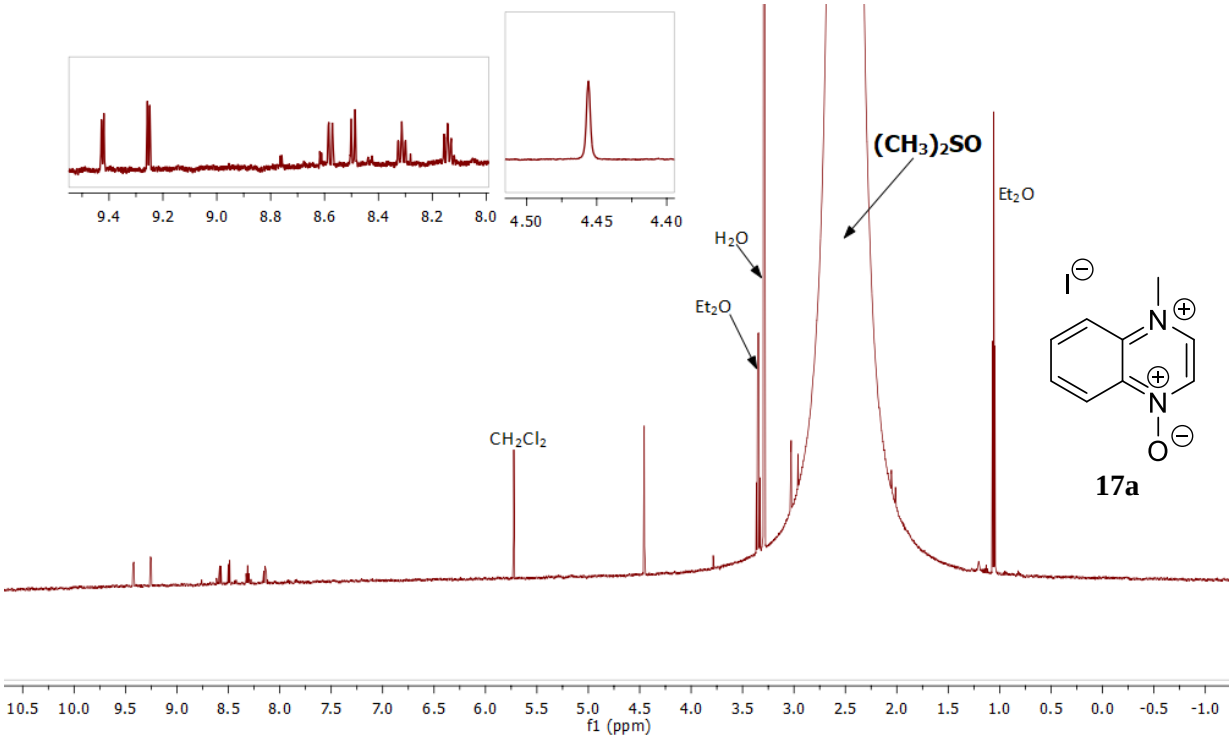


Figure S49: Full ^{1}H NMR spectrum of **17a** in $(CH_3)_2SO$ (600 MHz) **acquired with solvent signal suppression**.

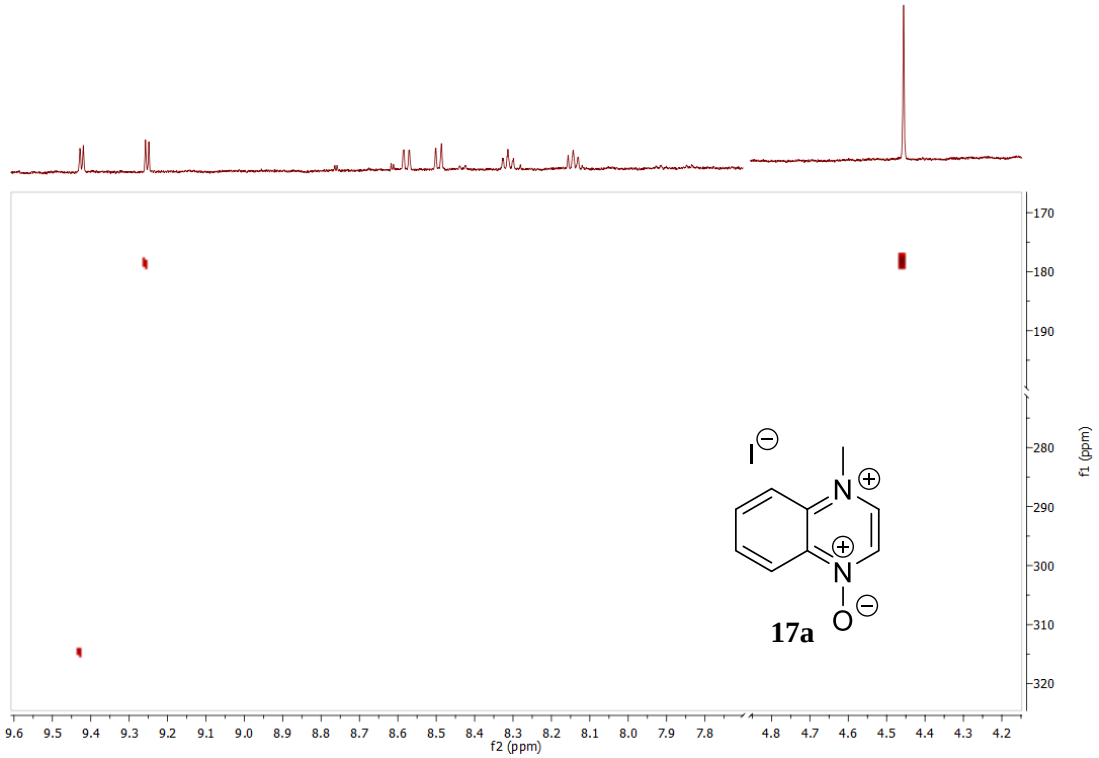


Figure S50: ^{1}H-^{15}N HMBC NMR spectrum of **17a** in $(CH_3)_2SO$ (150 MHz) acquired with solvent signal suppression.

17b in $(CD_3)_2SO$ (From Quinoxaline *N*-oxide (2) + MeOTf in CH_3CN)

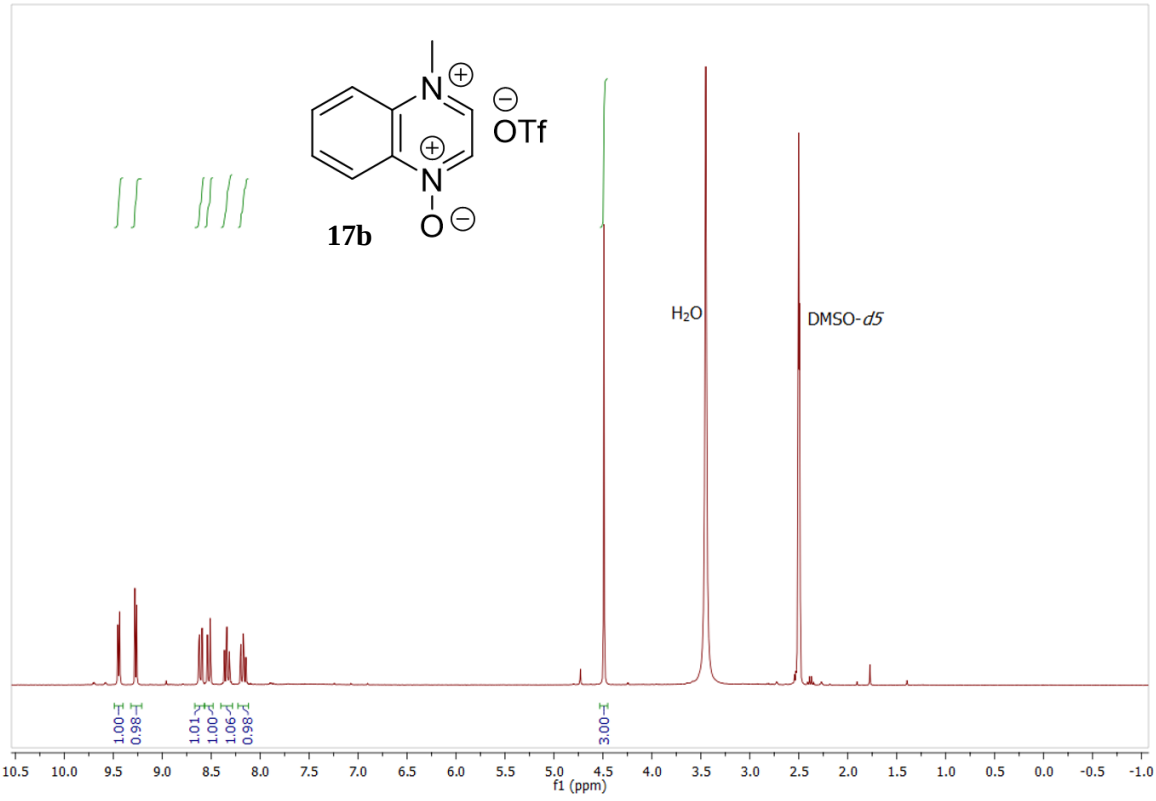


Figure S51 Full ^{1}H NMR spectrum of **17b** in $(CD_3)_2SO$ (300 MHz).

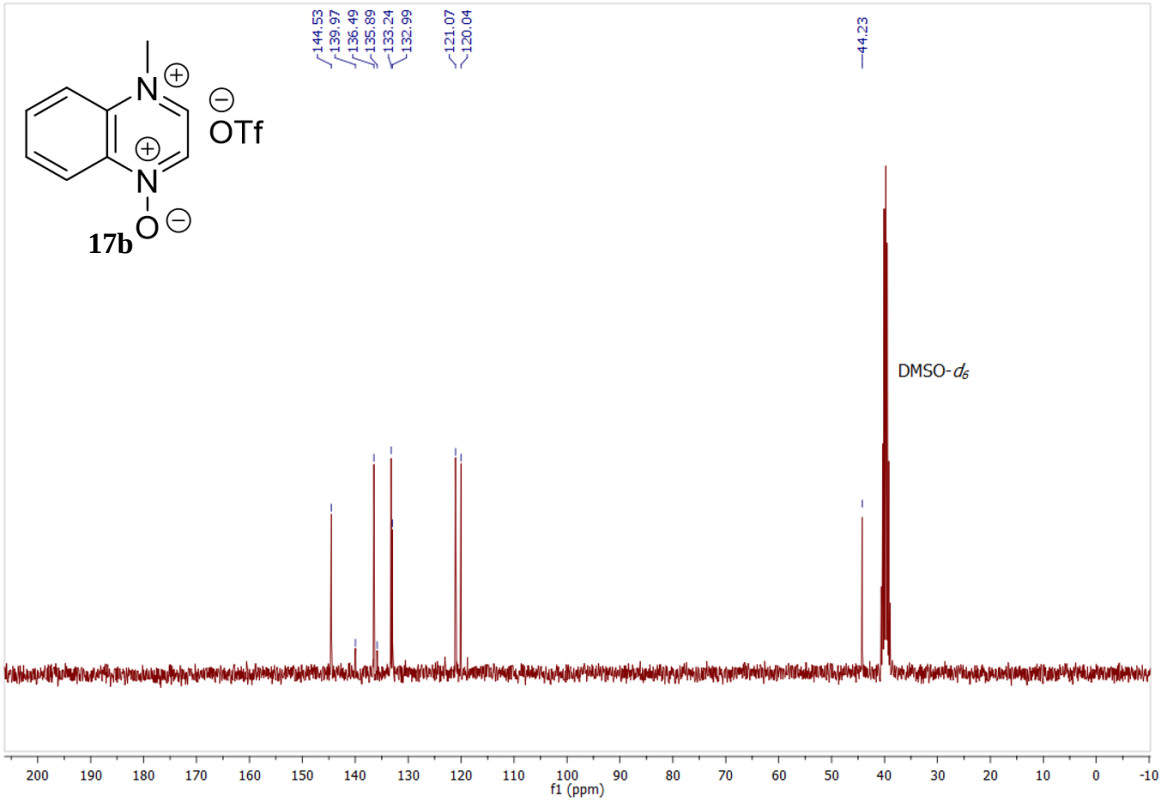


Figure S52: $^{13}C\{^{1}H\}$ NMR spectrum of **17b** in $(CD_3)_2SO$ (75 MHz).

17b and 19b in CD_3CN (From Quinoxaline *N*-oxide (2) + MeOTf in CD_3CN)

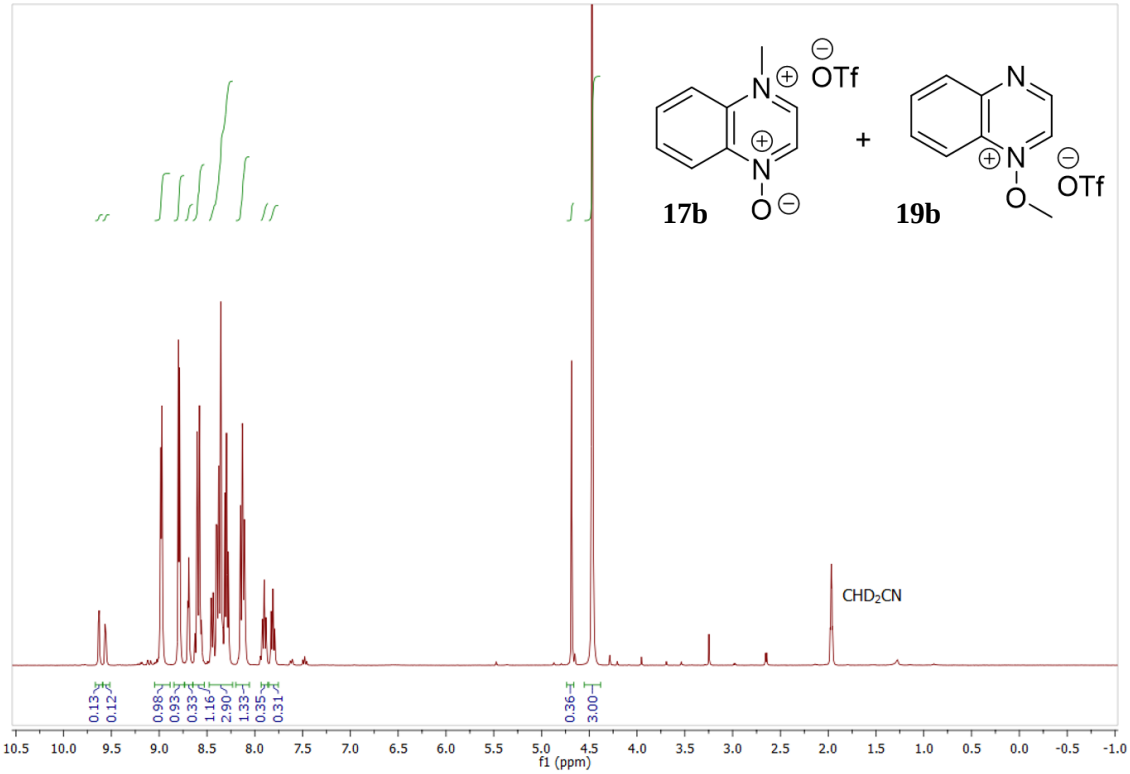


Figure S53: Full ^{1}H NMR Spectrum of **17b**, **19b** and **2** in CD_3CN (400MHz).

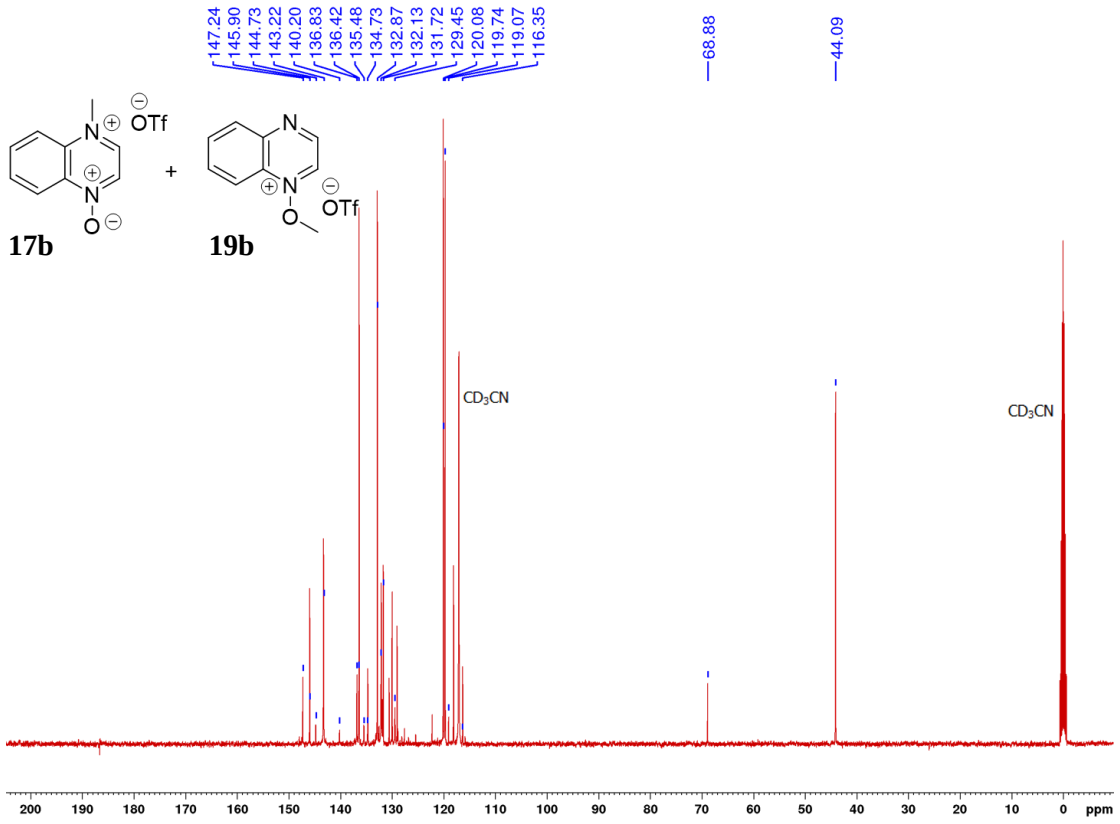


Figure S54: $^{13}C\{^{1}H\}$ NMR Spectrum of **17b**, **19b** and **2** in CD_3CN (100 MHz)

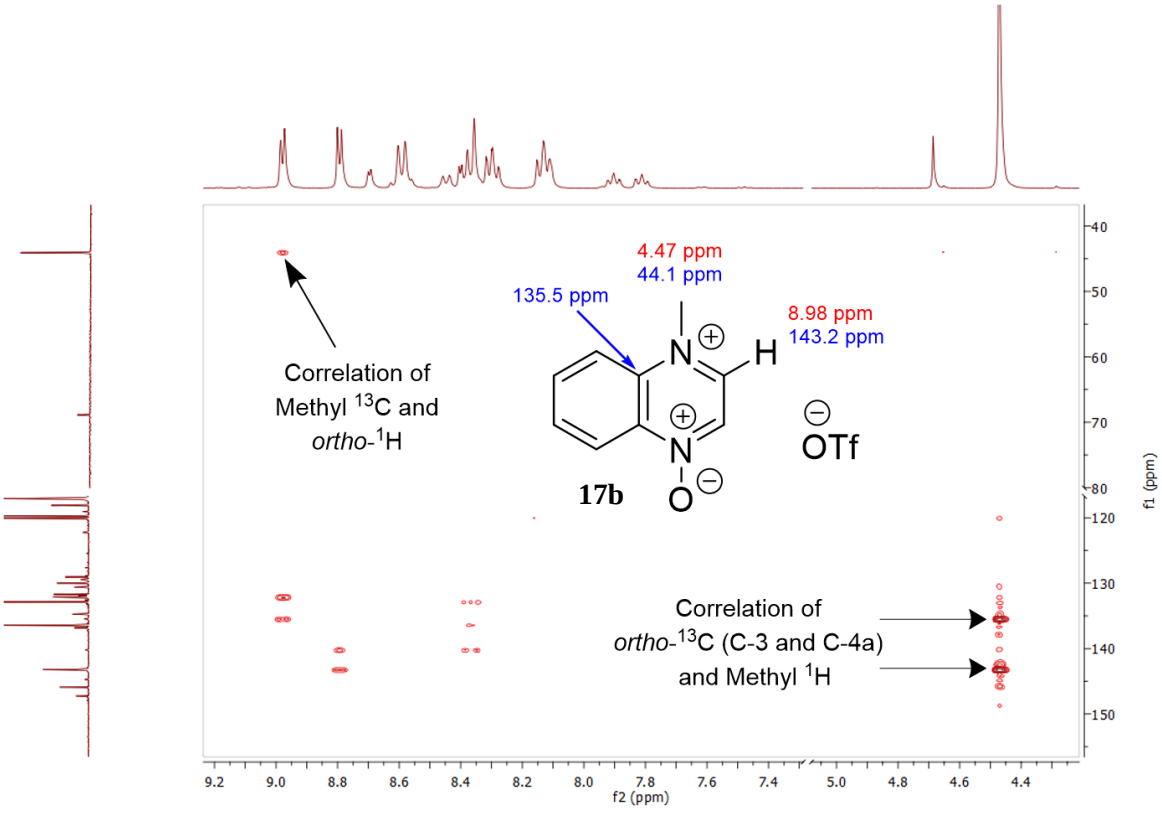


Figure S55: Section of ^{1}H-^{13}C HMBC NMR spectrum of **17b** in CD_3CN.

17b in $(CD_3)_2SO$ (From reaction of 2 + MeOTf in CD_3CN after solvent removal)

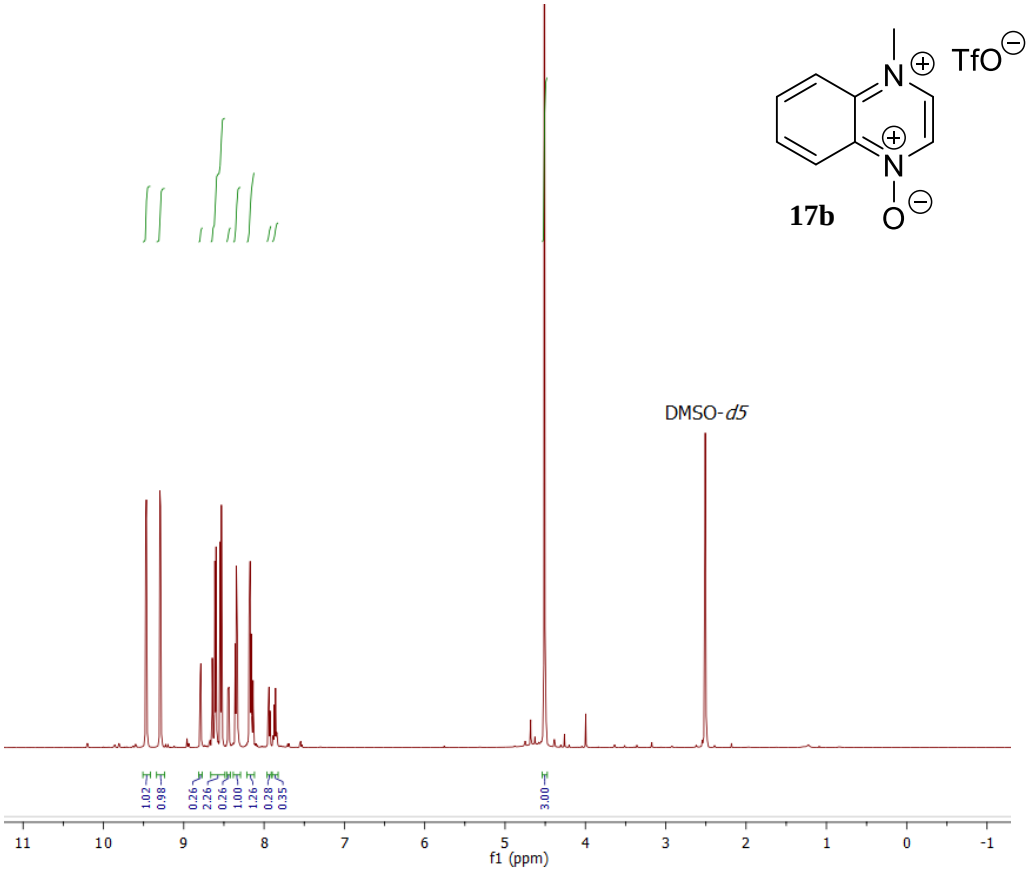


Figure S56: Full ^1H spectrum of **17b** and **2** in $(CD_3)_2SO$ (600 MHz). Removal of the CD_3CN caused the decomposition of **19b**.

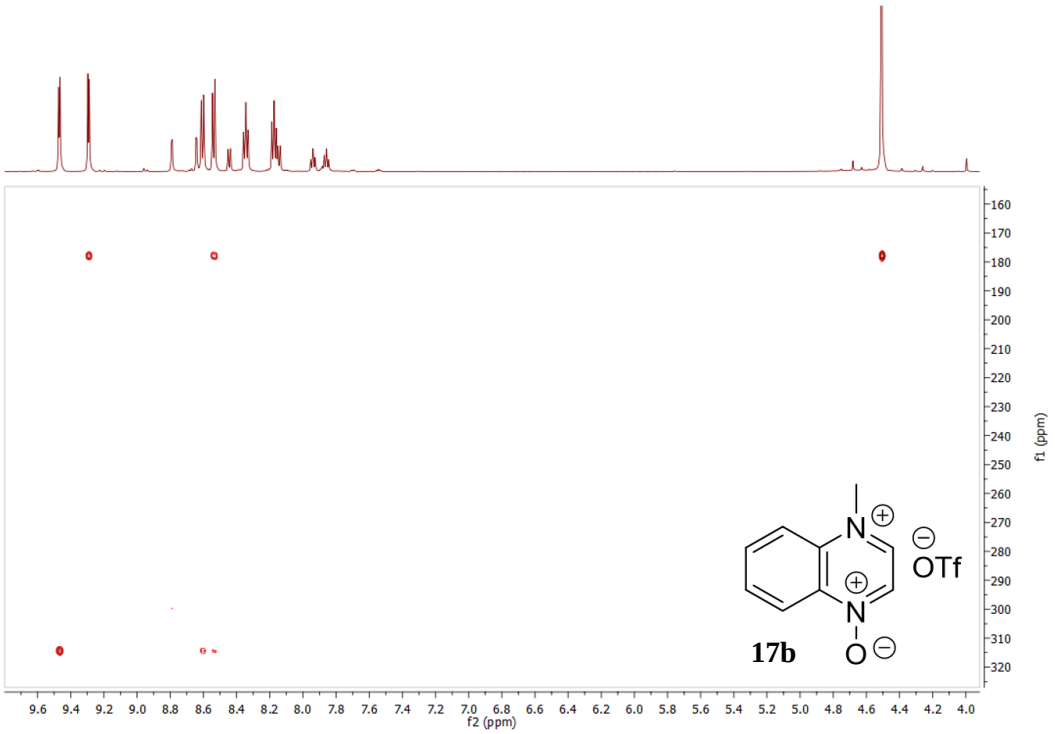


Figure S57: ^1H-^{15}N HMBC NMR spectrum of **17b** and **2** in $(CD_3)_2SO$. Removal of the CD_3CN caused the decomposition of **19b**.

17b in $(CD_3)_2SO$ (From Quinoxaline *N*-oxide (2) + MeOTf in $(CD_3)_2SO$)

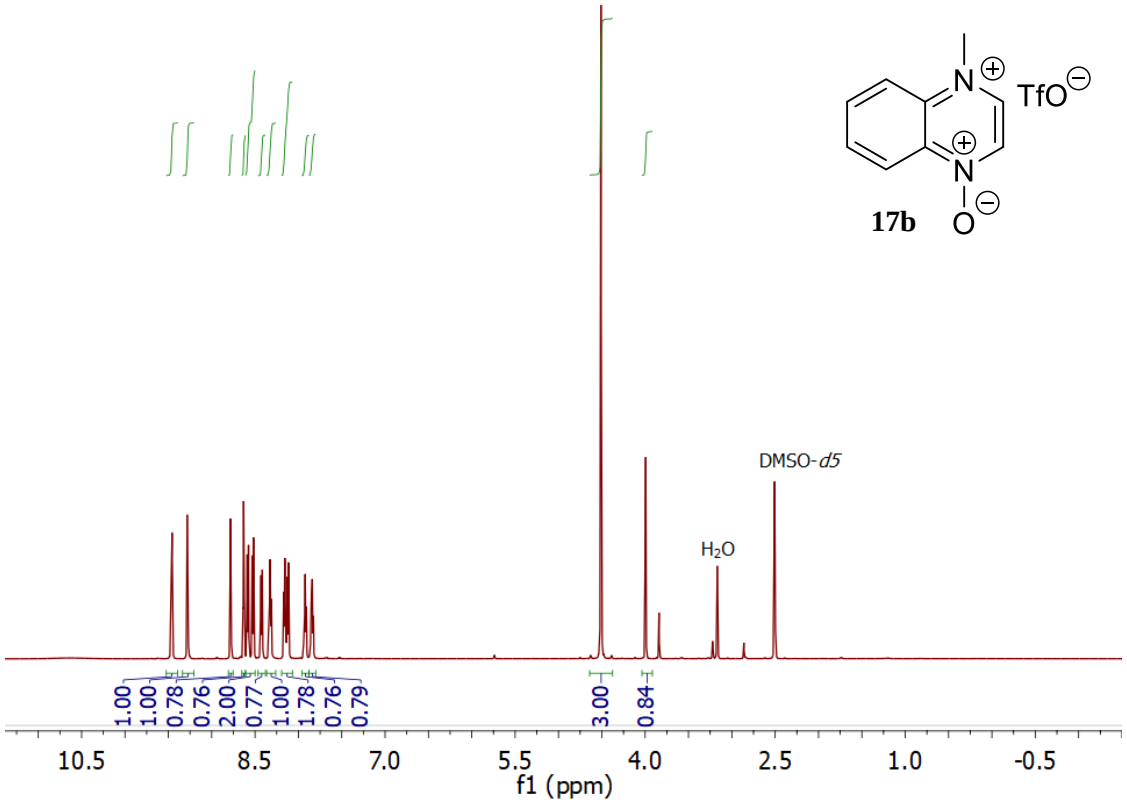


Figure S58: Full ^{1}H NMR spectrum of **17b** + starting material **2** in $(CD_3)_2SO$ (600 MHz). A signal assigned to the methoxydimethylsulfonium salt of $(CD_3)_2SO$ is present at 3.99 ppm.

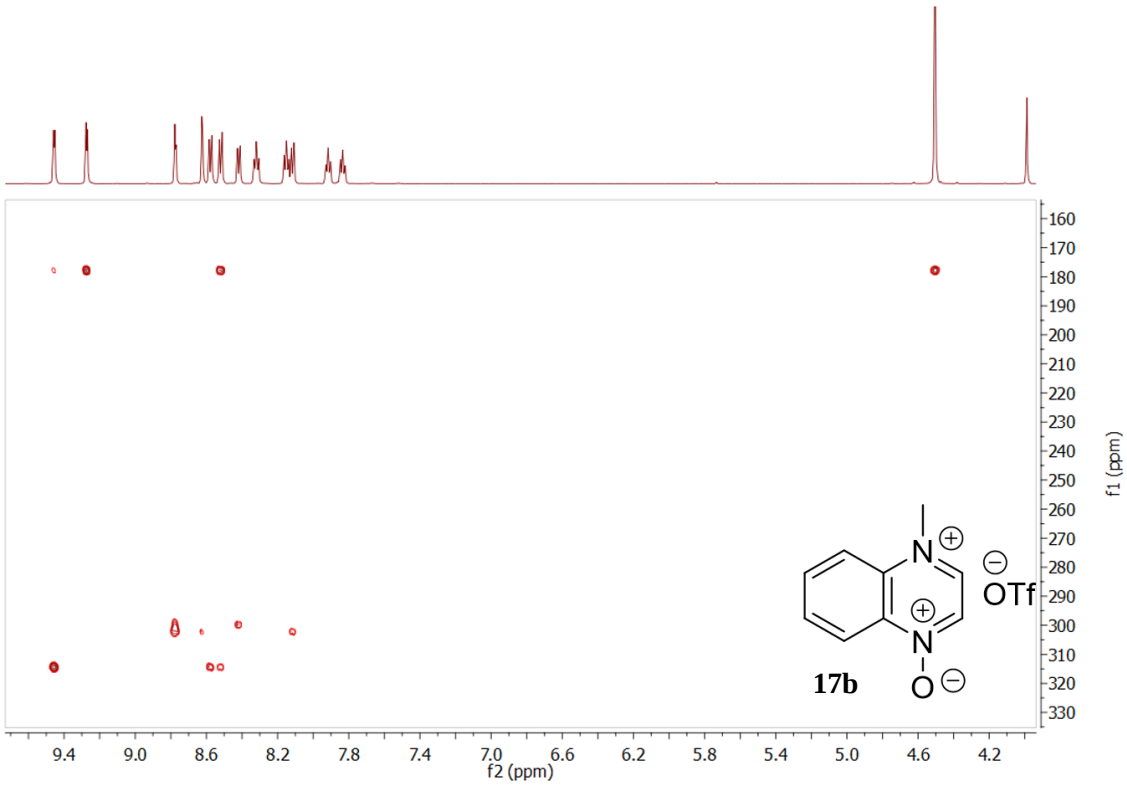


Figure S59: ^{1}H-^{15}N HMBC NMR spectrum of **17b** in $(CD_3)_2SO$, showing some **2**.

18 and 20 in CD_2Cl_2 (From reaction of 2 + 12 in CD_2Cl_2)

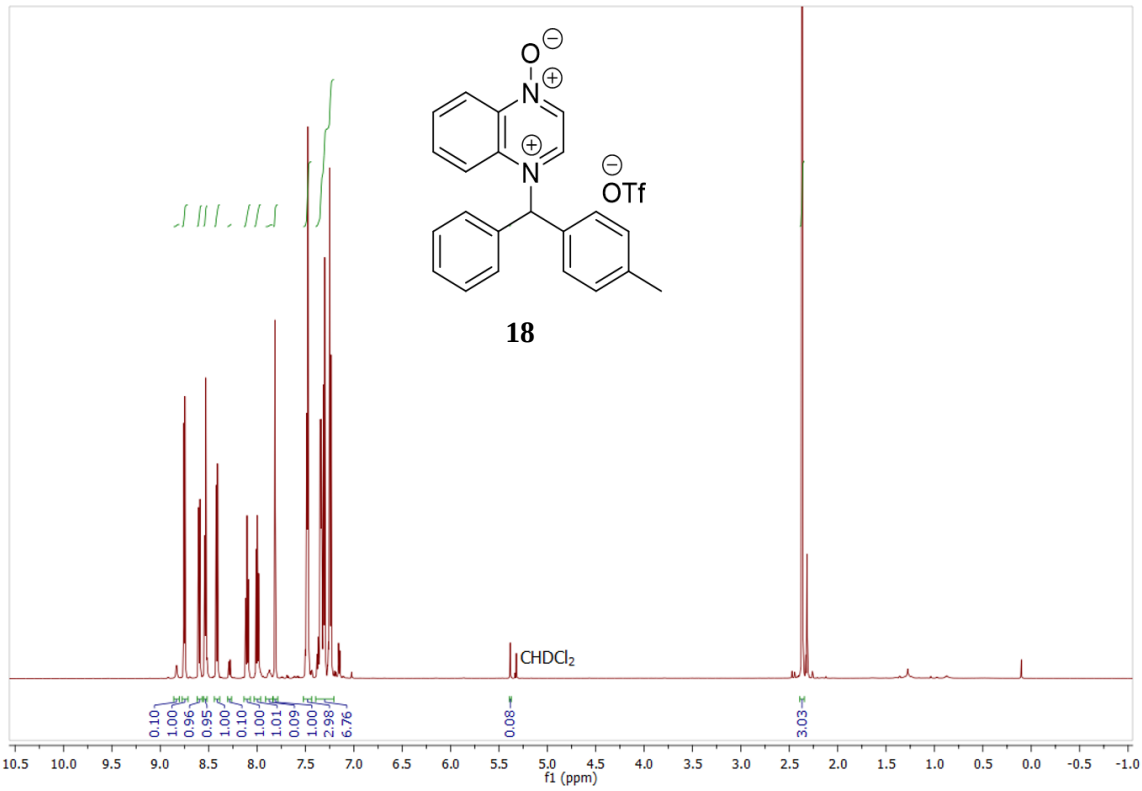


Figure S60: Full ^{1}H NMR spectrum of **18** in CD_2Cl_2 (600 MHz). Small signals assigned to **20** are also present.

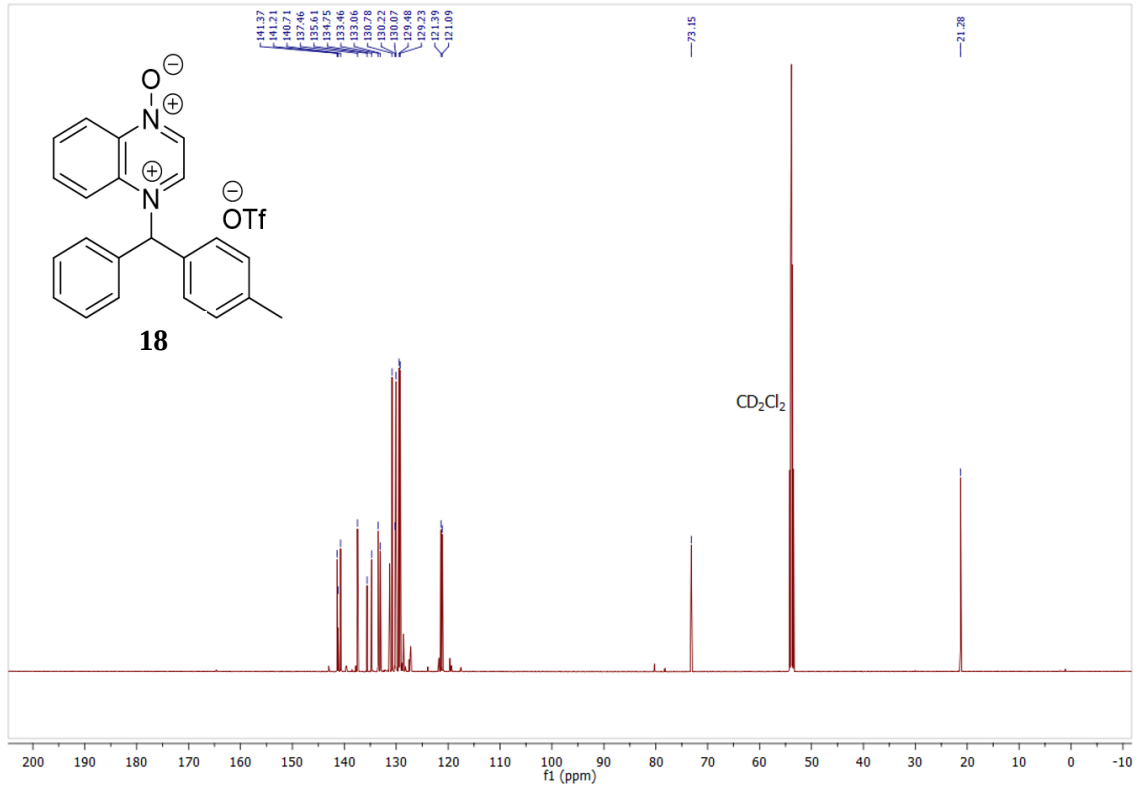


Figure S61: $^{13}C\{^{1}H\}$ NMR spectrum of **18** in CD_2Cl_2 (150 MHz). Small signals assigned to **20** are also present. A ^{13}C NMR signal assigned to the $CF_3SO_3^-$ ion is present at δ 120.7 ppm.

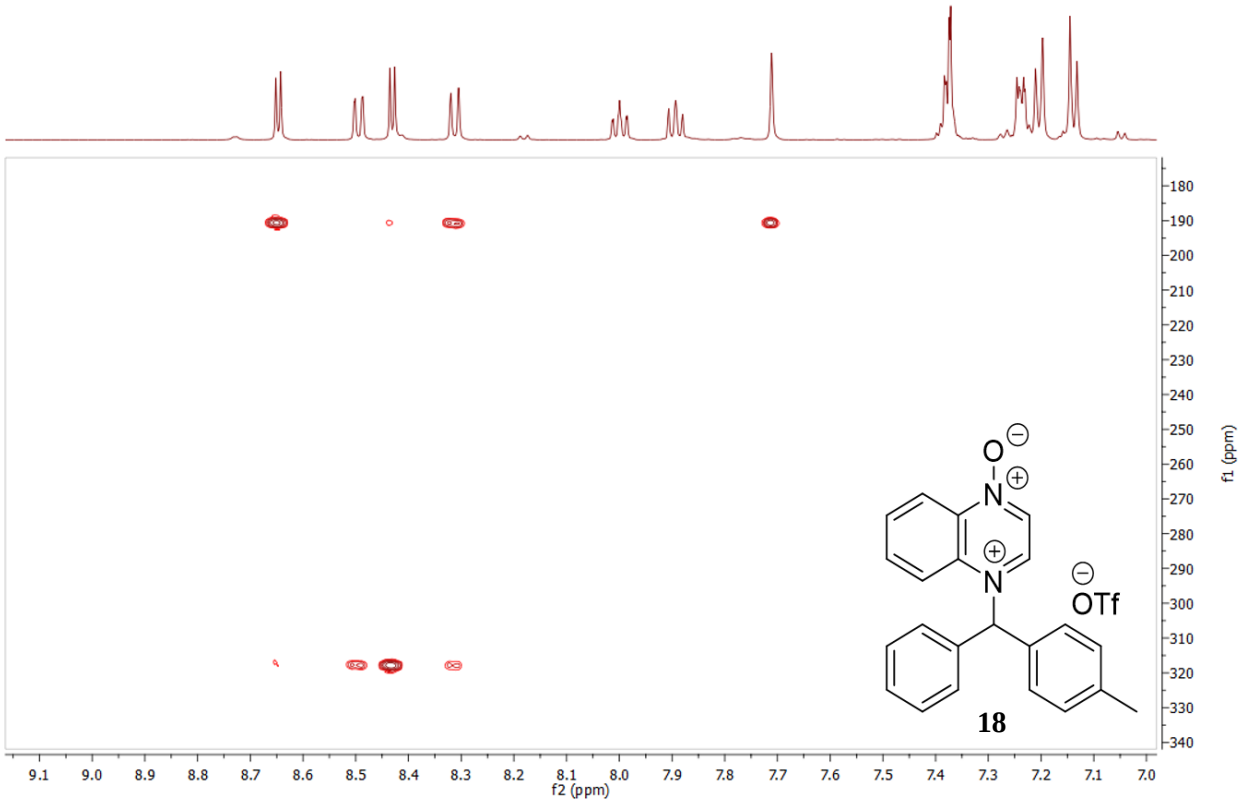


Figure S62: ^{1}H-^{15}N HMBC NMR spectrum of **18** in CD_2Cl_2.

23b in CD_3CN (From Pyrimidine *N*-oxide (3) + MeOTf in CD_3CN)

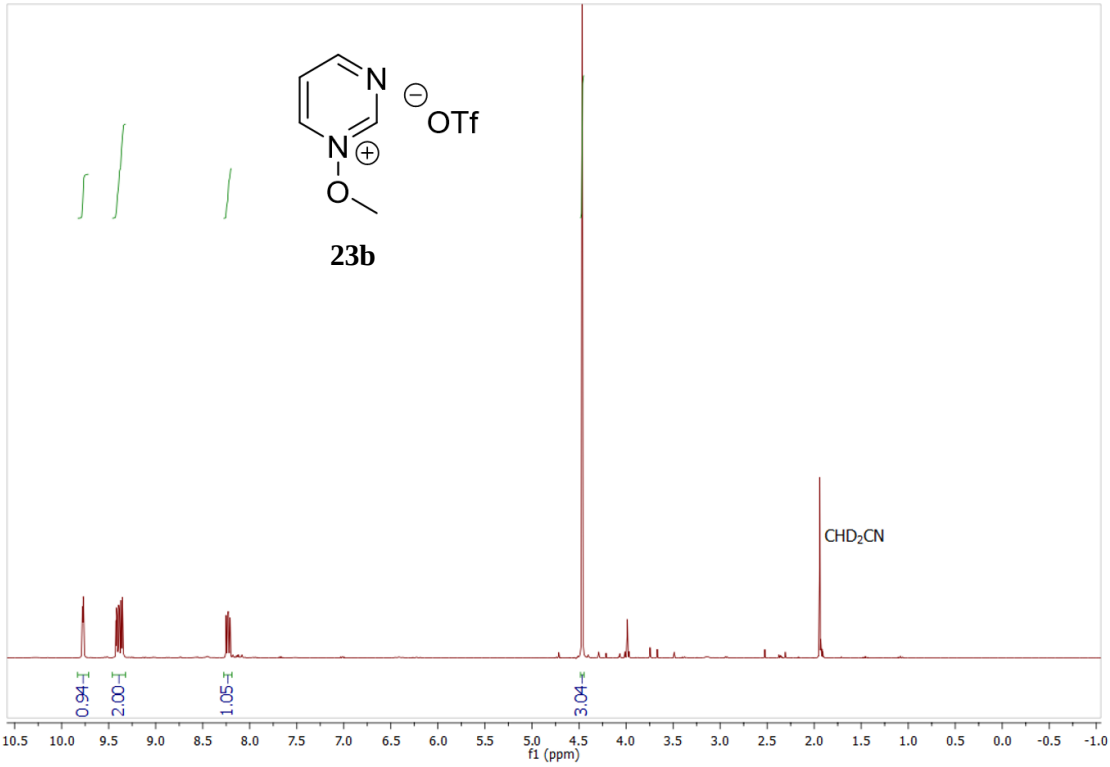


Figure S63: Full ^{1}H spectrum of **23b** in CD_3CN (300 MHz).

23b in $(CH_3)_2SO$ (From Pyrimidine *N*-oxide (3) + MeOTf in CH_3CN)

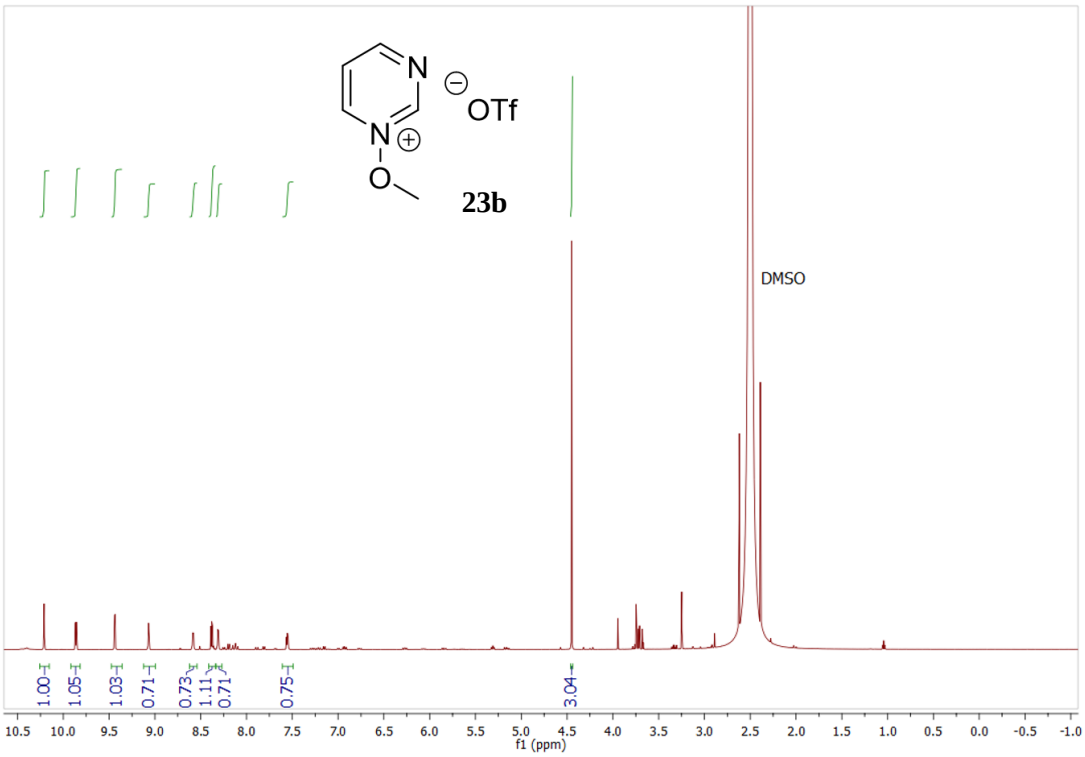


Figure S64: Full ^1H spectrum of **23b**, containing signals assigned to **3** in $(CH_3)_2SO$ (600 MHz) **acquired with solvent signal suppression**.

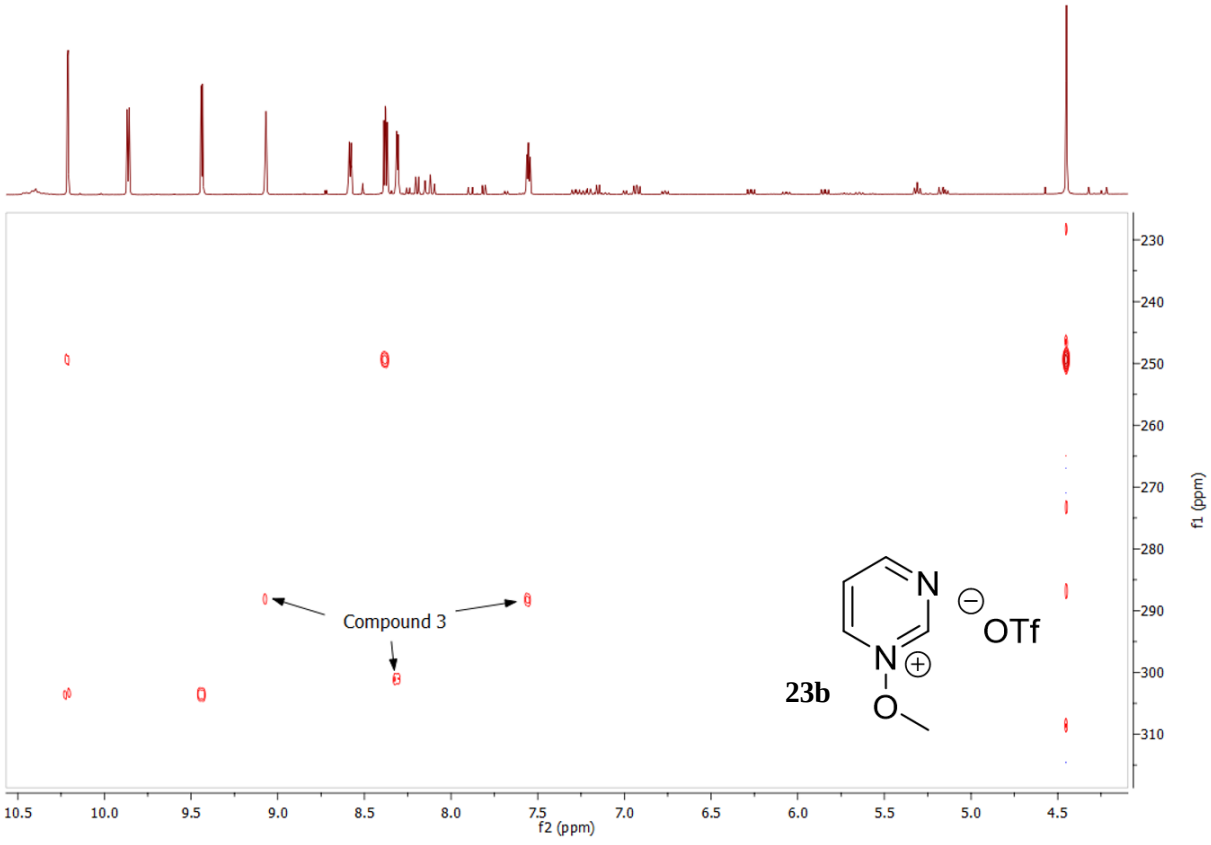


Figure S65: ^1H-^{15}N HMBC NMR spectrum of **23b**, containing signals assigned to **3** in $(CH_3)_2SO$ acquired with solvent signal suppression.

21b and 23b in CD_3CN (From Pyrimidine *N*-oxide (3) + MeOTf in CD_3CN)

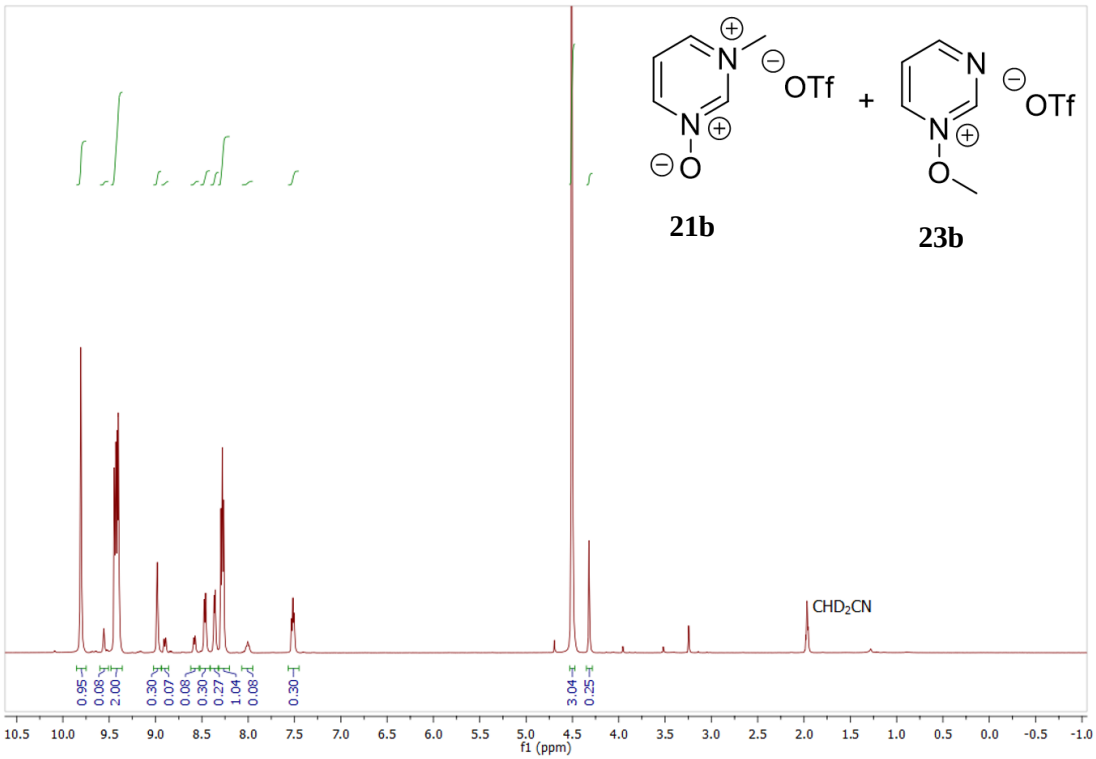


Figure S66: Full ^1H NMR spectrum containing signals assigned to **23b**, **21b** and **3** in CD_3CN (400 MHz).

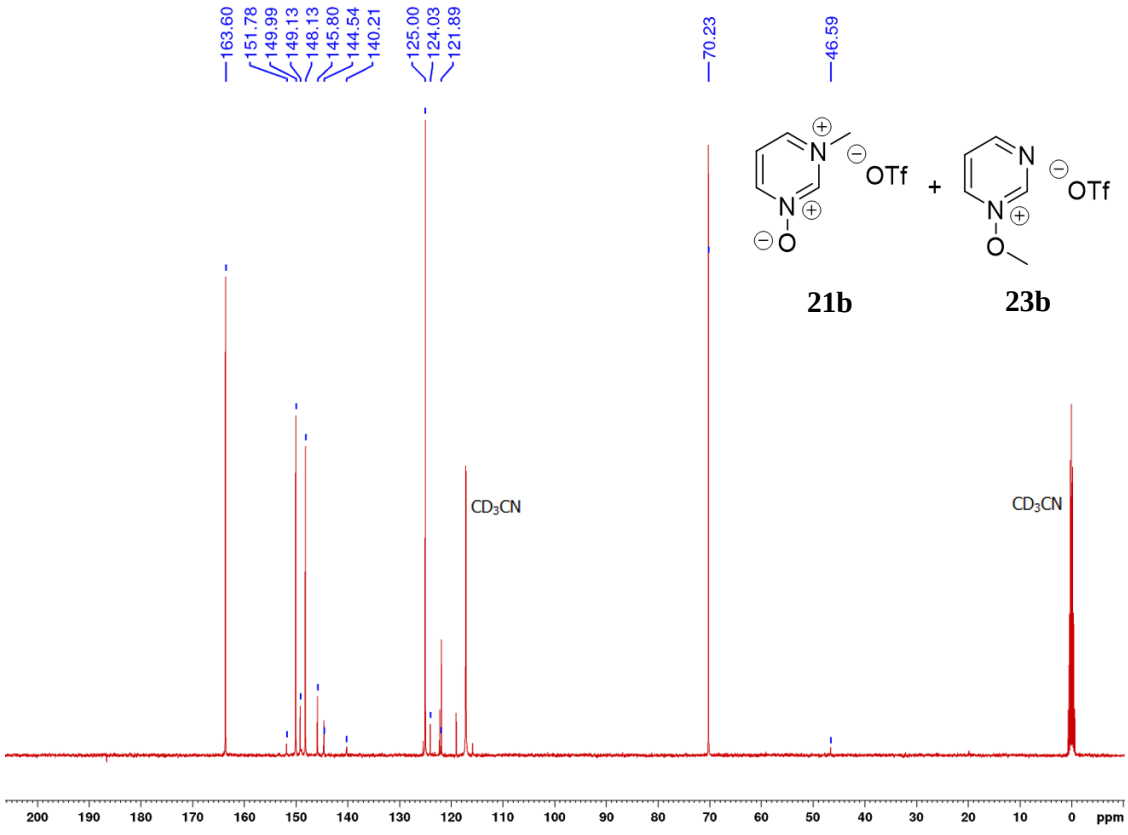


Figure S67: $^{13}C\{^1H\}$ NMR Spectrum of **23b**, **21b** and **3** in CD_3CN (100 MHz).

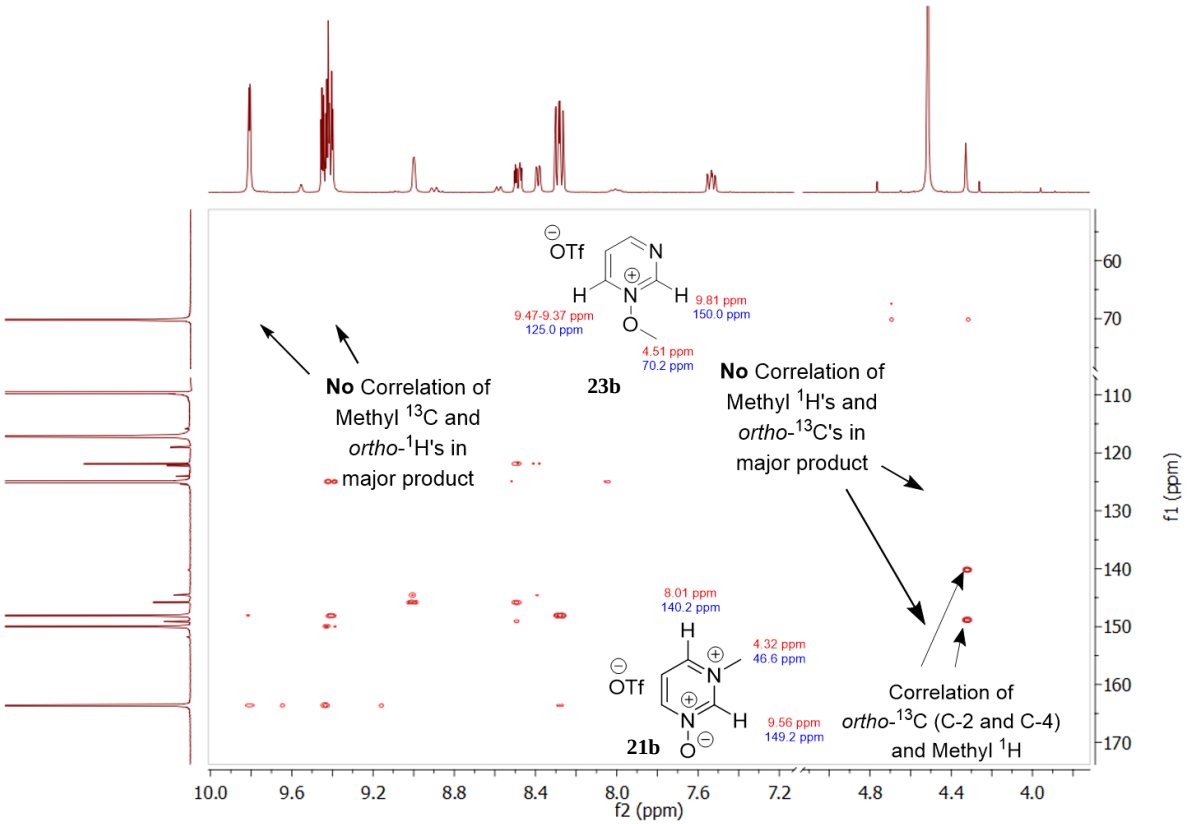


Figure S68: Section of ^{1}H-^{13}C HMBC NMR spectrum of **21b** and **23b** in CD_3CN.

23b in $(CD_3)_2SO$ (From 3 + MeOTf in CD_3CN, after solvent removal)

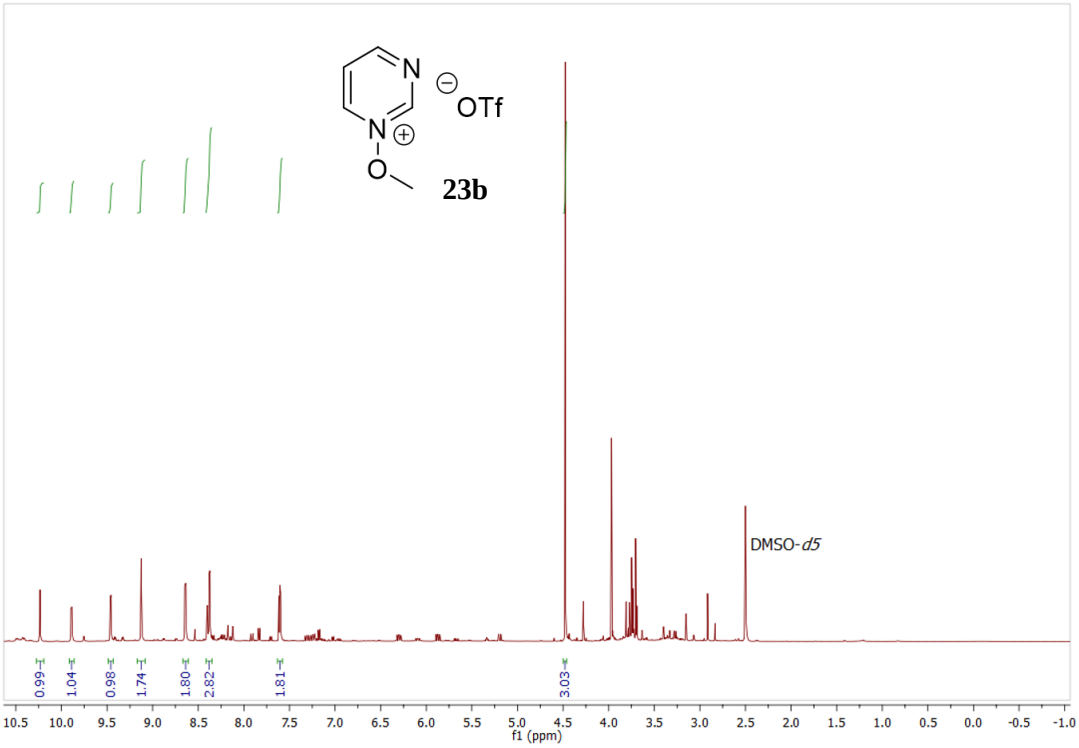


Figure S69: Full ^{1}H spectrum of **23b** and **3** in $(CD_3)_2SO$ (600 MHz). Removal of the CD_3CN caused the decomposition of **21b**. A large amount of decomposition product signals are present on the baseline.

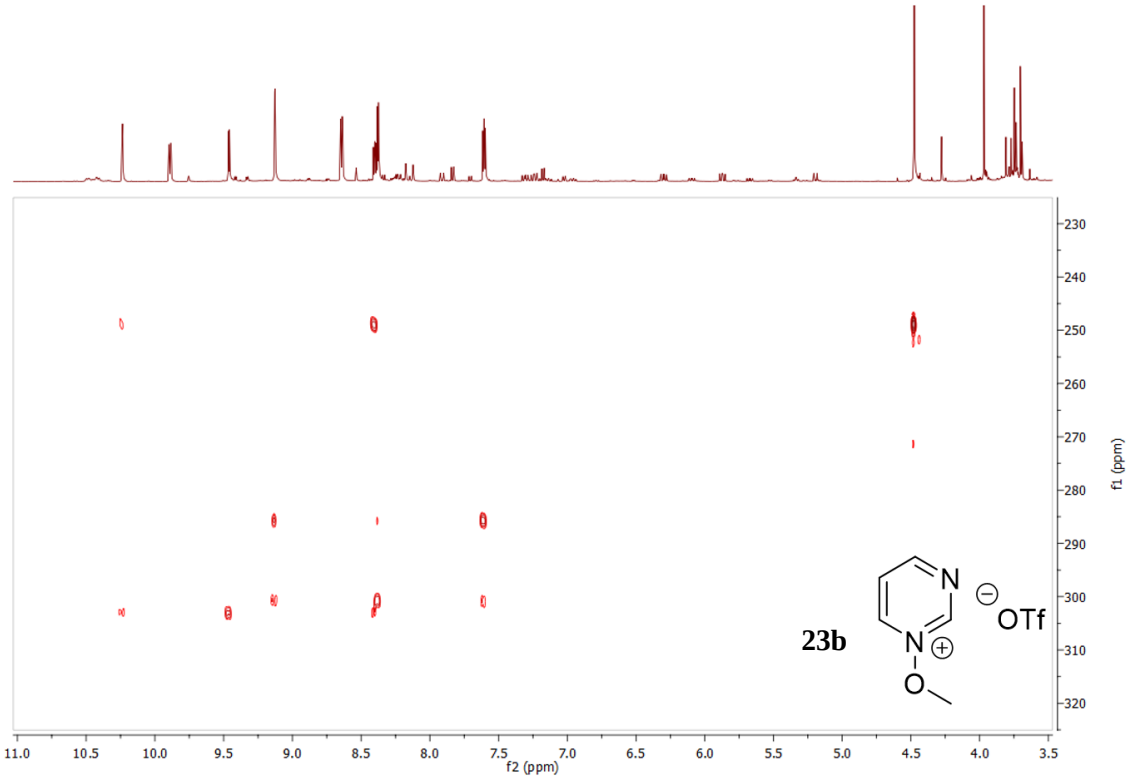


Figure S70: ^{1}H-^{15}N HMBC NMR spectrum of **23b**, containing signals assigned to **3** in $(CD_3)_2SO$.

21b and 23b in $(CD_3)_2SO$ (From Pyrimidine *N*-oxide (3) + MeOTf in $(CD_3)_2SO$)

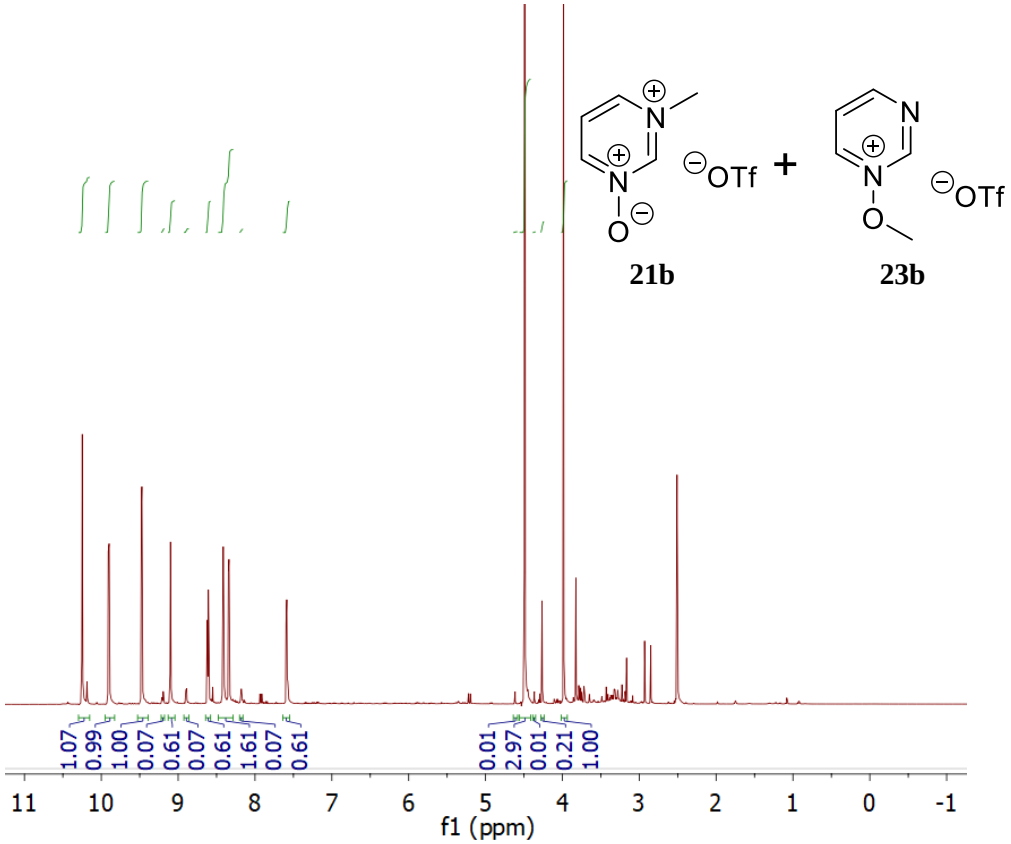


Figure S71: Full ^{1}H spectrum of containing signals assigned to **23b**, **21b** and **3** in $(CD_3)_2SO$ (600 MHz).

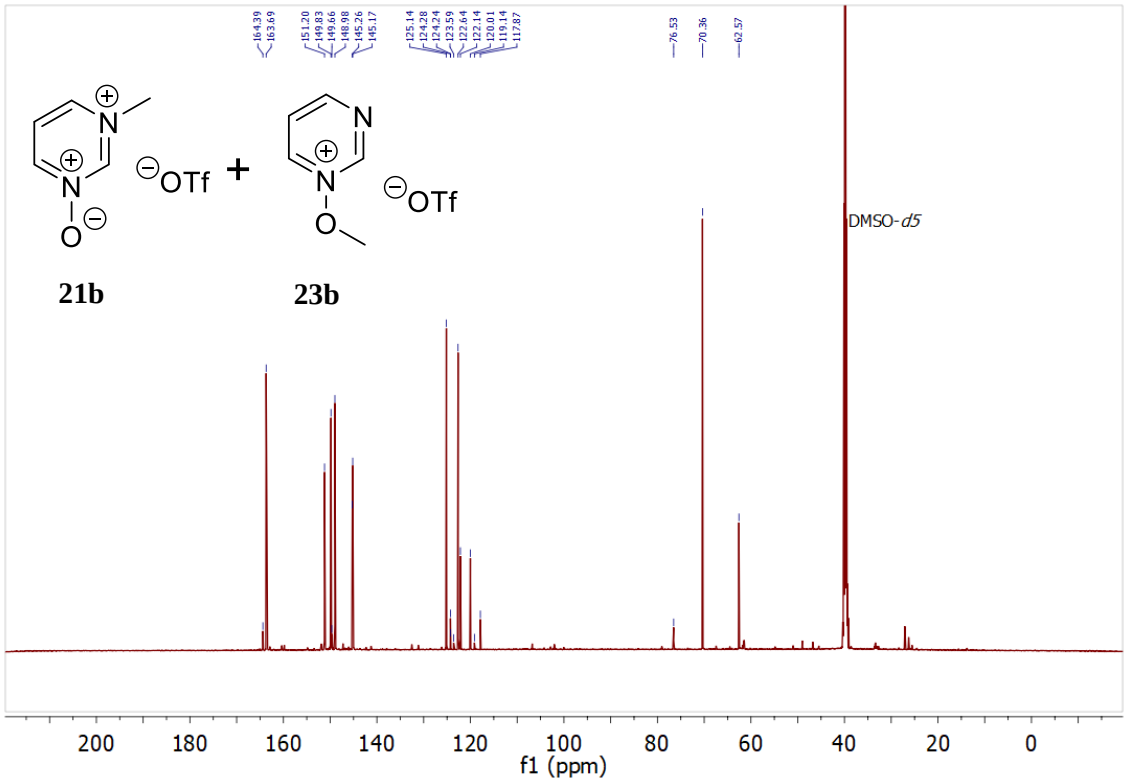


Figure S72: Full $^{13}C\{^{1}H\}$ NMR spectrum containing signals assigned to **23b** and **3** in $(CD_3)_2SO$ (600 MHz). No signals could be unambiguously assigned to the very small amount of **23b** shown to be present by the ^{1}H and ^{1}H-^{15}N HMBC NMR spectra.

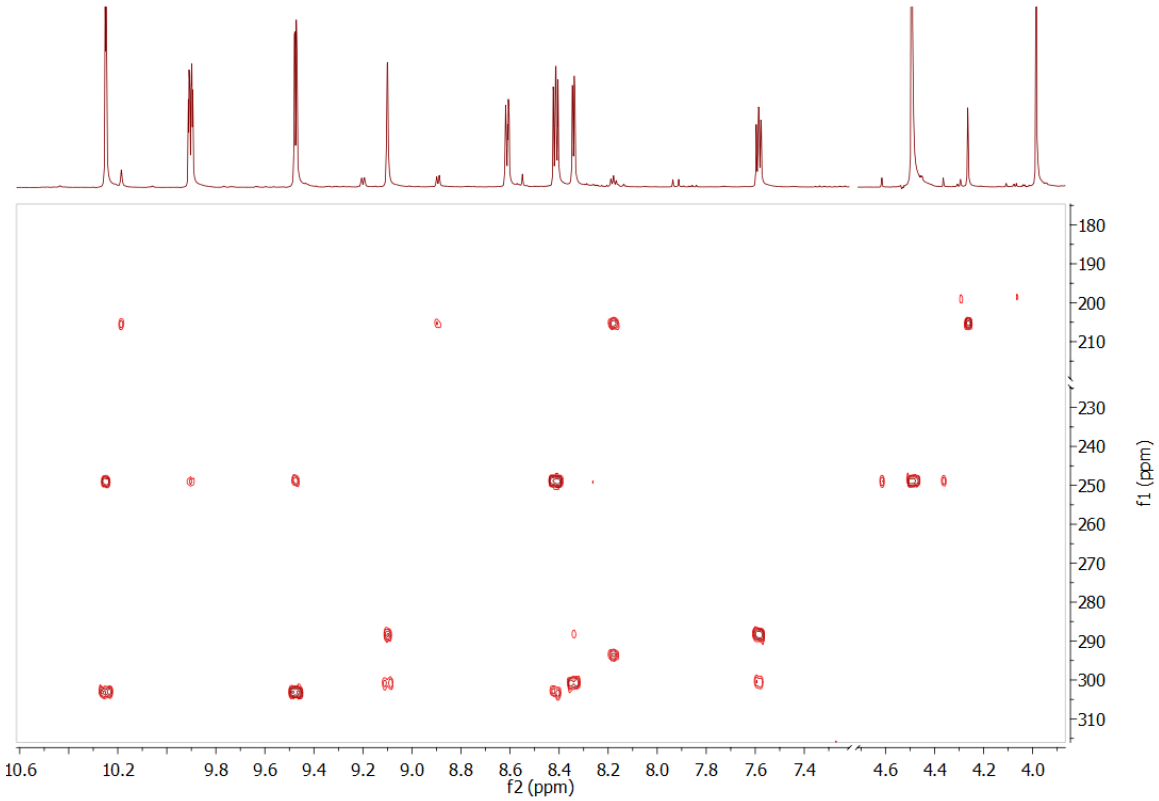


Figure S73: ^{1}H-^{15}N HMBC NMR spectrum containing signals assigned to **23b**, **21b** and **3** in $(CD_3)_2SO$. The two ^{15}N NMR corelations assigned to **21b** indicate ^{15}N resonances at 293.6 and 205.2 ppm.

Attempted Synthesis of 22 and/or 24 in CH_2Cl_2 (From 3 + 26 in CH_2Cl_2)

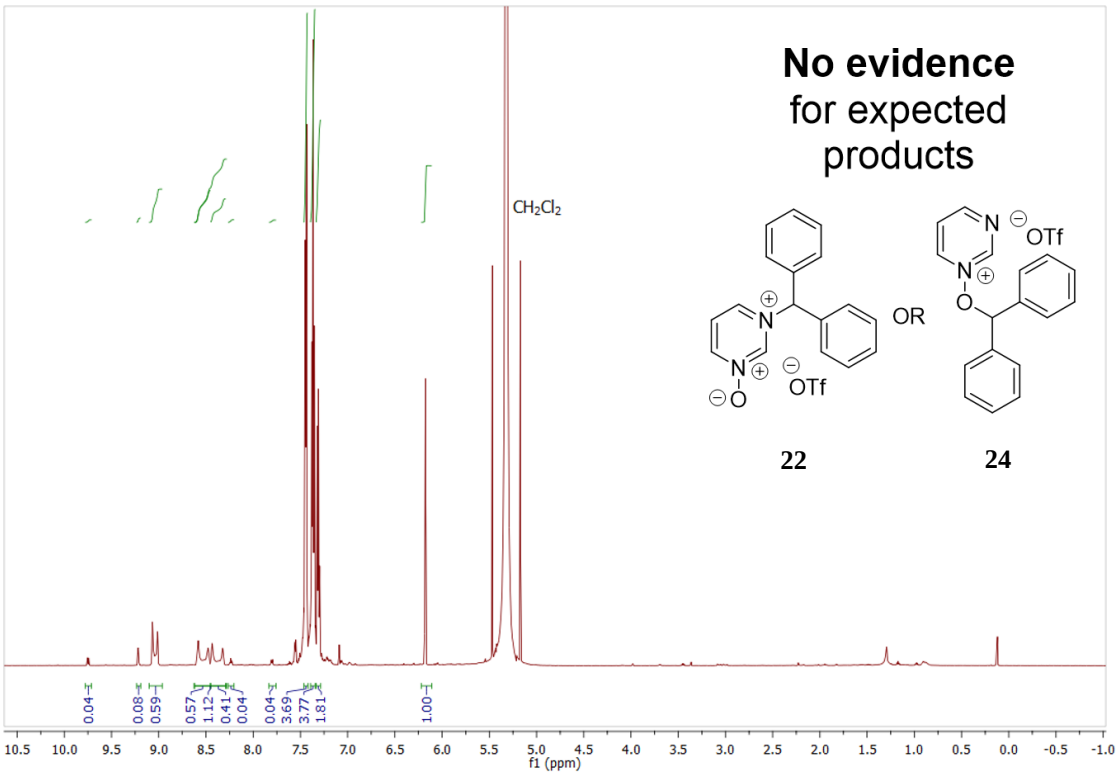


Figure S74: Full ^{1}H NMR spectrum of the crude reaction mixture from the reaction of **3** with **11** in CH_2Cl_2. Signals could not be definitively assigned to product **22** or **24**

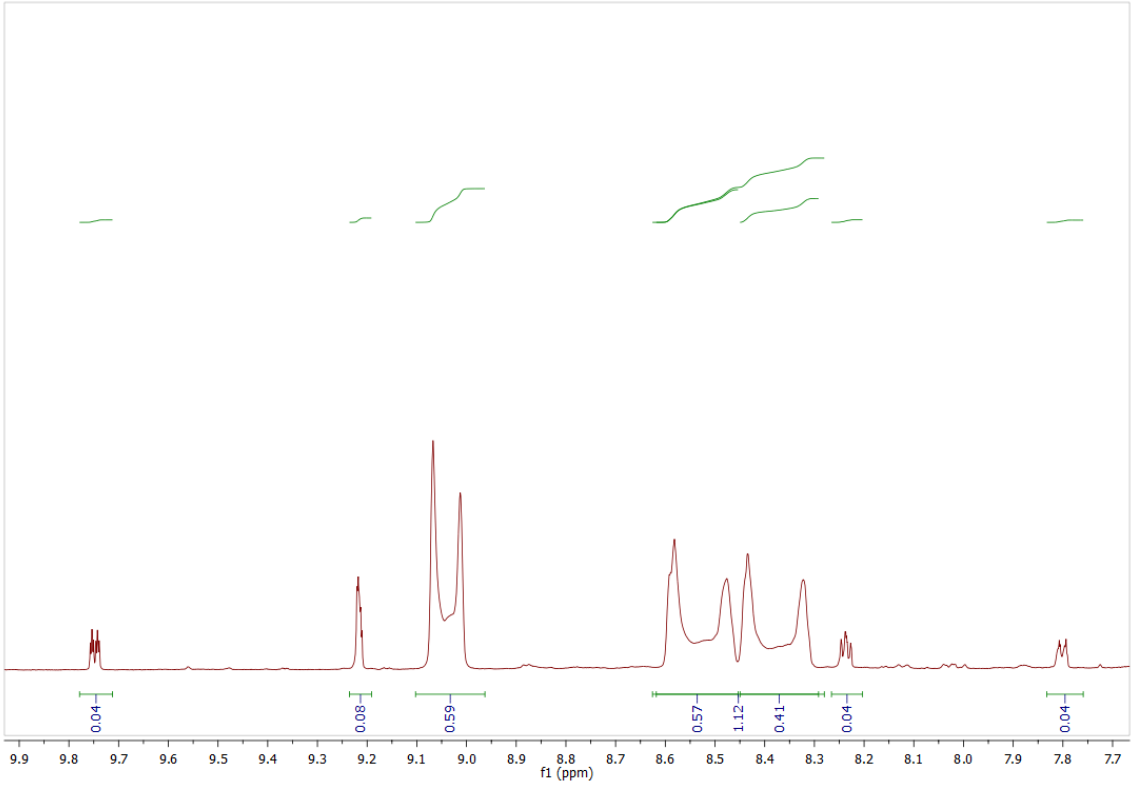
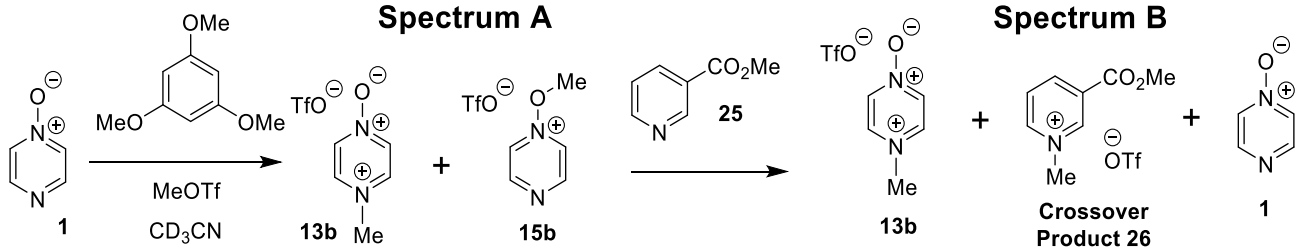


Figure S75: Expanded ^{1}H NMR spectrum of the crude reaction mixture from the reaction of **3** with **11** in CH_2Cl_2 (600 MHz). These unusually broad signals could not be definitively assigned to product **36** or **38**

Crossover experiment: 1 + MeOTf + 25 (reversibility of formation of 13b and 15b)



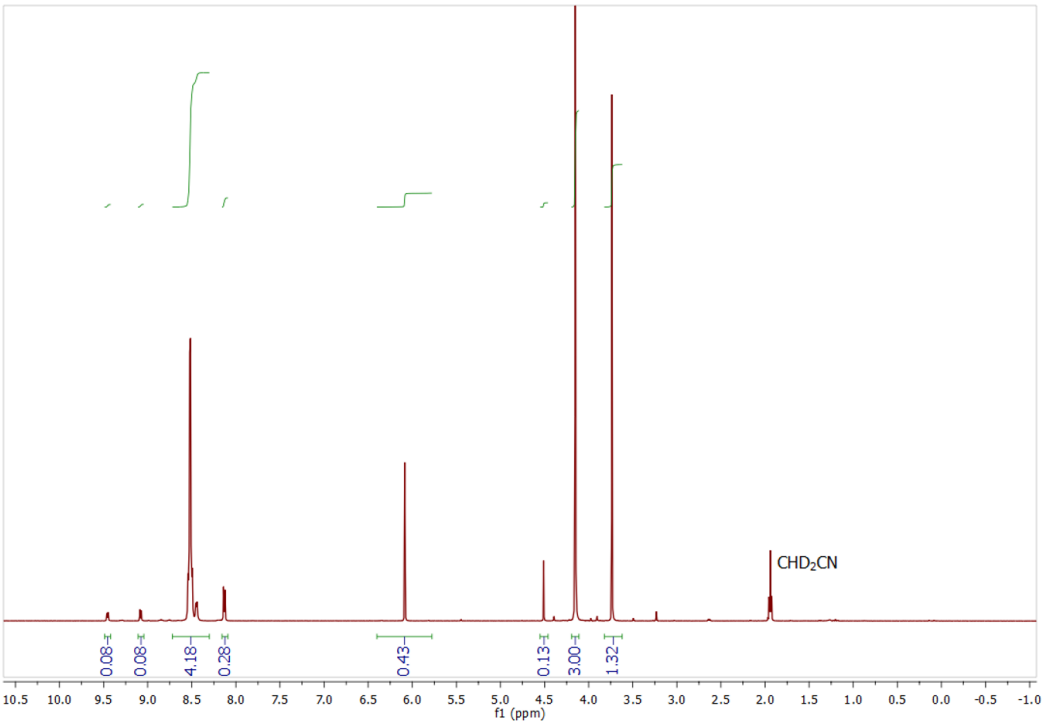


Figure S76: **Spectrum A**: Full ^{1}H NMR spectrum in CD_3CN (300 MHz) containing signals of **13b**, **15b**, **1** and 1,3,5-trimethoxybenzene.

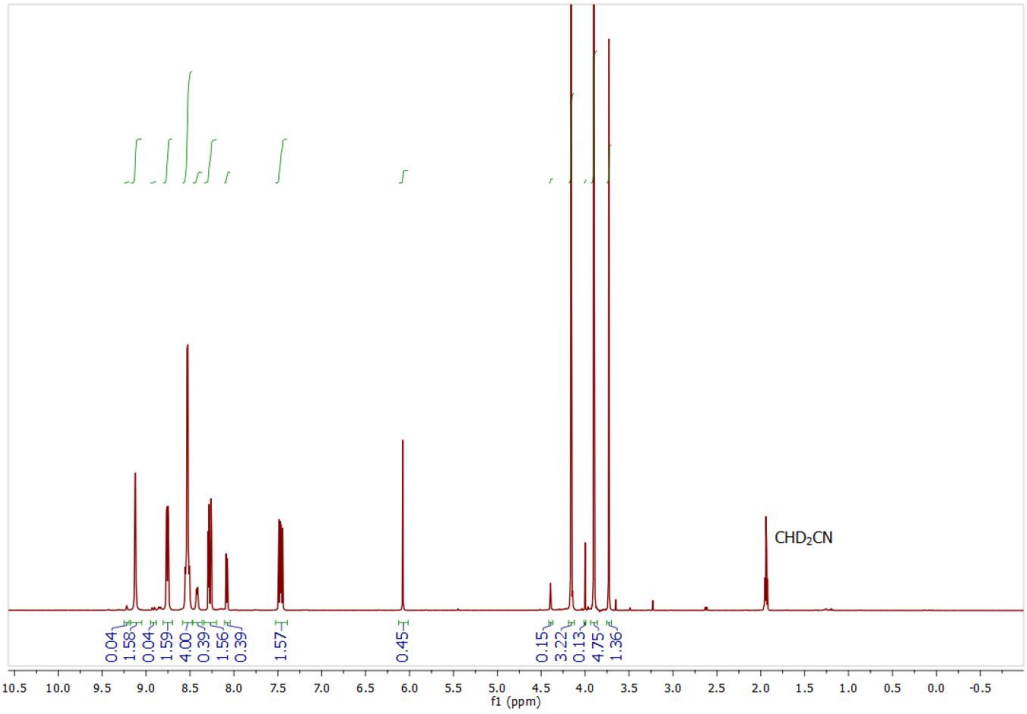
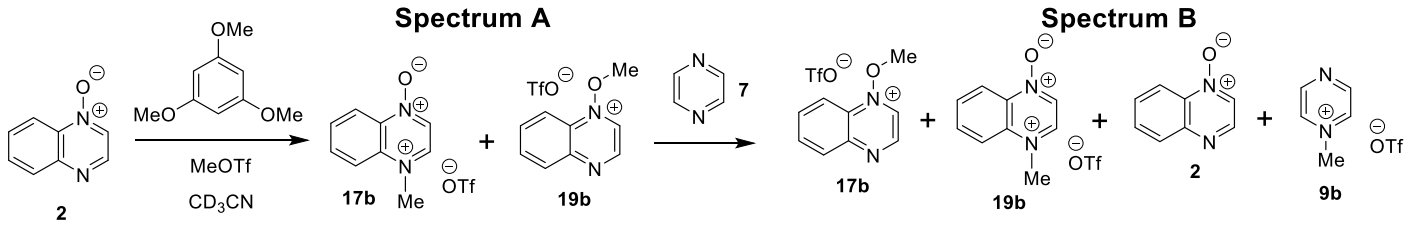


Figure S77: **Spectrum B**: Full ^{1}H NMR spectrum in CD_3CN (300 MHz) containing signals of **13b**, **25**, **26** (crossover product), **1** and 1,3,5-trimethoxybenzene.

Crossover experiment: 2 + MeOTf + 7 (reversibility of formation of 17b and 19b)



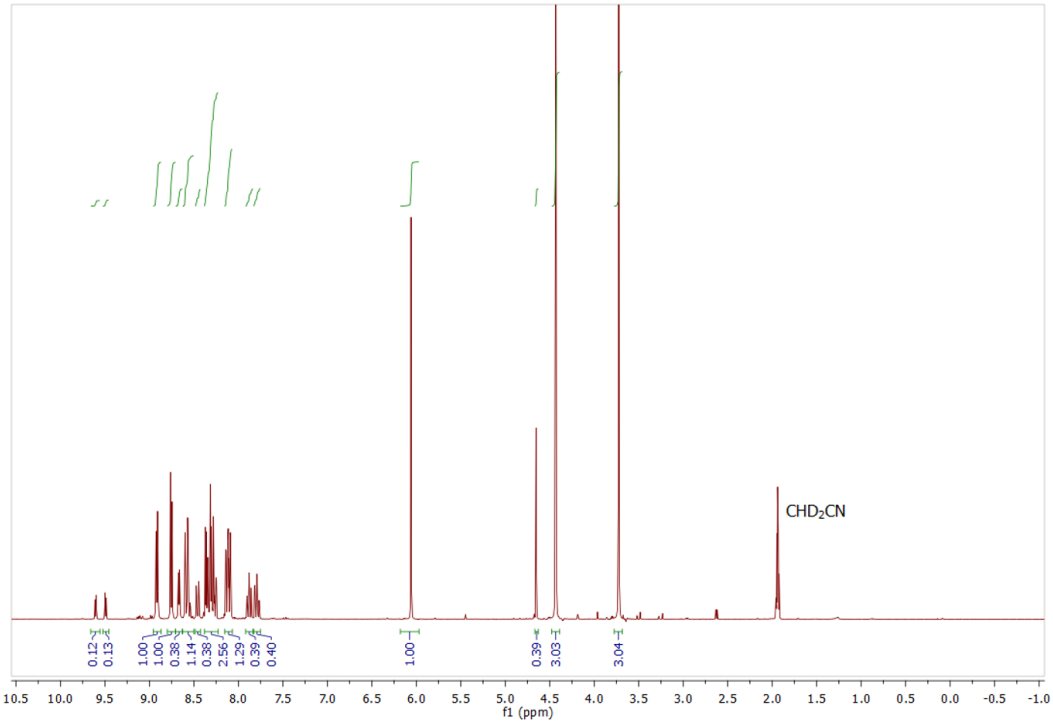


Figure S78: **Spectrum A**: Full ^{1}H NMR spectrum in CD_3CN (300 MHz) containing signals of **17b**, **19b**, **2** and 1,3,5-trimethoxybenzene.

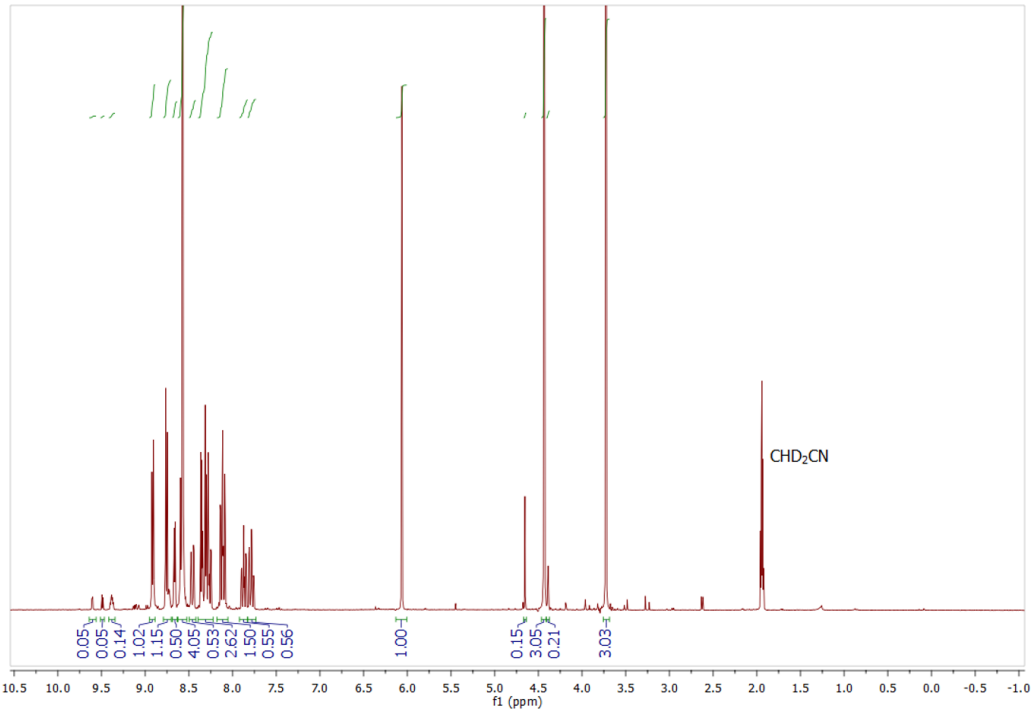
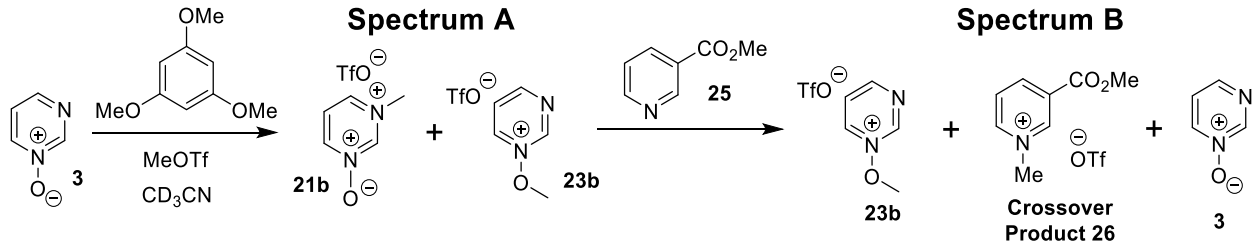


Figure S79: **Spectrum B**: Full ^{1}H NMR spectrum in CD_3CN (300 MHz) containing signals of **17b**, **7**, **9b** (crossover product**)**, **2** and 1,3,5-trimethoxybenzene.

Crossover experiment: 3 + MeOTf + 25 (reversibility of formation of 21b and 23b)



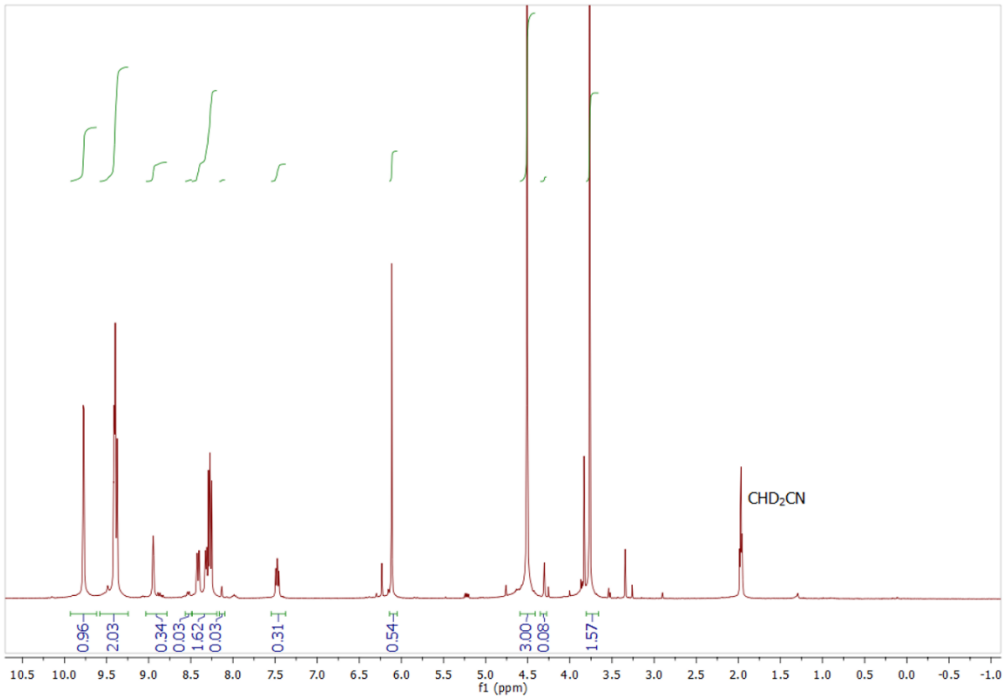


Figure S80: **Spectrum A –** Full ^{1}H NMR spectrum in CD_3CN (300 MHz) containing signals of **23b**, **21b**, **3** and 1,3,5-trimethoxybenzene.

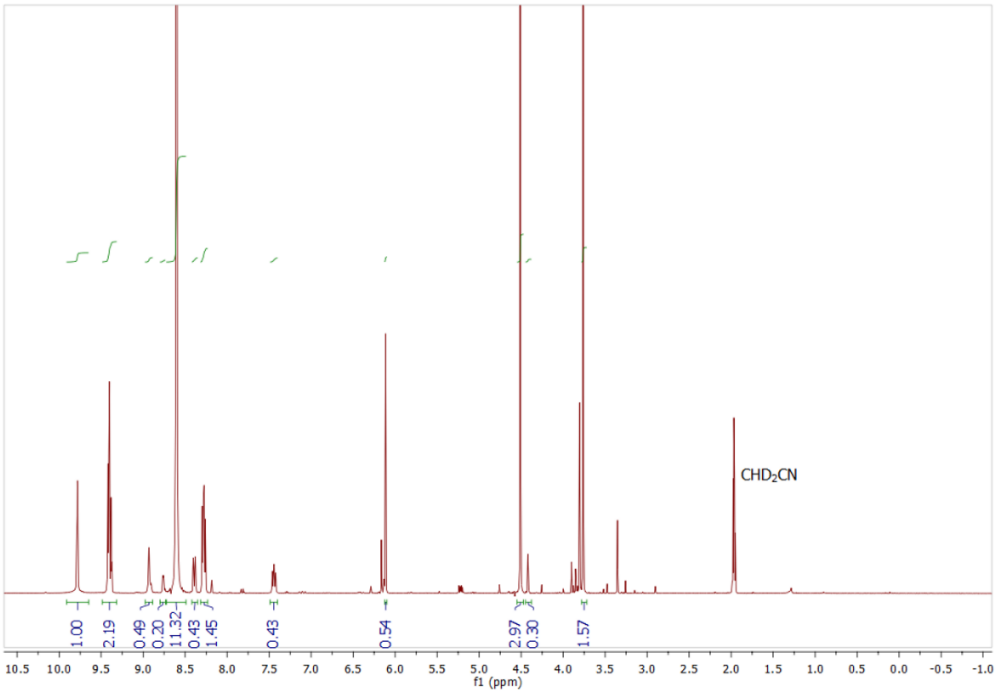


Figure S81: Spectrum B – Full ^{1}H NMR spectrum in CD_3CN (300 MHz) containing signals of **23b**, **3**, **9b** (crossover product) and 1,3,5-trimethoxybenzene

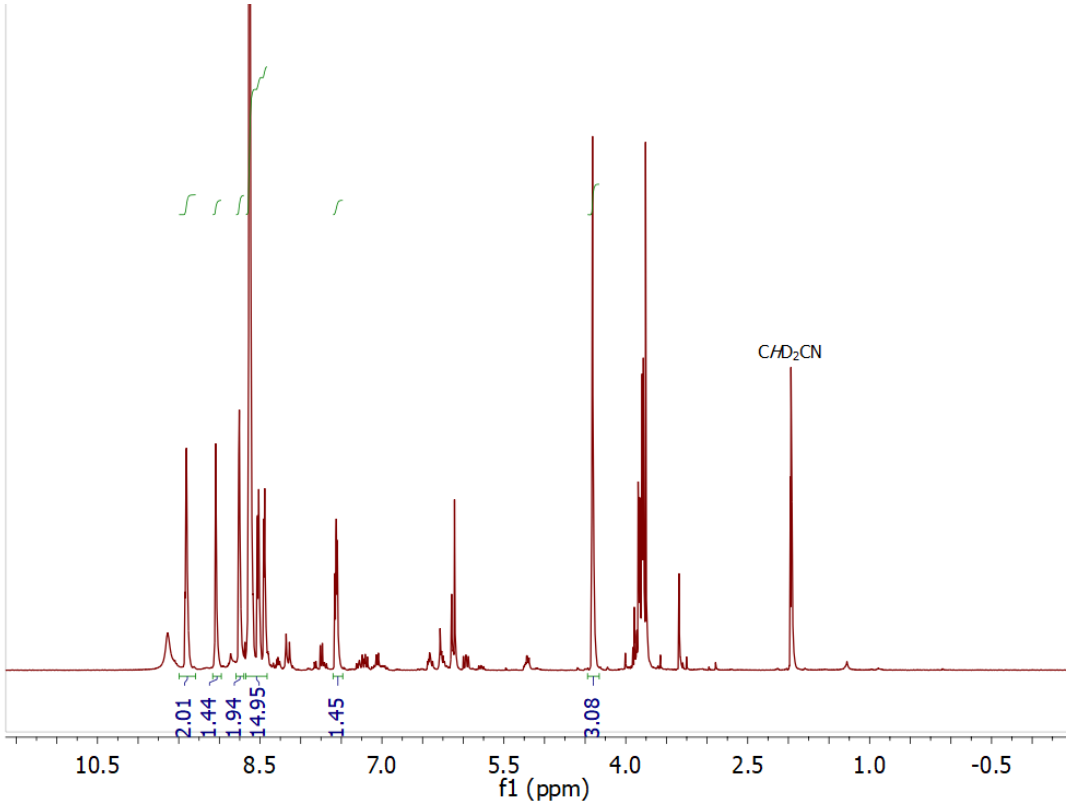
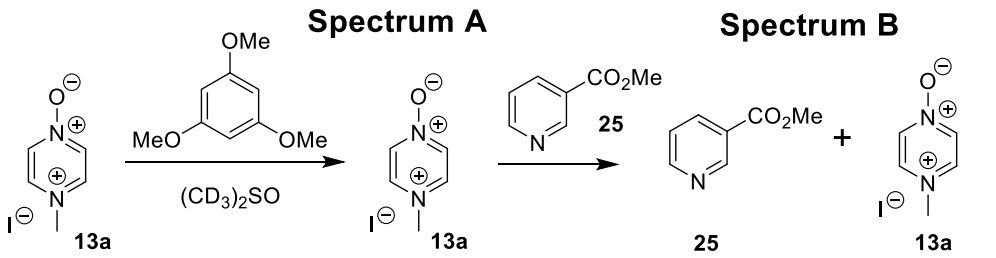


Figure S82: Spectrum C: Full ^{1}H NMR spectrum in CD_3CN (400 MHz) containing signals of **7**, **9b** (crossover product), **3** and 1,3,5-trimethoxybenzene.

Crossover experiment: 13a (From 1 + MeI) + 25 (reversibility of formation of 13a)



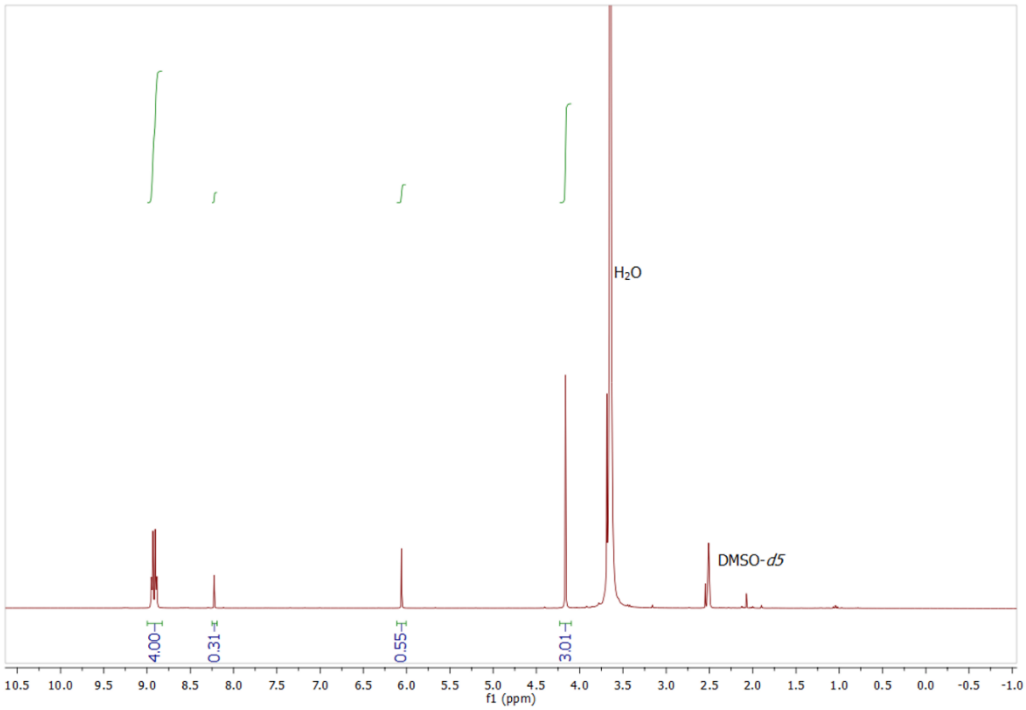


Figure S83: **Spectrum A**: Full ^{1}H NMR spectrum in $(CD_3)_2SO$ (300 MHz) containing signals of **13a** and 1,3,5-trimethoxybenzene.

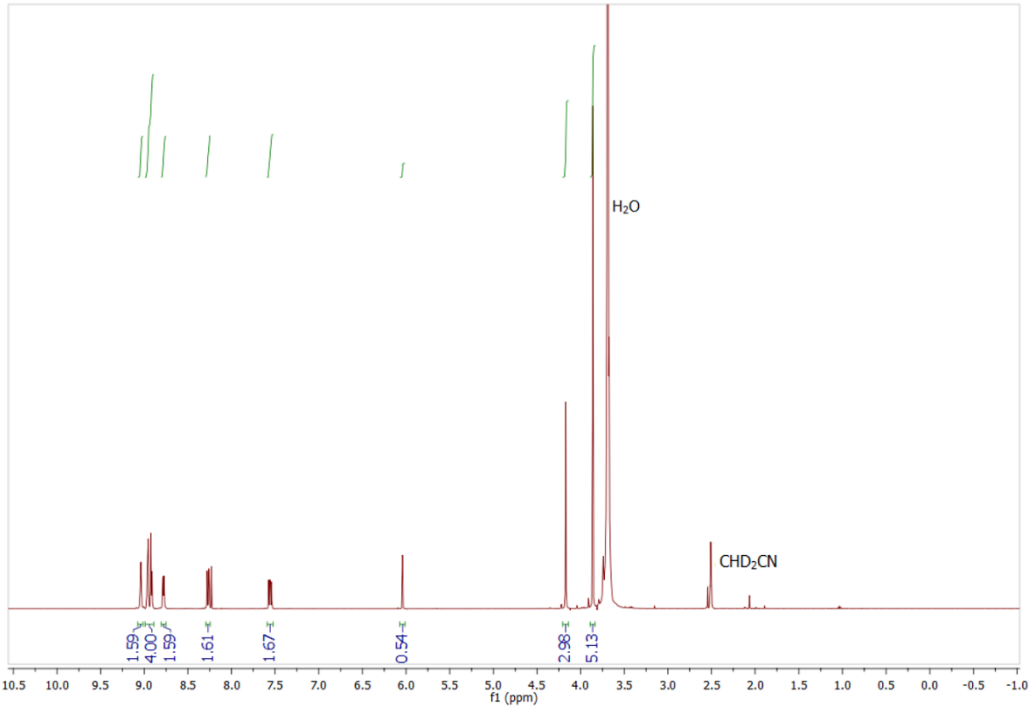


Figure S84: **Spectrum B**: Full ^{1}H NMR spectrum in $(CD_3)_2SO$ (300 MHz) containing signals of **13a**, **25**.and 1,3,5-trimethoxybenzene.

Competition experiment: 1 + 3 + benzhydrylium ion 31

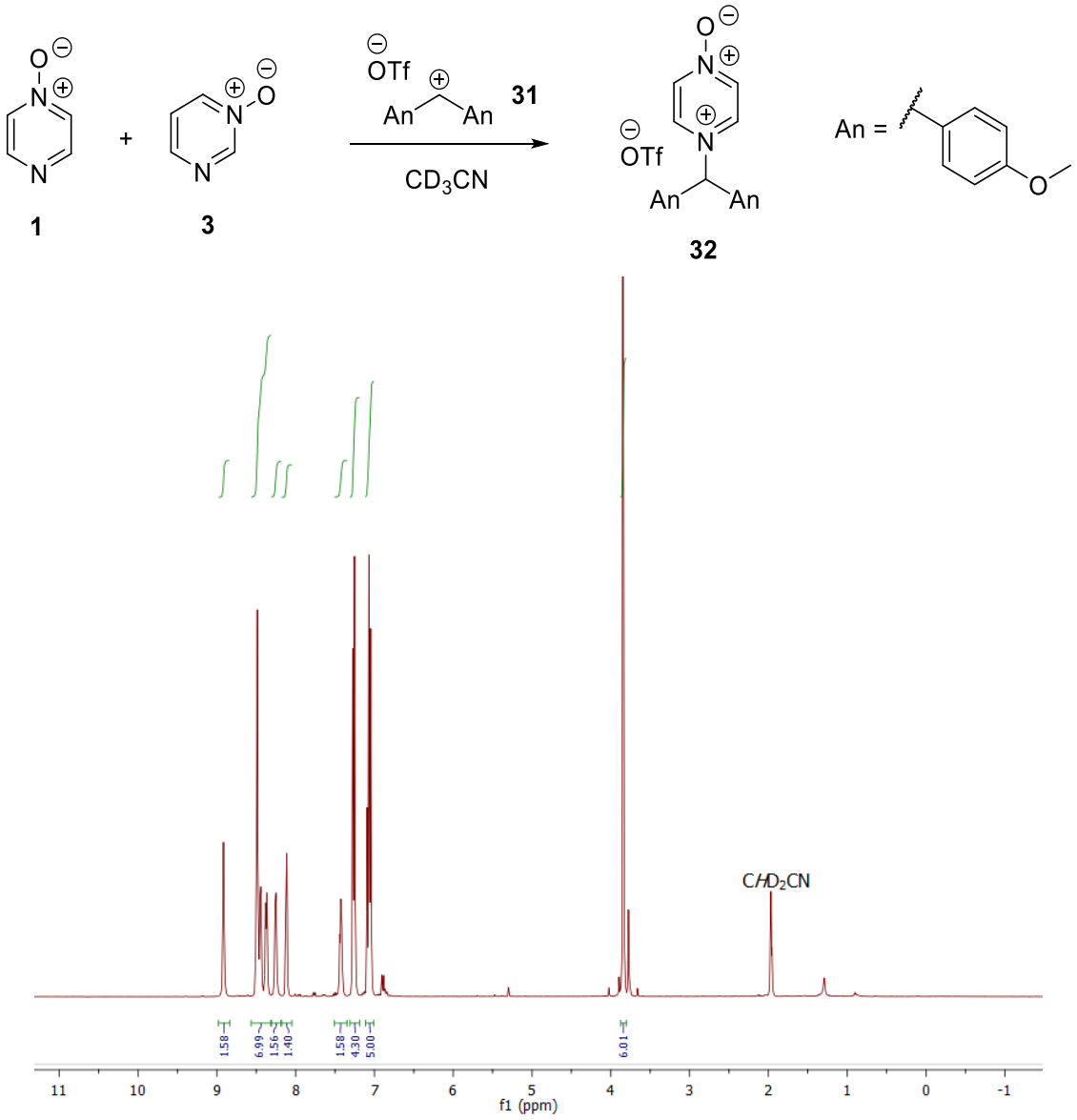


Figure S85: ^{1}H NMR spectrum in CD_3CN (400 MHz) containing signals of **1**, **3**, and **32**.

8. Calculations of Thermodynamic and Activation Parameter Values

Table S1: Activation Enthalpies ($\Delta H^{\ddagger}$, in kJ mol^{-1}), Activation Entropies ($\Delta S^{\ddagger}$, in J K^{-1} mol^{-1}), and Gibbs Energies of Activation ($\Delta G^{\ddagger}$, in kJ mol^{-1}) for Identity Methyl Transfer Reactions.

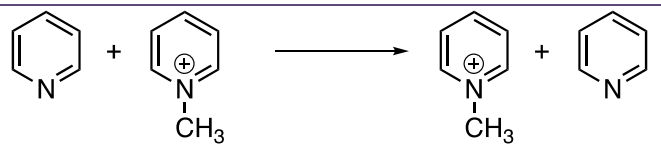
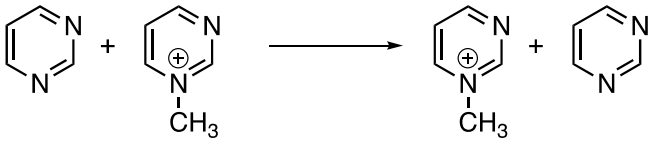
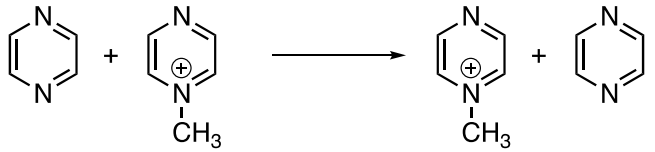
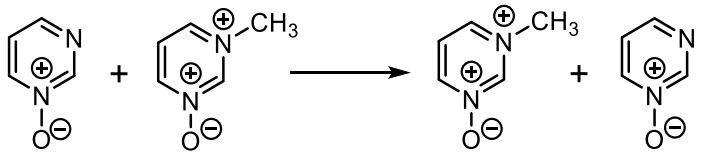
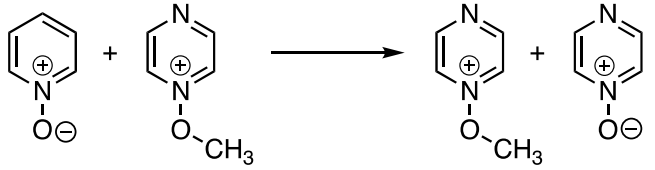
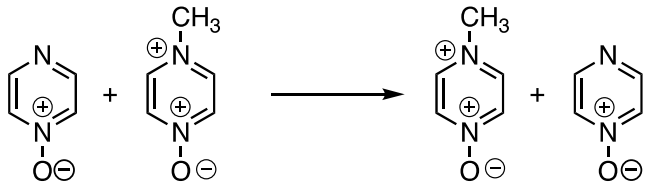
Reaction	$\Delta H^{\ddagger}$	$\Delta S^{\ddagger}$	$\Delta G^{\ddagger}$
	+127	–161	+175
	+123	–171	+175
	+121	–168	+171
	+87	–179	+141
	+73	–175	+125
	+117	–169	+167
	+88	–181	+142
	+125	–171	+176

Table S2: Values of Activation Parameters ($\Delta H^{\ddagger}$ (kJ mol^{-1}), $\Delta S^{\ddagger}$ (J K^{-1} mol^{-1})), $\Delta G^{\ddagger}$ (kJ mol^{-1})), and Thermodynamic Parameters ($\Delta_r H°$ (kJ mol^{-1}), $\Delta_r S°$ (J K^{-1} mol^{-1})), $\Delta_r G°$ (kJ mol^{-1})) for Methylation Reactions Using MeI.

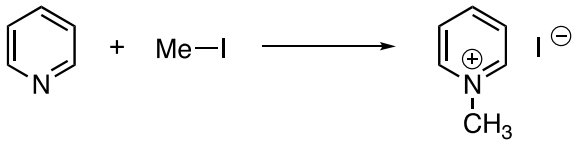
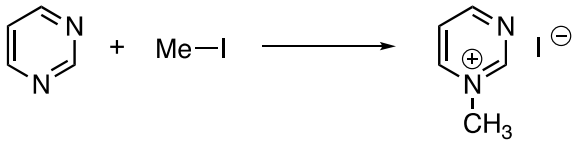
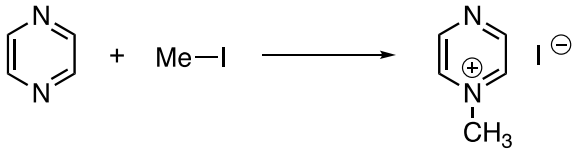
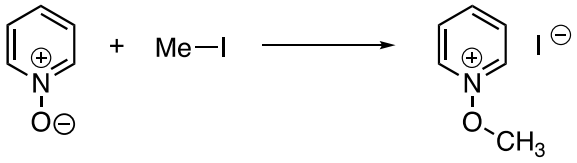
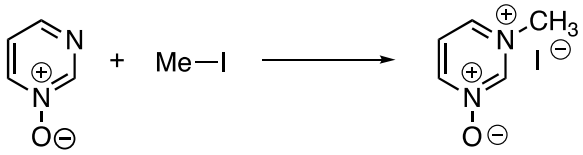
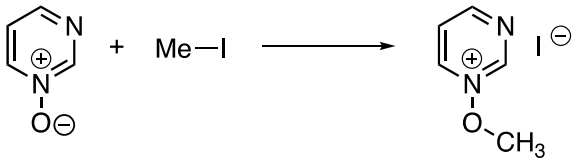
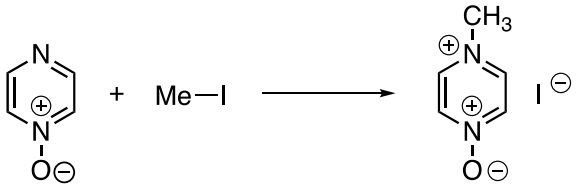
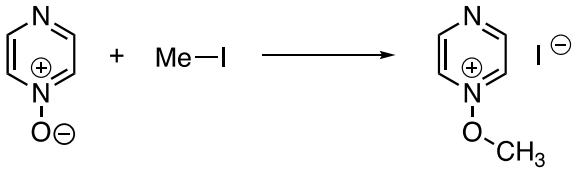
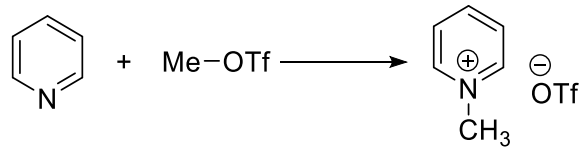
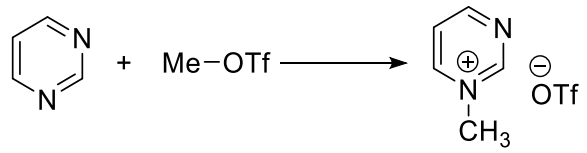
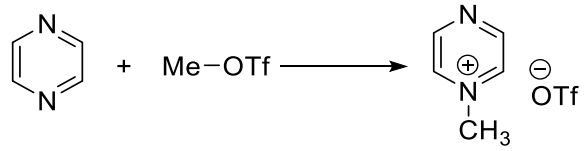
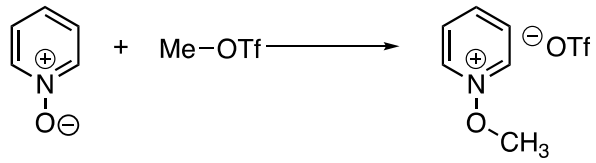
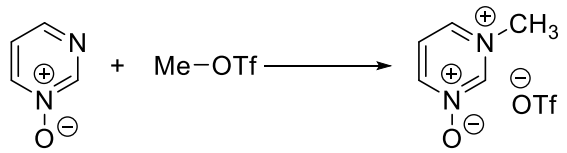
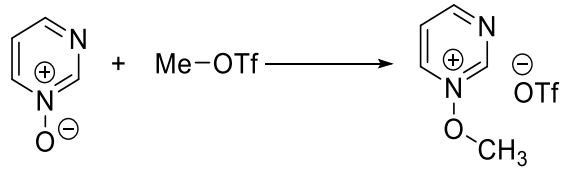
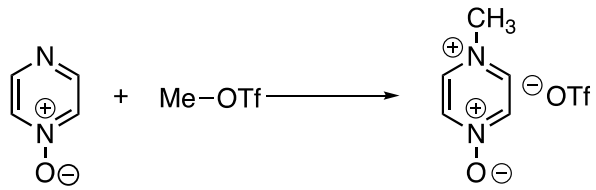
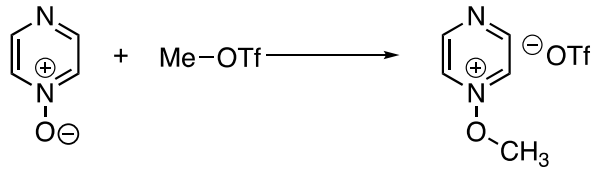
Reaction	$\Delta H^{\ddagger}$	$\Delta S^{\ddagger}$	$\Delta G^{\ddagger}$	$\Delta_r H°$	$\Delta_r S°$	$\Delta_r G°$
	+75	–150	+120	–64	–53	–48
	+84	–154	+130	–39	–52	–23
	+84	–156	+131	–37	–53	–21
	+75	–161	+123	–24	–56	–7
	+92	–154	+138	–13	–58	+4
	+80	–158	+127	+3	–59	+21
	+86	–158	+133	–37	–58	–20
	+92	–161	+140	+14	–55	+31

Table S3: Values of Activation Parameters ($\Delta H^{‡}$ (kJ mol^{-1}), $\Delta S^{‡}$ (J K^{-1} mol^{-1})), $\Delta G^{‡}$ (kJ mol^{-1})), and Thermodynamic Parameters ($\Delta_r H°$ (kJ mol^{-1}), $\Delta_r S°$ (J K^{-1} mol^{-1})), $\Delta_r G°$ (kJ mol^{-1})) for Methylation Reactions Using MeOTf.

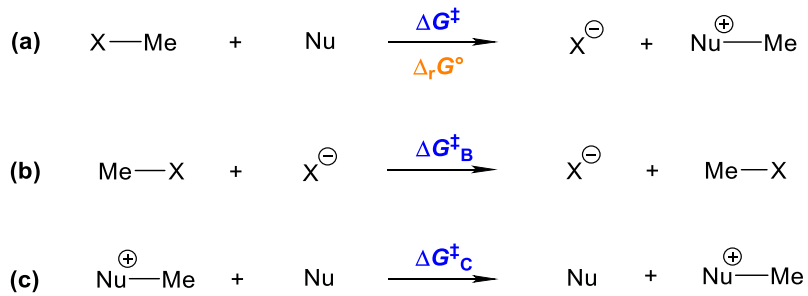
Reaction	$\Delta H^{‡}$	$\Delta S^{‡}$	$\Delta G^{‡}$	$\Delta_r H°$	$\Delta_r S°$	$\Delta_r G°$
	+47	–164	+96	–117	+1	–117
	+56	–171	+107	–91	+1	–91
	+55	–174	+107	–90	0	–90
	+44	–181	+97	–76	–3	–75
	+62	–173	+113	–66	–5	–64
	+51	–172	+103	–49	–6	–48
	+56	–174	+108	–90	–5	–88
	+61	–180	+115	–38	–2	–38

9. Calculation of Marcus Intrinsic Barriers

Let us consider an S_N2 reaction of a nucleophile (Nu) with an alkyl electrophile such as MeX (e.g. X = I, OTf, etc.), with a Gibbs energy of activation $\Delta G^{\ddagger}$ and a standard Gibbs energy of reaction $\Delta_r G°$. Such a reaction can be thought of as a methyl group transfer from X^- to the nucleophile (Scheme S1a). We wish to calculate $\Delta G^{\ddagger}$ using the Marcus equation (equation 1 in the main article), reproduced here:

$$\Delta G^{\ddagger} = \Delta G_0^{\ddagger} + \frac{\Delta_r G°}{2} + \frac{(\Delta_r G°)^2}{16\Delta G_0^{\ddagger}} \qquad (1)$$

In order to access the value of the Marcus intrinsic barrier ($\Delta G_0^{\ddagger}$) for the S_N2 reaction of Nu + MeX, one must first determine the Gibbs energies of activation for the reactions shown in Scheme S1b and S1c. These methyl group transfer reactions are identity reactions since the products and the reactants are the same. They are thermoneutral, i.e. $\Delta_r G° = 0$ for each one. The Gibbs energy of activation for methyl transfer from Me—X to X^- is $\Delta G^{\ddagger}_B$, and the Gibbs energy of activation for methyl transfer from Nu^+—Me to Nu is $\Delta G^{\ddagger}_C$.



Scheme S1. **(a)** Methyl transfer reaction from MeX to Nu, with Gibbs energy of activation = $\Delta G^{\ddagger}$ and $\Delta_r G° \neq 0$; **(b)** Methyl transfer identity reaction from MeX to X^-, with Gibbs energy of activation = $\Delta G^{\ddagger}_B$ and $\Delta_r G° = 0$; **(c)** Methyl transfer identity reaction from Nu^+—Me to Nu, with Gibbs energy of activation = $\Delta G^{\ddagger}_C$ and $\Delta_r G° = 0$.

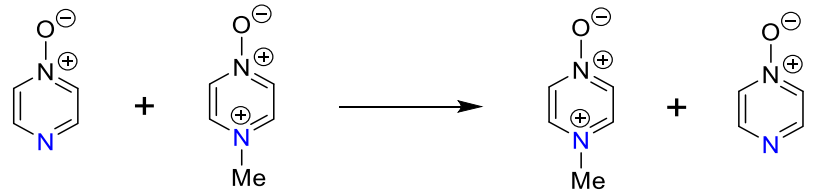
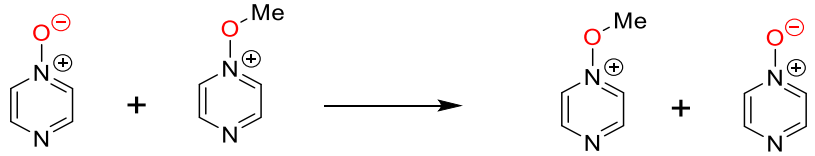
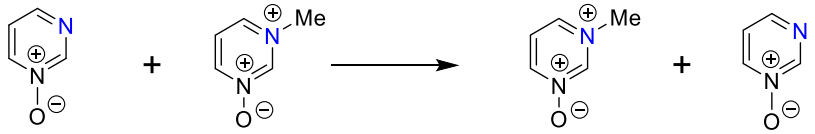
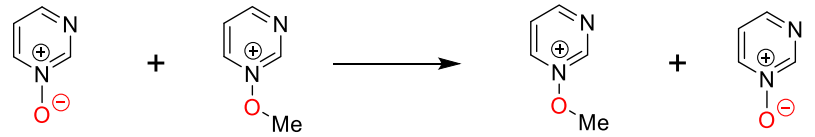
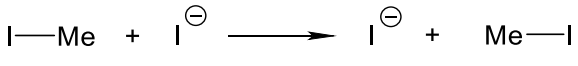
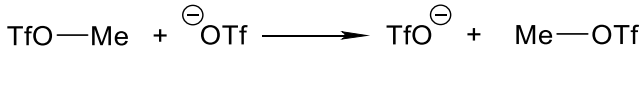
Using the Gibbs energies of activation of the identity reactions shown in Scheme S1b and S1c, the intrinsic barrier ($\Delta G_0^{\ddagger}$) for the reaction of the nucleophile (Nu) with MeX (Scheme S1a) can be calculated using equation 2:

$$\Delta G_0^{\ddagger} = \frac{1}{2}\left(\Delta G_B^{\ddagger} + \Delta G_C^{\ddagger}\right) \qquad (2)$$

i.e. $\Delta G_0^{\ddagger}$ for the methylation of the nucleophile is taken to be the average of the Gibbs energies of activation of the identity reactions shown in Scheme S1b and S1c.

In this study, we have calculated values of Gibbs energies of activation for methyl group transfer identity reactions of the type shown in Scheme S1b and S1c for nucleophiles **1** and **3** and also iodide and triflate (see Table S1). These calculations were done at the DLPNO-CCSD(T)/def2-TZVPPD/SMD//M06-2X-D3/6-311+G(d,p)/SMD level of theory.

Table S4. $\Delta G^{\ddagger}$ values for methyl transfer identity reactions of **1** and **3** at both the N and O nucleophilic sites, and of iodide and triflate. [a]

Reaction	Compound Number	Site of Methylation	$\Delta G^{\ddagger}$ of Identity Reaction
	**1**	N	**176**
	**1**	O	**142**
	**3**	N	**167**
	**3**	O	**125**
	Iodide	I	**112**
	Triflate	O	**123**

[a] Gibbs energy values were calculated at the DLPNO-CCSD(T)/def2-TZVPPD/SMD(CH3CN)//M06-2X-D3/6-311+G(d,p)/SMD(CH3CN) level of theory.

Calculation of $\Delta G^{\ddagger}$ using $\Delta G_0^{\ddagger}$ values in the Marcus Equation

Using the $\Delta G^{\ddagger}$ values calculated for the methyl transfer identity reactions (Table S4), values of the intrinsic barrier ($\Delta G_0^{\ddagger}$) were calculated for each of the reactions of compounds **1** and **3** with MeI and MeOTf using equation 2. These $\Delta G_0^{\ddagger}$ values are shown in Table S5 on pg. S90 (these values are also shown in Table 4 of the main article).

The value calculated for $\Delta G_0^{\ddagger}$ for each reaction was substituted into the Marcus equation (equation 1) along with the $\Delta_r G°$ value calculated for the reaction in question (these values are shown in Table 3 in the main article, and reproduced here in Table S5), enabling calculation of a value for $\Delta G^{\ddagger}$ according to the Marcus equation for the reaction of Nu + MeX. For ambident nucleophiles **1** and **3**, there are two $\Delta G^{\ddagger}$ values – one for reaction at each of the nucleophilic sites of the ambident nucleophile. For these nucleophiles, the product ratio predicted by the Marcus calculations just described was obtained using equation 3

$$\frac{k_{\mathrm{N}}}{k_{\mathrm{O}}} = e^{-\left(\frac{\Delta\Delta G^{\ddagger}}{RT}\right)} = e^{-\left(\frac{\Delta G^{\ddagger}(\mathrm{N}) - \Delta G^{\ddagger}(\mathrm{O})}{RT}\right)} \qquad (3)$$

where

k_{N} and $\Delta G^{\ddagger}(\mathrm{N})$ are the rate constant (L mol^{-1} s^{-1}) and Gibbs energy of activation (kJ mol^{-1}), respectively, for N-methylation,

k_{O} and $\Delta G^{\ddagger}(\mathrm{O})$ are the rate constant (L mol^{-1} s^{-1}) and Gibbs energy of activation (kJ mol^{-1}), respectively, for O-methylation,

R is the universal gas constant, and the temperature, T, was set to 298 K.

The product ratio calculated in this manner for methylation of **1** by MeOTf was 90:10 ± 2 (in favour of N-methylation), and for **1** + MeI the ratio was 97:3 ± 2 (O-methylation was also calculated to be reversible, i.e. $\Delta_r G° > 0$; experimentally no O-methylation is observed). The product ratio calculated for methylation of **3** by MeOTf was 0.4 : 99.6 ± 2 (in favour of O-methylation), and for **3** + MeI the ratio was calculated to be 1:99 ± 2 (both O and N-methylation were calculated to be reversible, i.e. $\Delta_r G° > 0$, and no product formation was observed experimentally). Further detail on these calculations is given below, in Tables S6 and S7.

Much of the information contained in Table S5 is reproduced from Table 4 in the main article. This was done by design to allow straightforward comparison of the extra results included there (from calculations done using the Zhu equation – see below) with results derived from the Marcus equation, and direct DFT calculations.

Calculation of $\Delta G^{\ddagger}$ using the Zhu Equation

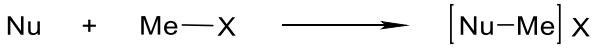
Zhu and co-workers have developed an alternative to the Marcus equation to rationalize the outcomes of hydride transfer reactions.[28] Here, we have adapted the Zhu equation to apply to methyl group transfer reactions. Our adaptation of the Zhu equation is shown in equation 4:

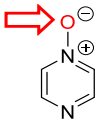
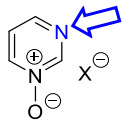
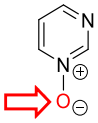
$$\Delta G^{\ddagger} = \frac{1}{2}\left(\Delta G^{\ddagger}_{\mathrm{XMe/X}} + \Delta G^{\ddagger}_{\mathrm{NuMe/Nu}}\right) + \frac{\Delta_r G^{\circ}}{2} \qquad (4)$$

where $\Delta G^{\ddagger}_{\mathrm{XMe/X}} = \Delta G^{\ddagger}_{\mathrm{B}}$ from Scheme S1b on pg. S86, $\Delta G^{\ddagger}_{\mathrm{NuMe/Nu}} = \Delta G^{\ddagger}_{\mathrm{C}}$ from Scheme S1c on pg. S86 (i.e. $\Delta G^{\ddagger}_{\mathrm{XMe/X}}$ and $\Delta G^{\ddagger}_{\mathrm{NuMe/Nu}}$ are the Gibbs energies of activation for the methyl group transfer identity reactions shown in Scheme S1b and S1c, for which $\Delta_r G^{\circ} = 0$), and $\Delta G^{\ddagger}$ and $\Delta_r G^{\circ}$ are, respectively, the Gibbs energy of activation and standard Gibbs energy of reaction for the methyl group transfer reaction shown in Scheme S1a on pg. S86.

The first term in equation 4 (involving the activation barriers for the identity reactions) is identical to the expression for the Marcus intrinsic barrier shown in equation 2, and the second term is identical to the second term of the Marcus equation (equation 1 in the main article). So the Marcus equation and Zhu equation differ only in the exclusion of the quadratic term of the Marcus equation from the latter equation. We have calculated $\Delta G^{\ddagger}$ values using the adapted Zhu equation (equation 4) using our computational data from the methyl transfer identity reactions (values from Table S4) along with our directly calculated $\Delta_r G^{\circ}$ values for the methylation reactions of **1** and **3** (shown in Table S5). These $\Delta G^{\ddagger}$ values, calculated according to the adapted Zhu equation (shown in Table S5), are essentially identical to the values calculated using equation 1. This is because the quadratic term of equation 1 is very small in all reactions investigated here due to the relatively small $\Delta_r G^{\circ}$ values of these reactions. Consequently, there is close agreement between the $\Delta G^{\ddagger}$ values calculated using equation 4 (Zhu equation) and equation 1 (Marcus equation) and those calculated directly at the DLPNO-CCSD(T)/def2-TZVPPD/SMD//M06-2X-D3/6-311+G(d,p)/SMD level of theory. Naturally, therefore, the product ratios determined using these three different methods of calculation agree quite closely. All of these methods of determining the product ratios are close to the true values observed experimentally, as discussed in the main article.

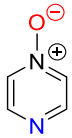
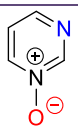
Table S5. Values of intrinsic barriers ($\Delta G_0^{\ddagger}$) for methylation reactions of nucleophiles **1** and **3**, and derived values of $\Delta G^{\ddagger}$ for methylation reactions of these nucleophiles (Scheme S1a with Nu = N or O nucleophilic site of **1** or **3**) calculated using Marcus equation (equation 1) and Zhu equation (equation 4) by employing values of $\Delta_r G°$ from Table 4 of the main article (and reproduced here). The site of methylation of each nucleophile is indicated by an arrow. The Gibbs energy values have units of kJ mol^{-1}.



Nucleophile (Nu)	#	Product. No.	X	$\Delta G^{\ddagger}$ Me transfer MeX + X$^-$	$\Delta G^{\ddagger}$ Me transfer MeNu$^+$ + Nu	$\Delta G_0^{\ddagger}$	$\Delta_r G°$	Marcus $\Delta G^{\ddagger}$	Zhu $\Delta G^{\ddagger}$	DFT $\Delta G^{\ddagger}$
	(i)	**13b**	OTf	123	176	+149.5	−88	+108.7	+105.5	+108
	(ii)	**13a**	I	112	176	+144	−20	+134.2	+134	+133
	(iii)	**15b**	OTf	123	142	+132.5	−38	+114.3	+113.5	+115
	(iv)	**15a**	I	112	142	+127.0	+31	+143.0	+142.5	+140
	(v)	**21b**	OTf	123	167	+145.0	−64	+114.8	+113	+113
	(vi)	**21a**	I	112	167	+139.5	+4	+141.5	+141.5	+138
	(vii)	**23b**	OTf	123	125	+124.0	−48	+101.2	+100	+103
	(viii)	**23a**	I	112	125	+118.5	+21	+129.2	+129	+127

Example calculation to obtain the product ratio predicted by the Marcus calculations

Table S6. Values of activation barriers ($\Delta G^{\ddagger}$) for methylation reactions of nucleophiles **1** and **3** with MeOTf, with calculations of the terms used in equation 3. The Gibbs energy values have units of kJ mol^{-1}.

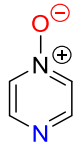
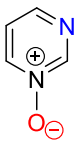
Nucleophile (Nu) and Product Number		Entry	Site of Methylation	Marcus $\Delta G^{\ddagger}$	$\Delta\Delta G^{\ddagger}$	$\left(\frac{\Delta\Delta G^{\ddagger}}{RT}\right)$
	**1**	(i)	N	+108.7	−5.44	−2.20
		(ii)	O	+114.3		
	**3**	(iii)	N	+114.8	+13.6	+5.49
		(iv)	O	+101.2		

In the case of **1** + MeOTf:

$$\frac{k_{\mathrm{N}}}{k_{\mathrm{O}}} = e^{-(-2.20)} = 9.03$$

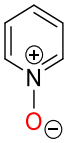
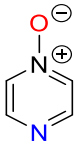
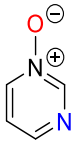
$$\frac{k_{\mathrm{N}}}{k_{\mathrm{O}}} = \frac{9.03}{1 + 9.03} = 90.0\%\ \text{N-methylation}$$

Table S7. Calculated ratios of N vs O methylation for reactions of nucleophiles **1** and **3** with MeOTf and MeI. The Gibbs energy values have units of kJ mol^{-1}.

Nucleophile (Nu) and Product Number	Entry	Method	Electrophile	$\Delta\Delta G^{\ddagger}$	$\left(\frac{\Delta\Delta G^{\ddagger}}{RT}\right)$	N/O Ratio
 **1**	(i)	Marcus	MeOTf	−5.4	−2.2	90 : 10
	(ii)	Marcus	MeI	−8.8	−3.6	97 : 3
	(iii)	Zhu	MeOTf	−8.0	−3.2	96 : 4
	(iv)	Zhu	MeI	−8.5	−3.4	97 : 3
	(v)	DFT	MeOTf	−7.0	−2.8	94 : 6
	(vi)	DFT	MeI	−7.0	−2.8	94 : 6
 **3**	(vii)	Marcus	MeOTf	+13.6	+5.5	0.4 : 99.6
	(viii)	Marcus	MeI	+12.3	+5.0	0.7 : 99.3
	(ix)	Zhu	MeOTf	+13.0	+5.3	0.5 : 99.5
	(ix)	Zhu	MeI	+12.5	+5.0	0.6 : 99.4
	(x)	DFT	MeOTf	+10.0	+4.0	1.7 : 98.3
	(xi)	DFT	MeI	+11.0	+4.4	1.2 : 98.8

10. Charge Density Calculations

Table S8. Charge density calculations using different computational methods (NBO,[13] Merz-Singh-Kollman,[14] ChelpG,[15] AIM[16]) at the M06-2X-D3/6-311+G(d,p)/SMD(CH_3CN) level of theory.

Nucleophile	 **28**	 **7**	 **27**	 **8**	 **1**		 **3**	
Nucleophilic Site	N	N	N	O	N	O	N	O
NBO	−0.514	−0.460	−0.528	−0.656	−0.490	−0.589	−0.484	−0.648
Merz-Singh-Kollman	−0.842	−0.564	−0.917	−0.719	−0.732	−0.679	−0.704	−0.300
ChelpG	−0.719	−0.558	−0.921	−0.710	−0.745	−0.700	−0.706	−0.665
AIM	−1.245	−1.215	−1.238	−0.669	−1.205	−0.616	−1.228	−1.215

11. Calculation of Activation Barriers for Methyl Transfer Identity Reactions

11.1 Methyl Transfer Involving Iodide

11.1.1 Methyl iodide

SCF energy:	–336.980594 hartree
Zero-point correction:	+0.036760 hartree
Enthalpy correction:	+0.040854 hartree
Free energy correction:	+0.011036 hartree
Truhlar's Delta G correction:	+0.011036 hartree
Grimme's Delta G correction:	+0.011036 hartree

Cartesian Coordinates

C	0.00000	-1.81320	0.00000
H	-1.03708	-2.13422	0.00000
H	0.51854	-2.13422	0.89813
H	0.51854	-2.13422	-0.89813
I	0.00000	0.32607	0.00000

11.1.2 Iodide

SCF energy:	–297.318803 hartree
Zero-point correction:	+0.000000 hartree
Enthalpy correction:	+0.002360 hartree
Free energy correction:	–0.016848 hartree
Truhlar's Delta G correction:	–0.016848 hartree
Grimme's Delta G correction:	–0.016848 hartree

Cartesian Coordinates

I	0.00000	0.00000	0.00000

11.1.3 Transition State Identity Reaction

SCF energy:	–634.267049 hartree
Zero-point correction:	+0.036306 hartree
Enthalpy correction:	+0.042259 hartree
Free energy correction:	+0.004451 hartree
Truhlar's Delta G correction:	+0.004451 hartree
Grimme's Delta G correction:	+0.004620 hartree
Imaginary Frequency:	509.4 *i*cm^{-1}

Cartesian Coordinates

C	-0.00002	-0.00726	-0.00073
H	0.00014	0.55232	-0.92086
H	-0.00002	-1.08424	-0.02511
H	-0.00018	0.51002	0.94379
I	-2.64394	0.00062	0.00006
I	2.64394	0.00062	0.00006

11.2 Methyl Transfer Involving Pyrimidine *N*-Oxide (3)

11.2.1 Pyrimidine *N*-Oxide (**3**)

SCF energy:	–338.948361 hartree
Zero-point correction:	+0.081611 hartree
Enthalpy correction:	+0.087483 hartree
Free energy correction:	+0.052978 hartree
Truhlar's Delta G correction:	+0.052978 hartree
Grimme's Delta G correction:	+0.052974 hartree

Cartesian Coordinates

C	0.26487	-1.15272	0.00000
N	0.94851	0.02630	-0.00000
C	0.23736	1.17892	-0.00000
N	-1.04443	-1.23702	-0.00000
C	-1.14071	1.13449	0.00000
C	-1.75816	-0.10771	-0.00000
H	0.89179	-2.03487	0.00000
H	0.82933	2.08392	0.00000
H	-1.70979	2.05411	0.00000
O	2.23462	0.03240	0.00000
H	-2.83702	-0.20519	0.00000

11.2.2 *N*-Methyl Pyrimidinium *N*-Oxide Ion (**21**$^+$)

SCF energy:	–378.619925 hartree
Zero-point correction:	+0.123063 hartree
Enthalpy correction:	+0.130750 hartree
Free energy correction:	+0.091756 hartree
Truhlar's Delta G correction:	+0.092170 hartree
Grimme's Delta G correction:	+0.092167 hartree

Cartesian Coordinates

C	-0.01615	-0.94658	-0.00865
N	1.22271	-0.41278	0.00011
C	1.35312	0.94382	0.00578
N	-1.09916	-0.17328	-0.01202
C	0.23842	1.74862	0.00269
C	-1.01290	1.16655	-0.00731
H	-0.10598	-2.02271	-0.01230
H	2.37320	1.30223	0.01158
H	0.34526	2.82390	0.00599
O	2.24047	-1.17740	0.00201
H	-1.94320	1.71722	-0.01098
C	-2.43513	-0.81592	0.01102
H	-2.31843	-1.86849	-0.22917
H	-2.84743	-0.69125	1.01057
H	-3.05610	-0.31825	-0.72955

11.2.3 O-Methyl Pyrimidinium *N*-Oxide Ion (**23**$^+$)

SCF energy:	–378.613655 hartree
Zero-point correction:	+0.123086 hartree
Enthalpy correction:	+0.130726 hartree
Free energy correction:	+0.091645 hartree
Truhlar's Delta G correction:	+0.092374 hartree
Grimme's Delta G correction:	+0.092257 hartree

Cartesian Coordinates

C	0.50632	-1.25048	-0.00002
N	-0.39237	-0.23937	-0.00001
C	-0.01000	1.04487	-0.00002
N	1.79283	-1.03301	0.00000
C	1.34576	1.30953	-0.00000
C	2.22073	0.23658	0.00002
H	0.08592	-2.24882	-0.00001
H	-0.76781	1.81597	-0.00004
H	1.69061	2.33361	0.00000
O	-1.68674	-0.66793	0.00001
H	3.29330	0.38890	0.00003
C	-2.68892	0.36351	0.00001
H	-2.61912	0.96986	-0.90453
H	-3.61660	-0.20344	0.00019
H	-2.61892	0.97003	0.90443

11.2.4 Transition State Identity Reaction N → N

SCF energy:	–717.523828 hartree
Zero-point correction:	+0.204107 hartree
Enthalpy correction:	+0.218130 hartree
Free energy correction:	+0.161539 hartree
Truhlar's Delta G correction:	+0.164702 hartree
Grimme's Delta G correction:	+0.164263 hartree
Imaginary Frequency:	621.4 *i*cm^{-1}

Cartesian Coordinates

C	0.00368	-0.25554	0.01894
N	-1.95733	-0.26162	-0.11354
C	-2.67025	0.70881	0.41227
C	-2.54612	-1.27727	-0.74632
N	-4.02639	0.73300	0.34367
H	-2.20240	1.53757	0.92773
C	-3.92668	-1.31416	-0.85191
H	-1.89987	-2.04368	-1.15736
C	-4.65680	-0.28782	-0.29314
H	-4.43332	-2.12393	-1.35828
N	1.96541	-0.29454	0.14773
C	2.59356	-1.30528	0.74728
C	2.64293	0.70089	-0.38143
C	3.97821	-1.31126	0.81527
H	1.98085	-2.09523	1.16444
N	3.99821	0.75617	-0.34892
H	2.13911	1.52524	-0.86963
C	4.66918	-0.26052	0.25464

H	4.51601	-2.11735	1.29468
H	-0.01922	0.65635	0.59685
H	0.07119	-0.21079	-1.05734
H	-0.04091	-1.21209	0.51782
H	-5.73542	-0.21415	-0.31586
H	5.74603	-0.16196	0.24923
O	4.61778	1.74416	-0.87646
O	-4.68124	1.69857	0.8704

11.2.5 Transition State Identity Reaction O → O

SCF energy:	–717.534306 hartree
Zero-point correction:	+0.204429 hartree
Enthalpy correction:	+0.218231 hartree
Free energy correction:	+0.162267 hartree
Truhlar's Delta G correction:	+0.165731 hartree
Grimme's Delta G correction:	+0.165175 hartree
Imaginary Frequency:	669.6 *i*cm^{-1}

Cartesian Coordinates

C	0.00001	1.11739	-0.00005
O	1.51505	1.13662	-1.14294
O	-1.51504	1.13663	1.14291
N	2.48404	0.41906	-0.60057
C	2.61022	-0.88536	-0.93581
C	3.33311	0.97778	0.28306
N	3.54349	-1.66117	-0.43794
H	1.88437	-1.24885	-1.65249
C	4.32902	0.19885	0.83146
H	3.16906	2.02583	0.49681
C	4.40055	-1.13104	0.44012
H	5.02521	0.62421	1.54066
N	-2.48406	0.41908	0.60061
C	-3.33314	0.97779	-0.28303
C	-2.61027	-0.88532	0.93589
C	-4.32900	0.19883	-0.83149
H	-3.16911	2.02584	-0.49676
N	-3.54349	-1.66116	0.43796
H	-1.88447	-1.24880	1.65263
C	-4.40049	-1.13107	-0.44017
H	-5.02518	0.62418	-1.54070
H	-0.00013	0.03614	-0.00021
H	0.53455	1.65965	0.76593
H	-0.53444	1.66001	-0.76584
H	-5.16228	-1.79106	-0.83793
H	5.16241	-1.79099	0.83781

11.3 Methyl Transfer Involving Pyrazine *N*-Oxide (1)

11.3.1 Pyrazine *N*-Oxide (**1**)

SCF energy:	–338.948037 hartree
Zero-point correction:	+0.081835 hartree
Enthalpy correction:	+0.087670 hartree
Free energy correction:	+0.053220 hartree
Truhlar's Delta G correction:	+0.053220 hartree
Grimme's Delta G correction:	+0.053215 hartree

Cartesian Coordinates

C	0.26352	1.16424	0.00000
N	0.96464	-0.00000	0.00000
C	0.26352	-1.16424	0.00000
C	-1.11658	1.12880	0.00000
C	-1.11658	-1.12879	-0.00000
N	-1.82670	-0.00000	0.00000
H	-1.65916	2.06716	-0.00000
H	0.85431	2.06847	-0.00000
H	0.85431	-2.06847	0.00000
H	-1.65916	-2.06716	-0.00000
O	2.23512	0.00000	-0.00000

11.3.2 *N*-Methyl Pyrazinium *N*-Oxide (**13**$^{+}$)

SCF energy:	–378.628807 hartree
Zero-point correction:	+0.123428 hartree
Enthalpy correction:	+0.131048 hartree
Free energy correction:	+0.092405 hartree
Truhlar's Delta G correction:	+0.092411 hartree
Grimme's Delta G correction:	+0.092584 hartree

Cartesian Coordinates

C	-0.77370	-1.17472	-0.00042
N	-1.47508	0.00000	0.00347
C	-0.77370	1.17472	-0.00042
C	0.59252	-1.15896	-0.00910
C	0.59253	1.15896	-0.00910
N	1.27293	0.00001	-0.01579
H	1.16492	-2.07690	-0.01408
H	-1.36003	-2.08123	0.00032
H	-1.36004	2.08123	0.00033
H	1.16492	2.07690	-0.01410
O	-2.72232	-0.00000	0.00797
C	2.74757	-0.00001	0.01595
H	3.10059	0.89266	-0.49342
H	3.10059	-0.89237	-0.49397
H	3.07136	-0.00030	1.05594

11.3.3 O-Methyl Pyrazinium *N*-Oxide (**15**$^{+}$)

SCF energy:	–378.608535 hartree
Zero-point correction:	+0.122591 hartree
Enthalpy correction:	+0.130352 hartree
Free energy correction:	+0.091208 hartree
Truhlar's Delta G correction:	+0.091495 hartree
Grimme's Delta G correction:	+0.091554 hartree

Cartesian Coordinates

C	0.20982	-1.17502	-0.16268
N	-0.41529	-0.00005	-0.28265
C	0.20974	1.17497	-0.16274
C	1.57163	-1.14105	0.10083
C	1.57154	1.14112	0.10078
N	2.24151	0.00006	0.23065
H	2.11521	-2.07185	0.20156
H	-0.38356	-2.07150	-0.28497
H	-0.38365	2.07144	-0.28511
H	2.11506	2.07196	0.20145
O	-1.74032	-0.00013	-0.60425
C	-2.56366	0.00008	0.59187
H	-3.58194	-0.00005	0.21160
H	-2.36828	0.90208	1.17241
H	-2.36820	-0.90170	1.17276

11.3.4 Transition State Identity Reaction N → N

SCF energy:	–717.529061 hartree
Zero-point correction:	+0.204595 hartree
Enthalpy correction:	+0.218532 hartree
Free energy correction:	+0.162293 hartree
Truhlar's Delta G correction:	+0.165360 hartree
Grimme's Delta G correction:	+0.164983 hartree
Imaginary Frequency:	639.2 *i*cm^{-1}

Cartesian Coordinates

C	0.00011	-0.03639	0.00449
N	1.95349	-0.04288	0.02048
C	2.66242	-1.12875	-0.28129
C	2.61320	1.07790	0.31038
C	4.03868	-1.12143	-0.29861
H	2.12139	-2.03818	-0.51788
C	3.98708	1.13968	0.30656
H	4.65047	-1.97873	-0.53676
N	-1.95319	-0.02845	-0.02524
C	-2.65434	-1.11935	0.27794
C	-2.62110	1.08765	-0.31327
C	-4.03020	-1.12198	0.29846
H	-2.10530	-2.02458	0.51231
C	-3.99573	1.13956	-0.30644

N	-4.71089	0.02127	0.00376
H	-4.63564	-1.98357	0.53744
N	4.71073	0.02621	-0.00250
O	5.97214	0.05826	-0.01388
O	-5.97246	0.04420	0.01740
H	-4.57519	2.02164	-0.53508
H	-2.04500	1.97273	-0.55904
H	-0.00415	-1.10596	-0.14965
H	-0.00963	0.36396	1.00679
H	4.55998	2.02585	0.53605
H	2.02962	1.95869	0.55432
H	0.01426	0.63397	-0.84151

11.3.5 Transition State Identity Reaction O → O

SCF energy:	–717.523094 hartree
Zero-point correction:	+0.204513 hartree
Enthalpy correction:	+0.218210 hartree
Free energy correction:	+0.163041 hartree
Truhlar's Delta G correction:	+0.165687 hartree
Grimme's Delta G correction:	+0.165467 hartree
Imaginary Frequency:	687.0 *i*cm^{-1}

Cartesian Coordinates

C	-0.00003	-0.84277	0.00000
O	-1.47072	-0.86673	-1.20899
O	1.47061	-0.86638	1.20908
N	-2.51771	-0.31668	-0.63878
C	-3.36095	-1.07469	0.08617
C	-2.73834	1.00375	-0.77540
C	-4.45426	-0.46528	0.67827
H	-3.12677	-2.12779	0.15422
C	-3.84944	1.55524	-0.16018
H	-2.02415	1.55335	-1.37202
N	-4.70554	0.83662	0.56246
H	-5.14050	-1.06730	1.26128
H	-4.03781	2.61661	-0.26710
N	2.51766	-0.31651	0.63881
C	2.73841	1.00391	0.77524
C	3.36085	-1.07471	-0.08600
C	3.84958	1.55522	0.15998
H	2.02424	1.55367	1.37175
C	4.45425	-0.46549	-0.67814
H	3.12658	-2.12780	-0.15391
N	4.70565	0.83640	-0.56251
H	4.03805	2.61658	0.26675
H	5.14045	-1.06766	-1.26104
H	-0.56412	-1.38609	0.74425
H	0.56382	-1.38696	-0.74379
H	0.00021	0.23837	-0.00047

12 Calculations on Reactions with Methyl Iodide and Methyl Triflate

12.1 Methylation of Pyridine (28)

12.1.1 Methyl Triflate

SCF energy:	–1000.213262 hartree
Zero-point correction:	+0.068039 hartree
Enthalpy correction:	+0.078169 hartree
Free energy correction:	+0.032986 hartree
Truhlar's Delta G correction:	+0.033685 hartree
Grimme's Delta G correction:	+0.033748 hartree

Cartesian Coordinates

O	0.14961	1.83242	-0.76112
S	0.41956	0.67876	0.04845
O	0.80716	0.78320	1.43023
O	1.40565	-0.24861	-0.75382
C	-1.11715	-0.36119	-0.00014
F	-2.07844	0.27303	0.64814
F	-0.88290	-1.52575	0.58292
F	-1.48201	-0.56039	-1.25300
C	2.27344	-1.18381	-0.03564
H	1.67126	-1.89244	0.52961
H	2.82132	-1.68966	-0.82497
H	2.94757	-0.62619	0.61004

12.1.2 Triflate Ion

SCF energy:	–960.567597 hartree
Zero-point correction:	+0.027777 hartree
Enthalpy correction:	+0.035760 hartree
Free energy correction:	–0.004526 hartree
Truhlar's Delta G correction:	–0.004057 hartree
Grimme's Delta G correction:	–0.004078 hartree

Cartesian Coordinates

O	-1.23298	-1.37549	0.38099
S	-0.90907	-0.00016	0.00006
O	-1.23319	1.01766	1.00037
O	-1.23278	0.35740	-1.38158
C	0.94417	-0.00001	0.00010
F	1.42517	-0.31444	1.20518
F	1.42405	1.20128	-0.33017
F	1.42541	-0.88617	-0.87498

12.1.3 Transition State for Methyl Iodide

SCF energy:	–584.799693 hartree
Zero-point correction:	+0.127449 hartree

Enthalpy correction:	+0.136820 hartree
Free energy correction:	+0.090730 hartree
Truhlar's Delta G correction:	+0.092049 hartree
Grimme's Delta G correction:	+0.092055 hartree
Imaginary Frequency:	547.9 *i*cm^{-1}

Cartesian Coordinates

C	0.13742	0.01418	-0.01218
H	0.08277	-0.38754	0.98579
H	0.10008	1.08084	-0.16385
H	0.09180	-0.64956	-0.85970
I	2.65999	-0.00134	0.00346
C	-2.68248	1.16435	-0.01176
C	-2.64062	-1.14048	-0.01245
C	-4.07140	1.18497	0.00838
H	-2.10187	2.08151	-0.01960
C	-4.02730	-1.21263	0.00760
H	-2.02535	-2.03503	-0.02039
C	-4.75335	-0.02655	0.01809
H	-4.59847	2.13048	0.01633
H	-4.51914	-2.17695	0.01491
N	-1.99232	0.02433	-0.02238
H	-5.83684	-0.04637	0.03393

12.1.4 Transition State for Methyl Triflate

SCF energy:	–1248.041686 hartree
Zero-point correction:	+0.157223 hartree
Enthalpy correction:	+0.172913 hartree
Free energy correction:	+0.111304 hartree
Truhlar's Delta G correction:	+0.116184 hartree
Grimme's Delta G correction:	+0.115162 hartree
Imaginary Frequency:	609.9 *i*cm^{-1}

Cartesian Coordinates

C	0.59052	-0.78365	-0.36165
H	0.51364	-0.57423	0.69468
H	0.93741	-1.75400	-0.68029
H	0.55833	0.02389	-1.07479
C	3.62842	-1.12267	-0.40148
C	2.93930	0.96797	0.27716
C	4.96680	-0.77889	-0.25811
H	3.33192	-2.11203	-0.73594
C	4.24872	1.39693	0.44785
H	2.09699	1.62401	0.47701
C	5.27992	0.50463	0.17450
H	5.73871	-1.50409	-0.48179
H	4.44833	2.40552	0.78666
N	2.64291	-0.26449	-0.13796
H	6.31374	0.80598	0.29692
O	-1.13569	-1.25271	-0.61487
S	-2.22823	-0.80612	0.32915
C	-2.53909	0.92263	-0.25376

F	-3.48071	1.49202	0.48845
F	-1.42293	1.63989	-0.15361
F	-2.93294	0.92494	-1.52092
O	-1.76545	-0.64845	1.69541
O	-3.46712	-1.51371	0.08754

12.2 Methylation of Pyrimidine (27)

12.2.1 Transition State for Methyl Iodide

SCF energy:	–600.829663 hartree
Zero-point correction:	+0.115790 hartree
Enthalpy correction:	+0.125116 hartree
Free energy correction:	+0.078790 hartree
Truhlar's Delta G correction:	+0.080442 hartree
Grimme's Delta G correction:	+0.080332 hartree
Imaginary Frequency:	558.2 *i*cm^{-1}

Cartesian Coordinates

C	0.09976	-0.02447	0.00012
H	0.06600	0.51333	0.93315
H	0.06581	0.51364	-0.93272
H	0.08339	-1.10271	-0.00007
I	2.65135	0.00453	-0.00004
C	-2.65071	1.13772	0.00018
C	-2.71138	-1.14956	0.00014
C	-4.03480	1.17525	-0.00011
H	-2.04400	2.03794	0.00030
H	-2.15390	-2.08039	0.00022
C	-4.69108	-0.04865	-0.00023
H	-4.57612	2.11133	-0.00026
N	-2.00001	-0.02603	0.00030
H	-5.77483	-0.09958	-0.00043
N	-4.03694	-1.21327	-0.00011

12.2.2 Transition State for Methyl Triflate

SCF energy:	–1264.071957 hartree
Zero-point correction:	+0.145638 hartree
Enthalpy correction:	+0.161203 hartree
Free energy correction:	+0.099993 hartree
Truhlar's Delta G correction:	+0.104642 hartree
Grimme's Delta G correction:	+0.103700 hartree
Imaginary Frequency:	616.2 *i*cm^{-1}

Cartesian Coordinates

C	0.62496	-0.79366	-0.32206
H	0.52486	-0.53283	0.72097
H	0.95324	-1.78601	-0.58826
H	0.58922	-0.02748	-1.07930
C	3.65098	-1.05993	-0.48735

C	2.95555	0.92367	0.41197
N	4.94119	-0.76058	-0.40261
H	3.37769	-2.02434	-0.90305
C	4.27311	1.32816	0.54271
H	2.12261	1.55008	0.71715
C	5.24457	0.43380	0.11268
H	4.53098	2.29262	0.95826
N	2.65286	-0.26954	-0.10208
H	6.29888	0.68027	0.18237
O	-1.12680	-1.26806	-0.56905
S	-2.21693	-0.78914	0.35780
C	-2.54166	0.91038	-0.29835
F	-3.47808	1.50995	0.42692
F	-1.42727	1.63570	-0.24172
F	-2.94815	0.85545	-1.56053
O	-1.74946	-0.56714	1.71426
O	-3.45480	-1.51226	0.15734

12.3 Methylation of Pyrazine (7)

12.3.1 Transition State for Methyl Iodide

SCF energy:	–600.820701 hartree
Zero-point correction:	+0.115661 hartree
Enthalpy correction:	+0.124908 hartree
Free energy correction:	+0.078918 hartree
Truhlar's Delta G correction:	+0.080343 hartree
Grimme's Delta G correction:	+0.080317 hartree
Imaginary Frequency:	541.4 *i*cm^{-1}

Cartesian Coordinates

C	-0.08206	0.00012	0.02625
H	-0.07076	-0.85202	0.68612
H	-0.04869	-0.14657	-1.04064
H	-0.07307	0.99806	0.43311
I	-2.65195	0.00003	-0.00728
C	2.65978	-1.14071	0.02674
C	2.67047	1.14733	0.02659
C	4.05031	-1.13956	-0.01914
H	2.08575	-2.06060	0.04421
C	4.06124	1.13264	-0.01973
H	2.10600	2.07302	0.04453
N	4.74994	-0.00664	-0.04263
H	4.60005	-2.07349	-0.03718
H	4.61974	2.06136	-0.03862
N	1.98945	0.00662	0.04976

12.3.2 Transition State for Methyl Triflate

SCF energy:	–1264.063294 hartree
Zero-point correction:	+0.145460 hartree
Enthalpy correction:	+0.160955 hartree

Free energy correction:	+0.100467 hartree
Truhlar's Delta G correction:	+0.104420 hartree
Grimme's Delta G correction:	+0.103812 hartree
Imaginary Frequency:	614.4 *i*cm^{-1}

Cartesian Coordinates

C	0.61921	-0.76025	-0.38232
H	0.95470	-1.72286	-0.73525
H	0.56766	0.06813	-1.07047
H	0.52987	-0.58925	0.68022
N	2.64423	-0.24920	-0.15028
C	3.63093	-1.10860	-0.38282
C	2.95439	0.98036	0.25055
C	4.95709	-0.72367	-0.20805
H	3.36448	-2.10784	-0.70941
C	4.28366	1.35266	0.42094
H	2.13734	1.66941	0.43673
N	5.28392	0.50305	0.19283
H	5.76187	-1.42461	-0.39743
H	4.53646	2.35476	0.74769
O	-1.12747	-1.23221	-0.64981
S	-2.21756	-0.81761	0.30817
O	-3.45560	-1.52410	0.05663
O	-1.75048	-0.69121	1.67689
C	-2.54033	0.92389	-0.22795
F	-3.47594	1.47269	0.53731
F	-2.94687	0.95748	-1.49084
F	-1.42496	1.64216	-0.12119

12.4 Methylation of Pyridine *N*-Oxide (8)

12.4.1 Transition State for Methyl Iodide

SCF energy:	–659.875011 hartree
Zero-point correction:	+0.131927 hartree
Enthalpy correction:	+0.141913 hartree
Free energy correction:	+0.094439 hartree
Truhlar's Delta G correction:	+0.095943 hartree
Grimme's Delta G correction:	+0.095738 hartree
Imaginary Frequency:	582.5 *i*cm^{-1}

Cartesian Coordinates

C	-0.40236	0.85146	0.00027
H	-0.16830	0.36790	0.93520
H	-0.16825	0.36817	-0.93478
H	-0.84408	1.83395	0.00041
I	-2.73001	-0.24897	-0.00007
O	1.38142	1.73258	0.00038
C	2.76647	0.31523	-1.17623
C	2.76634	0.31459	1.17637
C	3.72902	-0.67432	-1.19761
H	2.32958	0.76767	-2.05561

C	3.72889	-0.67497	1.19732
H	2.32934	0.76653	2.05596
H	4.08128	-1.03616	-2.15436
H	4.08104	-1.03734	2.15391
N	2.30844	0.79269	0.00018
C	4.22201	-1.18012	-0.00026
H	4.97738	-1.95578	-0.00042

12.4.2 Transition State for Methyl Triflate

SCF energy:	–1323.118407 hartree
Zero-point correction:	+0.161735 hartree
Enthalpy correction:	+0.178020 hartree
Free energy correction:	+0.115592 hartree
Truhlar's Delta G correction:	+0.120598 hartree
Grimme's Delta G correction:	+0.119490 hartree
Imaginary Frequency:	662.1 *i*cm^{-1}

Cartesian Coordinates

C	-0.12073	1.75711	0.53653
H	-0.20297	1.49019	-0.50658
H	-0.32510	1.03808	1.31362
H	0.00019	2.79504	0.80178
O	1.68877	1.45706	0.63364
S	2.36265	0.52759	-0.34536
O	1.80479	0.60930	-1.68340
O	3.80189	0.53118	-0.18948
C	1.81545	-1.13163	0.26899
F	2.33970	-2.09203	-0.48271
F	0.48791	-1.22192	0.21151
F	2.19794	-1.31569	1.52652
O	-2.11379	2.07976	0.47804
N	-2.65313	0.91379	0.17329
C	-3.01567	0.07175	1.16395
C	-2.80624	0.57298	-1.12377
C	-3.56114	-1.16130	0.86552
H	-2.84807	0.44348	2.16546
C	-3.34631	-0.65161	-1.46389
H	-2.48256	1.32005	-1.83534
H	-3.84499	-1.81442	1.67995
H	-3.45808	-0.89702	-2.51165
C	-3.73124	-1.53506	-0.46237
H	-4.15676	-2.49859	-0.71245

12.5 Methylation of Pyrimidine *N*-Oxide (3)

12.5.1 Transition State for N-Alkylation by Methyl Iodide

SCF energy:	–675.895370 hartree
Zero-point correction:	+0.119727 hartree
Enthalpy correction:	+0.129865 hartree
Free energy correction:	+0.081050 hartree

Truhlar's Delta G correction:	+0.083450 hartree
Grimme's Delta G correction:	+0.083041 hartree
Imaginary Frequency:	565.7 *i*cm^{-1}

Cartesian Coordinates

C	-0.40825	0.10800	-0.02109
H	-0.40752	0.39037	1.01899
H	-0.32897	-0.93107	-0.29811
H	-0.45853	0.86632	-0.78588
I	-2.98134	-0.07450	0.00577
C	2.40596	-0.79600	-0.02549
C	2.19303	1.49356	-0.01549
N	3.76323	-0.73092	0.00429
H	1.97784	-1.78985	-0.03990
C	3.57155	1.63338	0.01505
H	1.51523	2.33888	-0.02387
C	4.34738	0.49444	0.02449
O	4.46222	-1.80463	0.01305
H	4.04147	2.60702	0.03113
N	1.64921	0.27670	-0.03649
H	5.42839	0.48323	0.04787

12.5.2 Transition State for O-Alkylation by Methyl Iodide

SCF energy:	–675.900119 hartree
Zero-point correction:	+0.119877 hartree
Enthalpy correction:	+0.129857 hartree
Free energy correction:	+0.081965 hartree
Truhlar's Delta G correction:	+0.083777 hartree
Grimme's Delta G correction:	+0.083499 hartree
Imaginary Frequency:	610.2 *i*cm^{-1}

Cartesian Coordinates

C	0.40228	-0.79009	-0.21577
H	0.82738	-1.71587	-0.56671
H	0.21074	-0.65241	0.83628
H	0.14842	-0.01449	-0.92109
I	2.75010	0.22783	0.06714
O	-1.39251	-1.62034	-0.45066
C	-2.75801	0.08714	-1.20203
C	-2.85350	-0.61665	1.02717
C	-3.74083	1.01247	-0.92382
H	-2.29081	-0.05872	-2.16708
N	-3.79011	0.24908	1.33322
H	-2.44728	-1.30387	1.75852
C	-4.23782	1.06189	0.37117
H	-4.10359	1.67118	-1.70046
N	-2.32712	-0.72535	-0.21624
H	-5.01213	1.76712	0.64826

12.5.3 Transition State for N-Alkylation by Methyl Triflate

SCF energy:	–1339.138179 hartree
Zero-point correction:	+0.149359 hartree

Enthalpy correction:	+0.165756 hartree
Free energy correction:	+0.102444 hartree
Truhlar's Delta G correction:	+0.107541 hartree
Grimme's Delta G correction:	+0.106444 hartree
Imaginary Frequency:	622.1 *i*cm^{-1}

Cartesian Coordinates

C	0.33838	-0.66903	-0.32745
H	0.20728	-0.46948	0.72565
H	0.71008	-1.63130	-0.64280
H	0.23950	0.12443	-1.05066
N	2.29943	-0.02935	-0.08249
C	2.49918	1.24284	0.26531
C	3.31812	-0.83822	-0.26393
C	3.78824	1.72127	0.43622
H	1.61951	1.86116	0.40203
N	4.60763	-0.43539	-0.11383
H	3.17463	-1.87332	-0.54573
C	4.84120	0.85450	0.23873
H	3.97885	2.74784	0.71718
O	5.56922	-1.26093	-0.30344
O	-1.40587	-1.24438	-0.60205
S	-2.52061	-0.85126	0.33208
O	-3.71958	-1.63282	0.11235
O	-2.06836	-0.63926	1.69596
C	-2.93609	0.84563	-0.27822
F	-3.89925	1.37799	0.46460
F	-3.34427	0.80391	-1.54059
F	-1.86005	1.62640	-0.20554
H	5.88510	1.11670	0.34255

12.5.4 Transition State for O-Alkylation by Methyl Triflate

SCF energy:	–1339.142371 hartree
Zero-point correction:	+0.149567 hartree
Enthalpy correction:	+0.165930 hartree
Free energy correction:	+0.102106 hartree
Truhlar's Delta G correction:	+0.108124 hartree
Grimme's Delta G correction:	+0.106580 hartree
Imaginary Frequency:	664.2 *i*cm^{-1}

Cartesian Coordinates

C	-0.32305	1.33268	0.90702
H	-0.27637	0.28348	1.15519
H	-0.18415	2.06606	1.68491
H	-0.64349	1.64980	-0.07254
O	1.47546	1.45085	0.47348
S	2.03963	0.60603	-0.64029
O	1.01250	0.06432	-1.51268
O	3.21778	1.19752	-1.24002
C	2.67411	-0.85871	0.29682
F	3.17649	-1.75688	-0.54281

F	1.68364	-1.42429	0.98235
F	3.62401	-0.49345	1.14906
O	-2.25055	1.29688	1.44770
N	-2.89420	0.46662	0.65536
C	-2.95011	-0.84906	0.94215
C	-3.50009	0.94036	-0.45921
C	-3.63428	-1.69072	0.09135
H	-2.44333	-1.15365	1.84845
N	-4.16218	0.17483	-1.29396
H	-3.40225	2.00735	-0.61530
C	-4.23478	-1.13301	-1.02858
H	-3.69320	-2.74900	0.30419
H	-4.78618	-1.74485	-1.73256

12.6 Methylation of Pyrazine *N*-Oxide (1)

12.6.1 Transition State for N-Alkylation by Methyl Iodide

SCF energy:	–675.897471 hartree
Zero-point correction:	+0.119953 hartree
Enthalpy correction:	+0.129995 hartree
Free energy correction:	+0.082008 hartree
Truhlar's Delta G correction:	+0.083784 hartree
Grimme's Delta G correction:	+0.083620 hartree
Imaginary Frequency:	549.1 *i*cm^{-1}

Cartesian Coordinates

C	-0.50833	-0.00072	0.03533
H	-0.50406	-0.85522	0.69210
H	-0.47253	-0.14285	-1.03195
H	-0.50476	0.99535	0.44667
I	-3.08243	-0.00037	-0.01323
C	2.23958	-1.13643	0.04718
C	2.24724	1.14517	0.04675
C	3.61517	-1.17019	-0.00135
H	1.67630	-2.06259	0.06556
C	3.62328	1.16932	-0.00205
H	1.69097	2.07550	0.06518
N	4.31689	-0.00271	-0.02645
H	4.20437	-2.07497	-0.02153
H	4.21845	2.07017	-0.02301
N	1.55719	0.00682	0.07269
O	5.57998	-0.00718	-0.07132

12.6.2 Transition State for O-Alkylation by Methyl Iodide

SCF energy:	–675.894942 hartree
Zero-point correction:	+0.120147 hartree
Enthalpy correction:	+0.129989 hartree
Free energy correction:	+0.082700 hartree
Truhlar's Delta G correction:	+0.084231 hartree
Grimme's Delta G correction:	+0.084004 hartree
Imaginary Frequency:	594.7 *i*cm^{-1}

Cartesian Coordinates

C	-0.35380	0.85037	0.00167
H	-0.80973	1.82663	0.00415
H	-0.15547	0.34868	0.93598
H	-0.15619	0.35307	-0.93512
I	-2.74387	-0.23868	-0.00047
O	1.39219	1.69632	0.00276
C	2.78722	0.29184	-1.16689
C	2.78646	0.28734	1.16789
C	3.75896	-0.69342	-1.13546
H	2.36934	0.72085	-2.06650
C	3.75821	-0.69782	1.13329
H	2.36805	0.71293	2.06887
N	4.24835	-1.19156	-0.00188
H	4.14400	-1.08163	-2.07051
H	4.14260	-1.08966	2.06709
N	2.31773	0.77140	0.00128

12.6.3 Transition State for N-Alkylation by Methyl Triflate

SCF energy:	–1339.140028 hartree
Zero-point correction:	+0.149547 hartree
Enthalpy correction:	+0.165943 hartree
Free energy correction:	+0.102870 hartree
Truhlar's Delta G correction:	+0.107578 hartree
Grimme's Delta G correction:	+0.106785 hartree
Imaginary Frequency:	620.5 *i*cm^{-1}

Cartesian Coordinates

C	0.20351	-0.81501	-0.38943
H	0.50154	-1.80197	-0.70652
H	0.16978	-0.01446	-1.11055
H	0.12513	-0.59961	0.66591
N	2.24238	-0.36825	-0.19261
C	3.20559	-1.25890	-0.42067
C	2.60972	0.85591	0.18396
C	4.54176	-0.95391	-0.27999
H	2.91214	-2.25650	-0.72741
C	3.92936	1.21582	0.34059
H	1.82668	1.58275	0.37025
N	4.90913	0.29889	0.10627
H	5.34886	-1.64935	-0.45594
H	4.26459	2.19639	0.64411
O	-1.56481	-1.24069	-0.62872
S	-2.63073	-0.78173	0.33512
O	-3.88826	-1.46515	0.11813
O	-2.14053	-0.63612	1.69393
C	-2.92393	0.95451	-0.23387
F	-3.83921	1.53833	0.53017
F	-3.34452	0.97021	-1.49261
F	-1.79324	1.65221	-0.15511
O	6.12848	0.60429	0.24378

12.6.4 Transition State for O-Alkylation by Methyl Triflate

SCF energy:	–1339.138211 hartree
Zero-point correction:	+0.149981 hartree
Enthalpy correction:	+0.166123 hartree
Free energy correction:	+0.103765 hartree
Truhlar's Delta G correction:	+0.108854 hartree
Grimme's Delta G correction:	+0.107708 hartree
Imaginary Frequency:	671.4 *i*cm^{-1}

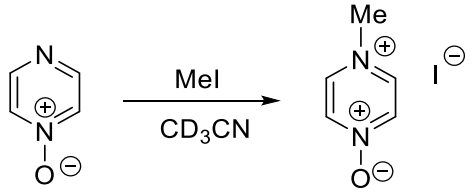
Cartesian Coordinates

C	-0.18773	-1.71515	-0.53991
H	-0.22393	-1.46338	0.50982
H	-0.36654	-0.97053	-1.29960
H	-0.06562	-2.74630	-0.82978
O	1.66585	-1.43996	-0.66131
S	2.37448	-0.56119	0.33403
O	1.80100	-0.63282	1.66724
O	3.81481	-0.62645	0.19573
C	1.91235	1.13006	-0.25997
F	2.45343	2.05583	0.52314
F	0.58784	1.27242	-0.23473
F	2.33401	1.32326	-1.50375
O	-2.14571	-2.02655	-0.46694
N	-2.70306	-0.88259	-0.16687
C	-3.11544	-0.05651	-1.14803
C	-2.84328	-0.51818	1.12268
C	-3.68350	1.15682	-0.79955
H	-2.97456	-0.40513	-2.16137
C	-3.41655	0.70924	1.40769
H	-2.49474	-1.22395	1.86347
N	-3.83642	1.54851	0.46362
H	-4.01907	1.82419	-1.58406
H	-3.53110	1.00753	2.44279

13 Determination of 2nd Order Rate Constant

Pyrazine *N*-oxide (**1**) (0.010 g, 0.10 mmol) was dissolved in dry CD_3CN (0.20 ml) in a glove box under nitrogen atmosphere. This solution was taken up in a syringe and the syringe was placed in a long Schlenk flask inside the glove box, and the Schlenk flask was sealed. Methyl iodide (0.147 g, 1.04 mmol, 10 equivalents) was dissolved in 0.65 ml dry CD_3CN in the glove box. This solution was placed in an NMR tube, which was sealed using a rubber septum. The seal was then wrapped with PTFE tape and Parafilm. Finally, the NMR tube was placed in a long Schlenk flask, which was then sealed inside the glove box. Both Schlenk flasks were removed from the glove box and brought to the NMR spectrometer (500 MHz instrument).

The Schlenk tubes were placed in the NMR spectrometer room for 20 minutes to allow them to equilibrate to the controlled room temperature of 25 °C. The NMR tube containing the MeI solution was removed from the Schlenk flask and placed in the NMR spectrometer. The probe of the spectrometer was also kept at 25 °C. After obtaining the first ^{1}H NMR spectrum and the correct shim for this sample, the NMR tube was ejected. The pyrazine *N*-oxide solution (0.18 ml, containing 0.090 mmol pyrazine *N*-oxide) in its syringe was removed from its Schlenk flask and added to the NMR tube by injection through the rubber septum. The septum was re-wrapped with parafilm after removal of the syringe. The NMR tube was inverted and then rapidly returned to the spectrometer to obtain NMR spectra of the ongoing reaction at certain intervals.



1 **13a**

Each spectrum was obtained using 4 scans, a 5 second relaxation delay and a 30° pulse. The time ascribed to each spectrum was when the spectrum measurement ended. In the obtained spectra, the C*H*D_2CN signal at δ 1.968 was set at a constant integral value throughout and the other signals are given relative to this value.

The following signals were observed in the spectra after addition.

^{1}H NMR (500 MHz, CD_3CN, 298K)

Assigned to **1**: δ 8.49 – 8.38 (m, 2H), 8.14 – 8.06 (m, 2H).

Assigned to MeI: δ 2.20 (s, 3H).

Assigned to **13a**: δ δ 8.65 – 8.59 (m, 2H), 8.57 – 8.52 (m, 2H), 4.19 (s, 3H, NCH_3).

Note: ^{13}C satellite peaks of the 2H signal of **1** at δ 8.10 appear at δ 8.30 – 8.28 and 7.92 – 7.90. These signals were included in the integration value for that signal. The aromatic signals of **13a** showed a variable chemical shift, moving downfield as the reaction progressed. The signal also initially appeared as a singlet, before splitting into two doublets as it moved downfield.

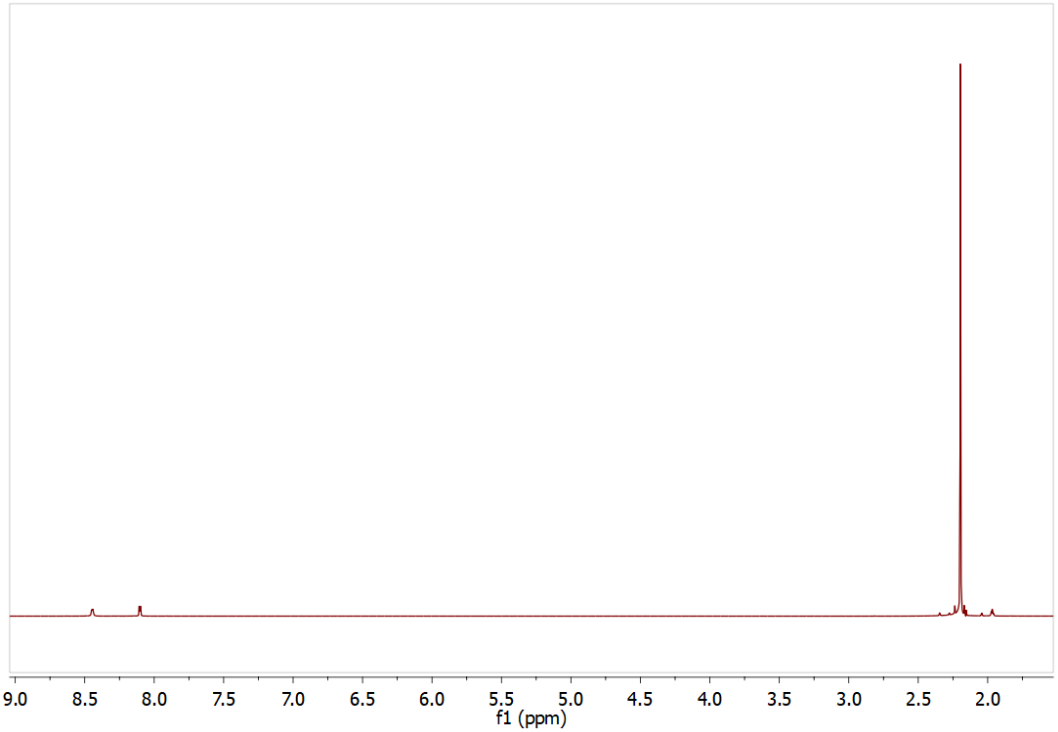


Figure S86: ^{1}H NMR spectrum in CD_3CN of the reaction of **1** and MeI. The MeI signal is disproportionately large compared to the signals of **1** and **13a** as there are 10 equivalents of MeI relative to **1**.

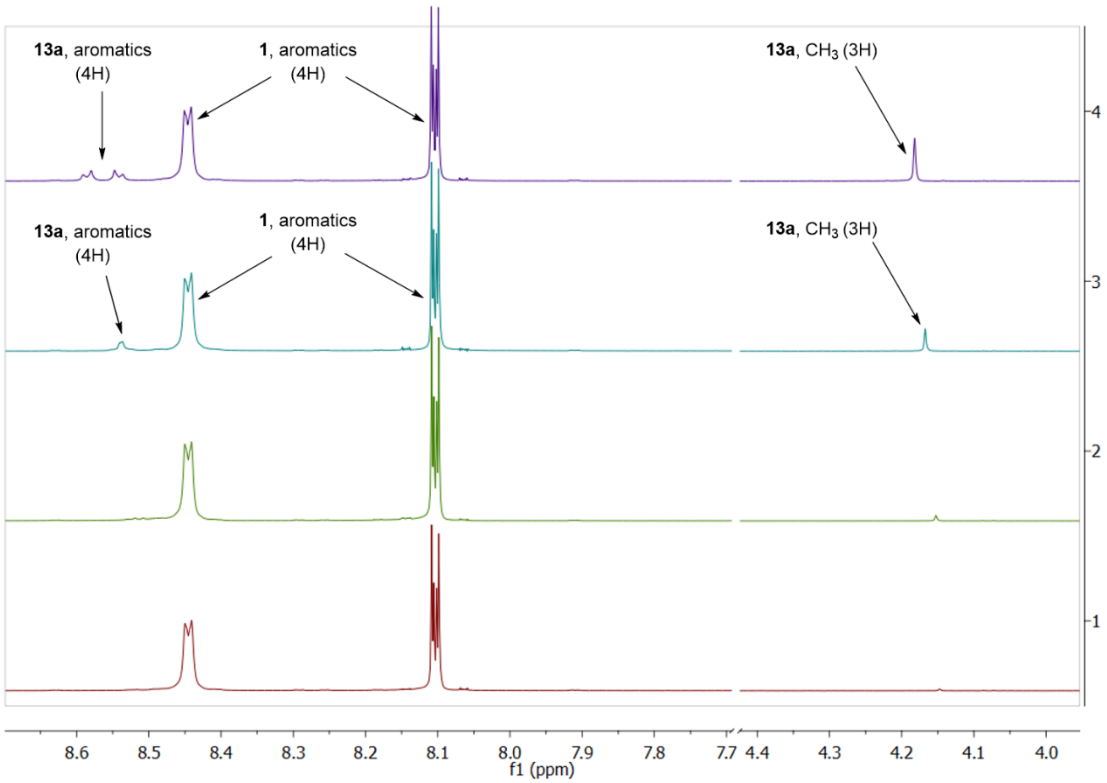


Figure S87: Stacked ^{1}H NMR spectra in CD_3CN of the reaction of **1** and MeI. The signals of **13a** appear as the reaction progresses. The aromatic signals associated with **13a** showed a variable chemical shift, in addition to being observed as both a singlet in earlier spectra, and a multiplet in later spectra.

The consumption of pyrazine *N*-oxide (**1**) was monitored by observing the decrease in the integration value at 8.10 ppm relative to the signal of C*H*D$_2$CN. The integration value was assigned a concentration value ([**1**]$_t$) relative to the concentration of (**1**) at t = 0.

At t = 0,

$$[\mathbf{1}]_{t=0} = \frac{\left(\frac{0.090\ \text{g}}{96.089\ \text{g mol}^{-1}}\right)}{0.83\ \text{ml}} = 0.113\ \text{mmol/ml}$$

At t = 713 seconds, the integration value of the signal at 8.10 ppm was 99.7% of its value at t = 0, giving:

$$[\mathbf{1}]_{t=713\ \text{s}} = (0.113\ \text{mmol/ml}) \times\ 0.997\ = 0.1127\ \text{mmol/ml}$$

This procedure was continued at various time points in order to monitor the consumption of pyrazine N-oxide. After 25 hours, conversion was approximately 28%. An approximate value of the 2nd order rate constant was derived based on data recorded for the reaction up to this level of conversion.

For each ^{1}H NMR spectrum (time t), the integrations of **1** and **13a** at time t ($I_{\mathbf{1}}$ and $I_{\mathbf{13a}}$, respectively) relative to the integration of the residual C*H*D$_2$CN were established (the integration of C*H*D$_2$CN in each spectrum was set equal to an arbitrary value of 15.2). The integration of **13a** ($I_{\mathbf{13a}}$) was scaled (multiplied by 2/3) to take account of the additional protons contributing to the signal used for the integration.

The total amount of **1** and **13a** present always equals the initial amount of **1** added, i.e.

$$n_{\mathbf{1}} + n_{\mathbf{13a}} = n_{\mathbf{1},t=0}$$

where:

$$n_{\mathbf{1}} = \text{amount of } \mathbf{1} \text{ (mmol) at time } t$$

$$n_{\mathbf{13a}} = \text{amount of } \mathbf{13a} \text{ (mmol) at time } t$$

$$n_{\mathbf{1},t=0} = \text{inital amount of } \mathbf{1} \text{ added (mmol)}$$

Hence, the quantity ($I_{\mathbf{1}}$ + $I_{\mathbf{13a}}$) – the sum of the integrations of the signals of **1** and **13a** (scaled appropriately) – was used to represent the initial amount of **1** added. The consumption of **1** at time t was then established as follows:

$$\text{Consumption of } \mathbf{1} \text{ at time } t = \frac{I_{\mathbf{1}}}{(I_{\mathbf{1}} + I_{\mathbf{13a}})} = \frac{[\mathbf{1}]_t}{[\mathbf{1}]_0}$$

See column 4 of Table S9 below for the quantities calculated in this manner.

Table S9. Recorded integration values (I) and calculated concentrations of **1** and **13a** at various time points, with derived values of ln ($[\mathbf{1}]_t$ / $[\mathbf{1}]_0$). Note that the integration value of **13a** shown here was scaled to take into account the additional protons contributing to the signal used for the integration.

Time (seconds)	$I_{\mathbf{1}}$	$I_{\mathbf{13a}}$	$[\mathbf{1}]_t$ / $[\mathbf{1}]_0$	ln ($[\mathbf{1}]_t$ / $[\mathbf{1}]_0$)
0	25.00	0	1	0
713	24.89	0.07	0.997	-2.7×10^{-3}
1080	24.87	0.09	0.996	-3.8×10^{-3}
1248	24.81	0.13	0.995	-5.1×10^{-3}
1620	24.77	0.15	0.994	-5.9×10^{-3}
1740	24.76	0.17	0.993	-6.7×10^{-3}
2160	24.74	0.19	0.992	-7.8×10^{-3}
2460	24.68	0.21	0.991	-8.6×10^{-3}
3060	24.63	0.25	0.990	-1.0×10^{-2}
3720	24.53	0.31	0.987	-1.3×10^{-2}
5460	24.32	0.45	0.982	-1.9×10^{-2}
7500	24.03	0.64	0.974	-2.6×10^{-2}
8100	23.97	0.69	0.972	-2.9×10^{-2}
11760	23.51	0.99	0.959	-4.1×10^{-2}
22560	22.48	1.68	0.930	-7.2×10^{-2}
29760	21.58	2.29	0.904	-1.0×10^{-1}
36960	20.83	2.79	0.882	-1.3×10^{-1}
54960	19.00	4.00	0.826	-1.9×10^{-1}
72960	16.96	5.36	0.760	-2.8×10^{-1}
90960	15.71	6.17	0.718	-3.3×10^{-1}

For the 2nd order reaction of **1** with MeI (and rate constant k):

$$\text{Rate} = -k[\mathbf{1}][\text{MeI}]$$

By including 10 equivalents of MeI, it can be assumed that:

$$[\text{MeI}]_t = [\text{MeI}]_0$$

Thus, for this pseudo-1st order reaction:

$$\text{Rate} = -k'[\mathbf{1}]$$

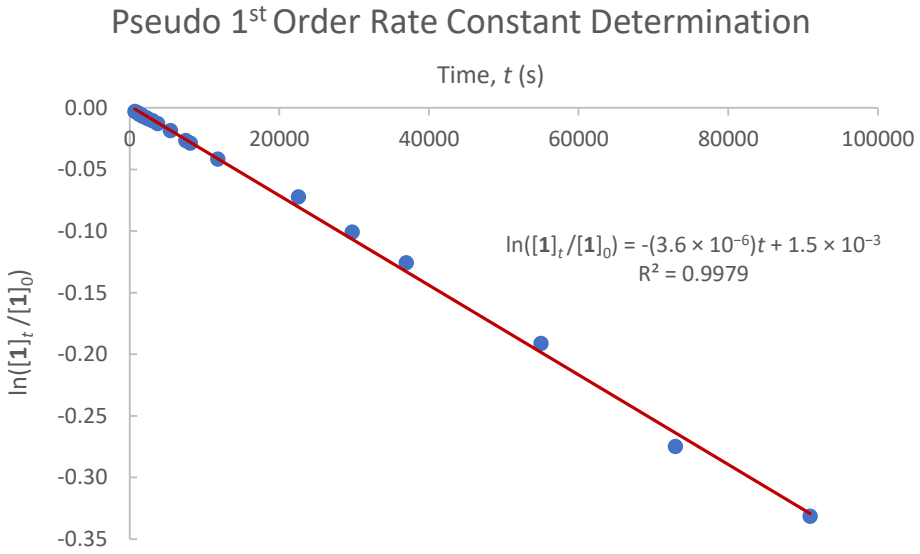
where $k' = k[\text{MeI}]_0$

The integrated rate equation for this reaction (under pseudo first-order conditions) is:

$$\ln\frac{[\mathbf{1}]_t}{[\mathbf{1}]_0} = -k't$$

where t is the time since the start of the reaction (s).

A plot of $\ln([\mathbf{1}]_t/[\mathbf{1}]_0)$ vs t (using the values shown in Table S9) is linear, as shown below. The slope of the line is $-k'$.



The slope of the plot is -3.6×10^{-6}, so $k' = -3.6 \times 10^{-6}\ \text{s}^{-1}$. Hence, since $[\text{MeI}]_0 = 1.25\ \text{mol L}^{-1}$,

$$k = (3.6 \times 10^{-6})\ \text{s}^{-1} \times (1.25\ \text{mol L}^{-1})$$

$$= 2.9 \times 10^{-6}\ \text{mol L}^{-1}\text{s}^{-1}$$

An identical value of the second order rate constant is also determined by monitoring the growth in the concentration of product **13a**.

This value of k may be related to $\Delta G^{\ddagger}$ by the Eyring equation:

$$k = \boldsymbol{\kappa} \frac{k_B T}{h} \times \frac{RT}{p^{\circ}} \, e^{-\frac{\Delta G^{\ddagger}}{RT}}$$

as seen in Atkins' Physical Chemistry, 9th ed. Section 22.4 pg. 848.[17] The transmission coefficient κ is taken to equal 1.

This equation can be rearranged to:

$$RT \ln \left(\left(\frac{1}{k} \right) \left(\frac{k_B T}{h} \right) \left(\frac{RT}{p^{\circ}} \right) \right) = \Delta G^{\ddagger}$$

giving:

$$\Delta G^{\ddagger} = 1.4 \times 10^{2} \text{ kJ mol}^{-1}$$

where:

$R = 3.14 \text{ J K}^{-1}\text{mol}^{-1}$ $T = 298 \text{ K}$
$p^{\circ} = 10^{5} \text{ N m}^{-2}$ $k_B = 1.38 \times 10^{-23} \text{ J K}^{-1}$ $h = 6.63 \times 10^{-34} \text{ J s}$

14 Additional Literature References from Main Article

S-1. Alkylation of amides (see also reference 19 of main article):

(a) Bredereck, H.; Gompper, R.; Rempfer, H.; Klemm, K.; Keck, H. *Chem. Ber*. **1959**, *92*, 329–337;

(b) Bredereck, H; Effenberger, F.; Simchen, G. *Chem. Ber*. **1963**, *96*, 1350 – 1355;

(c) Bredereck, H.; Gompper, R.; Theilig, G. *Chem. Ber*. **1954**, *87*, 537 – 546;

(d) Challis, B. C.; Challis, J. in *The Chemistry of Amides*; Zabicky, J., Ed.; Interscience: London, UK, **1970**; p. 731–858;

(e) Allouch, F.; Dwadnia, N.; Vologdin, N. V.; Svyaschenko,H. Cattey, Y. V.; Penouilh, M.-J.; Roger, J.; Naoufal, D.; Ben Salem, R.; Pirio, N.; Hierso, J.-C. *Organometallics* **2015**, *34*, 5015–5028;

(f) Smith, M. B.; Shroff, H. N. *J. Org. Chem*. **1984**, *49*, 2900–2906;

(g) Deslongchemps, P.; Caron, M. *Can. J. Chem*. **1980**, *58*, 2061 – 2068;

(h) Stirling, C. J. M. *J. Chem. Soc*. **1960**, 255 – 262;

(i) Ates, A.; Curran, D. P. *J. Am. Chem. Soc.* **2001**, *123*, 5130 – 5131.

S-2. Alkylation of amide anions (see also reference 21 of main article):

(a) See ref. S-1h above;

(b) See ref. S-1i above;

(c) Stein, A. R.; Tan, S. H. *Can. J. Chem.* **1974**, *52*, 4050 – 4061;

(d) Ragnarsson, U.; Grehn, L. *Acc. Chem. Res.* **1991**, *24*, 285 – 289.

S-3. Alkylation of anions of pyridone or quinolone (see also reference 22 of main article):

(a) Chung, N. M.; Tieckelmann, H. *J. Org. Chem*. **1970**, *35*, 2517–2520;

(b) Räth, C. *Liebigs Ann. Chem.* **1931**, *489*, 107–118;

(c) Effenberger, F.; Brodt, W.; Zinczuk, J. *Chem. Ber*. **1983**, *116*, 3011 – 3026;

(d) Nishiwaki, N.; Hisaki, M.; Ono, M.; Ariga, M. *Tetrahedron* **2009**, *65*, 7403-7407.

S-4. Alkylation of imide anions (see also reference 23 of main article):

(a) Gibson, M. S.; Bradshaw, R.W. *Angew. Chem. Int. Ed.* **1968**, *7*, 919 – 930;

(b) See ref. S-2d above.

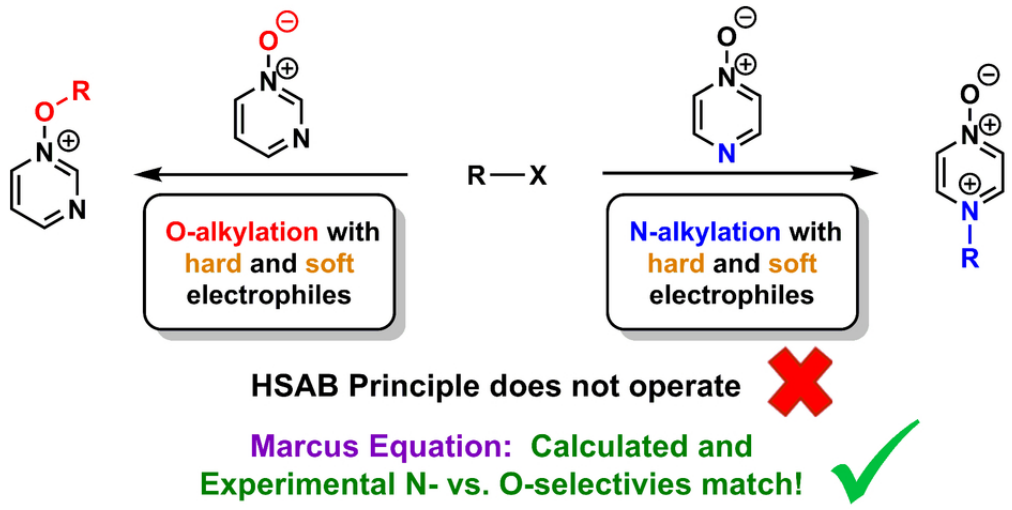
S-5. Examples of reactions of anionic ambident nucleophiles containing N- and O-centred nucleophilic sites in which coordination to a counter-cation influences site-selectivity, i.e. the selectivities are dependent on the identity and nature of the cation employed (see also reference 24 of main article):

(a) See ref. S-2c above.

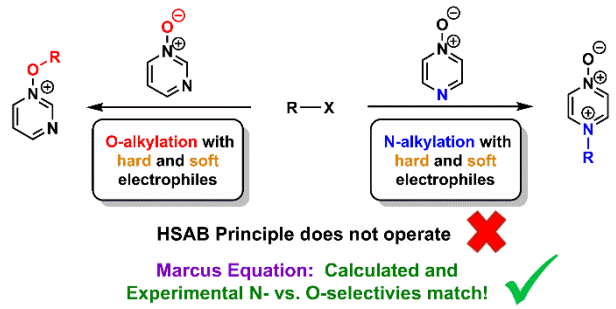
(b) See ref. S-3b above.

15 Supporting Information References

1. Williams, D. B. G.; Lawton, M. *J. Org. Chem.* **2010**, *75*, 8351–8354.
2. Shriver, D. F.; Drezdzon, M.A *The Manipulation of Air-Sensitive Compounds, 2nd Edition*; John Wiley & Sons: New York, 1986.
3. Kokatla, H. P.; Thomson, P. F.; Bae, S.; Doddi, V. R.; Lakshman, M. K. *J. Org. Chem.* **2011**, *76*, 7842–7848.
4. Procedure for synthesis of aromatic *N*-oxides: Leclerc, J. P.; Fagnou, K. *Angew. Chem. Int. Ed.* **2006**, *45*, 7781–7786
5. Głaszczka, R.; Jaźwiński, J.. *J. Mol. Struct.* **2014**, *1061*, 150–159.
6. Freire Franco, M. S.; de Paula, M. H.; Glowacka, P. C.; Fumagalli, F.; Clososki, G. C.; da Silva Emery, F. *Tetrahedron Lett.* **2018**, *59*, 2562–2566.
7. Larionov, O. V.; Stephens, D.; Mfuh, A. M.; Arman, H. D.; Naumova, A. S.; Chavez, G.; Skenderi, B. *Org. Biomol. Chem.* **2014**, *12*, 3026–3036.
8. Denegri, B.; Streiter, A.; Jurić, S.; Ofial, A. R.; Kronja, O.; Mayr, H. *Chem. Eur. J.* **2006**, *12*, 1648–1656
9. Jovanovic, M. V. **1985**, 23, 2299–2315
10. Forrester, J.; Jones, R. V. H.; Preston, P. N.; Simpson, E. S. C. *Perkin Trans.* **1995**, 2289–2291.
11. Ma, X.; Dang, H.; Rose, J. A.; Rablen, P.; Herzon, S. B. *J. Am. Chem. Soc.* **2017**, *139*, 5998–6007.
12. King, J. A.; Bryant, G. L. *Synthetic Commun.* **1994**, *24*, 1923–1935.
13. Breneman, C. M.; Wiberg, K. B. *J. Comput. Chem.* **1990**, *11*, 361–373.
14. (a) Singh, U. C.; Kollman, P. A. *J. Comput. Chem.* **1984**, *5*, 129–145; (b) Besler, B. H.; Merz Jr., K. M.; Kollman, P. A. *J. Comput. Chem.* **1990**, *11*, 431–439.
15. Glendening, E. D.; Badenhoop, J. K.; Reed, A. E.; Carpenter, J. E.; Bohmann, J. A.; Morales, C. M.; Landis, C. R.; Weinhold, F. *NBO 6.0*; Theoretical Chemistry Institute, University of Wisconsin, Madison, WI, 2013.
16. Bader, R. F. W. *Atoms in Molecules, A Quantum Theory*; Clarendon Press: Oxford, 1994.
17. Atkins, P. W.; De Paula, J. *Physical Chemistry, 9th Edition;* Oxford University Press: Oxford, 2010



79x39mm (300 x 300 DPI)



Marcus theory enables rationalisation and quantification of selectivities in reactions of ambident nucleophiles for which the HSAB Principle **cannot** operate.